Fachbereich Mathematik und Naturwissenschaften
Fachgruppe Physik
Bergische Universität Wuppertal

Influence of the Supersymmetric Bottom Sector on Higgs Production and Decay

Dissertation zur Erlangung des Doktorgrades
vorgelegt von
Franziska Hofmann

Mai 2009

Die Dissertation kann wie folgt zitiert werden:

urn:nbn:de:hbz:468-20090880
[http://nbn-resolving.de/urn/resolver.pl?urn=urn%3Anbn%3Ade%3Ahbz%3A468-20090880]

Contents

Chapter 1
1 Introduction

Particle physics aims at gaining a fundamental understanding of the elementary constituents of matter and radiation, and of the interactions between them. While researchers and philosophers speculated about the structure of matter for at least 2500 years, it was the research of the past century that revolutionized our physical understanding of this field. Triggered by the discovery of the electron (Thompson, 1887) and the realization that atoms must have a substructure (Rutherford, 1909), physicists started to systematically analyze the build-up of matter. It soon became clear that the physics at sub-atomic length scales is an incredibly fascinating field and far more complex than expected.

In a constant interplay between theory and experiment, more and more details on the structure of matter were resolved and the theoretical understanding started to improve in the early 20th century. Finally, the work culminated in the formulation of the so-called Standard Model (SM) of particle physics in the 1960s [1–8]. This theoretical model contains 12 elementary particles, which are the fundamental constituents of matter (cf. Fig. 1.1(a)). Furthermore, it describes the interaction between these particles and allows us to make accurate predictions of their scattering behavior. It groups together three of the four known fundamental forces, namely the electromagnetic force, the weak force and the strong force. Each of these forces is mediated by so-called gauge bosons (cf. Fig. 1.1(b)). The mediator of the electromagnetic force is the photon, the quantum of light. The force carriers of the weak force are called weak gauge bosons and the ones of the strong force are the gluons.

In the past decades, the predictions of the SM were thoroughly tested in a number of large-scale experiments. Today, all of the elementary SM particles are discovered and the theoretical predictions made by the SM were confirmed to astonishing accuracy. Thus, there can be little doubt that the Standard Model is an excellent description of the known elementary particles and their interactions.

Despite the unquestionable success of the Standard Model, there still is a number of theoretical and experimental challenges left:

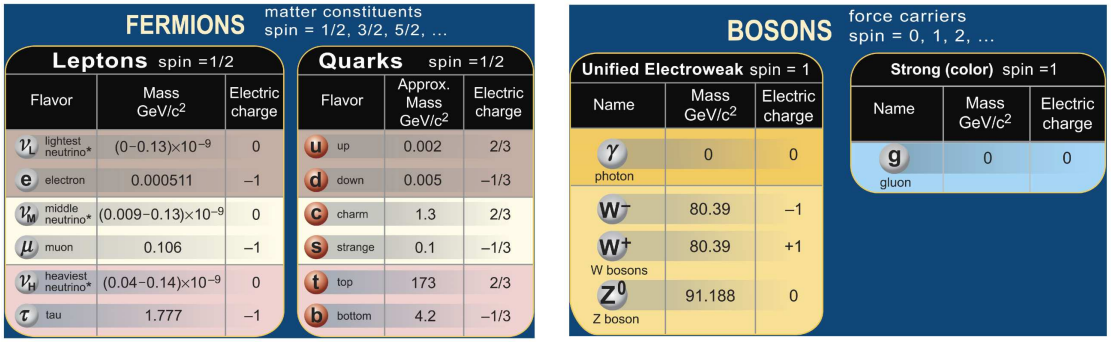

(a) (b)

Figure 1.1.: *(a) The 12 matter particles of the Standard Model. (b) The force carriers assigned to the fundamental forces that are combined in the Standard Model.*

- One of the fundamental problems is the origin of the masses of gauge bosons and elementary particles such as electrons and quarks. A priori, the theory contains massless particles. Since the gauge bosons that are mediating the weak force and electrons and quarks are observed to be massive in experiment, a mechanism to give masses to them is mandatory. The Standard Model incorporates a mechanism called spontaneous symmetry breaking to explain the masses [9, 10]. Through that mechanism one obtains the prediction of a massive Higgs boson which should be observable at colliders if this mechanism is realized in nature. Despite enormous efforts, the existence of this Higgs boson has not yet been confirmed experimentally.
- Gravity — the fourth fundamental force in nature — is not included in the model.
- From cosmological observations we know that only about 4% of the matter in the universe is visible and made up from baryons. So far it is not known what the rest is made up from. Additional 23% of the matter content of the universe is called dark matter. It is non-baryonic, non-luminous and cannot be explained within the Standard Model [11]. The residual 73% of the overall energy density of the universe is called dark energy. It is an energy form that permeates all of the universe and cosmology has not finally decided what it is.
- The forces of the Standard Model possess significantly different coupling constants. Theorists however expect the existence of a more fundamental Grand Unified Theory which describes the three forces with just one coupling constant [12, 13].

These problems have motivated theorists to work on possible solutions. Since the Standard Model is such a well-tested theory, the most promising new models are direct extensions. Those new models contain the SM and add a number of additional particles and/or interactions. One of the most promising extensions is the so-called Minimal Supersymmetric

Standard Model (MSSM) (see [14, 15] and references therein) where one practically doubles the content of the Standard Model by demanding that each Standard Model particle gets assigned a supersymmetric partner that only differs from the original particle by an amount of 1/2 in spin. This implies that bosons obtain fermions as superpartners and vice versa. This symmetry between fermions and bosons is called Supersymmetry (SUSY). The MSSM may provide solutions for the above mentioned shortcomings of the Standard Model.

Just like the SM, the MSSM allows us to predict the scattering behavior of particles after a collision. While no supersymmetric particle has ever been observed, the upcoming experiment of the Large Hadron Collider (LHC) at CERN will test the very energy scales at which extensions of the Standard Model predict new particles. The LHC is designed to search for the Higgs boson and extensions of the Standard Model like the MSSM.

Since the Higgs boson has not been found in experiments so far, it is important to investigate mechanisms that explain the observed masses within other models. In the MSSM one has the prediction of five physical Higgs bosons. In this thesis, we consider two of these Higgs bosons more closely in two scattering processes, which should allow for a direct comparison with experimental results that will be obtained at the LHC. For the experimental confirmation it is important to know the production and decay mechanisms of these Higgs bosons at the colliders built for their search. The main motivation for performing calculations for collider experiments is to obtain physical predictions for quantities that can be measured.

The LHC is a proton-proton collider. Besides two up quarks and one down quark, protons consist mainly of massless gluons. Thus, the so-called gluon fusion process is an important production mechanism for Higgs bosons at the LHC. Alongside the production of scalar and pseudoscalar Higgs bosons in the gluon fusion process, we investigate their decay into two photons, which could be an important channel for discovering Higgs bosons in case they are rather light. Massless particles such as gluons and photons cannot couple directly to Higgs bosons which were introduced to generate masses in the first place. For this reason gluons and photons can only couple to Higgs bosons via intermediate, massive particles in the SM and MSSM. This process is therefore sensitive to new massive particles, which can couple to the Higgs boson. Regarding fermions as intermediate particles, in the SM the top quark provides for the dominant contribution as it is the fermion with the largest mass.

In this thesis we investigate the production of pseudoscalar and scalar Higgs bosons via the gluon fusion process in the framework of the MSSM. The predictions the theory can provide for are only approximate. For the processes under consideration, to leading order (LO) in the strong coupling, the prediction is not a very good approximation to reality. The goal from the theory side is to access higher orders in the calculation to obtain better predictions. We calculate next-to-leading order (NLO) corrections that include contributions from quarks that are SM particles as well as their superpartners, the squarks. The

contributions from top quarks and their superpartners are known. The aim of the present thesis is to include the contributions from the second heaviest quarks, the bottom quarks and their superpartners into the calculation. The latter contributions can be enhanced in the MSSM in comparison to the SM. In addition to the superpartners of the quarks, the massive superpartner of the gluon, the gluino has to be included into the calculation as well.

This thesis introduces the concept of Supersymmetry in chapter 2. The parts relevant for our purposes of a phenomenological model of SUSY (MSSM) are presented in chapter 3. The regularization and renormalization with an emphasis on our calculations will be described in chapter 4. In chapter 5 the method of asymptotic expansions that is applied to the two-loop calculations performed in the context of this thesis is explained.

After these introductory chapters, chapter 6 presents results for the lightest scalar and pseudoscalar MSSM Higgs bosons decaying into two photons. In particular, the results for the partial decay widths of the photonic Higgs decay are investigated in terms of analytic expressions for the leading terms in certain mass hierarchies and in terms of numerical graphs. We especially investigate the influence of top quarks and their superpartners vs. bottom quarks and their superpartners on the amplitude and the decay rate.

The second main part of the results is presented in chapter 7. Those are the NLO-SQCD corrections to the production of scalar and pseudoscalar Higgs bosons in the gluon fusion process. Here, the bottom quarks and their superpartners have been included into the calculations as well. The thesis concludes with a summary and a short outlook.

Chapter 2
2 Supersymmetry (SUSY)

Supersymmetry (SUSY) denotes a symmetry between bosons and fermions. The theoretical foundations of supersymmetric theories were developed more than 30 years ago. As alluded to in the introduction, SUSY represents an appealing theoretical concept and potentially provides answers to some open questions within the Standard Model of particle physics (SM). In order to gain a better understanding of the concept of SUSY, this chapter begins with a brief historical overview. Subsequently, we discuss the main features of the Wess-Zumino Model and introduce the concept of superfields. Finally, a master Lagrangian for supersymmetric gauge field theories is presented.

2.1. The Beginning

The starting point for SUSY is a theorem formulated by Coleman and Mandula in 1967 [16], which usually is referred to as a "no-go" theorem. It states that every Lie group, which contains the Poincaré group $\mathcal{P}$ and an inner symmetry group G (e.g., the gauge group $G = SU(3)_C \otimes SU(2)_L \otimes U(1)_Y$ of the SM) has to be a direct product $\mathcal{P} \otimes G$. For a Lie group, the underlying product of the generators is the commutator $[.,.]$, which is defined as $[A, B] = AB - BA$ for operators A and B. The Poincaré group is an extension of the Lorentz group where, in addition to the Lorentz rotations and boosts ($M^{\mu\nu}$), translations in space and time (P^{μ}) are included as well. Particle states in the Standard Model are labeled with quantum numbers which are external ($m, s, \vec{p}, s_3$) and inner quantum numbers ($Q, I, I_3, Y, ...$). Let T^a be the generators of an inner symmetry group G. These are independent of spin and momentum. The statement of the "no-go" theorem is

$$[M^{\mu\nu}, T^a] = 0 \quad \text{and} \quad [P^{\rho}, T^a] = 0,$$

where $M^{\mu\nu}$ are the generators of the rotations and P^{ρ} denote the generators of the translations of the Poincaré group. This means that the T^a possess a trivial Lorentz-transformation since they do not change spin.

Further, it follows that a new group with generators Q_a, for which holds

$$[M^{\mu\nu}, Q_a] \neq 0 \quad \text{and} \quad [P^{\rho}, Q_a] \neq 0$$

is not allowed due to the theorem. This has to be understood in the sense that a new symmetry can only predict particles with the same spin and mass. A symmetry is defined to be a group of transformations that leave the action invariant and whose generators fulfill a certain algebra. A new symmetry that introduces particles with the same spin and mass is experimentally excluded because these particles would already have been observed in experiments. In other words, this means that no multiplet can group particles of different spins or masses together. There seems to be no way to bypass this no-go theorem and a non-trivial extension of a Quantum Field Theory (QFT) seems impossible.

However, this theorem does only hold for Lie algebras, where the product among generators is the commutator $[.,.]$. It does not apply to fermionic symmetries. For an extension of the group structure one is not allowed to use commutator but anti-commutator ($\{.,.\}$) relations among group generators are not excluded. The anti-commutator of two operators A and B is defined as $\{A, B\} = AB + BA$. The idea of circumventing the theorem and constructing new models is to enlarge the algebra by anti-commutator relations. One can divide the set of operators into even (bosonic) and odd (fermionic) operators. The association behind those names are bosons that possess integer spin and fermions with half-integer spin. If one denotes even (odd) operators by B (F) then a SUSY algebra possesses the following structure:

$$\begin{aligned} [F, B] &\sim F, \\ [B, B] &\sim B, \\ \{F, F\} &\sim B. \end{aligned} \tag{2.1}$$

The first expression in Eq. (2.1) indicates that the commutator of an odd and an even operator results in an odd operator and so forth. Therefore, a SUSY algebra makes a distinction between even and odd elements.

If one introduces, in addition to the Lorentz rotations and translations, a fermionic generator Q_a with spin 1/2 one obtains a so-called SUSY algebra or super algebra or graded Lie algebra. With the help of this fermionic operator, bosonic states are transformed into fermionic ones and vice versa:

$$Q_a \left|B\right\rangle = \left|F\right\rangle \qquad \text{and} \qquad Q_a \left|F\right\rangle = \left|B\right\rangle .$$

A super algebra is the only possibility of a graded Lie algebra that mixes integer and half-integer spin and changes statistics. It connects fermions and bosons. For a super algebra

with one ($N = 1$) fermionic generator Q the relations of Eq. (2.1) read

$$\begin{aligned} [P^\mu, Q_a] &= 0, \\ [Q_a, M^{\mu\nu}] &= (\Sigma^{\mu\nu})_{ab}\, Q_b, \\ \{Q_a, \overline{Q}_b\} &= 2\,(\gamma^\mu)_{ab}\, P_\mu. \end{aligned} \tag{2.2}$$

The indices a, b are spinor indices. For completeness, the known relations for the Poincaré algebra are given by

$$\begin{aligned} [P_\mu, P_\nu] &= 0, \\ [P_\mu, M_{\mu\nu}] &= i\,(g_{\mu\rho}P_\sigma - g_{\mu\sigma}P_\rho)\,, \\ [M_{\mu\nu}, M_{\rho\sigma}] &= i\,(g_{\nu\rho}M_{\mu\sigma} - g_{\nu\sigma}M_{\mu\rho} - g_{\mu\rho}M_{\nu\sigma})\,, \end{aligned} \tag{2.3}$$

where P^μ denote the generators of the translation, $M^{\mu\nu}$ are the Lorentz rotations, $\overline{Q}$ is the charge conjugate of Q and $\Sigma^{\mu\nu} = \frac{i}{4}[\gamma^\mu, \gamma^\nu]$. The γ_μ are the Dirac γ-matrices which fulfill the Clifford algebra $\{\gamma_\mu, \gamma_\nu\} = 2g_{\mu\nu}$ with the metric tensor $g_{\mu\nu}$. Together, Eqs. (2.2) and (2.3) form the super Poincaré algebra. Since Q does not commute with the Lorentz rotations we notice that it has a non-trivial Lorentz transformation that possesses a "non-zero" spin.

Haag, Lopuszanski and Sohnius showed in 1974 [17], that the above described graded Lie algebra is the only non-trivial unification of internal and space-time symmetries compatible with Quantum Field Theory. With this extension of the algebra, it is possible to group particles with integer and half-integer spin together into a multiplet if the number of bosonic degrees of freedom (d.o.f.) equals the number of fermionic degrees of freedom. But then one can show that for every fermionic state there is a bosonic one with equal mass. Let $|F\rangle$ be a fermionic state with mass m, $|B\rangle = Q_a\,|F\rangle$ and $P^2\,|F\rangle = m^2\,|F\rangle$ with the momentum operator P. It then follows

$$P^2\,|B\rangle = P^2 Q_a\,|F\rangle = Q_a m^2\,|F\rangle = m^2\,|B\rangle\,.$$

Thus, for every fermionic state there is a bosonic one with equal mass m.

This is excluded experimentally, because otherwise the supersymmetric partner particles of the Standard Model particles should have been observed so far. As a consequence, if supersymmetry exists it has to be broken in nature. Models with more than one supersymmetric charge do not lead to chiral fermions [18]. That is why they are excluded phenomenologically and we restrict ourselves henceforth to $N = 1$ supersymmetry.

2.1.1. The Wess-Zumino Model

In 1974, Wess and Zumino constructed the first linear realization of supersymmetry in four dimensions [19]. They worked out transformations that transform boson fields into fermion

fields and vice versa. We sketch the idea of SUSY transformations along the lines of their publication.

The infinitesimal supergauge transformations for two scalar fields A, B and a fermion field ψ are given by [19]

$$\begin{aligned} \delta A &= i\overline{\alpha}\psi && (B \to F), \\ \delta B &= i\overline{\alpha}\gamma_5\psi && (B \to F), \\ \delta\psi &= \partial_\mu (A - \gamma_5 B) && (F \to B). \end{aligned}$$

Here, a complex scalar field $\phi = (A + iB)/\sqrt{2}$ and a Majorana fermion $\psi = \psi^c = C\overline{\psi}^T$ are given. C is the charge conjugation matrix that satisfies $C\gamma_\mu^T C^{-1} = -\gamma_\mu$, $C^T = C^{-1} = -C$ and $[C, \gamma_5] = 0$. Here, α is an infinitesimal anti-commuting spinor parameter. From the transformations the mass dimension of α can be determined. The transformations given above preserve mass dimension, Lorentz invariance and parity. As the mass dimension of $[\psi] = \frac{3}{2}$, $[A] = [B] = 1$, it follows that the one of $[\alpha] = -\frac{1}{2} = [\overline{\alpha}]$. In Ref. [19] local gauge transformations are applied, which means that the generator of the transformations depends on the locality, i.e., $\alpha = \alpha(x)$. Assuming that $\alpha = \text{const}$ the calculations and results simplify a lot but nevertheless, the main ideas of the paper become clear.

As a starting point, we perform two SUSY transformations successively. The commutators of two such transformations are examined. A transformation with parameter α_1 (α_2) is denoted by δ_1 (δ_2). For the commutators of SUSY transformations, which are applied to boson fields, one obtains

$$\begin{aligned} [\delta_1, \delta_2]\, A &= \zeta^\mu(\partial_\mu A), \\ [\delta_1, \delta_2]\, B &= \zeta^\mu(\partial_\mu B), \end{aligned}$$

where $\zeta^\mu = 2i\overline{\alpha}_1\gamma^\mu\alpha_2$. One can read off the result that applying the transformation twice transforms a boson field back into a boson field ($B \to F \to B$). This corresponds to a translation in space-time as $\partial_\mu A$ indeed corresponds to the application of the momentum operator P_μ. It means that the result of applying a SUSY transformation twice leads to a translation in space-time, which belongs to the Poincaré algebra, i.e., remains within the super algebra. In this sense, one says that the algebra closes. For commutators applied to fermion fields the result reads

$$[\delta_1, \delta_2]\psi = \zeta^\mu(\partial_\mu\psi) + i(\overline{\alpha}_2\gamma_\nu\alpha_1)\gamma^\nu\,(\gamma^\mu\partial_\mu)\,\psi.$$

The algebra only closes, if the second term on the right hand side vanishes. This is only the case if the Dirac equation $i\,\partial\!\!\!/\psi = 0$ holds. Fermions that obey the Dirac equation are said to be on-shell. Thus, if the Dirac equation is imposed we obtain

$$[\delta_1, \delta_2]\psi = \zeta^\mu(\partial_\mu\psi).$$

Also, we observe that applying the SUSY transformation two times in a row on a fermion field ($F \to B \to F$), one again gets back a fermion field that is translated in space-time.

Our goal is to find a closed algebra for fermion fields with arbitrary masses and not being restricted to on-shell fermions (two d.o.f.). If the fermion field is off-shell, the number of bosonic degrees of freedom does not balance the fermionic one any longer. To reinstate this equality of bosonic and fermionic degrees of freedom, in addition to the boson fields A and B one introduces two more fields which are denoted by F and G. One then has 4 bosonic d.o.f., which correspond to the 4 fermionic ones an off-shell spinor possesses. With the new fields, the so-called auxiliary fields, one obtains the SUSY transformations listed below [19].

$$\begin{aligned}
\delta A &= i\overline{\alpha}\psi, \\
\delta B &= i\overline{\alpha}\gamma_5\psi, \\
\delta\psi &= \partial_\mu \left(A - \gamma_5 B\right)\gamma^\mu\alpha + F\alpha + G\gamma_5\alpha, \\
\delta F &= i\overline{\alpha}\gamma^\mu\partial_\mu\psi, \\
\delta G &= i\overline{\alpha}\gamma_5\gamma^\mu\partial_\mu\psi.
\end{aligned}$$

For the application of the SUSY transformations we now obtain

$$\begin{aligned}
\left[\delta_1, \delta_2\right] A &= \zeta^\mu(\partial_\mu A), \\
\left[\delta_1, \delta_2\right] B &= \zeta^\mu(\partial_\mu B), \\
\left[\delta_1, \delta_2\right] F &= \zeta^\mu(\partial_\mu F), \\
\left[\delta_1, \delta_2\right] G &= \zeta^\mu(\partial_\mu G),
\end{aligned}$$

and for the fermion field

$$\left[\delta_1, \delta_2\right]\psi = \zeta^\mu(\partial_\mu\psi).$$

Hence, the algebra closes. Again, $\zeta^\mu = 2i\overline{\alpha}_1\gamma^\mu\alpha_2$. The newly introduced auxiliary fields are non-physical. As F and G possess mass dimension two, a kinetic term for them is forbidden. It would be of the form $(\partial_\mu F)^2$ and would have a mass dimension six, which is not allowed in the Lagrangian with mass dimension four.

By grouping the four boson fields and the spinor field together, we obtain a multiplet in which the number of bosonic and fermionic d.o.f. are matched, as required. The Lagrangian of the multiplet (A, B, F, G, ψ) is

$$\mathcal{L} = -\frac{1}{2}\left(\partial_\mu A\right)\left(\partial^\mu A\right) - \frac{1}{2}\left(\partial_\mu B\right)\left(\partial^\mu B\right) - \frac{1}{2}i\overline{\psi}\gamma^\mu\partial_\mu\psi + \frac{1}{2}\left(F^2 + G^2\right).$$

From the Euler-Lagrange equations it follows that $F = 0$ and $G = 0$. If one examines this Lagrangian under a SUSY transformation, one finds that it is invariant only up to a total derivative [19]. Therefore, the action $S = \int d^4x\mathcal{L}$ is invariant.

Finally, it should be noted that Wess and Zumino were not the first to consider supersymmetry. There is a really nice book which narrates the beginnings of SUSY by letting

the protagonists have their say [20]. Golfand and Likhtman [21] were the first to consider SUSY-QED. Volkov and Akulov [22, 23] laid the foundations for spontaneously broken SUSY. They were able to obtain Goldstone particles with spin 1/2 due to an extension of the Poincaré group. Volkov and Soroka [24] were the first to consider local supersymmetry which leads to supergravity.

2.2. Steps Towards a Phenomenological Model of SUSY

In the last section we introduced the concept of SUSY transformations. There is still some work to be done to attain a viable phenomenological model for supersymmetry. In this thesis we will focus on the minimal supersymmetric extension of the Standard Model (MSSM). Its essential features needed for this work will be described in chapter 3. Beforehand, the superfield formalism will be introduced that provides general rules for how to construct supersymmetric Lagrangians. A master Lagrangian for supersymmetric theories will be presented at the end of this section. A very clear introduction to SUSY and the MSSM is given in the book by Baer and Tata [18].

2.2.1. Superfields

First, we establish supersymmetric multiplets. A chiral multiplet is composed of

$$\begin{aligned} S &= \frac{1}{\sqrt{2}}\left(A + iB\right), \\ \psi_L &= \frac{1-\gamma_5}{2}\psi, \\ \mathcal{F} &= \frac{1}{\sqrt{2}}\left(F + iG\right). \end{aligned}$$

S, ψ_L and $\mathcal{F}$ form a (left) chiral supermultiplet. We observe that, as required, the number of d.o.f. of ψ_L is equal to the number of scalar d.o.f. of $\mathcal{F}$ and S. The Lorentz group can be decomposed into two fundamental representations $\left(\frac{1}{2}, 0\right)$ and $\left(0, \frac{1}{2}\right)$. A $\left(\frac{1}{2}, 0\right)$ object transforms as a left-handed two-component Weyl spinor $\psi_{L,A}$ with $A = 1, 2$, whereas a $\left(0, \frac{1}{2}\right)$ object transforms as a right-handed two-component Weyl spinor $\psi_R^{\dot{A}}$ with $\dot{A} = 1, 2$. Spinors of the two fundamental SU(2) groups are distinguished by different indices A and $\dot{A}$. If we combine both representations by a direct sum, i.e., $\left(0, \frac{1}{2}\right) \oplus \left(\frac{1}{2}, 0\right)$, a four-component Dirac spinor is given by

$$\psi_a^D = \begin{pmatrix} \psi_{L,A} \\ \chi_R^{\dot{A}} \end{pmatrix}. \tag{2.4}$$

ψ_L and χ_R are independent. Since $(-i\sigma_2\psi_L^*)$ with the Pauli matrix σ_2 transforms as a $\left(0, \frac{1}{2}\right)$ representation, it transforms as χ_R. Consequently, we are able to construct a four-

component spinor whose right-handed piece is completely determined by its left-handed piece:

$$\psi_a = \begin{pmatrix} \psi_{L,A} \\ (-i\sigma_2\psi_L^*)^{\dot{A}} \end{pmatrix}. \tag{2.5}$$

ψ_a is called a Majorana spinor with $\chi_R = (-i\sigma_2\psi_L^*)$. In the following the four-component Majorana spinor notation is used. ψ_a^D then can be thought of as a combination of two Majorana spinors, like complex numbers as a combination of two real ones. Usually, one uses projectors to project out the left-handed (upper) components or right-handed (lower) components of spinor fields like $\psi_{R,L} = P_{R,L}\psi$ with $P_{R,L} = (1\pm\gamma_5)/2$ and the representation of $\gamma_5 = \mathrm{diag}(-1,-1,1,1)$.

The question now is how to combine S, ψ_L and $\mathcal{F}$ into a superfield. The problem we are facing is that S and ψ_L transform differently under Lorentz transformations. Therefore, it is not obvious how to combine them into one superfield. We are forced to introduce a new Majorana spinor θ with components θ_1, θ_2, θ_3 and θ_4, which can be combined with ψ to make a Lorentz scalar that can be "added" to S [18]. As ψ obeys anti-commutation relations, the components of θ are taken to be anti-commuting. They are called Grassmann numbers and fulfill $\{\theta_a, \theta_b\} = 0$ from which $\theta_a\theta_a = 0$ (no sum over a) is concluded. Further, $\{\theta_a, \psi_b\} = 0$. The Grassmann numbers are not operators but anti-commuting numbers. They anti-commute with fermionic operators and commute with bosonic operators. We impose the Majorana condition $\overline{\theta} = \theta^T C$. Therefore, the components of the conjugated spinor $\overline{\theta}$ are completely determined in terms of the four θ_a.

General superfields are denoted by $\hat{\phi} = \hat{\phi}(x,\theta)$. A hat is put on top of the superfield to distinguish it from usual fields. x and θ span the superspace. A superfield can be expanded in terms of the various possible θ combinations.

A general scalar superfield can be expressed as [18]

$$\begin{aligned} \hat{\phi}(x,\theta) = S &- i\sqrt{2}\,\overline{\theta}\gamma_5\psi - \frac{i}{2}\left(\overline{\theta}\gamma_5\theta\right)\mathcal{M} + \frac{1}{2}\left(\overline{\theta}\theta\right)\mathcal{N} \\ &+ \frac{1}{2}\left(\overline{\theta}\gamma_5\gamma_\mu\theta\right)V^\mu + i\left(\overline{\theta}\gamma_\mu\theta\right)\left\{\overline{\theta}\left(\lambda + \frac{i}{\sqrt{2}}\,\partial\!\!\!/\psi\right)\right\} \\ &- \frac{1}{\sqrt{4}}\left(\overline{\theta}\gamma_5\theta\right)^2\left(\mathcal{D} - \frac{1}{2}\Box S\right). \end{aligned} \tag{2.6}$$

Here, the coefficients are sixteen component fields. S, $\mathcal{M}$, $\mathcal{N}$ and $\mathcal{D}$ are the scalar ones, V^μ denotes a vector field and ψ and λ are spinor fields. As demanded, the eight scalar d.o.f. balance the eight spinorial d.o.f.. If the lowest spin component has spin-zero, one speaks of a chiral scalar superfield, otherwise of a chiral spinor superfield. Eq. (2.6) is not unique but it can be regarded as the canonical form in the sense that any scalar superfield can be straightforwardly reduced to Eq. (2.6) with identities among Grassmann variables.

We define the superfield to be real $\hat{\phi}^\dagger = \hat{\phi}$. Therefore, it follows that the boson fields are real and the fermion fields are Majorana $\psi = \psi^c$ and $\lambda = \lambda^c$.

The spinorial generator Q of SUSY transformations can be realized as a differential operator in superspace acting on superfields $\hat{\phi}(x, \theta)$. First, derivatives with respect to Grassmann numbers have to be defined:

$$\frac{\partial \theta_a}{\partial \theta_b} = \delta_{ab}, \quad \frac{\partial \overline{\theta}_a}{\partial \overline{\theta}_b} = \delta_{ab}.$$

From $\theta_a = c_{ab}\overline{\theta}_b$ it follows that $\frac{\partial \theta_a}{\partial \overline{\theta}_b} = c_{ab}$.

$$\frac{\partial}{\partial \theta_c}(\theta_a \theta_b) = \delta_{ac}\theta_b - \theta_a \delta_{bc},$$

where we used the fact that the anti-commutator of two θs is zero. For the action of the spinor operator Q on superfields one obtains [18]

$$[\overline{\alpha}Q, \hat{\phi}] = i\left(\overline{\alpha}\frac{\partial}{\partial \overline{\theta}} + i\overline{\alpha}\ \not{\partial}\theta\right)\hat{\phi}. \tag{2.7}$$

It changes the Lorentz properties of the individual terms of the superfield by taking away or adding a θ term. With the help of Eq. (2.7) it can be computed how a general superfield changes under an infinitesimal supersymmetric transformation. The variation of $\hat{\phi}$ is $\delta\hat{\phi} = i[\overline{\alpha}Q, \hat{\phi}]$ and by working $\delta\hat{\phi}$ into the canonical form of Eq. (2.6) the transformation laws of the component fields are obtained. Ultimately, the transformation laws of the components of a general scalar superfield are given by [18]

$$\begin{aligned}
\delta S &= i\sqrt{2}\overline{\alpha}\gamma_5\psi, \\
\delta\psi &= -\frac{\alpha\mathcal{M}}{\sqrt{2}} - i\frac{\gamma_5\alpha\mathcal{N}}{\sqrt{2}} - i\frac{\gamma_\mu\alpha V^\mu}{\sqrt{2}} - \frac{\gamma_5\ \not{\partial}S\alpha}{\sqrt{2}}, \\
\delta\mathcal{M} &= \overline{\alpha}\left(\lambda + i\sqrt{2}\ \not{\partial}\psi\right), \\
\delta\mathcal{N} &= \overline{\alpha}\gamma_5\left(\lambda + i\sqrt{2}\ \not{\partial}\psi\right) \\
\delta V^\mu &= -i\overline{\alpha}\gamma^\mu\lambda + \sqrt{2}\overline{\alpha}\partial^\mu\psi, \\
\delta\lambda &= -i\gamma_5\alpha\mathcal{D} - \frac{1}{2}[\not{\partial}, \gamma_\mu]V^\mu\alpha, \\
&\boxed{\delta\mathcal{D} = \overline{\alpha}\ \not{\partial}\gamma_5\lambda}.
\end{aligned} \tag{2.8}$$

As expected, the variation of a boson field is proportional to a fermionic one and vice versa.

Next, left-chiral scalar superfields will be defined. By choosing $\lambda = 0 = \mathcal{D}$ and $V_\mu = \partial_\mu\xi$ the multiplet can be reduced into two multiplets such that the field components of each multiplet transform only among themselves.

We obtain a left-chiral superfield consisting of

$$\frac{\partial^\mu S - iV^\mu}{\sqrt{2}}, \quad \psi_L, \quad \frac{\mathcal{M} - i\mathcal{N}}{\sqrt{2}}$$

and a right-chiral superfield composed of

$$\frac{\partial^\mu S + iV^\mu}{\sqrt{2}}, \quad \psi_R, \quad \frac{\mathcal{M} + i\mathcal{N}}{\sqrt{2}}.$$

Having started with the real superfield $\hat{\phi}$ of Eq. (2.6), those two chiral superfields are related. By setting $\psi_R = 0$, $V^\mu = i\partial^\mu S$ and $\mathcal{N} = i\mathcal{M} \equiv i\mathcal{F}$ into Eq. (2.6), we obtain what we call a left-chiral scalar superfield $\hat{S}_L$. By setting $\psi_L = 0$, $V^\mu = -i\partial^\mu S$ and $\mathcal{N} = -i\mathcal{M} \equiv \mathcal{F}$ into Eq. (2.6), we obtain what we call a right-chiral scalar superfield $\hat{S}_R$. Note that $\hat{S}_L^\dagger$ has the form of a right-chiral scalar superfield.

A left-chiral superfield is expressed by [18]

$$\begin{aligned}\hat{S}_L =& S + i\sqrt{2}\,\overline{\theta}\psi_L + i\overline{\theta}\theta_L\mathcal{F} + \frac{i}{2}\left(\overline{\theta}\gamma_5\gamma_\mu\theta\right)\partial^\mu S \\ &- \frac{1}{\sqrt{2}}\overline{\theta}\gamma_5\theta\cdot\overline{\theta}\;\partial\!\!\!/\psi_L + \frac{1}{8}\left(\overline{\theta}\gamma_5\theta\right)^2\Box S.\end{aligned} \tag{2.9}$$

In Eq. (2.9) the chiral representation is applied like in Eq. (2.5) for θ, i.e., $(\theta_1, \theta_2, \theta_3, \theta_4) = (\theta_{L1}, \theta_{L2}, \theta_{R1}, \theta_{R2})$. With this $\overline{\theta}\theta_L = 2\theta_{L1}\theta_{L2}$. The transformation laws for the component fields are [18]

$$\begin{aligned}\delta S &= -i\sqrt{2}\,\overline{\alpha}\psi_L, \\ \delta\psi_L &= -\sqrt{2}\mathcal{F}\alpha_L + \sqrt{2}\;\partial\!\!\!/ S\alpha_R, \\ &\boxed{\delta\mathcal{F} = i\sqrt{2}\,\overline{\alpha}\;\partial\!\!\!/\psi_L}.\end{aligned} \tag{2.10}$$

By defining $\hat{x}_\mu = x_\mu + \frac{i}{2}\overline{\theta}\gamma_5\gamma_\mu\theta$ a shorter expression for the left-chiral superfield is obtained.

$$\hat{S}_L(x,\theta) = S(\hat{x}) + i\sqrt{2}\,\overline{\theta}\psi_L(\hat{x}) + i\overline{\theta}\theta_L\mathcal{F}(\hat{x}). \tag{2.11}$$

A product of any number of left-chiral scalar superfields is a left-chiral superfield and a product of a left-chiral with a right-chiral scalar superfield is a general superfield [18].

Starting from the real general scalar superfield (2.6), one can work with all but the λ, V^μ and $\mathcal{D}$ components set to zero which then make up a gauge potential superfield $\hat{\Phi}$. The vector potentials are enclosed in them. Under a general supersymmetric local gauge transformation the gauge potential superfield transforms as

$$e^{g\hat{\Phi}} \to e^{-ig\hat{S}_L^\dagger} e^{g\hat{\Phi}} e^{ig\hat{S}_L}.$$

Here, g is the gauge coupling and $\hat{S}_L$ is a left-chiral scalar superfield. For the Abelian case, this transformation is [18]

$$\hat{\Phi}' \to g\hat{\Phi} + i\left(\hat{S}_L - \hat{S}_L^\dagger\right). \tag{2.12}$$

Performing this Abelian gauge transformation, starting from a multiplet $(S, \psi, \mathcal{M}, \mathcal{N}, V^\mu, \lambda, \mathcal{D})$ and choosing the component fields of $\hat{S}_L$ appropriately, one can set the following gauge-transformed parts to zero: S', ψ', $\mathcal{M}'$, $\mathcal{N}'$. This is called Wess-Zumino (WZ) gauge. The WZ gauge is not supersymmetric because after applying it and performing another SUSY transformation, one re-generates these components again [18]. Since there is a WZ gauge even for non-Abelian gauge theories, it is compatible with the usual gauges. In WZ gauge a gauge potential superfield (vector superfield) can be written as [18]

$$\hat{\Phi}_A = \frac{1}{2}\left(\overline{\theta}\gamma_5\gamma_\mu\theta\right)V_A^\mu + i\overline{\theta}\gamma_\mu\theta\overline{\theta}\lambda_A - \frac{1}{4}\left(\overline{\theta}\gamma_5\theta\right)^2\mathcal{D}_A,$$

with gauge group index A.

2.2.2. Lagrangians for Chiral Superfields

So far, we gathered together the information needed for constructing actions that are invariant under SUSY transformations. This invariance means that the variation of $\mathcal{L}$ can at most be a total derivative. In fact, $\mathcal{L}$ can never be invariant under SUSY transformations [18]. First, we observe that the $\mathcal{D}$-component (cf. Eq. (2.8)) of any superfield and the $\mathcal{F}$-component (cf. Eq. (2.10)) of chiral superfields transform as a total derivative under SUSY transformations. If the product of any number of chiral superfields with their hermitian conjugates is taken, the so-called $\mathcal{D}$-term (cf. Eq. (2.6)) of the product superfield changes only by a total derivative under SUSY transformations. Similarly, if the product of only left-chiral scalar superfields is taken, the so-called $\mathcal{F}$-term (cf. Eq. (2.9)) changes only by a total derivative.

Therefore, $\mathcal{D}$ and $\mathcal{F}$-terms are candidates for a SUSY Lagrangian.
In order to obtain SUSY invariant actions we concentrate on two functions, namely the so-called Kähler potential $K = K(\hat{S}_{Li}^\dagger, \hat{S}_{Lj})$ and the superpotential $\hat{f} = \hat{f}(\hat{S}_{Li})$. $\hat{S}_{Li}$ denotes a set of left-chiral superfields with $i = 1, ..., N$, $\hat{S}_{Li}^\dagger$ is a set of right-chiral superfields and K is a general superfield. The $\mathcal{D}$-term of K and the $\mathcal{F}$-term of $\hat{f}$ are candidates for a SUSY Lagrangian.

In the same way that a scalar potential specifies any theory of spin-zero and spin-1/2 fields in a usual field theory, a SUSY theory is specified by the Kähler potential and the superpotential. To obtain the Kähler potential contributions to the Lagrangian, we compute the coefficients of $(\overline{\theta}\gamma_5\theta)^2$ which means the $\mathcal{D}$-term of K, short "$\mathcal{D}$-term" contributions to $\mathcal{L}$.

Imposing renormalizability, the general choice for the Kähler potential has the form [18]

$$K[\hat{S}^\dagger, \hat{S}] = \sum_{i=1}^{N} \hat{S}_i^\dagger \hat{S}_i.$$

For a single chiral scalar superfield the $\mathcal{D}$-term contribution to the Lagrangian that is by convention the coefficient of $-(1/2)\,(\overline{\theta}\gamma_5\theta)^2$ of the product $\hat{S}_L^\dagger \hat{S}_L$ is given by [18]

$$\mathcal{L}_\mathcal{D} = \partial_\mu S^\dagger \partial^\mu S + \frac{i}{2}\overline{\psi}\ \partial\!\!\!/\psi + \mathcal{F}^\dagger\mathcal{F}.$$

In order to extract the superpotential, the coefficient of $\overline{\theta}\theta_L$ of a product of left-chiral superfields has to be calculated, i.e., the $\mathcal{F}$-term of the superpotential. Those are called "$\mathcal{F}$-term" contributions. To obtain a renormalizable Lagrangian, the superpotential can at most be cubic in $\hat{S}$.

Formally, the superpotential can be written as a power series about $\hat{S} = S$

$$\begin{aligned}\hat{f}\left(\hat{S}\right) = \hat{f}\left(\hat{S} = S\right) &+ \sum_i \frac{\partial\,\hat{f}}{\partial\hat{S}_i}\bigg|_{\hat{S}=S}\left(\hat{S} - S\right)_i \\ &+ \frac{1}{2}\sum_{i,j}\frac{\partial^2\,\hat{f}}{\partial\hat{S}_i\partial\hat{S}_j}\bigg|_{\hat{S}=S}\left(\hat{S} - S\right)_i\left(\hat{S} - S\right)_j \\ &+ \ldots\end{aligned}$$

S is the scalar component of $\hat{S}$. Only the second and third term will contribute, since the first does not contain θs. The second term contributes with the $\overline{\theta}\theta_L$ term of $(\hat{S} - S)_i$ and the third term contributes when $(\hat{S} - S)_i$ and $(\hat{S} - S)_j$ each contribute a term linear in θ.

Inserting all the possible terms one obtains the Hermitian Lagrangian which is by convention the coefficient of $(-\overline{\theta}\theta_L)$ [18]

$$\begin{aligned}\mathcal{L}_\mathcal{F} = &-i\sum_i \frac{\partial\,\hat{f}}{\partial\hat{S}_i}\bigg|_{\hat{S}=S}\mathcal{F}_i - \frac{1}{2}\sum_{i,j}\frac{\partial^2\,\hat{f}}{\partial\hat{S}_i\partial\hat{S}_j}\bigg|_{\hat{S}=S}\overline{\psi}_i P_L\psi_j \\ &+ i\sum_i\left(\frac{\partial\,\hat{f}}{\partial\hat{S}_i}\right)^\dagger\bigg|_{\hat{S}=S}\mathcal{F}_i^\dagger - \frac{1}{2}\sum_{i,j}\left(\frac{\partial^2\,\hat{f}}{\partial\hat{S}_i\partial\hat{S}_j}\right)^\dagger\bigg|_{\hat{S}=S}\overline{\psi}_i P_R\psi_j.\end{aligned}$$

By adding the $\mathcal{F}$-and $\mathcal{D}$-term Lagrangians from above we obtain a master Lagrangian for chiral scalar superfields. The auxiliary fields $\mathcal{F}_i$ can be eliminated with the help of the Euler-Lagrange equations.

For a general supersymmetric Lagrangian for theories with just scalars and spinors one finally gets [18]

$$\begin{aligned}\mathcal{L} =& \mathcal{L}_{\mathcal{D}} + \mathcal{L}_{\mathcal{F}} = \sum_i \left(\partial_\mu S_i\right)^\dagger \left(\partial^\mu S_i\right) + \frac{i}{2}\sum_i \overline{\psi}\ \not{\partial}\psi \\ & - \sum_i \left|\frac{\partial\,\hat{f}}{\partial \hat{S}_i}\right|^2_{\hat{S}=S} - \frac{1}{2}\sum_{i,j}\left(\left.\frac{\partial^2\,\hat{f}}{\partial\hat{S}_i\partial\hat{S}_j}\right|_{\hat{S}=S}\overline{\psi}_i\frac{1-\gamma_5}{2}\psi_j + h.c.\right).\end{aligned} \tag{2.13}$$

The third term in Eq. (2.13) is the scalar potential that is quartic if $\hat{f}$ is cubic in the fields and the last term contains the masses and Yukawa interactions of fermions.

The model dependence enters the Lagrangian via the choice of the superpotential.

Working in superspace, the action becomes an integral over superspace. First, we have to define an integral over Grassmann numbers η: $\int d\eta = 0$ and $\int d\eta\,\eta = 1$.

Using an explicit representation for $\gamma_5 = \mathrm{diag}(-1,-1,1,1)$ one obtains that $(\overline{\theta}\gamma_5\theta)^2 = 8\theta_4\theta_3\theta_2\theta_1$. We then define $d^4\theta \equiv d\theta_1 d\theta_2 d\theta_3 d\theta_4$. For the $\mathcal{D}$-term part, i.e., the coefficient of $-\frac{1}{2}(\overline{\theta}\gamma_5\theta)^2$ of the action we get

$$\int d^4x \mathcal{L}_{\mathcal{D}} = -\frac{1}{4}\int d^4x\, d^4\theta\ K\left(\hat{S}^\dagger, \hat{S}\right).$$

For $\overline{\theta}\theta_L = 2\theta_{L2}\theta_{L1}$ we define $d^2\theta_L \equiv d\theta_{L1}d\theta_{L2}$.
The $\mathcal{F}$-term part of the action is

$$\int d^4x \mathcal{L}_{\mathcal{F}} = -\frac{1}{2}\int d^4x\, d^2\theta_L\ \hat{f}\left(\hat{S}\right) + h.c.$$

2.2.3. A Master Lagrangian for SUSY Gauge Theories

Besides the Kähler and superpotential, two more terms are permitted in a locally gauge-invariant SUSY Lagrangian. These are a gauge kinetic term, which provides for the kinetic terms for the gauge superfields, including the gauge fields and their superpartners, the gauginos. Furthermore, one has a gauge part in which chiral scalar superfields are coupled to gauge superfields. In addition, the $\mathcal{D}$-term of a gauge potential superfield is gauge invariant if the gauge group is abelian. These terms are put into the Lagrangian as well. A master Lagrangian for SUSY gauge theories is given by [18]

$$
\begin{aligned}
\mathcal{L} = & \sum_i \left(\partial_\mu S_i\right)^\dagger \left(\partial^\mu S_i\right) + \frac{i}{2}\sum_i \overline{\psi}_i \not{D} \psi_i + \sum_{\alpha,A}\left[\frac{i}{2}\overline{\lambda}_{\alpha A}\left(\not{D}\lambda_{\alpha A}\right) - \frac{1}{4}F_{\mu\nu\,\alpha A}F^{\mu\nu}_{\alpha A}\right] \\
& - \sqrt{2}\sum_{i,\alpha,A}\left(S_i^\dagger g_\alpha t_{\alpha A}\overline{\lambda}_{\alpha A}\frac{1-\gamma_5}{2}\psi_i + h.c.\right) \\
& - \frac{1}{2}\sum_{\alpha,A}\left[\sum_i S_i^\dagger g_\alpha t_{\alpha A} S_i + \xi_{\alpha A}\right]^2 - \sum_i \left|\frac{\partial\,\hat{f}}{\partial \hat{S}_i}\right|_{\hat{S}=S} \\
& - \frac{1}{2}\sum_{i,j}\overline{\psi}_i\left[\left(\frac{\partial^2\,\hat{f}}{\partial\hat{S}_i\partial\hat{S}_j}\right)\Big|_{\hat{S}=S}\frac{1-\gamma_5}{2} + \left(\frac{\partial^2\,\hat{f}}{\partial\hat{S}_i\partial\hat{S}_j}\right)^\dagger\Big|_{\hat{S}=S}\frac{1+\gamma_5}{2}\right]\psi_j.
\end{aligned}
\tag{2.14}
$$

The covariant derivatives are defined as

$$
\begin{aligned}
D_\mu S &= \partial_\mu S + i\sum_{\alpha,A} g_\alpha t_{\alpha A} V_{\mu\alpha A} S, \\
D_\mu \psi &= \partial_\mu \psi + i\sum_{\alpha,A} g_\alpha \left(t_{\alpha A} V_{\mu\alpha A}\right)\psi_L - i\sum_{\alpha,A} g_\alpha \left(t^*_{\alpha A} V_{\mu\alpha A}\right)\psi_R, \\
\left(\not{D}\lambda\right)_{\alpha A} &= \not{\partial}\lambda_{\alpha A} + i g_\alpha \left(t^{\mathrm{adj}}_{\alpha B}\not{V}_{\alpha B}\right)_{AC}\lambda_{\alpha C}, \\
F_{\mu\nu\alpha A} &= \partial_\mu V_{\nu\alpha A} - \partial_\nu V_{\mu\alpha A} - g_\alpha f_{\alpha ABC} V_{\mu\alpha B} V_{\nu\alpha C}.
\end{aligned}
$$

i, j denote matter field types and A is the gauge group index. The index α is there to allow for several gauge couplings. ξ are coupling constants with $[\xi] = 2$. t_A are the matrix representations of the generators of the gauge group and satisfy the Lie algebra $[t_A, t_B] = i f_{ABC} t_C$, with the structure functions f_{ABC}. The occurrence of t^* has the origin in that if ψ_L transforms according to a representation given by t_A, then ψ_R transforms according to the conjugate representation given by $(-t^*_A)$. (t^{adj}_A) denote the generators in the adjoint representation.

Let us comment on the different parts of this Lagrangian [18].

* The first line displays the usual gauge-invariant kinetic energies for the components of the chiral and gauge superfields. The covariant derivatives are each in the appropriate representation in which the fields belong. For quarks the covariant derivative contains triplet $SU(3)_C$ matrices. The couplings of all particles to gauge bosons is completely determined by those terms.

* The second line represents the interactions of gauginos with the scalar and fermion components of chiral superfields. Thus, it describes how gauginos couple matter fermions to their superpartners and Higgs bosons to their superpartners. Those interactions are completely determined by the gauge couplings.

* In the third line the scalar potential is given. The first part is determined only by gauge interactions. As it originates from the auxiliary $\mathcal{D}$-field, it is referred to as the $\mathcal{D}$-term contribution to the scalar potential. The second term is from the superpotential $\hat{f}$. It is referred to as the $\mathcal{F}$-term contribution to the scalar potential.

* In the last line, superpotential interactions of matter and Higgs fields and fermion mass terms are given. This means that all the Yukawa couplings are contained in the superpotential.

2.2.4. SUSY Breaking

As is known from experiments, SUSY cannot be an exact symmetry in nature due to the lack of observation of supersymmetric particles. Thus, supersymmetry has to be broken by assuming that the masses of bosons and fermions in a multiplet differ from each other, i.e., $m_F \neq m_B$.

The mechanism of how SUSY is broken in nature is not yet understood.

What is common to all SUSY breaking mechanisms is that they occur in a sector of the theory that differs from that containing Standard Model particles and their superpartners. This is because SUSY models where the SUSY breaking occurs in the Standard Model sector of the theory lead to phenomenological problems (e.g. light scalars) [18].

This raises the question of how to convey the information of SUSY breaking to the observable sector of the Standard Model particles and their superpartners. One possible scenario of SUSY breaking is gravity-mediated SUSY breaking since gravity couples universally to energy. There, the SUSY breaking is dispatched to the low-energy SUSY model via gravitational interactions.

As the dynamics of SUSY breaking is unknown, it is most common to parameterize SUSY breaking effects by adding terms to the Lagrangian that are consistent with the desired unbroken symmetries at the SUSY breaking scale, that only have couplings with positive mass dimension and do not introduce new quadratic divergences. Terms fulfilling these requirements are called *soft* SUSY breaking terms.

Chapter 3
3 The Minimal Supersymmetric Standard Model (MSSM)

Initially, the investigation of SUSY was driven by aesthetic reasons to find larger symmetry groups not yet explored in theory. Later on, it was found that a phenomenological SUSY model is very attractive due to the fact that it offers possible solutions to some problems that cannot be answered in the Standard Model. In this chapter, we introduce a very popular phenomenological supersymmetric model, the minimal supersymmetrization of the Standard Model (MSSM).

First, some motivations for studying phenomenological SUSY models are highlighted. Afterwards, we introduce the MSSM with an emphasis on the Higgs sector and the mechanism of spontaneous symmetry breaking within this model. We describe how to obtain the physical lightest and pseudoscalar MSSM Higgs boson with respect to the fact that we will later on study their decay into two photons and their production in the gluon fusion process. Finally, we comment on the supersymmetric partners of the quarks of the third family whose effects we include into our calculations.

3.1. Motivations for Investigating Phenomenological SUSY Models

The Standard Model describes physics up to an energy range that is sixteen orders of magnitude below the natural mass scale, i.e., the Planck scale $M_P = (8\pi G_{Newton})^{-1/2} \approx 1.2 \times 10^{19}$ GeV [25]. Physicists agree on the fact that there should be new physics at the Planck scale since gravity becomes very strong at that scale. The actuality that the natural scale is gigantic compared to the electroweak symmetry breaking scale of about $v \sim 250$ GeV is called the hierarchy problem. It describes a sensitivity of the Higgs potential towards new physics. By calculating radiative corrections to the Higgs boson mass squared, one obtains quadratic divergences in the cut-off scale Λ up to which the Standard Model is assumed to

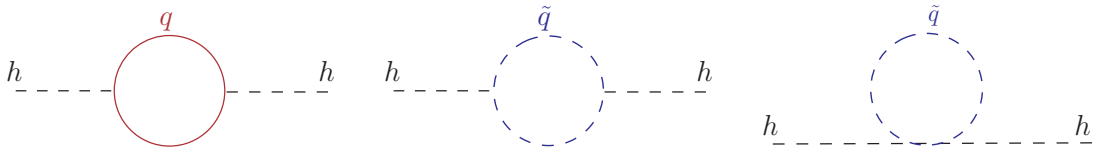

Figure 3.1.: *Lowest order diagrams contributing to quadratic divergences in the propagator of the Higgs boson h.*

be valid. These originate from loop insertions of fermions, gauge bosons and Higgs bosons into the Higgs propagator. The quadratic divergences occurring due to quark contributions are displayed on the left of Fig. 3.1. Choosing Λ of the order of the Planck scale requires a considerable amount of fine-tuning to obtain a Higgs mass of the order of the electroweak symmetry breaking scale favored by electroweak precision measurements. SUSY prevents the Higgs mass from obtaining very large radiative corrections due to a cancellation of the fermion contributions with the contributions from their scalar superpartners, which come into play with opposite signs [15]. Those contributions are displayed in Fig. 3.1 for quarks q and their scalar superpartners, the squarks $\tilde{q}$. This cancellation stabilizes the hierarchy between the Planck and electroweak scale without much fine-tuning, if it is assumed that the masses of the squarks are in the TeV-range.

SUSY may also solve the cosmological constant problem. In quantum field theory the cosmological constant $\Lambda_c \sim M_P^4$ but experimentally $\Lambda_c \sim (10^{-12}\ \text{GeV})^4$ [26]. If SUSY were an exact symmetry $\Lambda_c \equiv 0$ and in softly broken SUSY theories it can be assumed to be in the ball-park of the experimental limit [26].

The studies of the fluctuations in the spectrum of the relic microwave background from the Big Bang have established the existence of non-baryonic matter called dark matter. Galaxies are surrounded by a halo of dark matter. The flat rotation curves of spiral galaxies provide direct evidence for a large amount of dark matter. Only about 4 % of the energy content of the universe is of baryonic origin. Dark matter provides for about 23 % of the remaining energy content. A particle that is absolutely stable, fairly massive, electrically neutral and only weakly interacting could make up for this 23 %. The Standard Model does not provide for such a candidate of dark matter. SUSY models provide for a candidate for dark matter if a new symmetry called R-parity is imposed. R-parity is a symmetry under which the usual fields (fermions, Higgs and gauge bosons) are even while their superpartners (sfermions, higgsinos and gauginos) are odd. Imposing R-parity, all interactions involve an even number of supersymmetric particles and these can only be produced in pairs. Therefore, any sparticle decay must lead to an odd number of sparticles and the lightest supersymmetric particle (LSP) is stable. The LSP is a candidate for dark matter [18].

At the GUT (Grand Unified Theory) scale $\sim 10^{16}$ GeV, the theory describes the electromagnetic, weak and strong force within a single gauge group as, e.g. $SU(5)$ or $SO(10)$

and the different couplings become indistinguishable. In the Standard Model the renormalization group evolution of the three gauge couplings of $SU(3)_C \otimes SU(2)_L \otimes U(1)_Y$ fail to meet at a common point. Due to the introduction of SUSY particles into the spectrum the slopes of the three gauge couplings are altered in the renormalization group evolution. They tend to meet at an energy of around 10^{16} GeV and thus SUSY may cause gauge coupling unification [27].

Furthermore, SUSY theories have a strong connection to superstring theories that are considered to be candidates for theories that include a finite quantum theory of gravity.

Although SUSY has not been discovered in experiments so far, the data gathered at LEP is not inconsistent with SUSY since the radiative corrections to electroweak observables rapidly decouple with the SUSY masses [18]. This means that the heavier the SUSY masses are the less visible their effects in the observables.

All in all, there are strong arguments in favor of investigating phenomenological SUSY theories more closely.

3.2. The MSSM

The Minimal Supersymmetric Standard Model (MSSM) is a direct supersymmetrization of the Standard Model (SM) with two Higgs doublets. It is minimal in the sense that it introduces the smallest number of new particle states and new interactions consistent with phenomenology. For constructing the MSSM one proceeds as follows [18]:

- First, the gauge group is chosen to be $SU(3)_C \otimes SU(2)_L \otimes U(1)_Y$. The generator of the $SU(3)_C$ is the color, the generator of $SU(2)_L$ is the weak isospin I and the generator of the $U(1)_Y$ is the hypercharge Y. The gauge bosons of the SM are then promoted to gauge superfields. Descriptively, this means that, in addition to gauge boson fields, spin-1/2 gaugino fields are introduced. The nomenclature is such that the fermionic partners of the gauge boson fields get the name of the gauge boson with a suffix "ino". This means that the superpartners of the photon, Z, $W^{\pm}$ and the gluons are the photino $\tilde{\gamma}$, Z-ino, $W^{\pm}$-ino and the gluino $\tilde{g}$.

- The matter content is realized as left-chiral scalar superfields with the same gauge quantum numbers as in the SM. Quarks and leptons get spin-0 partners, called squarks and sleptons or collectively sfermions. Each SM fermionic d.o.f. obtains a superpartner. Therefore, squarks and sleptons obtain two partners corresponding to their chirality. They are denoted "left" and "right" $\tilde{f}_L$ and $\tilde{f}_R$. In contrast to spinors, sfermions are scalar particles. That is why the indices L and R are just labels.

- In the Higgs sector, two left-chiral scalar superfields $\hat{H}_u$ and $\hat{H}_d$ with opposite hypercharge are chosen. Both are needed in order to give masses to up- and down-type

fermions and to avoid anomalies [28]. The two doublets possess eight degrees of freedom. After the spontaneous symmetry breaking three of them become the longitudinal modes of the two W-bosons and the Z-boson which are thus massive. Five physical degrees of freedom remain which correspond to five Higgs particles. One obtains two neutral, CP-even (h, H), a neutral, CP-odd (A) and two charged Higgs bosons ($H^{\pm}$). Accompanying with the Higgs fields are their spin-1/2 superpartners, the higgsinos.

- In the next step the superpotential $\hat{f}$ is chosen that fixes the masses and couplings of the matter fields.
- Then one computes the SUSY Lagrangian with the help of Eq. (2.14).
- All possible *soft* SUSY breaking terms consistent with gauge and Poincaré invariance are added. As already emphasized before, softly broken SUSY theories have the virtue that they do not suffer from quadratic divergences.

The masses of the superpartners set the scale for radiative corrections to the Higgs mass and hence the weak scale. That is why we consider weak scale supersymmetry. Therefore, it is required that the SUSY breaking parameters and μ_{susy} are in the range of the weak scale $\mathcal{O}(100\ \text{GeV})$, or at least not larger than a TeV [18].

3.2.1. Higgs Superfields

Analogously to the Standard Model we want to break the $SU(3)_C \otimes SU(2)_L \otimes U(1)_Y$ gauge symmetry to an $SU(3)_C \otimes U(1)_{em}$. Through this breaking the $W^{\pm}$ and Z-bosons and the fermions acquire masses as in the Standard Model. The Higgs doublet ϕ of the SM is promoted to a doublet of left-chiral superfields

$$\phi = \begin{pmatrix} \phi^+ \\ \phi^0 \end{pmatrix} \quad \rightarrow \hat{H}_u = \begin{pmatrix} \hat{H}_u^+ \\ \hat{H}_u^0 \end{pmatrix}.$$

This transforms as a doublet **2** under $SU(2)_L$ and has hypercharge $Y = 1$. The Yukawa interactions of its scalar component with matter fermions must arise via the superpotential [18]. The vacuum expectation value (vev) of the scalar component of $\hat{H}_u^0$ gives masses to up-type quarks.

It cannot give a mass to $I_3 = -1/2$ down-type fermions. This is because a $Y = -1$ field needed to give mass to these would have to be the scalar component of the right-chiral superfield $\hat{H}_u^{0\dagger}$ but that is not allowed in the superpotential. This is in contrast to the SM where $\phi^c = i\sigma_2\phi^*$ with $Y = -1$ can lead to masses for down type fermions.

Thus, an additional Higgs doublet has to be introduced

$$\hat{H}_d = \begin{pmatrix} \hat{H}_d^0 \\ \hat{H}_d^- \end{pmatrix}.$$

which is a doublet **2** under $SU(2)_L$ that possesses hypercharge $Y = -1$. The masses of the fermions of the up-type are obtained with $\hat{H}_u$, the ones of the down type with the help of $\hat{H}_d$. The entries $\hat{H}_u^0$, $\hat{H}_d^0$ are electrically neutral and $\hat{H}_u^+$ and $\hat{H}_u^-$ carry the electrical charge one. The superpotential for the interaction of Higgs bosons with fermions is given by [18]

$$\hat{f} = \sum_{i,j=1}^{3} \left[(\mathbf{f}_e)_{ij}\, \epsilon_{ab} \hat{L}_i^a \hat{H}_d^b \hat{E}_j^c + (\mathbf{f}_d)_{ij}\, \epsilon_{ab} \hat{Q}_i^a \hat{H}_d^b \hat{D}_j^c + (\mathbf{f}_u)_{ij}\, \epsilon_{ab} \hat{Q}_i^a \hat{H}_u^b \hat{U}_j^c \right] + \mu_{susy} \epsilon_{ab} \hat{H}_u^a \hat{H}_d^b. \quad (3.1)$$

The superfields occurring in Eq. (3.1) and their corresponding SM fields are given in Tab. 3.1. The generation indices of the quarks and leptons are denoted by i, j. The 3×3-matrices $\mathbf{f}_d$, $\mathbf{f}_u$ and $\mathbf{f}_e$ contain dimensionless Yukawa couplings as entries, which occur in the quark and lepton mass terms. The occurrence of the ϵ-tensor reflects the fact that it is the antisymmetric combination of two doublets that is a SU(2) singlet. The hypercharge of each term in the superpotential sums up to zero, which means that the superpotential is invariant under $U(1)_Y$. The Lagrangian derived from this superpotential is given by [18]

$$\mathcal{L} = -\sum_i \left| \frac{\partial \hat{f}}{\partial \hat{S}_i} \right|^2_{\hat{S}=S} - \frac{1}{2} \sum_{i,j} \overline{\psi}_i \left[\left(\frac{\partial^2 \hat{f}}{\partial \hat{S}_i \partial \hat{S}_j} \right) \Big|_{\hat{S}=S} \frac{1-\gamma_5}{2} + \left(\frac{\partial^2 \hat{f}}{\partial \hat{S}_i \partial \hat{S}_j} \right)^\dagger \Big|_{\hat{S}=S} \frac{1+\gamma_5}{2} \right] \psi_j. \quad (3.2)$$

The sum over i runs over all scalar fields in the model. With the first term in Eq. (3.2) mass terms and interactions of the scalar fields are described. The second term describes masses and Yukawa interactions of the fermion fields. The *soft* SUSY breaking terms allowed in the gauge-invariant Lagrangian of the MSSM are added by hand [18]

$$\begin{aligned}
\mathcal{L}_{soft} = & -[\tilde{Q}_i^\dagger \mathbf{m}^2_{\mathbf{Q}_{ij}} \tilde{Q}_j + \tilde{d}_{Ri}^\dagger \mathbf{m}^2_{\mathbf{D}_{ij}} \tilde{d}_{Rj} + \tilde{u}_{Ri}^\dagger \mathbf{m}^2_{\mathbf{U}_{ij}} \tilde{u}_{Rj} \\
& + \tilde{L}_i^\dagger \mathbf{m}^2_{\mathbf{L}_{ij}} \tilde{L}_j + \tilde{e}_{Ri}^\dagger \mathbf{m}^2_{\mathbf{E}_{ij}} \tilde{e}_{Rj} + m^2_{H_u} |H_u|^2 + m^2_{H_d} |H_d|^2] \\
& - \frac{1}{2} \left[M_1 \overline{\lambda}_0 \lambda_0 + M_2 \overline{\lambda}_A \lambda_A + M_3 \overline{\tilde{g}}_B \tilde{g}_B \right] \\
& - \frac{i}{2} \left[M_1' \overline{\lambda}_0 \gamma_5 \lambda_0 + M_2' \overline{\lambda}_A \gamma_5 \lambda_A + M_3' \overline{\tilde{g}}_B \gamma_5 \tilde{g}_B \right] \\
& + \left[(\mathbf{a_u})_{ij}\, \epsilon_{ab} \tilde{Q}_i^a H_u^b \tilde{u}_{Rj}^\dagger + (\mathbf{a_d})_{ij}\, \epsilon_{ab} \tilde{Q}_i^a H_u^b \tilde{d}_{Rj}^\dagger + (\mathbf{a_e})_{ij}\, \epsilon_{ab} \tilde{L}_i^a H_u^b \tilde{e}_{Rj}^\dagger + h.c. \right] \\
& + \left[(\mathbf{c_u})_{ij}\, \epsilon_{ab} \tilde{Q}_i^a H_d^{*b} \tilde{u}_{Rj}^\dagger + (\mathbf{c_d})_{ij}\, \epsilon_{ab} \tilde{Q}_i^a H_u^{*b} \tilde{d}_{Rj}^\dagger + (\mathbf{c_e})_{ij}\, \epsilon_{ab} \tilde{L}_i^a H_u^{*b} \tilde{e}_{Rj}^\dagger + h.c. \right] \\
& + \left[B \mu_{susy} \epsilon_{ab} H_u^a H_d^b + h.c. \right].
\end{aligned} \quad (3.3)$$

It is understood that it is summed over the generation indices i, j, and over the $SU(2)$ indices a, b . The scalar mass matrices $\mathbf{m}$ in Eq. (3.3) are 3×3 Hermitian matrices with six real and three complex parameters each. The third row of Eq. (3.3) are the gaugino

Superfield	fermion field, spin	boson field, spin	$SU(3)_C$	$SU(2)_L$	$U(1)_Y$
$\hat{\Phi}_{U(1)_Y}$	λ_0, 1/2	B_μ, 1	**1**	**1**	0
$\hat{\Phi}^i_{SU(2)_L}$	λ^i, 1/2	W^i_μ, 1	**1**	**3**	0
$\hat{\Phi}^a_{SU(3)_C}$	$\tilde{g}^a$, 1/2	G^a_μ, 1	**8**	**1**	0
$\hat{Q}$	(u_L, d_L), 1/2	$\left(\tilde{u}_L, \tilde{d}_L\right)$, 0	**3**	**2**	$\frac{1}{3}$
$\hat{U}^c$	$\overline{u}_R$, 1/2	$\tilde{u}^*_R$, 0	$\mathbf{3}^*$	**1**	$-\frac{4}{3}$
$\hat{D}^c$	$\overline{d}_R$, 1/2	$\tilde{d}^*_R$, 0	$\mathbf{3}^*$	**1**	$\frac{2}{3}$
$\hat{L}$	(ν_L, e_L), 1/2	$(\tilde{\nu}_L, \tilde{e}_L)$, 0	**1**	**2**	-1
$\hat{E}^c$	$\overline{e}_R$, 1/2	$\tilde{e}^*_R$, 0	**1**	**1**	2
$\hat{H}_u$	$\left(\tilde{H}^+_u, \tilde{H}^0_u\right)$, 1/2	(H^+_u, H^0_u), 0	**1**	**2**	1
$\hat{H}_d$	$\left(\tilde{H}^0_d, \tilde{H}^-_d\right)$, 1/2	$\left(H^0_d, H^-_d\right)$, 0	**1**	**2**	-1

Table 3.1.: *The superfields and particle content of the MSSM. The group representation of the non-Abelian groups $SU(3)_C$ and $SU(2)_L$ is given in bold numbers that denote the dimension of the representation. For the Abelian group $U(1)_Y$ the hypercharges are shown.*

mass terms, whereas in the fourth row the CP-odd gaugino mass terms are given. The latter violate CP invariance. The six gaugino mass parameters (M_i, M'_i) are real. The label $i = 1, 2, 3$ corresponds to the 3 factors of the MSSM gauge group. The **a** and **c** matrices are general 3×3 complex matrices. Those parts describe trilinear scalar interactions. The terms proportional to **c** are frequently omitted because they are strongly suppressed in many models [18], but they are allowed by the theory. $m^2_{H_u}$ and $m^2_{H_d}$ are real and $B\mu_{susy}$ is in general taken to be complex.

3.3. Electroweak Symmetry Breaking in the MSSM

In order to investigate the symmetry breaking in the MSSM, the minima of the scalar potential have to be examined. Here we only investigate the parameter regions where the scalar potential develops a minimum with respect to the Higgs scalars.

Three different sources contribute to the scalar Higgs potential at tree-level: $V_{\text{Higgs}} = V_{\mathcal{D}} + V_{\mathcal{F}} + V_{\text{soft}}$ [18]. First, the $\mathcal{D}$-terms which contain the quartic Higgs interactions are given by [18]

$$V_{\mathcal{D}} = \frac{1}{2} \sum_A \left[\sum_i S^\dagger_i g t_A S_i \right]^2 ,$$

where i is the sum over the scalar Higgs fields. In component fields they are [29]

$$U(1)_Y : V_{\mathcal{D}}^1 = \frac{1}{2}\left[\frac{g_1}{2}\left(|H_u|^2 - |H_d|^2\right)\right]^2$$
$$SU(2)_L : V_{\mathcal{D}}^2 = \frac{1}{2}\left[\frac{g_2}{2}\left(H_d^{i*}\tau_{ij}^a H_u^j + H_u^{i*}\tau_{ij}^a H_d^j\right)\right]^2$$

g_1 and g_2 are the coupling constants of the $U(1)_Y$ and $SU(2)_L$ respectively. $\tau^a = \sigma^a/2$ with the Pauli matrices σ^a. Adding those two contributions together, one obtains

$$V_{\mathcal{D}} = \frac{g_1^2}{8}\left[|H_u|^2 - |H_d|^2\right]^2 + \frac{g_2^2}{8}\left[4\left|H_d^\dagger H_u\right|^2 - 2\,|H_d|^2\,|H_u|^2 + \left(|H_d|^2\right)^2 + \left(|H_u|^2\right)^2\right].$$

From the $\mathcal{F}$-term of the superpotential one obtains [29]

$$V_{\mathcal{F}} = \sum_i \left|\frac{\partial \hat{f}}{\partial \hat{S}_i}\right|^2_{\hat{S}=S} = |\mu_{susy}|^2\left(|H_u|^2 + |H_d|^2\right).$$

The third part comes from the *soft* SUSY breaking scalar Higgs mass terms and the bilinear terms [18]

$$V_{soft} = m_{H_d}^2 H_d^\dagger H_d + m_{H_u}^2 H_u^\dagger H_u + B\mu_{susy}\left(\epsilon_{ab} H_u^a H_d^b + h.c.\right).$$

The scalar potential for the Higgs fields is then the sum of the three terms from above

$$\begin{aligned} V_{Higgs} = {} & \left(|\mu_{susy}|^2 + m_{H_u}^2\right)|H_u|^2 + \left(|\mu_{susy}|^2 + m_{H_d}^2\right)|H_d|^2 \\ & + \left(B\mu_{susy}\left(H_u^+ H_d^- - H_u^0 H_d^0\right) + h.c.\right) \\ & + \frac{1}{8}\left(g_1^2 + g_2^2\right)\left(|H_u|^2 - |H_d|^2\right)^2 + \frac{1}{2}g_2^2\left|H_u^+ H_d^{0*} + H_d^0 H_u^{-*}\right|^2. \end{aligned} \tag{3.4}$$

Now there is the requirement that the minimum of the potential breaks the electroweak to an electromagnetic symmetry, $SU(2)_L \otimes U(1)_Y \to U_{em}(1)$. The $SU(2)_L$-gauge symmetry freedom allows to rotate the vev of H_u to its lower component which was defined to be neutral. At the minimum of the potential one can always choose $\langle H_d^- \rangle = 0$ because of $SU(2)$ symmetry. By taking $\partial V/\partial H_d^- = 0$ one automatically obtains $\langle H_u^+ \rangle = 0$.

This means that in the minimum of the potential the electromagnetism is unbroken since the charged components of the Higgs doublets do not acquire vevs. Therefore, there is no breaking of the symmetry in the charged directions and it is secured that the electric charge is conserved in the Higgs sector. As the charged parts in the Higgs potential are set to zero during the minimization process, only the scalar potential for the "neutral fields" has to be minimized. It reads

$$\boxed{\begin{aligned} V_{neutral} = {} & \left(|\mu_{susy}|^2 + m_{H_u}^2\right)\left|H_u^0\right|^2 + \left(|\mu_{susy}|^2 + m_{H_d}^2\right)\left|H_d^0\right|^2 \\ & - \left(B\mu_{susy} H_u^0 H_d^0 + h.c.\right) + \frac{1}{8}\left(g_1^2 + g_2^2\right)\left(\left|H_u^0\right|^2 - \left|H_d^0\right|^2\right)^2. \end{aligned}} \tag{3.5}$$

Some comments can be made on the Higgs potential [29].

The quartic Higgs couplings are completely fixed by the $SU(2)_L \otimes U(1)_Y$ couplings. One has the freedom to choose $B\mu_{susy}$, which is the only part depending on complex phases to be real. This can be done by redefining the phases of H_u and H_d. It follows that CP is not broken spontaneously by the scalar Higgs potential as all vevs and couplings can be chosen to be real at the same time. The Higgs mass eigenstates are CP eigenstates as well [15]. The scalar potential is thus CP conserving at tree-level. In order to have electroweak symmetry breaking and not obtain $\langle H_u^0 \rangle = 0$ and $\langle H_d^0 \rangle = 0$, we must have a local maximum of the scalar potential. We are therefore interested in evaluating the second derivatives with respect to the fields. Then just the bilinear terms contribute.

The condition obtained for electroweak symmetry breaking to take place is then

$$(B\mu_{susy})^2 > \left(|\mu_{susy}|^2 + m_{H_u}^2\right)\left(|\mu_{susy}|^2 + m_{H_d}^2\right).$$

In the direction where $|H_u^0| = |H_d^0|$, the quartic term vanishes. $V_{neutral}$ is then bounded from below only when it is positive. The additional requirement for symmetry breaking thus is

$$m_{H_u}^2 + m_{H_d}^2 + 2|\mu_{susy}|^2 > 2\,|B\mu_{susy}|\,.$$

The previous two conditions only hold if $\left(|\mu_{susy}|^2 + m_{H_u}^2\right) \neq \left(|\mu_{susy}|^2 + m_{H_d}^2\right)$.

Therefore, the requirement is that the *soft* SUSY breaking masses are unequal, i.e.,

$$m_{H_u}^2 \neq m_{H_d}^2.$$

This implies that in order to break the electroweak symmetry one needs to break SUSY as well. We observe that there is a connection between gauge-symmetry breaking and SUSY breaking.

For a minimum of the potential in Eq. (3.5) one demands that the product $H_u^0 H_d^0$ is real and positive such that $\langle H_u^0 \rangle$ and $\langle H_d^0 \rangle$ carry opposite phases. With the help of an $U(1)_Y$-transformation both vevs of the neutral Higgs fields can be chosen to be real. In that is no loss of generality as H_u and H_d carry opposite hypercharges (± 1). Commonly the vevs are denoted by

$$\left\langle H_u^0 \right\rangle = v_u \quad \text{and} \quad \left\langle H_d^0 \right\rangle = v_d.$$

The vevs of the two Higgs fields v_u and v_d can be expressed by v [29]:

$$v^2 = v_u^2 + v_d^2 = \frac{4M_Z^2}{g_2^2 + g_1^2} \approx (246\ \text{GeV})^2. \tag{3.6}$$

where $M_Z \approx 91.1876$ GeV is the mass of the Z-boson. Through convention the ratio of the two vevs is chosen to be a free parameter of the theory

$$\boxed{\tan\beta \equiv \frac{v_u}{v_d}.} \tag{3.7}$$

Since v_u and v_d were chosen to be real and positive we have $0 < \beta < \pi/2$. Minimizing the scalar potential with respect to H_u^0 and H_d^0, one is able by using Eqs (3.6) and (3.7) to replace $B\mu_{susy}$ and $|\mu_{susy}|$ with the help of $\tan\beta$ [29]:

$$B\mu_{susy} = \frac{\left(m_{H_d}^2 - m_{H_u}^2\right)\tan 2\beta + M_Z^2 \sin 2\beta}{2},$$
$$|\mu_{susy}|^2 = \frac{m_{H_u}^2 \sin^2\beta - m_{H_d}^2 \cos^2\beta}{\cos 2\beta} - \frac{M_Z^2}{2}.$$

Given the *soft* breaking Higgs masses, the second equation can be used to fix the magnitude of μ_{susy} to reproduce the experimental Z mass. Nevertheless, those do not fix the phase of μ_{susy}.

3.3.1. The Physical Neutral MSSM Higgs Bosons

For determining the physical Higgs fields and their masses one first splits the neutral fields into real and imaginary parts [18]

$$H_d = \begin{pmatrix} H_d^0 \\ H_d^- \end{pmatrix} = \begin{pmatrix} \frac{H_{d,R}^0 + iH_{d,I}^0}{\sqrt{2}} \\ H_d^- \end{pmatrix}, \qquad H_u = \begin{pmatrix} H_u^+ \\ H_u^0 \end{pmatrix} = \begin{pmatrix} H_u^+ \\ \frac{H_{u,R}^0 + iH_{u,I}^0}{\sqrt{2}} \end{pmatrix}.$$

Then the only non-vanishing vevs are $\left\langle H_{u,R}^0 \right\rangle = \sqrt{2}v_u$ and $\left\langle H_{d,R}^0 \right\rangle = \sqrt{2}v_d$. All the other vevs are set to zero. Due to conservation of the electric charge, there is no mixing between the charged and neutral Higgs fields. Therefore, one obtains one matrix for the charged sector and one for the neutral sector. Because CP invariance is assumed in the Higgs sector the real and imaginary components of the neutral Higgs bosons do not mix. Therefore, the 4×4 matrix in the neutral sector decomposes into two 2×2 blocks. The mass terms for the imaginary components of the neutral fields can be written as [18]

$$\mathcal{L} \ni \frac{1}{2}\left(H_{u,I}^0, H_{d,I}^0\right) \mathcal{M}_{H_{i,I}^0}^2 \begin{pmatrix} H_{u,I}^0 \\ H_{d,I}^0 \end{pmatrix}$$

with

$$\mathcal{M}_{H_{i,I}^0}^2 = \begin{pmatrix} \left.\frac{\partial^2 V}{\partial H_{u,I}^{02}}\right|_{h_i \to v_i} & \left.\frac{\partial^2 V}{\partial H_{u,I}^0 \partial H_{d,I}^0}\right|_{h_i \to v_i} \\ \left.\frac{\partial^2 V}{\partial H_{d,I}^0 \partial H_{u,I}^0}\right|_{h_i \to v_i} & \left.\frac{\partial^2 V}{\partial H_{d,I}^{02}}\right|_{h_i \to v_i} \end{pmatrix}. \tag{3.8}$$

Evaluating Eq. (3.8) one obtains

$$\mathcal{M}^2_{H^0_{i,I}} = \begin{pmatrix} B\mu_{susy}\cot\beta & B\mu_{susy} \\ B\mu_{susy} & B\mu_{susy}\tan\beta \end{pmatrix}. \tag{3.9}$$

The eigenvalues of this matrix are the mass of the pseudoscalar Higgs boson A and massless Goldstone boson

$$m_A^2 = \frac{2B\mu_{susy}}{\sin 2\beta} \quad \text{and} \quad m_G^0 = 0.$$

The pseudoscalar Higgs field A, that is obtained from the imaginary parts of the neutral parts in the Higgs doublets is then

$$\begin{pmatrix} G^0 \\ A \end{pmatrix} = \begin{pmatrix} \sin\beta & -\cos\beta \\ \cos\beta & \sin\beta \end{pmatrix} \begin{pmatrix} H^0_{u,I} \\ H^0_{d,I} \end{pmatrix}.$$

In unitary gauge, where only physical fields are present, the Goldstone boson G^0 becomes the longitudinal mode of the Z-boson. The fields of the two neutral Higgs bosons are obtained analogously to the procedure for the imaginary parts by replacing those with the real parts of the Higgs fields $H^0_{u,I} \to H^0_{u,R}$ and $H^0_{d,I} \to H^0_{d,R}$.
The mass matrix one obtains is then given by [18]

$$\mathcal{M}^2_{H^0_{i,R}} = \begin{pmatrix} m_A^2\cos^2\beta + M_Z^2\sin^2\beta & -(m_A^2+M_Z^2)\sin\beta\cos\beta \\ -(m_A^2+M_Z^2)\sin\beta\cos\beta & m_A^2\sin^2\beta + M_Z^2\cos^2\beta \end{pmatrix}. \tag{3.10}$$

At tree level their masses are

$$m^2_{H,h} = \frac{1}{2}\left(m_A^2 + M_Z^2 \pm \sqrt{\left(m_A^2+M_Z^2\right)^2 - 4m_A^2M_Z^2\cos^2 2\beta}\right).$$

h and H characterize the lighter and heavier of the neutral scalar mass eigenstates. Their physical fields are given by

$$\begin{pmatrix} h \\ H \end{pmatrix} = \begin{pmatrix} \cos\alpha & \sin\alpha \\ -\sin\alpha & \cos\alpha \end{pmatrix} \begin{pmatrix} H^0_{d,R} \\ H^0_{u,R} \end{pmatrix}.$$

α is denoted the Higgs mixing angle.

Given that, in this thesis only calculations which include either scalar or pseudoscalar Higgs bosons are performed, a discussion of the charged Higgs bosons is omitted. Usually m_A and $\tan\beta$ are chosen to be the free parameters of the MSSM Higgs sector, as one can express all mass eigenstates of the other Higgs particles through them. For the Higgs mixing angle the following relation holds [18]

$$\tan\alpha = \frac{(m_A^2 - M_Z^2)\cos 2\beta + \sqrt{\left(m_A^2-M_Z^2\right)^2 - 4m_A^2M_Z^2\cos^2 2\beta}}{(m_A^2+M_Z^2)\sin 2\beta}.$$

For the lighter neutral Higgs boson h one obtains the mass limits [18]

$$m_h \leq M_Z \left|\cos 2\alpha\right| \leq m_H. \tag{3.11}$$

Eq. (3.11) implies that $m_h = 0$ for $\tan\beta = 1$. It only holds at tree level. Radiative corrections allow h to be heavier than M_Z. This is very fortunate for otherwise LEP2 would have excluded the MSSM.

There are two essential differences between the neutral CP-even $\mathcal{H} = \{h, H\}$ and the pseudoscalar (CP-odd) Higgs boson A [30]:

1. In contrast to the production of scalar Higgs bosons there is no contribution from squarks in the first order of perturbation theory in the production of pseudoscalar Higgs bosons via the gluon fusion process. The same holds for the Higgs decaying into two photons. The Lagrangian is proportional to $(\mathcal{H} + iA)$. As it is real the following real expression for the coupling terms follow [18]:

   $$\mathcal{H}\tilde{q}_L^\dagger \tilde{q}_L, \quad \mathcal{H}\tilde{q}_R^\dagger \tilde{q}_R \quad \text{and} \quad \mathcal{H}\left(\tilde{q}_R^\dagger \tilde{q}_L + \tilde{q}_L^\dagger \tilde{q}_R\right)$$

   For the coupling of two squark fields to a pseudoscalar Higgs boson A only pure imaginary parts of the form

   $$A\left(\tilde{q}_R^\dagger \tilde{q}_L - \tilde{q}_L^\dagger \tilde{q}_R\right).$$

   exist. Two squarks of the same 'chirality' cannot couple to a pseudoscalar Higgs boson A. But gluons and photons can only couple to squarks of the same 'chirality', which is why a coupling of squarks to A in the gluon fusion and decay into two photons is only possible by including the gluino at two-loop level.

2. For the A boson the Born coupling to electroweak vector boson pairs (AVV) does not exist. The coupling of CP-even scalar Higgs bosons to a pair of massive vector bosons results from $(D_\mu S_i^\dagger)(D^\mu S_i)$, $S_i = H_u, H_d$ in the Lagrangian. In a CP conserving theory, this mechanism does not generate a coupling for the CP-odd A: A is derived from $\mathrm{Im}(S_i)$ but the vev of S_i and all the couplings are chosen to be real in the Higgs mechanism [28]. Therefore, $\langle A \rangle = 0$ which results in a vanishing AVV coupling.

The Yukawa couplings of Higgs bosons to quarks of down and up-type can be read off Tab. 3.2.

3.3.2. Squark-Mixing and Mass Eigenstates

In the SM, flavor eigenstates do not coincide with mass eigenstates of the particles in general. There, the B and W^i mix to become the physical γ, Z and $W^\pm$ fields. This always happens upon spontaneous symmetry breaking, where fields with the same color,

ϕ	g_u^ϕ	g_d^ϕ
h	$\cos\alpha/\sin\beta$	$-\sin\alpha/\cos\beta$
H	$\sin\alpha/\cos\beta$	$\cos\alpha/\cos\beta$
A	$\cot\beta$	$\tan\beta$

Table 3.2.: *The couplings of the neutral Higgs bosons to quarks.*

electric charge and spin may mix. The superfields in the MSSM are affected by this as well. Gauginos and higgsinos are not the physical fields but the mixing of the neutral higgsino and gaugino fields form the neutral fermion mass eigenstates, the so-called neutralinos. The mixing of the charged higgsino fields and the superpartner of the W-fields make up the charged fermion fields, called charginos.

Mixing takes place for the squark fields as well. As we only need the masses and mixing of the squark fields in our calculation, we only consider these in the following. The mixing determines the properties of the squarks and is related to the question of how SUSY is broken [31].

The masses of matter fermions arise only from the superpotential Yukawa interactions. Simply adding fermion mass terms would introduce new quadratic divergences into the theory and is not allowed [18].

Four distinct sources of mass terms for sfermions exist [18]. One part arises from the superpotential and is a mass term equal to the corresponding fermion mass term. These are pure mass ($m_i \tilde{f}_i^\dagger \tilde{f}_i,\ i = R, L$) terms and the ones with intra-generational mixing ($m(\tilde{f}_L^\dagger \tilde{f}_R + \tilde{f}_R^\dagger \tilde{f}_L)$). These mass terms vanish if the corresponding fermion Yukawa couplings are zero. Second, there are *soft* SUSY breaking scalar masses of Eq. (3.3). Those will be present whether or not electroweak symmetry is spontaneously broken. The third contribution arises due to *soft* SUSY breaking trilinear terms of squarks with neutral Higgs bosons. The fourth part originates from $\mathcal{D}$-term contributions from cross terms between squark and Higgs boson fields.

The squark mass eigenstates are obtained if one diagonalizes two 6×6-matrices. One for the squarks of the up-type and one for the ones of the down-type. By neglecting the mixing between the generations, the matrices split into 2×2-matrices, which describe squarks of a special flavor each. Taking into account experimental results of the $K^0 - \overline{K}^0$ and $D^0 - \overline{D}^0$-mixing one can neglect the mixing of the squarks of the first two generations, as their masses are degenerate [31]. They will be considered to be equal. Anyhow, their masses are small compared to the soft SUSY breaking masses [18].

For the third family the mixing cannot be neglected. Stop mixing can occur due to the large top mass and sbottom mixing due to the possibly large value of $\tan\beta$. Therefore, in case of the squarks, one has to consider only the $\tilde{q} = \{\tilde{t}, \tilde{b}\}$. The part of the Lagrangian containing the masses of the squarks of the third family is given by [18]

$$\mathcal{L} \ni -\left(\tilde{q}_L^\dagger, \tilde{q}_R^\dagger\right) \mathcal{M}_{\tilde{q}}^2 \begin{pmatrix} \tilde{q}_L \\ \tilde{q}_R \end{pmatrix}.$$

For the squarks one obtains for the mass matrix [18]

$$\mathcal{M}_{\tilde{q}}^2 = \begin{pmatrix} m_{\tilde{q}_L}^2 + m_t^2 + D(\tilde{q}_L) & m_q \left(-A_q + \mu_{susy} \begin{Bmatrix} \cot\beta \\ \tan\beta \end{Bmatrix}\right) \\ m_q \left(-A_q + \mu_{susy} \begin{Bmatrix} \cot\beta \\ \tan\beta \end{Bmatrix}\right) & m_{\tilde{q}_R}^2 + m_q^2 + D(\tilde{q}_R) \end{pmatrix} \tag{3.12}$$

with

$$D(\tilde{q}_L) = M_Z^2 \cos 2\beta \left(I_{3,q} - Q_q \sin^2\theta_W\right),$$
$$D(\tilde{q}_R) = M_Z^2 \cos 2\beta \left(Q_q \sin^2\theta_W\right).$$

A_q is the soft SUSY breaking trilinear coupling, $I_{3,q}$ is the isospin three component of the quark with $I_{3,t} = 1/2$, $I_{3,b} = -1/2$ and Q_q the charge of the quark with $Q_t = 2/3$ and $Q_b = -1/3$. $\sin\theta_W = \sqrt{1 - M_W^2/M_Z^2}$ with the mass of the Z (W) boson M_Z (M_W). The upper part of {} holds for stops and the lower component for sbottoms.

The eigenvalues of the matrix in Eq. (3.12) are calculated to be [18]

$$m_{\tilde{q}_{1,2}}^2 = \frac{1}{2}\left(m_{\tilde{q}_L}^2 + m_{\tilde{q}_R}^2\right) \begin{Bmatrix} + \\ - \end{Bmatrix} \frac{1}{4} M_Z^2 \cos 2\beta + m_q^2$$
$$\mp \sqrt{\left[\frac{1}{2}\left(m_{\tilde{q}_L}^2 - m_{\tilde{q}_R}^2\right) \begin{Bmatrix} + \\ - \end{Bmatrix} M_Z^2 \cos 2\beta \left(\frac{1}{4} - |Q_q| \sin^2\theta_W\right)\right]^2 + m_t^2 \left(\mu_{susy} \begin{Bmatrix} \cot\beta \\ \tan\beta \end{Bmatrix} - A_t\right)^2}.$$

As a convention $\tilde{q}_1$ is defined to be lighter than the $\tilde{q}_2$ mass eigenstates. The superpartners of the quarks belonging to the chiral eigenstates $\tilde{q}_L$ and $\tilde{q}_R$ are connected with the mass eigenstates $\tilde{q}_1$ and $\tilde{q}_2$ in the following manner

$$\begin{pmatrix} \tilde{q}_1 \\ \tilde{q}_2 \end{pmatrix} = \mathcal{R}^{\tilde{q}} \begin{pmatrix} \tilde{q}_L \\ \tilde{q}_R \end{pmatrix}, \quad \mathcal{R}^{\tilde{q}} = \begin{pmatrix} \cos\theta_{\tilde{q}} & \sin\theta_{\tilde{q}} \\ -\sin\theta_{\tilde{q}} & \cos\theta_{\tilde{q}} \end{pmatrix}.$$

$\theta_{\tilde{q}}$ is the squark mixing angle. For the squark mixing angle $\theta_{\tilde{q}}$ the relations given below hold [18]

$$\tan\theta_{\tilde{q}} = \frac{m_{\tilde{q}_q}^2 + m_q^2 + D(\tilde{q}_L) - m_{\tilde{q}_1}^2}{m_q \left(-A_q + \mu_{susy} \begin{Bmatrix} \cot\beta \\ \tan\beta \end{Bmatrix}\right)}.$$

Furthermore, one has $m_{\tilde{q}_1} \leq m_{\tilde{q}_{L,R}} \leq m_{\tilde{q}_2}$ and $0 \leq \theta_{\tilde{q}} < \pi$.

The couplings of two squarks to the light neutral Higgs boson h and to the pseudoscalar Higgs boson A, i.e., $\tilde{q}\tilde{q}h$ and $\tilde{q}\tilde{q}A$ are given in App. A. They arise due to quartic interactions of Higgs bosons and squark fields when one of the Higgs fields acquires a vacuum expectation value. In addition, *soft* SUSY breaking scalar trilinear couplings (A-terms) are sources of these interactions as well.

Gluino mass

The gluino is a color octet fermion. Since $SU(3)_C$ is not broken, the gluino cannot mix with any other fermion and must be a mass eigenstate. Its mass term arises from the *soft* SUSY breaking gaugino mass term already given in Eq. (3.3)

$$\mathcal{L} \ni -\frac{1}{2} M_3 \bar{\tilde{g}} \tilde{g}.$$

Its tree level mass is $m_{\tilde{g}} = |M_3|$. The gluino is taken to be a Majorana fermion.

Chapter 4
4 Regularization and Renormalization

At tree-level approximation the parameters in the Lagrangian that are called bare parameters are directly related to observables like masses and couplings measured in experiments. These days, the precision of the experiments requires us to go beyond the tree-level approximation and take into account higher order corrections.

Such higher order corrections that are quantum effects result from loop insertions into Feynman diagrams. Due to loop corrections the bare parameters in the Lagrangian become divergent and the relations between the bare parameters and the observables change. The divergences of the loop integrals can be parameterized by so-called regulators. To treat the divergences properly requires a regularization scheme that respects Lorentz and gauge invariance. In the end, the result should be independent of the regulator to recover the original theory. This is accomplished by a redefinition of the parameters of the Lagrangian called renormalization. Altogether, the regularization and its physical interpretation constitute the renormalization of the theory.

First, the need for regularization with respect to loop calculations is motivated. Subsequently, two regularization schemes, dimensional regularization (DREG) and dimensional reduction (DRED) are presented. The latter is particularly well suited for calculations performed in a SUSY framework. The application of DRED and DREG in the calculations under consideration in this work is emphasized. At the end of this chapter we comment on the running of the strong coupling and the bottom mass through the introduction of the renormalization scale.

4.1. Implications for Loop Calculations

In order to present the essential features that show the need for regularization in dealing with loop calculations (see for e.g. [32,33]), we consider the simplest one-loop integral that

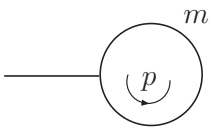

Figure 4.1.: *Massive (mass m) one-loop tadpole diagram with loop momentum p.*

is the scalar tadpole diagram from Fig. 4.1. Its assigned integral is given by

$$A(m) = \frac{1}{i\pi^2} \int \frac{d^4p}{(2\pi)^4} \frac{1}{(p^2 - m^2 + i\epsilon)} \sim \int \frac{d^4p}{p^2} \sim \int dp\, p. \tag{4.1}$$

As demonstrated above, according to power counting, this integral is quadratically divergent in four dimensions. For large p it is ultra-violet (UV) divergent and therefore has to be regularized. The factor $(i\pi^2)^{-1}$ is there by definition.

By applying dimensional regularization or reduction, the calculations are performed in d instead of four dimensions. The loop integrals then converge for small enough d and the usual calculational rules such as linearity, translational and rotational invariance can be used. The analytic structure of these integrals allows for an analytic continuation to arbitrary complex values of d. The ultra-violet divergences manifest themselves as poles at integer values of d as can be observed below. By changing the dimension of the integral, the dimension of $A(m)$ is changed as well. This is compensated with an additional factor and thereby the integration volume is replaced in the following way

$$\int \frac{d^4p}{(2\pi)^4} \to \mu^{4-d} \int \frac{d^dp}{(2\pi)^d},$$

where μ is a reference mass. Using dimensional regularization or reduction implies that integrals that do not depend on any scale other than the loop momentum vanish

$$\int d^4p\, \left(p^2\right)^\alpha = 0, \qquad \text{for all } \alpha. \tag{4.2}$$

The integrand given in Eq. (4.1) would be divergent for $p^2 = m^2$, if the $+i\epsilon$ part were absent. This $i\epsilon$ part is important to keep track of how to perform the integration contour in the complex plane. We especially have to keep in mind that we have those $+i\epsilon$ summands to define how functions are continued analytically. They are important in case our results for instance contain logarithms with negative arguments that develop an imaginary part. For instance

$$\ln(a \pm i\epsilon) = \ln(-a) \pm i\pi, \quad a < 0.$$

For later application we are interested in the evaluation of integrals of type $A(m)$ with arbitrary powers of denominators and define

$$A(m; n_1) = \frac{\mu^{4-d}}{i\pi^2} \int \frac{d^dp}{(2\pi)^{d-4}} \frac{1}{(p^2 - m^2 + i\epsilon)^{n_1}},\ n_1 \geq 1. \tag{4.3}$$

The aim is to perform the integration over the loop momentum of an integral of the form

$$I_n(R) = \int d^d p \frac{1}{(p^2 - R + i\epsilon)^n}. \tag{4.4}$$

The momentum integration is over Minkowski space with $p^\mu = (p^0, p^1, ..., p^{d-1})$ and $p^2 = (p^0)^2 - \vec{p}^2$ if the d- dimensional metric is by convention $g_{\mu\nu} = \text{diag}(1,-1,-1,...,-1)$.

$$I_n(R) = \int_{-\infty}^{+\infty} dp^0 \int d^{d-1}\vec{p}\, \frac{1}{((p^0)^2 - \vec{p}^2 - R + i\epsilon)^n}. \tag{4.5}$$

It should be noted that there is a subtlety in evaluating the integral given in Eq. (4.5) because the p^0-component is treated differently from the p^i components. That is why the integral cannot be evaluated directly. In order to perform the momentum integration nonetheless, a trick called Wick rotation is introduced, with which one then is able to work in Euclidean space instead of Minkowski space. We define $p^0 \equiv ip_E^0$ and $\vec{p} = \vec{p}_E$. With these replacements $p^2 = (p^0)^2 - \vec{p}^2 = -(p_E^0)^2 - \vec{p}_E^2 = -p_E^2$ and hence all the coordinates are treated alike. Then one can perform the integral using d-dimensional spherical coordinates. If one performs the Wick rotation and afterwards the evaluation of the momentum integral in Euclidean space, one has to transform momenta back to Minkowski coordinates in the end. The evaluation of the integral in Eq. (4.4) is illustrated with intermediate steps in [33, 34]. The final result for the integral under investigation is [34]

$$I_n(R) = i(-1)^n \pi^{(d/2)} \frac{\Gamma\left(n - \frac{d}{2}\right)}{\Gamma(n)} (R - i\epsilon)^{\frac{d}{2}-n}. \tag{4.6}$$

with the Euler Γ function

$$\Gamma(z) = \int_0^\infty dt\, t^{z-1} e^{-t}$$

that has the basic properties

$$\Gamma(z+1) = z\Gamma(z), \qquad \Gamma(z+1) = z!, \qquad \Gamma\left(\frac{1}{2}\right) = \sqrt{\pi},$$

and first order poles at $z = 0, -1, -2, -3, ...$
$\Gamma(z+1) = \frac{1}{z} + \gamma_E + \mathcal{O}(z)$ with the Euler-Mascheroni constant $\gamma_E = -\Gamma'(1) = 0.5772....$
One observes that analytic continuation in d and R holds.

Since the starting point was an integral over four physical dimensions, one usually takes $d = 4 - 2\epsilon$. The ultraviolet divergences then manifest themselves as poles in ϵ. For the original integral $A(m, 1)$ one then obtains [33]

$$A(m,1) = m^2 \left(\frac{1}{\epsilon} - \gamma_E + \ln 4\pi - \ln\left(\frac{m^2}{\mu^2} - i\epsilon\right) + 1\right) + \mathcal{O}(\epsilon^2). \tag{4.7}$$

The ultra-violet singularity is manifest for $\epsilon \to 0$ which corresponds to the limit $d \to 4$. It should be noted that the ϵ originating from going from four to $d = 4 - 2\epsilon$ dimensions is not the same as the $+i\epsilon$ that appears in the propagators to fix the integration contour in the complex p^0 plane. It is unfortunate that the same symbol is used for different quantities in the literature but it should always be clear from the context which one is meant.

4.2. Dimensional Regularization (DREG) and γ_5

Dimensional regularization (DREG) according to 't Hooft and Veltman [35] is an established regularization method, which respects Lorentz and gauge invariance and the symmetries of the Standard Model. The Feynman diagrams are calculated as analytic functions in d space-time dimensions. For small enough d the loop momentum integral converges and the Ward identities are conserved. Ward identities express current conservation which is a consequence of the gauge invariance of the theory. In the end, the results for observables have to possess a well defined limit for $d \to 4$. A common choice is $d = 4 - 2\epsilon$. In order to formulate the dimensional regularization in theories with fermions consistently, one needs a set of matrices γ^μ ($\mu = 0, 1, 2, ..., d-1$), which fulfill the Clifford algebra

$$\{\gamma^\mu, \gamma^\nu\} = 2g^{\mu\nu}\mathbf{1}.$$

The metric tensor $g^{\mu\nu}$ is defined below

$$g^{\mu\nu} = \begin{cases} g^{00} = 1 \\ g^{ii} = -1, \quad i = 1, ..., d-1 \\ g^{\mu\nu} = 0, \quad \mu \neq \nu \end{cases}$$

In addition one needs a definition of the γ_5-matrix. It plays a role for the pseudoscalar current at the vertex of quarks q and a pseudoscalar Higgs boson $q\bar{q}A$: $j_5 = \overline{\psi}\gamma_5\psi$. In four dimensions γ_5 is

$$\gamma_5 = i\gamma^0\gamma^1\gamma^2\gamma^3,$$

with a four dimensional representation of the γ^μ. It anti-commutes with the other γ-matrices

$$\{\gamma_5, \gamma_\mu\} = 0.$$

One would assume that the relation above can be continued dimensionally and holds in d dimensions as well. But there is an inconsistency which is described below. The γ_5 occurring at the vertex $q\bar{q}A$ is rewritten after 't Hooft and Veltman [35] in

$$\gamma_5 = \frac{i}{4!}\epsilon^{\mu\nu\rho\sigma}\gamma_\mu\gamma_\nu\gamma_\rho\gamma_\sigma \tag{4.8}$$

to make it suitable for loop calculations performed in DREG. The totally antisymmetric Levi-Civita tensor is a four dimensional object defined as

$$\epsilon_{\mu\nu\rho\sigma} = \begin{cases} 1 & , \quad (\mu\nu\rho\sigma) = \text{even permutation of (0123)} \\ -1 & , \quad (\mu\nu\rho\sigma) = \text{odd permutation of (0123)} \\ 0 & , \quad \text{otherwise} \end{cases}$$

In the definition in Eq. (4.8) γ_5 remains four dimensional because the ϵ-tensor is a four dimensional object. The advantage of this definition is that the γ-matrices in the loop integrals can be treated as d-dimensional. Products of two Levi-Civita tensors can be replaced by metric tensors which can be interpreted as d-dimensional objects

$$\epsilon_{\mu\nu\rho\sigma}\epsilon^{\mu_1\nu_1\rho_1\sigma_1} = -g_\mu^{[\mu_1} g_\nu^{\nu_1} g_\rho^{\rho_1} g_\sigma^{\sigma_1]}.$$

An inconsistency occurs in the calculation of traces of products of γ_5 with an even number of Dirac matrices [32]. For the trace of γ_5 with four Dirac matrices one obtains for $d = 4$

$$\text{tr}\,(\gamma_5\gamma_\mu\gamma_\nu\gamma_\rho\gamma_\sigma) = 4i\epsilon_{\mu\nu\rho\sigma} \quad (d = 4). \tag{4.9}$$

To be able to analytically continue this expression to d dimensions, one now takes γ_5 in d dimensions to be anti-commuting. One then obtains for the same trace [32]

$$\begin{aligned} &(d-4)\text{tr}\,(\gamma_5\gamma_\mu\gamma_\nu\gamma_\rho\gamma_\sigma) = 0 \\ &\Rightarrow \text{tr}\,(\gamma_5\gamma_\mu\gamma_\nu\gamma_\rho\gamma_\sigma) = 0 \quad (d \neq 4). \end{aligned} \tag{4.10}$$

By examining Eq. (4.10), here in $(d = 4)$ dimensions the non-zero definition of the trace in Eq. (4.9) is prohibited, if the trace in d dimensions is a meromorphic function. If one takes γ_5 to be anti-commuting in d dimensions no analytic continuation of Eq. (4.10) to four dimensions exists. This is an inconsistency in dealing with γ_5. The anti-commutation relations of γ_5 with the d-dimensional γ_μ are lost for $d \neq 4$. That is why Ward identities and with that gauge invariance of the theory is violated. A possible solution of this dilemma is described in the next section.

Renormalization constant Z_5^p for the pseudoscalar current in QCD

In this section we demonstrate how the anti-commutativity of γ_5 can be recovered explicitly. It covers the QCD case. It is not known whether there is a similar procedure for supersymmetric theories. The pseudoscalar current that occurs at the vertex $q\bar{q}A$ in the calculation of the QCD corrections to the gluon fusion process and the Higgs decay into two photons has the form

$$P(x) = \overline{\psi}(x)\gamma_5\psi(x) = \frac{i}{4!}\epsilon_{\mu\nu\rho\sigma}\overline{\psi}(x)\gamma_\mu\gamma_\nu\gamma_\rho\gamma_\sigma\psi(x).$$

In order to renormalize the current correctly a finite constant Z_5^p in addition to the ultra violet renormalization constant Z_{MS}^p is introduced. The renormalized current is given by

$$P_R = Z_5^p Z_{MS}^p P_B = Z_5^p Z_{MS}^p \frac{i}{4!} \epsilon_{\mu\nu\rho\sigma} \overline{\psi}(x)_B \gamma_\mu \gamma_\nu \gamma_\rho \gamma_\sigma \psi(x)_B.$$

The index R denotes the renormalized and B the non-renormalized or bare parameters. The finite renormalization constant Z_5^p is needed to restore Ward identities which have been violated by the assumption of the anti-commutativity of γ_5 in d dimensions. Z_5^p is determined by the requirement of the restoration of the anti-commutativity of γ_5.

In five flavor QCD one obtains [36]

$$Z_5^p = 1 - \frac{\alpha_s}{\pi} 2 C_F + \mathcal{O}\left(\alpha_s^2\right), \tag{4.11}$$

with the Casimir operator $C_F = 4/3$ in SU(3). To conclude, for practical QCD calculations where γ_5 is taken to be anti-commuting in d dimensions, the result has to be multiplied with the finite Z_5^p.

4.3. Dimensional Reduction (DRED)

Dimensional regularization (DREG) violates SUSY as the transition from space-time dimension 4 to $d = 4 - 2\epsilon$ introduces a mismatch between the number of degrees of freedom of gauge bosons and their supersymmetric fermionic partners (gauginos). A spinor field in d dimensions is $2^{d/2}$-dimensional, whereas a vector field is d-dimensional. Thus, the dimensions of the fields only match for $d = 2$ and $d = 4$ dimensions. One can apply DREG nonetheless if one adds finite counterterms which restore the supersymmetric Ward identities [37–39]. The existence of such counterterms is granted by the renormalizability of supersymmetric gauge theories [40–42].

Besides the violation of SUSY the second reason not to use DREG is the appearance of γ_5 in our calculations. If one uses γ_5 in DREG to be anti-commuting Ward identities are violated which have to be restored by adding finite counterterms. This counterterm is only known for the calculation in the SM (cf. Eq. (4.11)) [36]. As it is not known how such a counterterm would read for a calculation including supersymmetric contributions, or if it even exists, our preferred choice of regularization scheme in a SUSY calculation is not DREG.

A different possibility is the use of a regularization scheme in which the momentum integrals are taken to be in $d = 4 - 2\epsilon$ dimensions and the Lorentz indices of the gauge bosons are taken to be 4-dimensional. While the momentum integration further stays in d dimensions, the number of field components remains unchanged and SUSY is conserved. This procedure is called dimensional reduction (DRED) [43]. In DRED only the momenta are treated in d dimensions whereas the γ-matrices and gauge fields remain in 4 dimensions.

Therefore, a direct breaking of SUSY, as occurs in DREG, is circumvented. The idea of dimensional reduction consists in assuming that all field variables depend on a subset of the whole number of space-time dimensions; in this case $d = 4-2\epsilon$. One now introduces 4 and d-dimensional objects. The indices $\mu, \nu, ...$ denote 4-dimensional and $i, j, ...$ d-dimensional objects. The associated metric tensors are $g_{\mu\nu}$ and g_{ij}. Additionally, one introduces symbols with a hat ($\hat{g}_{\mu\nu}$,$\hat{\gamma}^{\mu}$) , which agree with the d-dimensional objects in the d-dimensional subspace and carry zeros as entries in $(4-d)$ dimensions. Momenta p^{μ} only exist in d dimensions and therefore do not obtain a hat symbol. In DRED for instance the following relations hold

$$\begin{aligned} \not{p} &= p_{\mu}\gamma^{\mu} = p_{\mu}\hat{\gamma}^{\mu}, \\ g^{\mu\nu}g_{\mu\nu} &= 4, \quad \hat{g}^{\mu\nu}\hat{g}_{\mu\nu} = g^{ij}g_{ij} = d, \\ \hat{g}^{\mu\nu}g^{\lambda}_{\nu} &= \hat{g}^{\mu\lambda}, \quad \hat{g}^{\mu\nu}\gamma_{\nu} = \hat{\gamma}^{\mu}. \end{aligned}$$

In order to obtain 4-dimensional vector fields W_{μ} on d-dimensional space-time x^j, each vector field (Yang-Mills-gauge field) gets an additional scalar field W_{σ}. This scalar field is called an ϵ-scalar because it transforms as a scalar field under gauge transformations. In dimensional reduction the vector fields are thus split into a d-dimensional and an ϵ-dimensional part [44]

$$W^a_{\mu}\left(x^j\right) = \left\{W^a_i\left(x^j\right), W^a_{\sigma}\left(x^j\right)\right\},$$

with

$$\delta^i_i = \delta^j_j = d \quad \text{and} \quad \delta_{\sigma\sigma} = \epsilon.$$

In leading order the new regularization scheme manifests itself in a way that the Dirac algebra is performed in four dimensions whereas the loop integrations still remain in d dimensions. By applying DRED to supersymmetric theories, one does not run into problems as W_i and W_{σ} behave like W_{μ} under renormalization [44]. Even in higher orders of perturbation theory the only effect of ϵ-scalars is that the Dirac algebra is performed in 4 dimensions. Inserting the fields and their ϵ-scalars into the Lagrangian, one obtains

$$\mathcal{L}^4_B = \mathcal{L}^d_B + \mathcal{L}^{\epsilon}_B.$$

The Lagrangian contains a d-dimensional and an ϵ-dimensional part. In dimensional regularisization (DREG) only $\mathcal{L}^d_B$ is considered. The newly introduced part $\mathcal{L}^{\epsilon}_B$ is needed to recover the supersymmetric Ward identities in one-loop order in SUSY theories [44].

4.3.1. Dimensional Reduction and γ_5

One could conjecture that γ_5 in DRED does not pose any problems as the whole Dirac algebra can be executed in four dimensions. Nevertheless, it has been shown that, as in DREG (see Sec. 4.2), in a mathematically consistent formulation of DRED an inconsistency

with γ_5 exists. This is revealed by the transition from d to four dimensions in the trace of γ_5 with other γ-matrices [45]. Assuming that the anti-commutativity of γ_5, $\{\gamma_\mu, \gamma^5\} = 0$, in four dimensions holds in d dimensions as well one obtains as in DREG that

$$(d-4)\mathrm{tr}\left(\gamma^5\hat{\gamma}^\mu\hat{\gamma}^\nu\hat{\gamma}^\rho\hat{\gamma}^\sigma\right) = 0 \quad (d \neq 4).$$

The result given above requires that the trace vanishes for $(d = 4)$ dimensions. This is in contradiction to the results in four dimensions

$$\mathrm{tr}\left(\gamma^5\gamma^\mu\gamma^\nu\gamma^\rho\gamma^\sigma\right) = 4i\epsilon^{\mu\nu\rho\sigma}.$$

This results in problems analogous to the ones in DREG in handling γ_5.

Concluding remarks

In our calculations we take γ_5 to be anti-commuting and the Dirac-Algebra (traces, etc.) is conducted in four dimensions. After the anti-commutation γ_5 is replaced with Eq. (4.8) ((6.6)) in case the projector from Eq. (6.3) ((6.5)) is applied.

In general, in an MSSM calculation in DRED one would have to introduce ϵ-scalars which occur when vector bosons are generated in the loops. In our calculations the only gauge bosons that appear are gluons. We do not calculate the pure QCD parts contributing to the Higgs production and Higgs decay at two-loop order. In case of the pseudoscalar Higgs production as well as decay the NLO-SUSY contributions to the amplitude do not have gluon insertions in the loops. For the Higgs decay and production squark diagrams with one internal gluon line occur. The $g\tilde{q}\tilde{q}$ coupling however does not obtain a counterpart with an ϵ-scalar. In addition, in the Higgs production processes only the virtual part for the pure SUSY contributions is evaluated by ourselves. Those are inserted into an effective $gg\phi$ vertex we take from the literature. To conclude, in the calculations presented in this thesis, we do not have to introduce ϵ-scalars into the computation.

4.4. Renormalization

Renormalization is needed to absorb UV-divergences that originate from large loop momenta. Via renormalization the bare parameters of the Lagrangian are related to measurable physical quantities like couplings and masses. Hence, the theory can make predictions for experiments. In a renormalizable theory divergences can appear to all orders in perturbation theory. Nevertheless, it is possible to remove them via a finite number of parameter renormalizations. The MSSM and SM are renormalizable non-Abelian gauge theories.

On the one hand, radiative corrections can be calculated from the bare Lagrangian where the bare parameters are transformed into the physical ones afterwards. On the other hand one can consider a Lagrangian that contains counterterms from the beginning to compensate for the divergences and obtain a finite result. We choose the first renormalization

procedure that goes by the name of multiplicative renormalization. In doing so, the bare coupling constants and masses g_B are expressed through the physical coupling constants and masses g with the help of multiplicative factors Z_g in the following manner

$$g_B = Z_g g = (1 + \delta Z_g)\, g.$$

The factors δZ_g contain poles and have to be inserted into our calculations to the appropriate order in the strong coupling constant α_s.

$$\delta Z_g \sim \alpha_s + \mathcal{O}(\alpha_s^2).$$

The δZ_g contain poles in $1/\epsilon$ to compensate for UV-divergences appearing in Feynman diagrams.

Various renormalization schemes exist which tie the renormalization of the parameters to various boundary conditions. They are all equivalent and can be converted into each other. In comparison with the calculation in leading order, in a next-to-leading order calculation one has to renormalize the parameters that appear in the leading order. The renormalization of the coupling constants is performed in the $\overline{MS}$-scheme (modified minimal subtraction). In the MS-scheme that is applied if the underlying regularization scheme is DREG after the transition from 4 to $d = 4 - 2\epsilon$ dimensions the $1/\epsilon$-poles from the loop integrations are subtracted. In addition to this subtraction, in the $\overline{MS}$-scheme finite parts $-\gamma_E + \ln(4\pi)$ as in Eq. (4.7) are subtracted as well. In both cases a finite result is obtained. If the applied regularization scheme is DRED, the underlying renormalization scheme is called DR or $\overline{DR}$-scheme analogously to MS or $\overline{MS}$.

For our calculation of the gluon fusion process the coupling α_s of the strong interaction has to be renormalized. This is not the case for the Higgs decay into two photons, because there the leading order is independent of α_s.

In these processes we perform the renormalization of the masses of the fields that occur as internal lines in the leading order in the on-shell scheme. On-shell means that the boundary conditions are taken for particles on their mass shell. The mass of particles that are on-shell is given by the real part of the pole of the propagator and is interpreted as the physical mass. Besides the pole term the on-shell mass counterterms contain finite parts as well. This is due to the fact that the real parts to the pole mass are absorbed in the counterterm. In the calculations involving pseudoscalar Higgs bosons only the quark mass is renormalized because there are no contributions from supersymmetric particles in leading order. In the scalar cases the squark masses and the squark mixing angle have to be renormalized as well.

4.5. DREG and DRED in our Calculations

The calculations we perform are the NLO-SQCD contributions to the Higgs decaying into two photons, where the Higgs can either be a scalar or a pseudoscalar MSSM Higgs boson. Furthermore, the NLO-SQCD contributions to the production of pseudoscalar and scalar MSSM Higgs bosons via the gluon fusion mechanism are determined. In all the processes we take the appearing masses to be on the mass shell. In our calculations we find that the naive treatment of taking γ_5 to be anti-commuting works. We even observe that our physical on-shell results that should not depend on a regulator agree in DRED and DREG if we perform the calculations carefully within each scheme.

For the pseudoscalar cases we find that the result in DRED with the on-shell quark mass counterterms (cf. App. B) in DRED and the one in DREG with on-shell quark mass counterterms in DREG agree, as expected.

The picture changes when one considers the cases for the scalar Higgs boson. Here, already at leading order there are contributions due to squarks that are absent in the pseudoscalar case because of its being CP-odd. If one performs the calculation in DRED with on-shell mass counterterms for the quarks, squarks and the squark mixing angle, only the quark mass depends on the DRED scheme. In DRED the Higgs-squark-squark couplings are taken as they naturally appear in the MSSM. The result is then the correct one.

In contrast to the calculation in DRED the one in DREG is more subtle. Naively changing the counterterm of the pole quark mass from DRED to DREG is not sufficient to obtain the same on-shell result in DREG as in DRED. The crux is that one has to perform shifts in the Higgs-squark-squark couplings in the calculation in DREG [46]. The relation between the renormalized coupling $m_q^2 g^h_{\tilde{q},ij}$ (cf. App. A) in DREG and DRED is [46]

$$\begin{aligned}\left(m_q^2 g^h_{\tilde{q},ij}\right)^{DREG} &= \left(m_q^2 g^h_{\tilde{q},ij}\right)^{DRED} + m_q \frac{\partial\left(m_q^2 g^h_{\tilde{q},ij}\right)}{\partial m_q}\left[\delta Z^{DRED}_{m_q} - \delta Z^{DREG}_{m_q}\right] + \mathcal{O}\left(\alpha_s^2\right) \\ &= \left(m_q^2 g^h_{\tilde{q},ij}\right)^{DRED} - \frac{1}{4} C_F \frac{\alpha_s}{\pi} m_q \frac{\partial\left(m_q^2 g^h_{\tilde{q},ij}\right)}{\partial m_q} + \mathcal{O}\left(\alpha_s^2\right).\end{aligned} \tag{4.12}$$

Having performed this shift in the Higgs-squark-squark couplings by applying DREG to the calculation we find that the on-shell result regularized in DRED agrees with the corresponding one regularized in DREG as required by the physical result that should be form invariant in both schemes. The reason for this shift in the Higgs-squark-squark couplings is due to the difference in the on-shell quark mass counterterms in DREG and DRED that appear in this coupling [46]. The shift given in Eq. (4.12) accommodates for that dependence such that the DRED result is recovered. The formula states that there is no shift in case the term of the coupling is independent of the quark mass. There is a shift if the dependence is linear and the shift is twice as big if the dependence of the quark mass is quadratic. In the coupling $m_q^2 g^h_{\tilde{q},ij}$ all three cases appear as can be checked in App. A.

4.6. Running of α_s and the Bottom Mass

Via renormalization, a scale μ is introduced into the parameters of the Lagrangian. It is the point at which the subtractions which remove the UV-divergences are performed. We consider a dimensionless observable R that only depends on a single energy scale Q more precisely on the ratio Q^2/μ^2 and the renormalized strong coupling α_s. α_s also depends on μ. This physical quantity R should be independent of the choice of μ provided that the bare parameters are kept fixed. This is expressed by the RG (renormalization group) equation

$$\mu^2 \frac{d}{d\mu^2} R\left(\frac{Q^2}{\mu^2}, \alpha_s\right) = 0.$$

The renormalized strong coupling α_s is not a constant but evolves with energy. It is large at low energies and becomes smaller at high energies. Therefore, perturbation theory works for high energies. The change in α_s is described by [47]

$$\mu^2 \frac{d}{d\mu^2} \frac{\alpha_s(\mu^2)}{\pi} = \beta(\alpha_s) = -\sum_{i\geq 0} \beta_i \left(\frac{\alpha_s}{\pi}\right)^{2+i}.$$

If coefficients higher than β_0 are neglected, the evolution is given by

$$\alpha_s(\mu) = \frac{\alpha_s(\mu_0)}{1 + \frac{\alpha_s(\mu_0)}{\pi}\beta_0 \ln\left(\frac{\mu}{\mu_0}\right)}.$$

Here, β_0 is the one-loop QCD β-function, which is given below. To evaluate the equation above, as a starting point one chooses the experimentally very well measured $\alpha_s(M_Z) = 0.1176$ [25] and extrapolates then to the desired energy scale.

The only quark masses we deal with in our calculations are the bottom quark mass and the top quark mass. Since besides those two mass scales the Higgs mass and the masses of the squarks and gluino are appearing in our calculations, the mass range we investigate is of the order of magnitude around 100 GeV to 1000 GeV. The top mass, the Higgs mass, the squark masses and the gluino masses are set to their pole masses in our calculations.

It has been suggested that one should use the $\overline{MS}$ bottom quark mass at the Higgs scale instead of the on-shell bottom mass for the virtual contributions of bottom quarks to the Higgs production [48]. In our calculations we will compare the results for on-shell bottom masses with taking $\overline{MS}$ bottom masses. Like the running strong coupling, minimally renormalized masses are affected by the energy scale under consideration. By taking a $\overline{MS}$ bottom mass, running effects have to be included. The running describes, that the bottom mass becomes larger, the smaller the energy scale and vice versa. The change in the running $\overline{MS}$ bottom quark mass $\overline{m}_b$ is described by [47]

$$\mu^2 \frac{d}{d\mu^2} \frac{\overline{m}_b(\mu^2)}{\pi} = \overline{m}_b \gamma_m = -\overline{m}_b \sum_{i\geq 0} \gamma_m^i \left(\frac{\alpha_s}{\pi}\right)^{1+i}.$$

The solution for the running mass $\overline{m}_b$ is given by [47]

$$\begin{aligned}\overline{m}_b(\mu) &= \overline{m}_b(\mu_0)\exp\left\{\frac{1}{\pi}\int_{\alpha_s(\mu_0)}^{\alpha_s(\mu)} dx\frac{\gamma_m(x)}{\beta(x)}\right\} \\ &= \overline{m}_b(\mu_0)\left(\frac{\alpha_s(\mu)}{\alpha_s(\mu_0)}\right)^{\frac{\gamma_m^0}{\beta_0}}\left[1+\left(\frac{\gamma_m^1}{\beta_0}-\frac{\beta_1\gamma_m^0}{\beta_0^2}\right)\left(\frac{\alpha_s(\mu)}{\pi}-\frac{\alpha_s(\mu_0)}{\pi}\right)\right]+\mathcal{O}\left(\alpha_s^2\right).\end{aligned}$$

γ_m is called the anomalous dimension. As reference value we take $\overline{m}_b(\mu_0 = 2\,\text{GeV}) = 4.2$ GeV [25]. Furthermore, we use the explicit relation between the on-shell mass and the $\overline{MS}$ mass which is given by [47]

$$\overline{m}_b(\mu) = M_b\left[1-\frac{\alpha_s(\mu)}{\pi}\left(\frac{4}{3}+\ln\left(\frac{\mu^2}{M_b^2}\right)\right)\right]+\mathcal{O}\left(\alpha_s^2\right).$$

With the help of this equation, the on-shell bottom mass is expressed through a running $\overline{MS}$ bottom mass. There is no limitation on the result since one can always convert between $\overline{MS}$ into $\overline{DR}$ masses. The β-functions needed are

$$\begin{aligned}\beta_0 &= \frac{1}{4}\left(11-\frac{2}{3}n_f\right), \\ \beta_1 &= \frac{1}{16}\left(102-\frac{38}{3}n_f\right), \\ \beta_2 &= \frac{1}{64}\left(\frac{2857}{2}-\frac{5033}{18}n_f+\frac{325}{54}n_f^2\right).\end{aligned}$$

The anomalous dimensions are given by

$$\begin{aligned}\gamma_m^0 &= \frac{1}{4}(3C_F), \\ \gamma_m^1 &= \frac{1}{16}\left(\frac{3}{2}C_F^2+\frac{97}{6}C_FC_A-\frac{10}{3}C_FTn_f\right),\end{aligned}$$

with $n_f = 5$, $C_F = 4/3$, $C_A = 3$ and $T = 1/2$.

Chapter 5
5 Asymptotic Expansions

The main topic of the present thesis are the production of Higgs bosons in the gluon fusion process ($gg \to \phi$) and the decay of Higgs bosons into two photons ($\phi \to \gamma\gamma$). Both processes are evaluated in next-to-leading order supersymmetric Quantum Chromodynamics (SQCD) for $\phi = h$ and A.

In the occurring two-loop diagrams, up to four massive scales arise due to the quarks, their superpartners and the gluino, all of which can be generated as intermediate particles. To make the calculations feasible, we employ the method of asymptotic expansions which is suited for higher order processes with several massive scales.

First, the method of asymptotic expansions in large masses is introduced. We comment on the program packages we use as an assistance for our two-loop calculations. Subsequently, the inclusion of the effects of bottom quarks with the help of the method of asymptotic expansions is described. In the last section we illustrate the implementation of additional one-loop routines needed for the inclusion of the bottom effects.

5.1. Asymptotic Expansions in Large Masses

When calculating loop corrections, one has to deal with Feynman diagrams which depend on external momenta and masses. Especially in higher orders of perturbation theory this gets increasingly difficult due to momentum integrations which occur in loops. Diagrams one is unable to calculate exactly due to their complexity one has to calculate approximately. A limit of large masses and momenta is defined by grouping the set of external momenta and internal masses of a Feynman diagram Γ into large $\underline{Q} \equiv \{Q_1, ..., Q_i, ...\}$ and small $\underline{q} \equiv \{q_1, ..., q_i, ...\}$ momenta and large $\underline{M} \equiv \{M_1, ..., M_i, ...\}$ and small $\underline{m} \equiv \{m_1, ..., m_i, ...\}$ masses. The associated Feynman integral is $F_\Gamma\left(\underline{Q}, \underline{q}, \underline{M}, \underline{m}\right)$. One can then expand the Feynman diagrams with respect to masses and/or momenta. Reviews of the method of asymptotic expansion are given in [49–51].

In our calculations we apply the method of expansions in large masses. A few exemplary

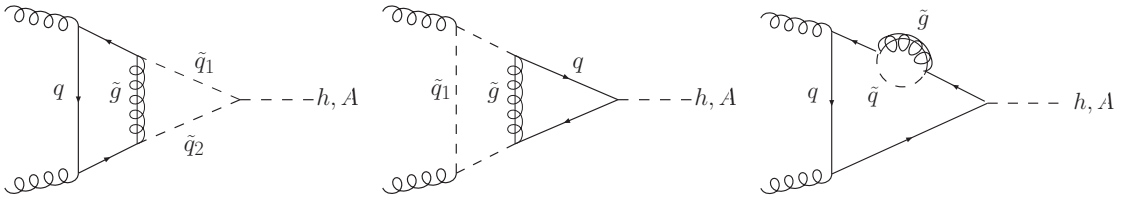

Figure 5.1.: *Two-loop (NLO) Feynman diagrams for Higgs production through gluon fusion ($gg \to \phi$).*

diagrams are displayed in Fig. 5.1. They can depend on the quark mass m_q, the two squark masses $m_{\tilde{q}_1}$, $m_{\tilde{q}_2}$ and on the gluino mass $m_{\tilde{g}}$, where $(q, \tilde{q}) = (t, \tilde{t})$ or $(b, \tilde{b})$. Therefore, we are dealing with up to four massive scales in a Feynman diagram. For processing the expansion, one in advance fixes a hierarchy among the magnitude of the masses appearing in the loops. In our calculations we performed asymptotic expansions for instance for the mass hierarchies

$$\begin{aligned}
&m_q \ll m_{\tilde{q}_1} \ll m_{\tilde{q}_2} \ll m_{\tilde{g}}, \qquad && m_q \ll m_{\tilde{q}_1} = m_{\tilde{q}_2} \ll m_{\tilde{g}}, \\
&m_q \ll m_{\tilde{q}_1} \ll m_{\tilde{q}_2} = m_{\tilde{g}}, \qquad && m_q \ll m_{\tilde{q}_1} = m_{\tilde{q}_2} = m_{\tilde{g}}, \\
&m \equiv m_t = m_{\tilde{t}_1} = m_{\tilde{t}_2} \ll m_{\tilde{g}},
\end{aligned}$$

where $(q, \tilde{q}) = (b, \tilde{b})$ or $(t, \tilde{t})$. One has to keep in mind that the convergence of the expansion is only given in the assumed mass hierarchy. The method of expansion in the limit of large masses $\underline{M}$ is depicted in the formula below [49]

$$F_\Gamma\left(\underline{q}, \underline{M}, \underline{m}; \epsilon\right) \sim \sum_\gamma F_{\Gamma/\gamma}\left(\underline{q}, \underline{m}; \epsilon\right) \circ \mathcal{T}_{\underline{q}^\gamma, \underline{m}^\gamma} F_\gamma\left(\underline{q}^\gamma, \underline{M}, \underline{m}^\gamma; \epsilon\right).$$

F_Γ is the integral belonging to a Feynman diagram Γ. Γ/γ is a diagram in which the subdiagram γ has been shrunk to a point. $\mathcal{T}_{\underline{q}^\gamma, \underline{m}^\gamma}$ denotes the Taylor expansion in all small mass scales $\underline{m}^\gamma$ and external momenta $\underline{q}^\gamma$ of the subgraph γ. In this way, loop momenta of the diagram under consideration can become external momenta of subgraphs. The sum runs over all subdiagrams γ, which

1. contain all lines with large masses

2. are one particle irreducible with respect to the lines of small masses.

The integrals are calculated in $d = 4 - 2\epsilon$ dimensions. The asymptotic expansions in our calculation are performed with the help of EXP [52, 53]. The software packages used are described in the next section.

5.2. Methods and Auxiliary Material

One of the main difficulties in our calculations performed in the MSSM is the occurrence of more than one massive scale $m_i \in \{m_q, m_{\tilde{q}_1}, m_{\tilde{q}_2}, m_{\tilde{g}}\}$ with $(q, \tilde{q}) = (t, \tilde{t})$ or $(b, \tilde{b})$. For the calculation of the two-loop amplitudes (NLO) we use existing software programs. The generation and calculation of the diagrams is completely automatized.

With the help of the program QGRAF [54] the diagrams contributing to the given process are generated. For this we implement the Feynman rules in terms of propagators and vertices in the notation of QGRAF and determine the initial and final state for the process under consideration. The output of QGRAF contains the number of propagators, loops, ingoing and outgoing momenta and in addition for each propagator the momentum of the respective particle for each Feynman diagram. Lines which for instance merge into the same vertex carry the same number. From that information one can reconstruct the diagrams graphically. In our cases of the calculation we always deal with $\mathcal{O}(100 - 300)$ diagrams. The Feynman rules applied are given in App. C. Q2E [55] translates the symbolic notation of the diagrams given in QGRAF as an input into EXP.

EXP generates files that can be given directly to a FORM-program [56] for the calculation. EXP [52, 53] contains routines that process asymptotic expansions (cf. Sec. 5.1). For the expansion in large masses, one first has to fix arbitrary mass hierarchies among the massive particles occurring in the diagram. In the calculations under consideration — in one single Feynman diagram — up to four massive scales that are the gluino, the two squark masses and the quark mass can occur. The asymptotic expansions are carried out in the way that the program searches the single graphs for subgraphs which can be calculated with additional routines. The diagrams are classified by topologies which can be calculated with the same routines. If EXP detects a routine with which a subgraph can be calculated it is not fragmented any more. EXP does not apply asymptotic expansions in case routines for evaluating all graphs exist. EXP prepares the diagrams finally for the calculation by providing the essential information.

With the help of MATAD [57] or MINCER [58], which are implemented in the language FORM [56] the output of EXP is analyzed. MATAD is a program to calculate massive vacuum diagrams. It can deal with up to three-loop vacuum diagrams in which one massive scale occurs. With MINCER one can calculate diagrams of the propagator type which only depend on one non-vanishing external momentum. It can deal with up to three-loop graphs in the massless case. After the procedure of generating the Feynman diagrams, and having done the asymptotic expansions and evaluations of the diagrams with the automatized setup, the unrenormalized amplitudes of the respective process are obtained.

The renormalization and the calculation of physical observables like decay widths and cross sections remain yet to be done. The projectors that are described in Sec. 6.4 are implemented in addition. The treatment of γ_5 and the regularization scheme (see chapter 4) are handled user-defined.

The following flow chart abstracts the steps of the automatized setup described above

QGRAF	→	Q2E	→	EXP	→	MATAD/MINCER
generation		translation		asymptotic expansion (optional)		evaluation

5.3. The Method Applied in our Case

The goal of our calculations is an expression for the amplitudes in supersymmetric Quantum Chromodynamics (SQCD) for the photonic Higgs decay and the production of scalar and pseudoscalar MSSM Higgs bosons at the two-loop level. Since we are about to apply the method of asymptotic expansions, we have to set a hierarchy among the mass scales appearing in our calculations.

If one is just interested in performing the calculations including the top quark, its scalar superpartners and the gluino, one can make the assumption that the top quark is heavier than the Higgs boson and perform an expansion in $(m_\phi^2)/(4m_t^2)$, $\phi = h, A$, with the Higgs mass m_ϕ and top mass m_t. This seems to be a more or less valid assumption for $m_t = 172.4$ GeV and an assumed Higgs mass between 100 GeV and 200 GeV. The superpartners of the top quark and the gluino can be assumed to be heavier than the top anyway. The calculation then simplifies in a way that one can set the external momenta of the photons and gluons to zero and ends up with the evaluation of massive two-loop tadpole diagrams.

Having in mind to include the bottom quark and its superpartners into the calculation, the assumption of the quark being heavier than the Higgs boson clearly does not hold for a bottom quark with a mass of around $m_b = 5$ GeV. In this case, it is not permitted to set the external momenta of the process under consideration to zero. This clearly demands for another manner of including the bottom quark. The squarks and the gluino are still considered to be heavy. By including the bottom quark, we will nevertheless perform asymptotic expansions, only this time by keeping the external momenta non-vanishing.

Below, we want to describe the method to obtain this expansion in more detail. Applying the method of asymptotic expansions for the first diagram displayed in Fig. 5.1 in the limit $M_s \equiv m_{\tilde{b}_1} = m_{\tilde{b}_2} = m_{\tilde{g}} \gg m_\phi, m_b$ with the sbottom masses $m_{\tilde{b}_{1,2}}$ and gluino mass $m_{\tilde{g}}$ leads to the following relation

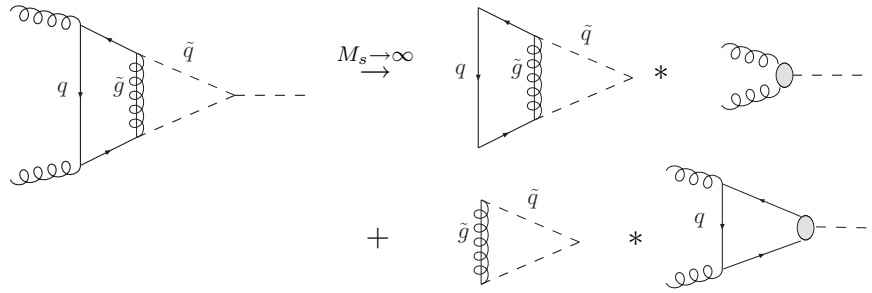

(5.1)

On the right hand side it is understood that the integrand of the Feynman integral left of $*$ is Taylor-expanded in terms of all its parameters (external momenta, masses) except for the heavy mass scale M_s (note that in the second term, also the loop momentum of the diagram to the right of $*$ counts as external momentum to the term left of $*$). This leads to massive tadpole integrals depending only on M_s which can be evaluated analytically. The resulting expression is inserted into the shaded blob in the diagram left of $*$ as an effective vertex. The dependence of the external momenta of the process is contained in the diagrams to the right of *. The triangle diagram to the lower right is a one-loop three-point function which gives rise to functions $F_\Delta(m_\phi, m_b)$ depending on the bottom and Higgs mass. Its evaluation will be described in more detail in Sec. 5.4. An analogous procedure can be applied to all other diagrams contributing to the gluon fusion process.

For clarity, let us give one other example for the second exemplary Feynman diagram in Fig. 5.1:

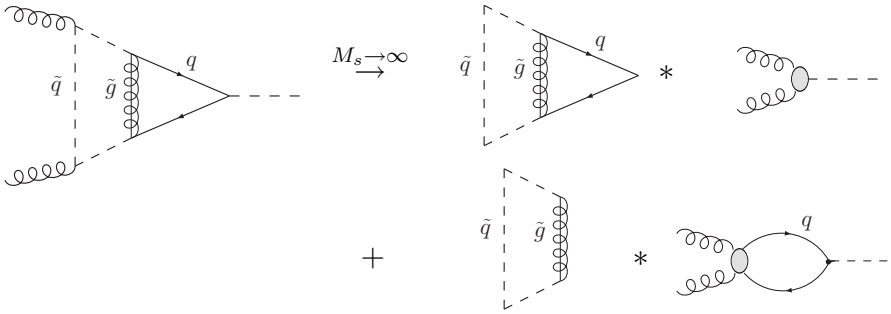

(5.2)

Here, an additional type of one-loop diagram appears that has to be evaluated with non-vanishing external momenta and results again in functions $F_O(m_\phi, m_b)$ depending on the bottom and Higgs mass. By performing an asymptotic expansion for the last diagram of Fig. 5.1 one has to evaluate triangle diagrams like in the one given in Eq. (5.1) with one propagator appearing in the triangle graph, raised by one power.

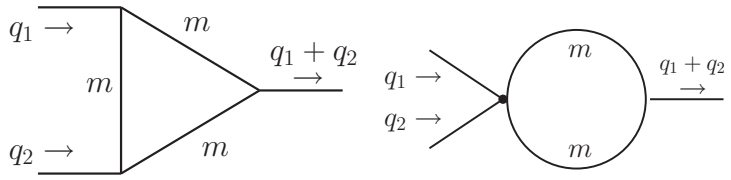

Figure 5.2.: *Diagrams calculable with the new routines.*

For the one-loop diagrams to the right of $*$ in the symbolic sketches of Eqs. (5.1) and (5.2) we implement additional routines into the setup described in Sec. 5.2 which allow us to evaluate them using standard Feynman parameterization. It should be noted that if these integrals are expressed in terms of analytic functions, the result is valid both below and above the cut at $m_\phi = 2m_q$. In particular, we can compare it to the expansions of Ref. [59,60] obtained in the limit $m_t > m_\phi$, which provides a welcome check.

The result obtained for the pure supersymmetric contributions to the amplitude is then expressed as a power series of the following form

$$\mathcal{A}_{susy} = \sum_n \left(\frac{m_\phi^2}{M_s^2}\right)^n F_{\Delta,O}(m_\phi, m_q)\,.$$

Above, we only illustrated asymptotic expansions for the production of Higgs bosons through gluon fusion. Of course, this is analogously applicable to the process where the Higgs decays into two photons via a loop. For the decay process Eqs. (5.1) and (5.2) from above can be taken with the modifications that initial and final state are interchanged and the two gluons are replaced by photons.

5.4. New Routines for Including the Bottom Quark

In order to include the bottom quark and its superpartners into our calculation, we implemented new routines. They are included in the topology file used by `EXP` [52, 53], which reads in the topologies that we assume for the diagrams during the calculation as follows

$$\{\text{mb1l}; 2; 1; 2; 2; ; (q_1 : 1, 2)(q_2 : 1, 2)(p_1 : 2, 1)(p_2 : 1, 2); 33\},$$

$$\{\text{3ptriangle}; 3; 1; 2; 3; ; (q_1 : 1, 3)(q_2 : 2, 3)(p_1 : 2, 1)(p_2 : 1, 3)(p_3 : 3, 2); 333\}.$$

The procedure 3ptriangle allows us to evaluate the leading order for the process $gg \rightarrow \phi$ and $\phi \rightarrow \gamma\gamma$ where either a top quark or a bottom quark are generated in the loop exactly,

i.e., without having to make an approximation. Furthermore, both of the new routines enable us to include the bottom quarks and their superpartners into our calculation in next-to-leading order (NLO) perturbation theory, as described in the previous section.

3ptriangle is implemented in order to calculate triangle (Δ) graphs with three massive propagators with one mass scale m ($m = m_q$) appearing in the loop and with non-vanishing external momenta. The type of diagrams that can be evaluated with 3ptriangle is shown on the left side in Fig. 5.2. The incoming external momenta are denoted q_1 and q_2. Those diagrams arise as subdiagrams in the expansion of diagrams of the type exhibited in Eq. (5.1).

mb1l is implemented in order to calculate two-point functions with two massive propagators with one mass scale m ($m = m_q$) and non-vanishing external momenta. Diagrams that can be calculated with mb1l are illustrated on the right side in Fig. 5.2. These arise as subdiagrams like the one depicted in Eq. (5.2) in the calculations.

In both routines, the two external four-momenta q_1, q_2 correspond to the two photon or gluon momenta. We assume that the photons and gluons are on the mass shell, i.e., $q_1^2 = 0 = q_2^2$ and that $(q_1 + q_2)^2 = 2q_1 \cdot q_2 = m_\phi^2$. The Higgs bosons are taken as real particles.

During the calculation projectors are applied, which project out the scalar parts of the amplitudes. We are then left to consider scalar integrals. Since we have to regularize the Feynman integrals appearing in our calculations we do so by evaluating loop integrals in $d = 4 - 2\epsilon$ rather than in 4 dimensions. This is done in dimensional regularization and dimensional reduction which were discussed in chapter 4.

In the routine 3ptriangle for evaluating Δ diagrams, the most complex integral appearing is the one with three propagators corresponding to three factors in the denominator of the integrand. The corresponding scalar integral is given by

$$C(q_1, q_2, m, m, m; n_1, n_2, n_3) = \frac{(2\pi\mu)^{4-d}}{i\pi^2} \int d^d p \frac{1}{(p^2 - m^2 + i\epsilon)^{n_1} \left((p+q_1)^2 - m^2 + i\epsilon\right)^{n_2} \left((p-q_2)^2 - m^2 + i\epsilon\right)^{n_3}}.$$

The factors in the denominator we face can contain one exponent $n_i = 2$ and the other exponents $n_j = 1$, $j \neq i$ in case the original diagram was of the type of the last diagram shown in Fig. 5.1. In this case, while processing the asymptotic expansion by taking out the squark/gluino loop of the original diagram, one is left with a triangle diagram, where the exponent of one propagator is increased by 1. For diagrams like the one shown left in Fig. 5.1 the exponents are $n_i = 1$ for $i = 0, 1, 2$.

In the routine mb1l diagrams with two propagators are evaluated. Their integrals can be expressed by

$$B(q_1,q_2,m,m;n_1,n_2) = \frac{(2\pi\mu)^{4-d}}{i\pi^2}\int d^dp \frac{1}{((p+q_1)^2-m^2+i\epsilon)^{n_1}\,((p-q_2)^2-m^2+i\epsilon)^{n_2}}, \tag{5.3}$$

$$B(q_1,m,m;n_1,n_2) = \frac{(2\pi\mu)^{4-d}}{i\pi^2}\int d^dp \frac{1}{(p^2-m^2+i\epsilon)^{n_1}\,((p+q_1)^2-m^2+i\epsilon)^{n_2}},$$

$$B(q_2,m,m;n_1,n_2) = \frac{(2\pi\mu)^{4-d}}{i\pi^2}\int d^dp \frac{1}{(p^2-m^2+i\epsilon)^{n_1}\,((p-q_2)^2-m^2+i\epsilon)^{n_2}}.$$

The B-type integrals occur in both routines. In the routine 3ptriangle we may have cancellations between numerators and denominators and the C-type integrals may be reduced to B-type ones.

Additionally, scalar integrals of the type already discussed in Sec. 4.1 occur

$$A(m;n_1) = \frac{(2\pi\mu)^{4-d}}{i\pi^2}\int d^dp \frac{1}{(p^2-m^2+i\epsilon)^{n_1}}.$$

In our calculations n_1 and n_2 are integer.

For the evaluation of these one-loop routines, we proceed as follows. First, we express the momenta (p_1, p_2 and p_3 in case of the Δ diagram) running in the loops with the help of the ones of the external gluons respective photons q_1 and q_2 and the loop momentum p. Afterwards, these momenta are rewritten in terms of the appearing denominators. In both routines an integration momentum p is present. Numerators that appear are expressed through denominators and reduced. One simplifies the structure of the integrals if one reduces the numerators first. Having the integrals C, B and A from above in mind, we write

$$\begin{aligned} p^2 =& (p^2-m^2)+m^2, \\ p\cdot q_1 =& \frac{1}{2}((p+q_1)^2-m^2) - \frac{1}{2}(p^2-m^2), \\ p\cdot q_2 =& -\frac{1}{2}((p-q_2)^2-m^2) + \frac{1}{2}(p^2-m^2). \end{aligned} \tag{5.4}$$

If Eq. (5.4) for instance is applied to the expression $p\cdot q_1\; C(q_1,q_2;1,1,1)$, it simplifies considering the complexity of the integrals remaining to be calculated. The reduced expression is $p\cdot q_1\; C(q_1,q_2;1,1,1) = \frac{1}{2}B(q_2,m,m;1,1) - \frac{1}{2}B(q_1,q_2,m,m;1,1)$. The example demonstrates that after the reduction one obtains new integrals which often have a simpler structure in the denominator.

The problem with the integrals above is that one has to reform them into an expression, that allows us to perform the integration over the loop momentum p. One method to

reformulate the integrals in a simpler way that allows for the integration over the loop momenta is Feynman parameterization. Here, the goal of this method is to reduce the various factors of the denominators in the integrals into a single quadratic polynomial in p, raised to some power. Then what remains is a spherically symmetric integral, that can be evaluated without any difficulties. As nothing comes for free, when one reduces the denominator to one single factor, additional parameters come into play, with integrations over them. The simplest identity has the form [61]

$$\frac{1}{AB} = \int_0^1 \frac{dx}{\left(xA + (1-x)B\right)^2} \tag{5.5}$$

with the so-called Feynman parameter x. We will demonstrate step by step how they are applied for the case of the Feynman integral of Eq. (5.3) by taking $A = ((p+q_1)^2 - m^2 + i\epsilon)$ and $B = ((p-q_2)^2 - m^2 + i\epsilon)$.

$$\begin{aligned}
&\frac{(2\pi\mu)^{4-d}}{i\pi^2}\int d^dp \frac{1}{AB} = \frac{(2\pi\mu)^{4-d}}{i\pi^2}\int d^dp \frac{1}{\left((p+q_1)^2 - m^2 + i\epsilon\right)\left((p-q_2)^2 - m^2 + i\epsilon\right)} \\
&= \frac{(2\pi\mu)^{4-d}}{i\pi^2}\int d^dp \int_0^1 dx \frac{1}{\left[x\left((p+q_1)^2 - m^2 + i\epsilon\right) + (1-x)\left((p-q_2)^2 - m^2 + i\epsilon\right)\right]^2} \\
&= \frac{(2\pi\mu)^{4-d}}{i\pi^2}\int d^dp \int_0^1 dx \frac{1}{\left[p^2 + 2pq_1x - 2(1-x)pq_2 - m^2 + i\epsilon\right]^2} \\
&= \frac{(2\pi\mu)^{4-d}}{i\pi^2}\int d^dp \int_0^1 dx \frac{1}{\left[p^2 + 2q_1q_2x(1-x) - m^2 + i\epsilon\right]^2} \\
&= \frac{(2\pi\mu)^{4-d}}{i\pi^2}\int d^dp \int_0^1 dx \frac{1}{\left[p^2 + m_\phi^2 x(1-x) - m^2 + i\epsilon\right]^2}.
\end{aligned} \tag{5.6}$$

In the last step we performed the substitution of setting $p' = p + q_1x - (1-x)q_2$ and afterwards relabeled p' back to p again. We also applied $q_1^2{=}0$ and $q_2^2 = 0$ and $Q^2 = (q_1+q_2)^2 = 2q_1q_2 = m_\phi^2$. The identity in Eq. (5.5) generalizes to having n factors $A_1, ..., A_n$ in the denominator with exponents m_i [61]

$$\begin{aligned}
\frac{1}{A^{m_1}A_2^{m_2}...A_n^{m_n}} = \frac{\Gamma\left(m_2 + ... + m_n\right)}{\Gamma\left(m_1\right)\Gamma\left(m_2\right)...\Gamma\left(m_n\right)}\int_0^1 dx_1 \int_0^1 dx_2 ... \int_0^1 dx_n \\
\delta\left(\sum x_i - 1\right)\frac{\prod x_i^{m_i-1}}{\left[\sum x_iA_i\right]^{\sum m_i}}.
\end{aligned} \tag{5.7}$$

This formula even holds for non-integer m_i. The special cases we need are given below, where we already eliminated one integration with the help of the δ-function which appears in Eq. (5.7)

$$\frac{1}{A^2BC} = \Gamma(4)\int_0^1 dx \int_0^{1-x} dy \frac{x}{(xA+yB+(1-x-y)C)^4},$$
$$\frac{1}{ABC} = \Gamma(3)\int_0^1 dx \int_0^{1-x} dy \frac{1}{(xA+yB+(1-x-y)C)^3},$$
$$\frac{1}{A^2B} = \Gamma(3)\int_0^1 dx \frac{x}{(xA+(1-x)B)^3}.$$

After having inserted the Feynman parameters into the Feynman integrals, we are left with just one denominator raised to a certain power. This then has to be expressed in the form $p^2 - R$, where the loop momentum p is separated from the rest R that is independent of p (cf. Eq. (5.6)). This is done with the help of substitution of momenta in the integral. In general, the function $R = R\,(q_1, q_2, ..., q_n; m_1, m_2, ..., m_n; x_1, x_2, ..., x_n)$ depends on the external momenta q_i, the masses m_i appearing in the propagators and the Feynman parameters x_i. After the Feynman parameterization and before performing the integration over the loop momentum p, powers of the denominator are reduced. In doing so, the numerators in which momenta p^2 appear are rewritten in the form $p^2 + R - R$ by adding zero and the first two terms are reduced against one power in the denominator. As an example, the following integral can be simplified by

$$\int d^dp \frac{p^2}{p^2-R} = \int d^dp \frac{p^2-R+R}{p^2-R} = R\int d^dp \frac{1}{p^2-R}.$$

Eq. (4.2) was applied to the first summand that then vanishes by definition. The aim then is to eliminate all powers of loop momenta in the numerator and just be left with integrals of the form [34]

$$I_n(R) = \int d^dp \frac{1}{(p^2-R+i\epsilon)^n} = i(-1)^n \pi^{(d/2)} \frac{\Gamma\left(n-\frac{d}{2}\right)}{\Gamma(n)} (R-i\epsilon)^{\frac{d}{2}-n},$$

where the result was already presented in Sec. 4.1.

Having performed the integration over the loop momentum, integrations over Feynman parameters remain to be done. The functions we obtain in our calculations and we are left with to solve are

$$f_{xy}(a,b,c,n) = \frac{(2\pi\mu)^{4-d}}{i\pi^2}\int_0^1 dx \int_0^{1-x} dy \int d^dp \frac{x^a\, y^b\, R_{xy}(q_1q_2,m,x,y)^c}{(p^2 - R_{xy}(q_1q_2,m,x,y)+i\epsilon)^n}$$
$$= (-1)^n \left(4\pi\mu^2\right)^\epsilon \frac{\Gamma(n-2+\epsilon)}{\Gamma(n)} \int_0^1 dx \int_0^{1-x} dy\; x^a\; y^b\; \left(R_{xy}(q_1q_2,m,x,y) - i\epsilon\right)^{c+2-n-\epsilon},$$

$$f_x\left(a,c,n\right) = \frac{\left(2\pi\mu\right)^{4-d}}{i\pi^2}\int_0^1 dx \int d^dp \frac{x^a\ R_x(q_1q_2,m,x)^c}{(p^2 - R_x(q_1q_2,m,x) - i\epsilon)^n}$$
$$= (-1)^n\left(4\pi\mu^2\right)^\epsilon \frac{\Gamma\left(n-2+\epsilon\right)}{\Gamma(n)}\int_0^1 dx\ x^a\ \left(R_x(q_1q_2,m,x) - i\epsilon\right)^{c+2-n-\epsilon},$$

where $d = 4 - 2\epsilon$ was employed. The functions can be written as an expansion in the infinitesimal parameter ϵ. To achieve this the expansion of the exponential function is used

$$R^{\pm\epsilon} = e^{\pm\epsilon \ln R} = 1 \pm \epsilon \ln R + \frac{\epsilon^2}{2}\ln^2 R \pm ....$$

In the final results for the amplitudes only integrals appear which are at most proportional to a logarithm squared.

Finally, three types of integrals remain to be solved

$$F_0(a,c,n) = (-1)^n\left(\frac{4\pi\mu^2}{m^2}\right)^\epsilon \frac{\Gamma\left(n-2+\epsilon\right)}{\Gamma(n)}\int_0^1 dx\ x^a (m^2)^{c+2-n}$$
$$= (-1)^n\left(\frac{4\pi\mu^2}{m^2}\right)^\epsilon \frac{(m^2)^{c+2-n}}{(a+1)},$$

$$F_1(a,c,n) = (-1)^n\left(\frac{4\pi\mu^2}{m_\phi^2}\right)^\epsilon \frac{\Gamma\left(n-2+\epsilon\right)}{\Gamma(n)}\int_0^1 dx\ x^a \left(x^2 - x + \frac{m^2}{m_\phi^2} - i\epsilon\right)^{(c+2-n)}$$
$$\cdot\left[1 - \epsilon\ln\left(x^2 - x + \frac{m^2}{m_\phi^2} - i\epsilon\right) + \mathcal{O}(\epsilon^2)\right],$$

$$F_2(a,b,c,n) = (-1)^n\left(\frac{4\pi\mu^2}{m_\phi^2}\right)^\epsilon \frac{\Gamma\left(n-2+\epsilon\right)}{\Gamma(n)}\int_0^1 dy \int_0^{1-x} dy\ x^a y^b$$
$$\left(-xy + \frac{m^2}{m_\phi^2} - i\epsilon\right)^{(c+2-n)} \cdot\left[1 - \epsilon\ln\left(-xy + \frac{m^2}{m_\phi^2} - i\epsilon\right) + \mathcal{O}(\epsilon^2)\right].$$

Here, we observe the use of μ as a reference mass in order to keep arguments of logarithms dimensionless. The expressions of R for the integrals above are $R_0 = m^2$, $R_1 = (x^2 - x)m_\phi^2 + m^2$ and $R_2 = -x\,y\,m_\phi^2 + m^2$.

Finally, this means that the results obtained with the help of the new routines are functions,

in case we apply them to quarks loops, depending on the quark mass m_q (denoted by m above) and the Higgs boson mass m_ϕ, i.e.,

$$\boxed{F_i = F_i\left(m_q, m_\phi\right), \quad (i = 0, 1, 2)}$$

The analytic expressions for the integrals as well as their expansions are calculated with the help of `mathematica` [62]. For some integrals it is not possible to evaluate them with `mathematica` directly. By applying substitutions and appropriate replacements, one can force the program to calculate the integrals step by step. The integrals we are left with are roughly $F_1(a, c, n)$ where $n = 1, 2, 3$, $a \in 0, ..., \mathcal{O}(10)$ and $c = 0, ..., 4$. For most of them we need the constant as well as the $\mathcal{O}(\epsilon)$ parts. Only for $F_1(0, 0, 2)$, $F_1(1, 0, 2)$, $F_1(2, 0, 2)$, $F_1(1, 0, 2)$ and $F_1(0, 0, 1)$ we need the $\ln^2$ part, i.e., the $\mathcal{O}(\epsilon^2)$ contribution. The most complicated integrals we are finally left with are $F_2(0, 0, 0, 3)$ and $F_2(0, 0, 0, 4)$. For the renormalization one needs to take the derivative of $F_2(0, 0, 0, 3)$ with respect to the quark mass, m_q. The term proportional to ϵ in $F_2(0, 0, 0, 3)$ is known in the literature [63, 64].

Validation and Remarks

The need for new routines is due to the inclusion of the bottom quarks. To all diagrams that contain mixed gluino/quark/squark contributions, the new routines are applied.

The new routines which were primarily designed to calculate the bottom contributions to the two-loop processes under consideration, are applicable in the case of the top quark as well. A welcome check of our routines is that we can compare the results obtained with them with the results obtained for the limit of large top masses. Therefore, we could test our new routines at leading order and next-to-leading order in perturbation theory. We calculated all limiting cases including top quarks and their superpartners in the limit of large top masses. With these results we checked our new routines by expanding the integrals obtained with them in the appropriate small parameter, i.e., $m_\phi^2/(4m_t^2)$ in the case of the top quark.

Applying the new routines to the two-loop diagrams that contain top quarks results in a larger radius of convergence compared to the result obtained in the limit of large top masses. In particular, they are valid for Higgs masses larger than the top mass.

In the renormalized results for the amplitudes of photonic decay of Higgs bosons, the integrals are kept analytically to evaluate the results obtained for the Higgs decay numerically. For the Higgs production via the gluon fusion they are expanded in the parameters m_q and m_ϕ. The expansion parameter is $4m_b^2/m_\phi^2$ for the bottom case and $m_\phi^2/(4m_t^2)$ in the top case. This is described in more detail in the chapters about Higgs decay and Higgs production.

Chapter 6
6 Higgs Decay

After having set the scene in the previous chapters, we now proceed to the main part of this thesis. First, we will briefly discuss the current status of the Higgs search. Next, the decay of Higgs bosons in general will be discussed and throughout the chapter we focus on the decay of scalar and pseudoscalar Higgs bosons into two photons. We calculate the latter process in the framework of NLO-SQCD, where we include contributions from tops, stops and gluinos as well as the — previously unknown — contributions from bottoms, sbottoms and gluinos. We will give explicit expressions for the leading terms of the amplitude in NLO-SQCD to the Higgs decay into two photons. Finally, we discuss the physical results for the partial decay widths of the process under consideration.

6.1. Theoretical and Experimental Bounds on the Higgs

The different experiments yielded certain limits on the Standard Model Higgs boson mass. From direct search the experiments at the Large Electron Positron Collider (LEP) concluded a lower bound for the Higgs mass which is $m_H \geq 114.4$ GeV at 95% confidence level [65]. From electroweak precision data the preferred value of the Higgs mass is $m_H = 90^{+36}_{-27}$ GeV at 68% confidence level including only the experimental uncertainty [65] and an upper bound of $m_H \leq 163$ GeV with 95% confidence level [65]. The upper bound increases to $m_H \leq 191$ GeV if the direct search limit of LEP is included [65].

From the theory side, the bounds for the Higgs mass depend on the underlying model. In the SM the Higgs mass is a priori a free parameter. Constraints come from the demand to have a non-zero Higgs potential which possesses a stable vacuum expectation value. In the SM the Higgs potential is given by $V_{Higgs} = \lambda(\phi^\dagger\phi)^2 - \mu^2(\phi^\dagger\phi)$ and the Higgs mass is $m_H = \sqrt{2}\mu = \sqrt{2\lambda}v$ [61]. Such as all couplings in a quantum field theory, the parameter λ exhibits an energy dependency. From its running, an upper limit called triviality bound for the Higgs mass is obtained by demanding that λ should not become singular. On the other hand in order to have spontaneous symmetry breaking at all requires a non-vanishing

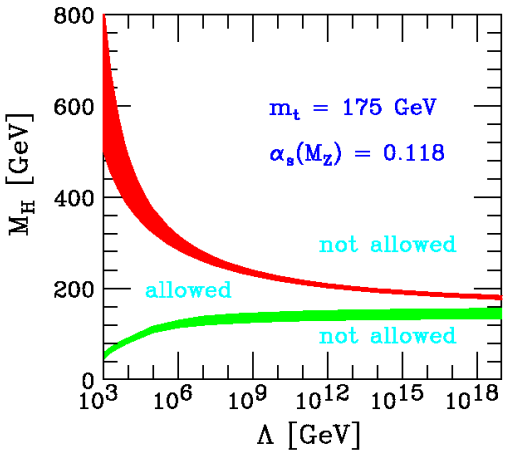

Figure 6.1.: *The triviality bound (upper) and the vacuum stability bound (lower) on the Higgs mass in dependence of a cut-off scale Λ up to which the SM is assumed to be valid. The allowed region is in between the bands. Taken from [67].*

λ at all energies. This is called stability bound and provides a lower limit on the Higgs mass. In case the SM fulfills these two requirements up to a certain energy scale Λ up to which the SM is assumed to be valid, the bounds can be read off in Fig. 6.1. If the validity of the SM is assumed up to $\Lambda \sim 10^{19}$ GeV the bounds on the Higgs mass are roughly 100 GeV $\leq m_H \leq$ 200 GeV. Fig. 6.1 displays that the upper bound on the Higgs mass increases to $m_H \leq 800$ GeV if one assumes for instance that new physics sets in at an order $\mathcal{O}(1$ TeV$)$.

With the end of data taking at LEP, the search for Higgs bosons has turned to hadron colliders. The Tevatron experiment at Fermilab is a proton-anti-proton collider with $\sqrt{s} =$ 1.96 TeV hadronic center of mass energy. Recently, the two Tevatron experiments D$\varnothing$ and CDF published a combined exclusion of a SM Higgs boson with a mass between 160 GeV to 170 GeV at 95% confidence level [66].

The LHC, which shall start operating in the end of 2009 is a proton-proton collider with $\sqrt{s} = 14$ TeV hadronic center of mass energy. There, it should be possible to discover a Higgs boson from the lower experimental mass limit up to a mass of about 1 TeV.

The above bounds were given for a Standard Model Higgs boson. Supposed the underlying model is the MSSM, there exist theoretical bounds on the lightest Higgs mass and on $\tan\beta$. For a SUSY scale of about $M_s \approx 1$ TeV one obtains $1 \lesssim \tan\beta \lesssim 60$ in models with universal boundary conditions at the GUT scale [29]. If one requires that the set of SUSY parameters fulfills the known theoretical and experimental constraints the lightest MSSM Higgs boson mass is at most $m_h \simeq 144$ GeV for $m_t = 175$ GeV [29].

Thorough reviews on SM and MSSM Higgs physics can be found in [28, 29, 68].

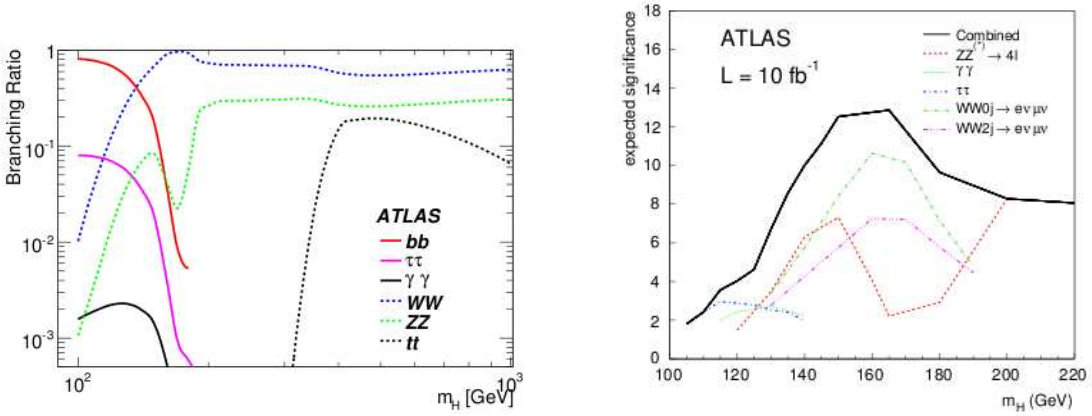

(a) (b)

Figure 6.2.: *(a) The main branching ratios for the Higgs decay in the SM in dependence of the Higgs mass. The color coding for the single decay channels is shown in the legend. (b) The expected significance of the combined channels in dependence of the Higgs mass for a luminosity of L=10 fb^{-1}. Both taken from [69].*

6.2. Higgs Decay

Since the existence of the Higgs boson has not been established experimentally, it is important to know its dominant decay channels. For the Higgs search it is necessary to examine these decay channels for different Higgs boson masses. The SM Higgs boson can directly decay into fermion pairs and massive gauge boson pairs (see Fig. 6.2).

The Higgs decay into bottom pairs $H \rightarrow b\bar{b}$ is the dominant decay mode for Higgs masses below the W^+W^- threshold ($m_H = 2m_W$). The second largest decay mode for light Higgs bosons is their decay into two τ leptons. In case the Higgs mass approaches and is above the W^+W^- threshold, the Higgs decays mainly into W pairs. Once the Z threshold opens up, the Higgs decays into these as well. Owing to the fact that the Zs are identical particles, the decay into Z pairs is a factor of two smaller than the one into W pairs. Below their thresholds, the decay into W or Z pairs can happen also, but with at least one W or Z-boson being virtual. The branching ratios for the decay into two electroweak gauge boson pairs then rises steeply towards their thresholds. For a very heavy Standard Model Higgs boson, starting around the top pair threshold, the decay into top quarks opens in addition to the decay into gauge bosons. But its branching ratio is smaller than the ones into gauge bosons.

For a Higgs boson with a mass larger than about 130 GeV, the main search channel for a discovery will be the decay of the Higgs boson into two W or Z bosons [69]. If the Higgs mass is smaller than about 130 GeV, the Higgs boson decays dominantly into $b\bar{b}$ pairs.

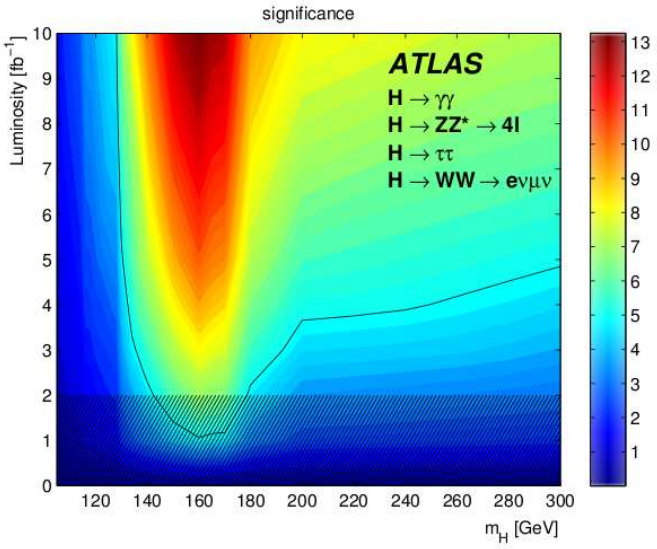

Figure 6.3.: *The significance vs. the Higgs mass for an integrated luminosity given in fb^{-1}. The black curve marks the 5σ discovery potential. Taken from [69].*

Since one will have a large QCD background of bottom quarks from other processes at the LHC one will not be able to distinguish the $b\bar{b}$ pairs from the Higgs decay and those from the QCD background. In this case one would have to look into the decay into two photons which possesses a small branching ratio of the order of 10^{-3} (see Fig. 6.2(a)). Already at leading order the decay into two photons is a loop induced Higgs decay. The Higgs decay into a photon and a Z boson is loop induced as well. Their branching ratios are rather small but provide a clean signal. The Higgs decay into two gluons is a one-loop process whose signature one would not be able to distinguish from the gluons from the QCD background.

Some combined Higgs decay channels are given in the significance plot in Fig. 6.3. The black curve reflects the 5σ discovery potential. The prospect for discovering a Higgs boson with a mass larger than about 120 GeV seems within reach. But the main concern might be a possibility of unobservability at the low mass end as displayed in Fig. 6.3.

In view of experimental limits some SUSY particles such as the charginos, neutralinos and possibly sleptons and the third generation of squarks could be light enough to give contributions in Higgs decays [29]. The contributions of these sparticles to the decay of the neutral Higgs bosons into the two photon or two gluon final state can be large and they can significantly alter the other decay modes through radiative corrections [29].

The decay channels described above are valid both for a Standard Model Higgs boson and the lightest MSSM Higgs boson h. For the pseudoscalar Higgs boson, the decay into WW

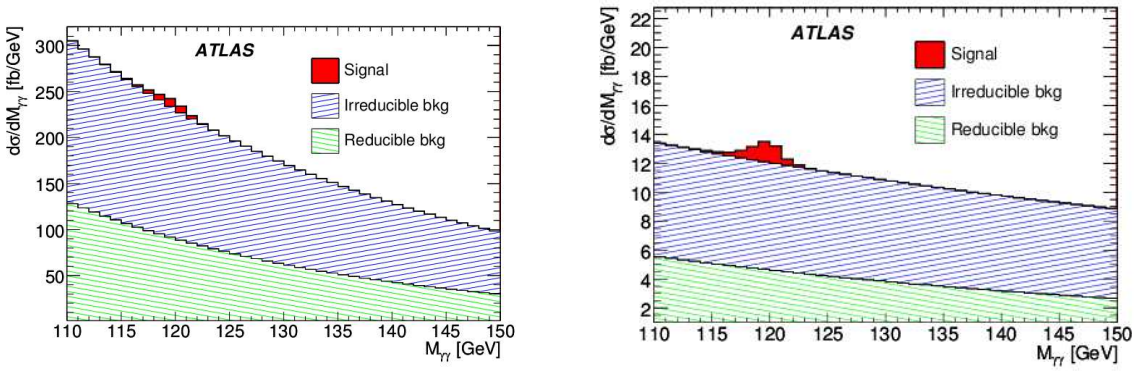

(a) (b)

Figure 6.4.: *The di-photon invariant mass spectrum in terms of cross sections in fb for a Higgs mass of 120 GeV. The contribution from various signal to background (bkg) processes are presented in stacked histograms. (a) Inclusive analysis (only the di-photon system) (b) beyond the inclusive analysis with one jet analysis. Taken from [69].*

and ZZ bosons does not exist.

In this thesis, the main focus will be on the decay of neutral MSSM Higgs bosons into two photons in NLO-SQCD.

6.3. $\phi \to \gamma\gamma$

One of the most important search channels for Higgs bosons of masses of up to $m_H \leq 130$ GeV is the decay into two photons ($H \to \gamma\gamma$). In spite of an expected large background one hopes for a clear signal on top of the background (Fig. 6.4(a),(b)) in case of the mass of the Higgs being in that range. Both figures display the cross sections in dependence of the invariant di-photon mass for a Higgs mass of 120 GeV. Fig. 6.4(a) is inclusive, i.e., one only looks at the di-photon system in the experiment and in 6.4(b) in addition one jet is required. The leading jet in the $gg \to Hj$ process tends to be more separated from the di-photon system than in background events [69]. Thus, taking the jet in addition to the di-photon system as the signal process, discriminates well the signal from the background. If one compares Fig. 6.4(a) with 6.4(b) the improvement of the signal/background ratio can be observed. By using distinctive features of different production mechanisms in addition to the inclusive analysis, one can enhance the signal to background ratio. The drawback is that the improved signal/background ratio comes with worse statistics and might be more sensitive to systematic uncertainties [69].

The so-called irreducible part of the background is generated mainly due to $q\overline{q} \to \gamma\gamma$ and $gg \to \gamma\gamma$. Irreducible contributions are the ones in which the background contains the

same particles in the final state as the signal process. A reducible part of the background is due to jets which are falsely detected as photons.

For a discovery of a Higgs boson with a mass less than about 130 GeV the decay channel into two photons has to be combined with all the other production channels or the $\tau\tau$ channel from the fusion of weak gauge bosons [69].

Status of the theoretical predictions

The status of the perturbative calculations for the decay of SM Higgs bosons into two photons will be briefly recollected. The LO decay rate was first presented in [70–72]. The references for the calculation of the two-loop QCD amplitudes are given in [68]. The general NLO-QCD result is known numerically [73, 74] and analytically [75, 76]. The NNLO-QCD effects are known only in the limit of large top masses [77]. The electroweak corrections have been evaluated in NLO as well [74]. For the decay of a pseudoscalar Higgs boson the NLO-electroweak corrections have been calculated in [78]. In our calculations the electroweak corrections will not be considered.

In this thesis we only calculate SQCD (supersymmetric QCD) corrections. If one performs the QCD calculation for a neutral, scalar MSSM Higgs boson h instead of a SM Higgs boson, one obtains an additional multiplicative factor $\cos\alpha/\sin\beta$ as the Feynman rule for the vertex $ht\bar{t}$ is modified in the MSSM (cf. App. C and Tab. 3.2). For the bottom contributions this corresponding factor is $-\sin\alpha/\cos\beta$ (cf. Tab. 3.2). α is the mixing angle in the Higgs sector and $\tan\beta = v_1/v_2$ is the ratio of the vacuum expectation values of the two Higgs doublets in the MSSM. The LO-MSSM Higgs decay into two photons is known for h and A. The references are given in [29]. The NLO-SQCD corrections to the photonic decay of light CP-even Higgs bosons in the limit of large top/stop and gluino masses have been derived in [79]. For the case of the decay of the lightest scalar MSSM Higgs bosons h with the inclusion of the supersymmetric partners of the bottom quarks, the sbottoms, the result is only known in leading order, which corresponds to a one loop calculation.

The aim of the presented work was to obtain the next-to-leading order corrections in SQCD to the process $h,\ A \to \gamma\gamma$ by not only including the top quark and its superpartners but also the bottom quark and its superpartners. The gluino, which is the massive superpartner of the gluon contributes to these corrections as well. For the pseudoscalar case in leading order no contribution due to supersymmetric particles exists, as the coupling of A to two squarks is non-diagonal in the two different squark flavors (cf. App. A). Those arise first one order higher. Here, we are interested in the NLO-SQCD corrections as well.

6.4. Projectors and d'Alembert Operators

We apply the projectors and d'Alembert operators described in this section both for the calculation of the amplitudes of the Higgs decaying into two photons and the Higgs being produced via the gluon fusion process. The calculation of the diagrams for the processes A and $h \to \gamma\gamma$ is done with the help of an expansion in the external momenta q_1 and q_2 of the photons. The result for the top contributions to the amplitude is an expansion in $m_h^2/(4m_t^2)$ with the Higgs mass m_h and the quark mass m_t. Its application to the MSSM calculation and the inclusion of the bottom quarks will be described at the end of this section.

The Lorentz structure of the amplitude of the decay of two on-shell photons with polarization vectors $\epsilon_\mu(q_1)$ and $\epsilon_\nu(q_2)$ into a CP-even Higgs boson is given by [77]

$$\mathcal{A}^{\mu\nu,h} = \sum_i A_i^{\mu\nu,h} = \sum_i \left(a_i^h q_1 q_2 g^{\mu\nu} + b_i^h q_1^\nu q_2^\mu + c_i^h q_1^\mu q_2^\nu\right) = (q_1 q_2 g^{\mu\nu} - q_1^\nu q_2^\mu) \sum_i a_i^h. \quad (6.1)$$

The sum runs over the number of diagrams which contribute to the given process.

Utilizing gauge invariance, i.e., $q_{1\mu} A^{\mu\nu,h} = 0$ and $q_{2\nu} A^{\mu\nu,h} = 0$ together with the fact that $q_1^2 = 0 = q_2^2$ for real photons, results in $\sum_i a_i^h = -\sum_i b_i^h$ and a vanishing coefficient $\sum_i c_i^h$. In order to have an additional check for the scalar parts of the amplitude, one can keep both, a_i^h and b_i^h. The projectors onto a_i^h and b_i^h possess the following properties [77]

$$a_i^h = \frac{A_i^{\mu\nu,h}}{(d-2)(q_1 q_2)^2} \left(q_1 q_2\, g_{\mu\nu} - q_{1\nu} q_{2\mu} - q_{1\mu} q_{2\nu}\right), \quad (6.2)$$

$$b_i^h = \frac{A_i^{\mu\nu,h}}{(d-2)(q_1 q_2)^2} \left(-q_1 q_2\, g_{\mu\nu} + q_{1\nu} q_{2\mu} + (d-1) q_{1\mu} q_{2\nu}\right).$$

They have been obtained by contracting Eq. (6.1) with $q_{1\mu} q_{2\nu}$, $q_{1\nu} q_{2\mu}$ and $g_{\mu\nu}$, where $g_{\mu\nu} g^{\mu\nu} = g_\mu^\mu = d$ in d dimensions.

These projectors are applied to simplify the calculation of Feynman diagrams contributing to the amplitude such that only scalar Feynman integrals have to be evaluated.

The amplitude for pseudoscalar Higgs bosons possesses a different Lorentz structure due to the CP properties of A:

$$\mathcal{A}^{\mu\nu,A} = \sum_i A_i^{\mu\nu,A} = \sum_i \left(\epsilon^{\mu\nu\alpha\beta} q_{1\alpha} q_{2\beta}\right) a_i^A.$$

The corresponding projector in this case is given by

$$a_i^A = -\frac{A_i^{\mu\nu,A}}{(d-2)(d-3)(q_1 q_2)^2} \epsilon_{\mu\nu\rho\sigma} q_1^\rho q_2^\sigma. \quad (6.3)$$

In connection with this projector we implement γ_5 as follows

$$\gamma_5 = \frac{i}{4!}\epsilon^{\mu\nu\rho\sigma}\gamma_\mu\gamma_\nu\gamma_\rho\gamma_\sigma. \tag{6.4}$$

As a test of the setup the projector given in [80] is implemented as well. The latter projector can be displayed as follows [80]

$$P^{\mu\nu\rho\sigma}_{\alpha\beta}(q_1,q_2) = q_1^{[\mu}q_2^{\nu}g_\alpha^{\rho}g_\beta^{\sigma]}. \tag{6.5}$$

The square brackets denote an anti-symmetrization in the Lorentz indices μ,ν,ρ and σ. In connection with this projector γ_5 is replaced with [80]

$$\gamma_5 \to \frac{i}{4!}\gamma^{[\mu}\gamma^{\nu}\gamma^{\rho}\gamma^{\sigma]}. \tag{6.6}$$

As expected, both projectors lead to the same results for the amplitude of a pseudoscalar Higgs boson decaying into two photons. Because the projector given in Eq. (6.3) is much more efficient with respect to running time if we are dealing with additional mass scales of supersymmetric particles in the diagrams, we mainly use that one.

Our observation is that we obtain the same results in the limit of large top masses for the QCD top contributions in the decay of two photons into a pseudoscalar Higgs boson if we use (a) the projector and γ_5 as given in Eqs. (6.5) and (6.6) and the finite counterterm $Z_5^p \neq 1$ (cf. Eq. (4.11)) [36] compared to the application of (b) the projector and γ_5 from Eqs. (6.3) and (6.4) together with $Z_5^p = 1$.

Since we are interested in a result which poses an expansion in m_ϕ, $\phi = h, A$, we will perform an expansion in the external photon momenta. If one performs a Taylor expansion in q_1 and q_2 for both h and A, the scalar part of the amplitude can be expressed by [77]

$$a_i^{h,A}(q_1,q_2) = \sum_{l,m,n=0}^{\infty} c_{lmn}^{i,h,A}\left(q_1^2\right)^l\left(q_2^2\right)^m(q_1q_2)^n. \tag{6.7}$$

Only the coefficients $c_{00n}^{i,h,A}$ contribute to the amplitude, as we calculate with photons or gluons on the mass shell, i.e., $q_1^2 = 0$ and $q_2^2 = 0$. In our calculations we always have $q_1q_2 = m_{h,A}^2/2$ since the Higgs is taken to be real. The $c_{00n}^{i,h,A}$ correspond to massive two-loop diagrams with vanishing external momenta.

By successively applying d'Alembert operators one obtains a system of equations, which is solved for $c_{00n}^{i,h,A}$. The d'Alembert operators are given by

$$\Box_{ij} = \frac{\partial^2}{\partial q_i^\mu \partial q_{j,\mu}}, \quad i,j = 1,2. \tag{6.8}$$

If one solves the system of equations, the solution for the coefficients is [77]

$$\begin{aligned}
c_{000}^{i,h,A} &= a_i^{h,A}, \\
c_{001}^{i,h,A} &= \frac{1}{d}\Box_{12} a_i^{h,A}, \\
c_{002}^{i,h,A} &= -\frac{1}{2(d-1)d(d+2)}\left(\Box_{11}\Box_{22} - d\,\Box_{12}^2\right) a_i^{h,A}, \\
c_{003}^{i,h,A} &= -\frac{1}{2(d-1)d(d+2)(d+4)}\left(\Box_{11}\Box_{22}\Box_{12} - \frac{1}{3}(d+2)\Box_{12}^3\right) a_i^{h,A}, \\
c_{004}^{i,h,A} &= \frac{1}{8(d-1)d(d+1)(d+2)(d+4)(d+6)} \\
&\quad \left(\Box_{11}^2\Box_{22}^2 - 2(d+2)\Box_{11}\Box_{22}\Box_{12}^2 + \frac{1}{3}(d+2)(d+4)\Box_{12}^4\right) a_i^{h,A}.
\end{aligned} \tag{6.9}$$

In addition, we employ $c_{005}^{i,h,A}$ and $c_{006}^{i,h,A}$.

All in all in the approximation in which $m_h^2 < 4m_t^2$, i.e., the limit of large top masses holds, the amplitude for the Higgs decay into two photons with only the contributions due to top quarks can be depicted as a series

$$\mathcal{A}^\phi(q_1,q_2) = c_0^\phi + c_1^\phi\left(\frac{m_\phi^2}{4m_t^2}\right) + c_2^\phi\left(\frac{m_\phi^2}{4m_t^2}\right)^2 + ...,$$

where we employed the convention $c_n^\phi \equiv \sum_i c_{00n}^{i,\phi}$, $q_1q_2 = m_\phi^2/2$ and $\phi = h,\, A$. By expanding in this manner, the calculation of the diagrams has been simplified in a way that one only has to deal with massive two-loop vacuum diagrams, i.e., ones where the external momenta vanish. In the supersymmetric two-loop calculation we performed, in addition to the top mass more massive scales occur. With the help of the vacuum diagrams one obtains the coefficient functions in dependence of the mass scales appearing in the diagrams, namely the top mass m_t, stop masses $m_{\tilde{t}_1}$, $m_{\tilde{t}_2}$ and the gluino mass $m_{\tilde{g}}$. Our aim is hence the determination of

$$c_n^{h,A} = c_n^{h,A}\left(m_t, m_{\tilde{t}_1}, m_{\tilde{t}_2}, m_{\tilde{g}}\right).$$

We apply the method of asymptotic expansions described in chapter 5 for calculating the Higgs production and decay amplitudes. In case one is just interested in contributions due to top quarks and their superpartners, these can all be assumed to be much larger than the Higgs mass so the method with the application of the d'Alembert operators can be applied. As a result the amplitude is an expansion in powers of m_h^2.

If we seek to include bottom quarks and their superpartners into the two-loop calculation the assumption that the quark mass is larger than the Higgs mass is not valid. In this calculation we perform asymptotic expansions in a certain hierarchy among the massive scales. To each Feynman diagram thus several subdiagrams contribute which have to be

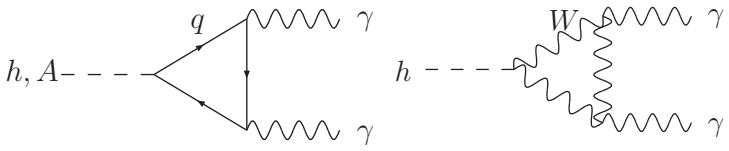

Figure 6.5.: *The Feynman diagrams in leading order of the photonic Higgs decay.*

calculated separately and summed up in the end. We only apply the d'Alembert operators in subdiagrams in which no new routines occur and obtain an expansion in ratios of the Higgs mass and the large supersymmetric mass scales that are the two sbottom masses and the gluino mass. In the cases where we deal with a bottom one-loop subdiagram we keep the external momenta in those diagrams non-zero and explicitly evaluate those one-loop diagrams.

To conclude, in our SQCD calculations we apply a mixture of applying d'Alembert operators which corresponds to calculating massive vacuum diagrams and of keeping the external momenta of one-loop quark subdiagrams non-zero. The projectors given in Eqs. (6.2) and (6.3) for the decay of scalar respective pseudoscalar Higgs bosons into two photons are always applied to each Feynman diagram to free them of the tensor structure and to be able to deal just with scalar integrals.

6.5. LO and NLO-(S)QCD Results

In the following section the decay of a Higgs boson into two photons, $\phi \to \gamma\gamma$, is investigated. As massless photons do not couple directly to Higgs bosons, this process is already at leading order in perturbation theory a one-loop process. In the SM either a fermion or charged W-bosons mediates the coupling of Higgs bosons to photons. We will not go into detail considering insertions of weak gauge bosons in the loops and higher order corrections of those which are electroweak corrections. We are just interested in the QCD parts of the amplitude. Fig. 6.5 displays the corresponding Feynman diagrams.

The cases where $\phi = h$ or A is a MSSM Higgs boson will be examined. Fermions couple proportional to their mass to Higgs bosons. If one considers the decay of a Standard Model Higgs boson, the dominant fermion contribution originates from the top quark. In the MSSM however, the Yukawa couplings are modified to be

$$g_t^h = \frac{\cos\alpha}{\sin\beta}, \quad g_b^h = -\frac{\sin\alpha}{\cos\beta},$$
$$g_t^A = \cot\beta, \quad g_b^A = \tan\beta.$$

Thus, for large $\tan\beta$ the effects through bottom quarks cannot be neglected in the MSSM.

The aim of this thesis is to include the two-loop MSSM corrections which contain the superpartners of the bottoms, the sbottoms in order to obtain an estimate of how large

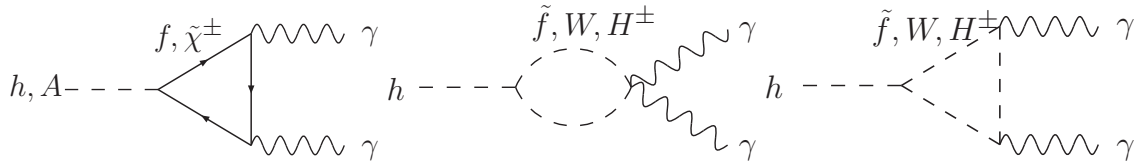

Figure 6.6.: *The LO Feynman diagrams which contribute to the decay of scalar and pseudoscalar Higgs bosons into two photons in the MSSM are displayed.*

their effects are. The two-loop QCD-corrections can be taken from the literature [76]. In spite of only considering MSSM Higgs bosons h and A and of the non-existence of a CP-odd Higgs boson in the SM, pure quark and gluon contributions, i.e., contributions from SM particles in the loops will be referred to as "QCD-" or "SM parts". For the decay of pseudoscalar Higgs bosons into two photons the leading order does not change when taking into account MSSM particles. The supersymmetric particles only supply a contribution in NLO. Contrary to the pseudoscalar case, in the decay of scalar Higgs bosons into two photons already at leading order we get shares due to supersymmetric particles (cf. Fig. 6.6).

By considering SQCD, which means that one is interested in an expansion in the coupling of the strong force α_s, contributions of quarks as well as their superpartners, the squarks have to be considered. As mentioned above, the Yukawa couplings in the MSSM are modified. That is why we take into account the top quarks as well as the bottom quarks as well as their superpartners. This means the introduction of two additional massive scales for each quark into the calculation in leading order coming from the two different masses of the squarks. Each Standard Model degree of freedom gets assigned a superpartner, that is why left and right-handed quarks obtain one massive superpartner each. The mass eigenstates of the squarks are denoted by $\tilde{q_1}$ and $\tilde{q_2}$. In leading order only one species of squarks, $\tilde{q_1}$ or $\tilde{q_2}$ can propagate in the loop at a time, as the photon cannot convert them. In case only the top quark is taken into account at leading order, the left Feynman diagram of Fig. 6.5 has to be evaluated. This triangle diagram exists for the squarks as well. There is an additional diagram which includes a four vertex where two squarks couple to the two photons. This coupling does not exist for quarks. The Standard Model and MSSM contributions are displayed in Figs. 6.5 and 6.6 respectively.

For completeness we cite the entire supersymmetric leading order contributions to the partial decay widths for $\phi \to \gamma\gamma$. These are given by [81]

$$\Gamma\left(h \to \gamma\gamma\right) = \frac{G_F \alpha^2 m_h^3}{128\sqrt{2}\pi^3} \Bigg| \sum_f N_{c,f} Q_f^2 g_f^h H_f\left(\tau_f\right) + g_W^h H_W^h\left(\tau_W\right) + g_{H^\pm}^h H_{H^\pm}\left(\tau_{H^\pm}\right) + \sum_{\tilde{\chi}^\pm} g_{\tilde{\chi}^\pm}^h H_{\tilde{\chi}^\pm}\left(\tau_{\tilde{\chi}^\pm}\right) + \sum_{\tilde{f}} N_{c,\tilde{f}} Q_{\tilde{f}}^2 g_{\tilde{f}}^h H_{\tilde{f}}\left(\tau_{\tilde{f}}\right) \Bigg|^2 ,$$

$$\Gamma\left(A \to \gamma\gamma\right) = \frac{G_F \alpha^2 m_A^3}{128\sqrt{2}\pi^3} \left| \sum_f N_{c,f} Q_f^2 g_f^A A_f\left(\tau_f\right) + \sum_{\tilde{\chi}^\pm} g_{\tilde{\chi}^\pm}^h A_{\tilde{\chi}^\pm}\left(\tau_{\tilde{\chi}^\pm}\right) \right|^2 ,$$

with the form factors

$$\begin{aligned} H_{f,\tilde{\chi}^\pm}\left(\tau\right) &= 2\tau\left[1 + \left(1-\tau\right) f(\tau)\right], \\ H_{\tilde{f},H^\pm}\left(\tau\right) &= -\tau\left[1 - \tau f(\tau)\right], \\ H_W\left(\tau\right) &= -\left[2 + 3\tau + 3\tau\left(2-\tau\right) f(\tau)\right], \\ A_{f,\tilde{\chi}^\pm}\left(\tau\right) &= 2\tau f(\tau). \end{aligned} \tag{6.10}$$

The function f has the shape

$$f(\tau) = \begin{cases} \arcsin^2 \frac{1}{\sqrt{\tau}} & , \tau \geq 1 \\ -\frac{1}{4}\left(\ln \frac{1+\sqrt{1-\tau}}{1-\sqrt{1-\tau}} - i\pi\right)^2 & , \tau < 1 \end{cases}$$

Here, $\tau_X = 4m_X^2/m_\phi^2$ with the mass m_X of particle X and $\phi = h, A$. The labels $H^\pm$ denote the charged Higgs bosons, f fermions, $\tilde{f}$ sfermions, $\tilde{\chi}^\pm$ charginos and W gauge bosons. $g_X^{h,A}$ are their respective dimensionless couplings to h and A bosons. The electric charge of the fermion (sfermion) is denoted Q_f ($Q_{\tilde{f}}$). For the decay of scalar Higgs bosons into two photons the contribution due to W bosons is dominant over the one due to fermions. For $\tau \to 0$ one obtains $H_W^h \to -7$ in contrast to $H_f^h \to \frac{4}{3}$ and $H_{\tilde{f}}^h \to \frac{1}{3}$.

In our calculations however, we exclusively consider the QCD and SQCD part including the third family of quarks and squarks given by

$$\boxed{\Gamma\left(h \to \gamma\gamma\right) = \frac{G_F \alpha^2 m_h^3}{128\sqrt{2}\pi^3} \left| \sum_{q=t,b} N_c Q_q^2 g_q^h H_q\left(\tau_q\right) + \sum_{\tilde{q}=\tilde{t}_1,\tilde{t}_2,\tilde{b}_1,\tilde{b}_2} N_c Q_{\tilde{q}}^2 g_{\tilde{q}}^h H_{\tilde{q}}\left(\tau_{\tilde{q}}\right) \right|^2} \tag{6.11}$$

and for the pseudoscalar Higgs boson we have

$$\boxed{\Gamma\left(A \to \gamma\gamma\right) = \frac{G_F \alpha^2 m_A^3}{128\sqrt{2}\pi^3} \left| \sum_{q=t,b} N_c Q_q^2 g_q^A A_q\left(\tau_q\right) \right|^2 .} \tag{6.12}$$

The charges $Q_{\tilde{q}}$ of the squarks are the same as for the respective quarks. For the top quark we have $Q_t = 2/3$ and for the bottom quark the electric charge is $Q_b = -1/3$. $N_c = 3$ is the number of colors and α is the fine-structure constant. The Fermi constant G_F is related to the vacuum expectation values of the Higgs fields via $v = \sqrt{v_1^2 + v_2^2} = 1/\sqrt{\sqrt{2} G_F}$.

The amplitude $\mathcal{H}\left(h \to \gamma\gamma\right)$ for the scalar Higgs decay will be defined as

$$\mathcal{H}\left(h \to \gamma\gamma\right) = \sum_{q\tilde{q}=t\tilde{t},b\tilde{b}} Q_q^2\, \mathcal{H}_{q\tilde{q}} = \sum_{q\tilde{q}} Q_q^2 \left(\mathcal{H}_{q\tilde{q}}^{(0)} + \frac{\alpha_s}{\pi}\mathcal{H}_{q\tilde{q}}^{(1)}\right) + \mathcal{O}\left(\alpha_s^2\right), \tag{6.13}$$

with

$$\mathcal{H}_{q\tilde{q}} = \mathcal{H}_q^{(0)} + \mathcal{H}_{\tilde{q}}^{(0)} + \frac{\alpha_s}{\pi}\left(\mathcal{H}_q^{(1)} + \mathcal{H}_{susy}^{(1)}\right) + \mathcal{O}\left(\alpha_s^2\right), \tag{6.14}$$

where $\mathcal{H}_q^{(0)} \equiv g_q^h H_q$ and $\mathcal{H}_{\tilde{q}}^{(0)} \equiv g_{\tilde{q}}^h H_{\tilde{q}}$ with the form factors H_q, $H_{\tilde{q}}$ given in Eq. (6.10). $\mathcal{H}_{q\tilde{q}}^{(0)}$ and $\mathcal{H}_{q\tilde{q}}^{(1)}$ denote the one- and two-loop SQCD contributions respectively.
In case only QCD contributions are considered, the amplitude is denoted by

$$\mathcal{H}\left(h \to \gamma\gamma\right) = \sum_{q=t,b} Q_q^2\, \mathcal{H}_q = \sum_q Q_q^2 \left(\mathcal{H}_q^{(0)} + \frac{\alpha_s}{\pi}\mathcal{H}_q^{(1)}\right) + \mathcal{O}\left(\alpha_s^2\right).$$

Similarly, the amplitude $\mathcal{A}\left(A \to \gamma\gamma\right)$ for the decay of pseudoscalar Higgs bosons is modified if higher order contributions are accounted for

$$\mathcal{A}\left(A \to \gamma\gamma\right) = \sum_{q\tilde{q}=t\tilde{t},b\tilde{b}} Q_q^2\, \mathcal{A}_{q\tilde{q}} = \sum_{q\tilde{q}} Q_q^2 \left(\mathcal{A}_{q\tilde{q}}^{(0)} + \frac{\alpha_s}{\pi}\mathcal{A}_{q\tilde{q}}^{(1)}\right) + \mathcal{O}\left(\alpha_s^2\right), \tag{6.15}$$

with

$$\mathcal{A}_{q\tilde{q}} = \mathcal{A}_q^{(0)} + \frac{\alpha_s}{\pi}\left(\mathcal{A}_q^{(1)} + \mathcal{A}_{susy}^{(1)}\right) + \mathcal{O}\left(\alpha_s^2\right), \tag{6.16}$$

where $\mathcal{A}_q^{(0)} \equiv g_q^A A_q$ and A_q from Eq. (6.10). In case only QCD corrections are referred to, the amplitude is written as

$$\mathcal{A}\left(A \to \gamma\gamma\right) = \sum_{q=t,b} Q_q^2\, \mathcal{A}_q = \sum_q Q_q^2 \left(\mathcal{A}_q^{(0)} + \frac{\alpha_s}{\pi}\mathcal{A}_q^{(1)}\right) + \mathcal{O}\left(\alpha_s^2\right).$$

The particle content of $\mathcal{H}_{susy}^{(1)}$ and $\mathcal{A}_{susy}^{(1)}$ will be specified in the next section.
In next-to leading order in QCD the diagrams to calculate are the ones where a gluon line is inserted into the leading order quark loop. Two example diagrams are shown in Fig. 6.7. There is no contribution from real gluon emission at that order in perturbation theory due to color conservation since the initial as well as final state are colorless. As a reminder, we present the results for NLO-QCD amplitudes for both the decay of scalar and pseudoscalar Higgs bosons into two photons for the top as well as for the bottom contributions. We display them as an expansion in the parameters

$$\tau = m_\phi^2/(4m_t^2) \qquad \text{and} \qquad \tau_b = 4m_b^2/m_\phi^2. \tag{6.17}$$

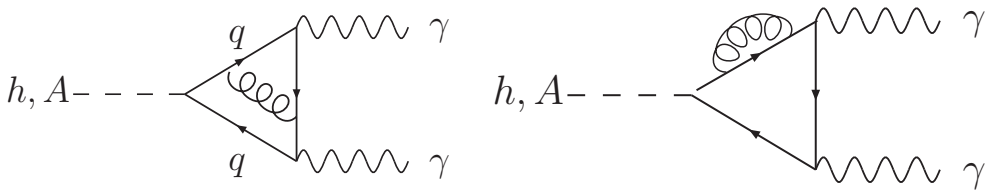

Figure 6.7.: *The Feynman diagram contributing to the NLO-QCD of the photonic Higgs decay.*

The on-shell result for the top contributions to the amplitude $h \to \gamma\gamma$ reads [77]

$$\begin{aligned}\mathcal{H}_t = &\frac{\cos\alpha}{\sin\beta}\left(1+\frac{7}{30}\tau+\frac{2}{21}\tau^2+\frac{26}{525}\tau^3+\frac{512}{17325}\tau^4+\mathcal{O}\left(\tau^5\right)\right)\\ &+\left(\frac{\alpha_s}{\pi}\right)\frac{\cos\alpha}{\sin\beta}\left(-1+\frac{122}{135}\tau+\frac{8864}{14175}\tau^2+\frac{209186}{496125}\tau^3+\frac{696616}{2338875}\tau^4+\mathcal{O}\left(\tau^5\right)\right).\end{aligned} \tag{6.18}$$

We take the on-shell result for the NLO contributions of bottom quarks from [76] and expand it in the parameter τ_b as follows

$$\begin{aligned}\mathcal{H}_b = &\frac{\sin\alpha}{\cos\beta}\left[\frac{3}{8}\left(L_{bh}^2-4\right)\tau_b+\frac{3}{8}\left(-L_{bh}^2+L_{bh}\right)\tau_b^2+\left(\frac{3}{32}-\frac{15L_{bh}}{64}\right)\tau_b^3\right.\\ &\left.+\left(-\frac{L_{bh}}{16}-\frac{3}{128}\right)\tau_b^4+\mathcal{O}\left(\tau_b^5\right)\right]+\left(\frac{\alpha_s}{\pi}\right)\frac{\sin\alpha}{\cos\beta}\left[\left(-\frac{L_{bh}^4}{48}+\frac{L_{bh}^3}{4}\right.\right.\\ &\left.-\frac{\pi^2L_{bh}^2}{6}+\left(-4\zeta(3)-\frac{\pi^2}{6}-3\right)L_{bh}+\zeta(3)-\frac{\pi^4}{20}-5\right)\tau_b+\left(\frac{L_{bh}^4}{48}\right.\\ &\left.-\frac{3L_{bh}^3}{4}+\left(\frac{\pi^2}{6}+\frac{5}{8}\right)L_{bh}^2+(4\zeta(3)+1)L_{bh}+\zeta(3)+\frac{\pi^4}{20}-\frac{\pi^2}{12}-4\right)\tau_b^2\\ &+\left(-\frac{L_{bh}^4}{384}+\frac{23L_{bh}^3}{192}+\left(-\frac{\pi^2}{48}-\frac{143}{128}\right)L_{bh}^2+\left(-\frac{1}{2}\zeta(3)+\frac{5\pi^2}{48}+\frac{15}{32}\right)L_{bh}\right.\\ &\left.\left.+\frac{5\zeta(3)}{4}-\frac{\pi^4}{160}+\frac{\pi^2}{96}+\frac{467}{256}\right)\tau_b^3+\left(\frac{5L_{bh}^3}{288}-\frac{7L_{bh}^2}{64}+\left(\frac{\pi^2}{144}-\frac{727}{1152}\right)L_{bh}\right.\right.\\ &\left.\left.+\frac{\zeta(3)}{12}+\frac{7\pi^2}{288}+\frac{1103}{1728}\right)\tau_b^4+\mathcal{O}\left(\tau_b^5\right)\right].\end{aligned}$$

with $L_{bh} = \ln(\tau_b/4) + i\pi$, τ_b and τ taken as in Eq. (6.17) and $\phi = h$.

The amplitude of $A \to \gamma\gamma$ through NLO-QCD in the on-shell scheme is [76]

$$\begin{aligned}\mathcal{A}_t = &\cot\beta\left(1+\frac{1}{3}\tau+\frac{8}{45}\tau^2+\frac{4}{35}\tau^3+\frac{128}{1575}\tau^4+\mathcal{O}\left(\tau^5\right)\right)\\ &+\left(\frac{\alpha_s}{\pi}\right)\cot\beta\left(\frac{16}{9}\tau+\frac{68}{45}\tau^2+\frac{53012}{42525}\tau^3+\frac{34712}{33075}\tau^4+\mathcal{O}\left(\tau^5\right)\right).\end{aligned} \tag{6.19}$$

Again, the corresponding on-shell result for the bottom quark contributions is taken from [76] and expanded in τ_b

$$\begin{aligned}
\mathcal{A}_b = \tan\beta \Bigg[& -\frac{L_{bA}^2 \tau_b}{4} - \frac{L_{bA}\tau_b^2}{4} + \left(-\frac{3L_{bA}}{32} - \frac{1}{16}\right)\tau_b^3 + \left(-\frac{5L_{bA}}{96} - \frac{3}{64}\right)\tau_b^4 \Bigg] + \mathcal{O}\left(\tau_b^5\right) \\
& + \left(\frac{\alpha_s}{\pi}\right)\tan\beta \Bigg[\left(\frac{L_{bA}^4}{72} - \frac{L_{bA}^3}{6} + \frac{\pi^2 L_{bA}^2}{9} + \left(\frac{8}{3}\zeta(3) + \frac{\pi^2}{9}\right) L_{bA} - \frac{2\zeta(3)}{3} + \frac{\pi^4}{30}\right)\tau_b \\
& + \left(\frac{L_{bA}^3}{9} - \frac{11 L_{bA}^2}{12} + \left(\frac{\pi^2}{9} + \frac{1}{3}\right) L_{bA} + \frac{4\zeta(3)}{3} + \frac{\pi^2}{18} + \frac{5}{3}\right)\tau_b^2 + \left(\frac{L_{bA}^4}{576} + \frac{L_{bA}^3}{32}\right. \\
& + \left(\frac{\pi^2}{72} - \frac{11}{64}\right) L_{bA}^2 + \left(\frac{1}{3}\zeta(3) + \frac{\pi^2}{24} - \frac{43}{48}\right) L_{bA} + \frac{\zeta(3)}{2} + \frac{\pi^4}{240} + \frac{7\pi^2}{144} + \frac{159}{128}\Bigg)\tau_b^3 \\
& + \left(\frac{L_{bA}^4}{576} + \frac{17 L_{bA}^3}{864} + \left(\frac{\pi^2}{72} - \frac{19}{192}\right) L_{bA}^2 + \left(\frac{1}{3}\zeta(3) + \frac{\pi^2}{27} - \frac{1145}{1728}\right) L_{bA}\right. \\
& \left. + \frac{4\zeta(3)}{9} + \frac{\pi^4}{240} + \frac{7\pi^2}{216} + \frac{8035}{10368}\right)\tau_b^4 + \mathcal{O}\left(\tau_b^5\right) \Bigg],
\end{aligned}$$

with $L_{bA} = \ln(\tau_b/4) + i\pi$, τ_b and τ as defined in Eq. (6.17) and $\phi = A$.

As a test of our setup of the programs we reproduce known results for the top quarks as an expansion in τ which corresponds to the limit of large top masses. In order to obtain the amplitude we calculate the two-loop QCD diagrams with the help of the projectors and the application of the d'Alembert operators described in Sec. 6.4. Furthermore, the top mass has to be renormalized. Its on-shell counterterm is given in Eq. (B.1) in App. B.

The next step is then to augment the calculation by the effects of the MSSM partners of the quarks, the squarks and the gluino to the photonic Higgs decay.

6.6. Diagrams in NLO-SQCD for $\phi \to \gamma\gamma$

In the following, characteristic Feynman diagrams contributing to the partial decay width of scalar and pseudoscalar Higgs bosons into two photons are exemplified.

From now on by "top sector" or "top case" we term the contributions generated by top quarks, top squarks and gluinos and analogous "bottom sector" or "bottom case" refers to the contributions generated by bottom quarks, sbottom squarks and gluinos.

For the scalar case there are $\mathcal{O}(300)$ and for the pseudoscalar Higgs decay $\mathcal{O}(100)$ diagrams for the top sector and the same amount of diagrams for the bottom sector.

The contributing diagrams can be categorized according to

1. pure quark contributions (SM- or QCD contributions) (Fig. 6.8(a), 6.8(b))
2. mixed quark-squark-gluino contributions ($q\tilde{g}$ contributions) (Fig. 6.8(c)-6.8(e))
3. pure squark contributions ($\tilde{q}$ contributions) (Fig. 6.8(f), 6.8(g))

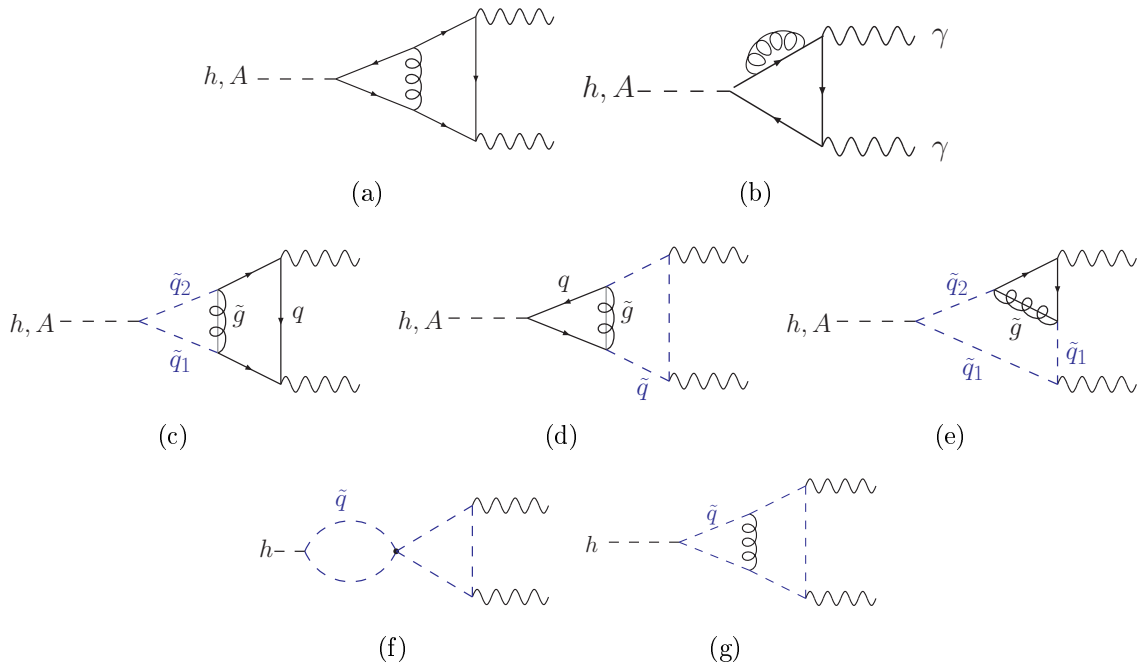

Figure 6.8.: *NLO-SQCD contributions to the decay of Higgs bosons into two photons: (a),(b): pure quark contributions; (c)-(e): mixed quark-squark-gluino contributions; (f),(g): pure squark contributions.*

The $q\tilde{g}$ and $\tilde{q}$ contributions together constitute what we call "SUSY" contributions to the given process. For the decay of scalar Higgs bosons in NLO-SQCD more diagrams exist because of the diagonal couplings of $h\tilde{q}_i\tilde{q}_i$. With this information on the two-loop contributions in SQCD we can further specify the amplitude in the notation introduced in Eqs. (6.13) and (6.14)

$$\mathcal{H}^{(1)}_{susy} = \mathcal{H}^{(1)}_{\tilde{q}} + \mathcal{H}^{(1)}_{q\tilde{g}}.$$

Thus, the supersymmetric part of the amplitude for the photonic decay of scalar Higgs bosons contains diagrams that only have pure squark (label $\tilde{q}$) insertions and diagrams that contain a gluino besides the quark and squark lines (label $q\tilde{g}$). Again, if the contributions to the amplitude are labeled with $q\tilde{q}$ the entire contributions are meant, if the label is $\tilde{q}$ (q) only the squarks (quarks) are included and with the label $q\tilde{g}$ we denote the contributions that contain a gluino as an internal particle. The gluino parts have an additional quark label (q) to further specify if we mean contributions from top quarks and top squarks in connection with the gluino or from bottom quarks and bottom squarks. Analogously, the two-loop part of the amplitude for the pseudoscalar case (cf. Eqs. (6.15) and (6.16)) is

expressed by

$$\mathcal{A}^{(1)}_{susy} = \mathcal{A}^{(1)}_{q\tilde{g}}.$$

6.7. Determination of the New Contributions

In both calculations, i.e., the scalar as well as pseudoscalar Higgs decay into two photons, the projectors given in Sec. 6.4 are applied. In the decay of pseudoscalar Higgs bosons, the coupling $Aq\overline{q} \sim \gamma_5$ occurs. Therefore, the antisymmetric projector of Eq. (6.3) or (6.5) in combination with the assigned implementation of γ_5 are applied in evaluating the diagrams. For the scalar case, the projector is given in Eq. (6.2). After the application of the projectors, one is left with a scalar structure and thus with scalar Feynman integrals to be evaluated.

Those are evaluated with the help of the method of asymptotic expansions according to the chosen hierarchy among the massive particles appearing in the Feynman diagrams. The massive scales are $m_q, m_{\tilde{q}_1}, m_{\tilde{q}_2}$ and $m_{\tilde{g}}$, where $q\tilde{q} = t\tilde{t},\ b\tilde{b}$. The asymptotically expanded diagrams contain several subdiagrams (cf. Eqs. (5.1) and (5.2)). If a subdiagram contains a quark subloop, this is evaluated with the help of the newly implemented one-loop routines described in Sec. 5.4. The other subloop is a one-loop tadpole which can be evaluated with MATAD. If a new routine is applied to a subloop, the external momenta are kept and the d'Alembert operators are not applied. In case a subdiagram is a two-loop tadpole diagram or a product of two one-loop tadpoles, the d'Alembert operators are applied as described in Eqs. (6.7)-(6.9) and the result is an expansion in ratios of m_ϕ^2/M_s^2 with the appearing heavy SUSY mass scales M_s.

The new routines which were originally designed for the inclusion of the bottom quark effects can of course be applied to the top quark subloops as well. We do that in order to push the validity of the top contributions to a higher energy scale. If the large top limit is applied, the result is valid for $m_\phi^2 < 4m_t^2$. Applying the new routines to the top sector in addition, the result is valid for $M_s^2 > m_\phi^2 > 4m_t^2$.

After the calculation of the diagrams as described above, the amplitude has to be renormalized.

6.7.1. Renormalization of the New Contributions

As we only calculate the contributions which contain at least one supersymmetric particle in the loop, i.e., squark or gluino, we have to make sure to obtain a finite result for them and to adjust the renormalization procedure. The pure QCD parts of the two-loop amplitude are taken from [76].

Parts of the amplitude which include at least one supersymmetric scale in the loop will be referred to as "SUSY parts". In the end, we have to make sure to add the QCD part and our SUSY part consistently together to obtain the full SQCD result.

By calculating only the SUSY parts of the amplitude, the counterterms have to be modified in comparison to the calculation in the full theory. The mass counterterms of the quarks and their superpartners are known [82] and explicitly given in App. B.

For both, the decay of scalar and pseudoscalar Higgs bosons, the quark mass has to be renormalized. The application of the new routines leads to amplitudes which depend on functions F of Feynman integrals. Those depend on the quark and Higgs mass, i.e., $F = F(m_q, m_\phi)$. We renormalize those functions in the following manner

$$F(m_q, m_\phi) = F(m_b, m_\phi) + \delta Z_{m_q} m_q F'(m_q, m_\phi) + \mathcal{O}(\delta Z_{m_q}^2).$$

F' denotes the derivative of F with respect to the quark mass m_q. At next-to-leading order, the Higgs mass is not renormalized.

For the pseudoscalar case, the result obtained by just taking the pure SUSY contributions in NLO and taking the MSSM counterterm for the quark mass, is not finite. Therefore, the counterterm for the quark mass has to be modified in a way that the difference between the MSSM counterterm and the QCD counterterm is applied to render a finite result. The bare quark mass is related to the renormalized one by $m_q^B = Z_{m_q} m_q = \left(1 + \delta Z_{m_q}\right) m_q$. The renormalization constant utilized for the quark mass renormalization is given by

$$\delta Z_{m_q,susy} = \delta Z_{m_q,\mathrm{MSSM}} - \delta Z_{m_q,\mathrm{QCD}}.$$

This formula is employed in DRED as well as DREG. In detail it reads

$$\begin{aligned}
\delta Z_{m_q,susy}^{\mathrm{DRED}} &= \delta Z_{m_q,\mathrm{MSSM}}^{\mathrm{DRED}} - \delta Z_{m_q,\mathrm{QCD}}^{\mathrm{DRED}} \\
\delta Z_{m_q,susy}^{\mathrm{DREG}} &= \delta Z_{m_q,\mathrm{MSSM}}^{DREG} - \delta Z_{m_q,\mathrm{QCD}}^{\mathrm{DREG}}
\end{aligned}$$

The counterterms are given in App. B. By taking the respective on-shell counterterms for the quark masses in DREG and DRED, both results agree in the on-shell scheme as required.

Moreover, an additional check of this subtraction in the quark mass counterterm for the renormalization of the SUSY parts is testing it in the limit of large top masses. In that limit we can always calculate the complete NLO result for the top sector that includes the two-loop QCD contributions of top quarks. This is a check of the calculation in which we employ modified counterterms. For the comparison of the new results for the top case with the result in the limit of large top masses, we expand it in the parameter $m_\phi^2/(2m_t^2)$ and find agreement.

For the process $h \to \gamma\gamma$, the renormalization is modified, due to the appearance of squark effects already at LO. Again, we calculate all the diagrams except for the pure QCD ones at two-loop level. Here, the squark masses and the squark-mixing angle are renormalized with the complete MSSM counterterms given in appendix B. For the renormalization of the quark mass we again subtract the pure QCD quark mass counterterm from the MSSM one. The only exception is the Higgs-squark-squark coupling. Since the $h\tilde{q}\tilde{q}$ coupling is

purely supersymmetric, the complete MSSM quark mass counterterm has to be employed in case this coupling is present.

No matter what limiting case is calculated with the method of asymptotic expansions and which SUSY scales are set equal (e.g. $m_{\tilde{q}_1} = m_{\tilde{q}_2}$), the complete LO MSSM result has to be taken into account. In particular, this means that the full dependence of $m_{\tilde{q}_1}$ and $m_{\tilde{q}_2}$ has to be included and both squark masses and the mixing angle $\theta_{\tilde{q}}$ have to be renormalized. Only after the renormalization of the LO result that contains the full mass dependence, one finally sets the scales according to the NLO part (e.g. $m_{\tilde{q}_1} = m_{\tilde{q}_2}$). Taking the limit at the LO before the renormalization, the result will not be finite.

The transition from $\overline{DR}$ to $\overline{MS}$ is given by [83]

$$\alpha_s^{\overline{DR}} = \alpha_s^{\overline{MS}} \left(1 + \frac{\alpha_s^{\overline{MS}}}{4\pi} + \mathcal{O}\left((\alpha_s^{\overline{MS}})^2 \right) \right). \tag{6.20}$$

This finite shift does not affect the results in NLO-SQCD as α_s is not renormalized. Therefore, this shift does not contribute to the NLO amplitude but one order higher. Thus, in the final result, $\alpha_s^{\overline{DR}}$ and $\alpha_s^{\overline{MS}}$ can be interchanged, depending on whether one is interested in the $\overline{DR}$ or $\overline{MS}$ result.

6.7.2. Correct Decoupling of the Contributions

An important check for the finite SUSY parts of the two-loop amplitude is that the result decouples in the sense that these vanish in the limit in which the couplings are fixed and the masses of the SUSY particles tend to infinity. In this limit, according to the decoupling theorem of Appelquist and Carazzone [84], the QCD result should be reproduced.

To clarify this limit with formulae, the on-shell results for the expansion up to $\mathcal{O}(\tau = m_\phi^2/(4m_t)^2)$ in the limit of large top and SUSY masses will be given explicitly for the limiting case where $m_t \ll M_s = m_{\tilde{t}_1} = m_{\tilde{t}_2} = m_{\tilde{g}}$.

For $\underline{A \to \gamma\gamma}$ this limit reads

$$\begin{aligned}
\mathcal{A}_{t\tilde{t}} &= \cot\beta \left[1 + \frac{1}{3}\tau + \frac{\alpha_s}{\pi}\tau \left[\tilde{q} \left(\frac{4}{9} - \frac{2}{9}l + \frac{2}{9}\ln\left(\frac{\mu^2}{M_s^2} \right) - \frac{2}{9} B_0^{fin}\left(m_t^2, M_s, M_s \right) l \right) \right.\right. \\
&\quad \left.\left. + q \left(\frac{14}{9} + \frac{2}{9} d_r \right) \right] + \mathcal{O}\left(\frac{1}{M_s} \right) \right] + \mathcal{O}\left(\tau^2 \right) \\
&= \cot\beta \left[1 + \frac{1}{3}\tau + \frac{\alpha_s}{\pi}\tau \left[\tilde{q} \left(\frac{4}{9} - \frac{2}{9}l \right) + q \left(\frac{14}{9} + \frac{2}{9} d_r \right) + \mathcal{O}\left(\frac{1}{M_s} \right) \right] \right] + \mathcal{O}\left(\tau^2 \right).
\end{aligned}$$

In the above formula we introduced labels $\tilde{q}$ and q ($q = 1$) to distinguish the SUSY parts from the QCD parts. From the results we can read off that in the QCD case ($\tilde{q} = 0$) in NLO only terms proportional to $q = 1$ occur. With l ($l = 1$) we denote the part which originates from the renormalization of the LO. We set $d_r = 1$, as we perform the calculation

in DREG in the pure QCD calculation. The coefficient of τ is therefore 16/9 as required (cf. Eq. (6.19)). By considering the SUSY case ($\tilde{q} = 1$), $d_r = 0$ in DRED, the QCD part then only provides for $(14/9)\tau$ and the $(4/9 - (2/9)\, l)\tau = (2/9)\, \tau$ that counts to the QCD limit which originate from the SUSY diagrams in NLO and the part which comes from the SUSY top mass renormalization of the LO. The term $\ln(\mu^2/M_s^2)$ cancels against the finite part of the MSSM top mass counterterm $B_0^{fin}(m_t^2, M_s, M_s) = \ln(\mu^2/M_s^2) + \mathcal{O}(1/M_s)$.

Therefore, in the limit of large SUSY masses working in DRED we obtain the on-shell QCD result of $(16/9)\, \tau$ as required. This non-trivial interplay between the SUSY and SM parts was already observed for the case of the production of pseudoscalar Higgs bosons in [60].

The analogous case for $\underline{h \to \gamma\gamma}$ is given by

$$\begin{aligned}\mathcal{H}_{t\bar{t}} = & \frac{\cos\alpha}{\sin\beta}\left[1 + \frac{7}{30}\tau + \frac{\alpha_s}{\pi}\left[\tilde{q}\,\tau\left(\frac{14}{45} - \frac{7}{45}l + \frac{7}{45}\ln\left(\frac{\mu^2}{M_s^2}\right)\right.\right.\right. \\ & \left.\left.\left. - \frac{7}{45}B_0^{fin}\left(m_t^2, M_s, M_s\right) l\right) + q\left(-1 + \tau\left(\frac{101}{135} + \frac{7}{45}d_r\right)\right)\right]\right] + \mathcal{O}\left(\frac{1}{M_s}, \tau^2\right) \\ = & 1 + \frac{7}{30}\tau + \frac{\alpha_s}{\pi}\left[\tilde{q}\,\tau\left(\frac{14}{45} - \frac{7}{45}l\right) + q\left(-1 + \tau\left(\frac{101}{135} + \frac{7}{45}d_r\right)\right)\right] + \mathcal{O}\left(\frac{1}{M_s}, \tau^2\right).\end{aligned}$$

Again, the logarithmic term cancels against the B_0^{fin} part originating from the finite part of the SUSY top quark mass counterterm, as described above. The parameters are chosen like in the pseudoscalar case. For the pure QCD result proportional to q ($q = 1$), the coefficient of τ in NLO is 122/135, as expected (cf. Eq. (6.18)). By performing the full MSSM calculation in the limit of large top masses and taking $d_r = 0$ in DRED, we again observe that the QCD result is recovered in the limit of large SUSY masses. But it is only obtained as an interplay between the pure SUSY parts with the renormalized LO parts (label $l = 1$) and the pure QCD parts.

Altogether for the amplitudes the "SM limit" reads

$$\begin{aligned}\mathcal{A}_{q\tilde{q}} &= \mathcal{A}_q + \boxed{\frac{1}{M_s}\mathcal{A}_{q\tilde{g}}} \xrightarrow{\lim M_s \to \infty} \quad \mathcal{A}_{q\tilde{q}} = \mathcal{A}_q \\ \mathcal{H}_{q\tilde{q}} &= \mathcal{H}_q + \boxed{\frac{1}{M_s}\left(\mathcal{H}_{q\tilde{g}} + \mathcal{H}_{\tilde{q}}\right)} \xrightarrow{\lim M_s \to \infty} \quad \mathcal{H}_{q\tilde{q}} = \mathcal{H}_q.\end{aligned}$$

$\mathcal{A}_q$ and $\mathcal{H}_q$ are the known QCD amplitudes. We only calculate the expressions in the $\square$es, which correspond to the contributions through supersymmetric particles.

For the decay of pseudoscalar Higgs bosons into two photons we observe that by letting the heaviest mass scale tend to infinity, the SUSY parts vanish.

In the decay of scalar Higgs bosons, by letting the largest mass scale tend to infinity the result vanishes only for the case where all the SUSY scales are set to one scale. By

assuming different SUSY masses, all of them have to be taken very large and thus the limit is zero. We then obtain ratios of masses in that limit which are always suppressed by a power of a SUSY mass scale, e.g. $\mu_{susy}\, m_{\tilde{t}_1}/m^2_{\tilde{t}_2} \to 0$ for $m_{\tilde{t}_1} \ll m_{\tilde{t}_2}$ and a fixed μ_{susy}.

To conclude, for both the decay of scalar and pseudoscalar Higgs bosons the SM limit is recovered in the limit of very large SUSY masses.

6.8. Explicit Results as an Expansion in Leading Terms

In order to investigate the two-loop results for the Higgs decaying into two photons, we will give explicit examples for the cases where we assume certain hierarchies among the masses of the supersymmetric particles. The simplest case is assuming one SUSY mass scale, i.e., $M_s \equiv m_{\tilde{q}_1} = m_{\tilde{q}_2} = m_{\tilde{g}}$. Further we apply the method of asymptotic expansions in the limit $m_q \ll M_s$.

For the top case and its superpartners, we explicitly checked that the results obtained with the routines described in Sec. 5.4 agree with the ones obtained in the limit of large top masses. To perform this check the new results are expanded in the parameter $\tau = m^2_{h,A}/(4m^2_t)$.

The amplitudes we are interested in are the ones in leading order and next-to-leading order.

For the photonic decay of scalar and pseudoscalar Higgs bosons the amplitudes can be written in the following form (cf. Eqs. (6.13) and (6.15))

$$\mathcal{H}\,(h \to \gamma\gamma) = \sum_{q\tilde{q}=t\tilde{t},b\tilde{b}} Q_q^2\, \mathcal{H}_{q\tilde{q}} = \sum_{q\tilde{q}=t\tilde{t},b\tilde{b}} Q_q^2 \left(\mathcal{H}^{(0)}_{q\tilde{q}} + \frac{\alpha_s}{\pi}\mathcal{H}^{(1)}_{q\tilde{q}}\right) + \mathcal{O}\left(\alpha_s^2\right),$$

$$\mathcal{A}\,(A \to \gamma\gamma) = \sum_{q\tilde{q}=t\tilde{t},b\tilde{b}} Q_q^2\, \mathcal{A}_{q\tilde{q}} = \sum_{q\tilde{q}=t\tilde{t},b\tilde{b}} Q_q^2 \left(\mathcal{A}^{(0)}_{q\tilde{q}} + \frac{\alpha_s}{\pi}\mathcal{A}^{(1)}_{q\tilde{q}}\right) + \mathcal{O}\left(\alpha_s^2\right).$$

This has to be understood in the sense that $q\tilde{q} = t\tilde{t}$ $(b\tilde{b})$ denotes the top (bottom) case which includes the stops (sbottoms) and gluinos as well. In addition to the Feynman integrals obtained with the new routines, the finite expressions, B_0^{fin} originating from the on-shell counterterms, are expanded according to the mass hierarchy given in the limiting case under consideration. The notation given in the table below will be applied to the explicit expressions of the two-loop on-shell amplitudes for which we display the leading

terms in the following sections.

$$
\begin{aligned}
&x_{\phi s} = \frac{m_\phi^2}{M_s^2},\ L_{\phi s} = \ln x_{\phi s} - i\pi,\ x_{qs} = \frac{m_q^2}{M_s^2},\ L_{qs} = \ln x_{qs},\ x_{q\tilde{g}} = x_{\tilde{g}q}^{-1} = \frac{m_q^2}{m_{\tilde{g}}^2},\\
&L_{q\tilde{g}} = \ln x_{q\tilde{g}},\ x_{\phi q} = x_{q\phi}^{-1} = \frac{m_\phi^2}{m_q^2},\ L_{\phi b} = \ln x_{\phi b} - i\pi,\ L_{\phi t} = \ln x_{\phi t},\\
&x_{1\tilde{g}} = x_{\tilde{g}1}^{-1} = \frac{m_{\tilde{q}_1}^2}{m_{\tilde{g}}^2},\ L_{1\tilde{g}} = \ln x_{1\tilde{g}},\ x_{2\tilde{g}} = x_{\tilde{g}2}^{-1} = \frac{m_{\tilde{q}_2}^2}{m_{\tilde{g}}^2},\ L_{2\tilde{g}} = \ln x_{2\tilde{g}},\ x_{\phi\tilde{g}} = \frac{m_\phi^2}{m_{\tilde{g}}^2},\\
&L_{\phi\tilde{g}} = \ln x_{\phi\tilde{g}} - i\pi,\ x_{12} = x_{21}^{-1} = \frac{m_{\tilde{q}_1}^2}{m_{\tilde{q}_2}^2},\ L_{12} = \ln x_{12},\ L_{\tilde{g}} = \ln\frac{\mu_R^2}{m_{\tilde{g}}^2},\\
&L_s = \ln\frac{\mu_R^2}{M_s^2},\ L_{\tilde{q}_1} = \ln\frac{\mu_R^2}{m_{\tilde{q}_1}^2},\ L_{\tilde{q}_2} = \ln\frac{\mu_R^2}{m_{\tilde{q}_2}^2},\ L_{\tilde{q}} = \ln\frac{\mu_R^2}{m_{\tilde{q}}^2},\ L_q = \ln\frac{\mu_R^2}{m_q^2},\\
&x_{\phi 1} = x_{1\phi}^{-1} = \frac{m_\phi^2}{m_{\tilde{q}_1}^2},\ x_{\phi 2} = x_{2\phi}^{-1} = \frac{m_\phi^2}{m_{\tilde{q}_2}^2} \qquad \text{with } \phi = h,\ A;\ q = t,\ b;\ \tilde{q} = \tilde{t},\ \tilde{b}.
\end{aligned}
\tag{6.21}
$$

6.8.1. Explicit Expressions for the Amplitude $A \to \gamma\gamma$

The contributions of the bottom sector to the two-loop amplitude for the decay of pseudoscalar Higgs bosons into two photons can be expressed through

$$
\boxed{\mathcal{A}_{b\tilde{b}} = \tan\beta\,\mathcal{A}_{0,b\tilde{b}} + \frac{\mu_{susy}}{M_x}\left(1+\tan^2\beta\right)\mathcal{A}_{1,b\tilde{b}},}
\tag{6.22}
$$

with

$$
\mathcal{A}_{i,b\tilde{b}} = \sum_n \left(\frac{m_b}{m_A}\right)^n \mathcal{A}_{i,b\tilde{b},n}.
$$

The analogous part of the amplitude of the top sector reads

$$
\boxed{\mathcal{A}_{t\tilde{t}} = \cot\beta\mathcal{A}_{0,t\tilde{t}} + \frac{\mu_{susy}}{M_x}\left(1+\cot^2\beta\right)\mathcal{A}_{1,t\tilde{t}},}
\tag{6.23}
$$

with

$$
\mathcal{A}_{i,t\tilde{t}} = \sum_n \left(\frac{m_A}{m_t}\right)^n \mathcal{A}_{i,t\tilde{t},n}.
$$

Furthermore,

$$
\mathcal{A}_{i,q\tilde{q}} = \mathcal{A}_{i,q\tilde{q}}^{(0)} + \frac{\alpha_s}{\pi}\mathcal{A}_{i,q\tilde{q}}^{(1)} + \mathcal{O}\left(\alpha_s^2\right), \qquad q\tilde{q} = t\tilde{t},\ b\tilde{b}
$$

and

$$\mathcal{A}_{i,q\tilde{q}}^{(j)} = \mathcal{A}_{i,q}^{(j)} + \mathcal{A}_{i,q\tilde{g}}^{(j)}.$$

The analogous decomposition applies to the coefficients $\mathcal{A}_{i,q\tilde{q},n}$. Here, M_x denotes the largest SUSY mass scale chosen in the limiting case. In the following sections, coefficients that are omitted vanish. The QCD parts for the top and bottom contributions are already given in Sec. 6.5. Since we choose a different expansion parameter we list the results again in the same expansion we apply to the SUSY parts of the amplitude. The leading order does not get a contribution from squarks in the MSSM. For the bottom case it reads

$$\begin{aligned}\mathcal{A}_{0,b}^{(0)} = &-L_{Ab}^2 x_{bA} - 4L_{Ab}x_{bA}^2 - (6L_{Ab}-4)x_{bA}^3 - \left(\frac{40L_{Ab}}{3}+12\right)x_{bA}^4 \\ &- \left(35L_{Ab}+\frac{107}{3}\right)x_{bA}^5 - \left(\frac{504L_{Ab}}{5}+110\right)x_{bA}^6 + \mathcal{O}\left(x_{bA}^7\right).\end{aligned}$$

The two-loop QCD contributions of bottoms through $\mathcal{O}\left(m_b^4\right)$ are given by [76]

$$\mathcal{A}_{0,b,2}^{(1)} = \frac{L_{Ab}^4}{18} - \frac{2L_{Ab}^3}{3} + \frac{4\pi^2 L_{Ab}^2}{9} + \left(\frac{4\pi^2}{9} - \frac{32\zeta(3)}{3}\right)L_{Ab} - \frac{8\zeta(3)}{3} + \frac{2\pi^4}{15},$$

$$\mathcal{A}_{0,b,4}^{(1)} = \frac{16L_{Ab}^3}{9} - \frac{44L_{Ab}^2}{3} + \left(\frac{16}{3}+\frac{16\pi^2}{9}\right)L_{Ab} + \frac{64\zeta(3)}{3} + \frac{8\pi^2}{9} + \frac{80}{3},$$

The amplitude in LO from top effects is

$$\mathcal{A}_{0,t}^{(0)} = 1 + \frac{x_{At}}{12} + \frac{x_{At}^2}{90} + \frac{x_{At}^3}{560} + \frac{x_{At}^4}{3150} + \mathcal{O}\left(x_{At}^5\right),$$

For the two-loop SM insertions due to top quarks we obtain

$$\mathcal{A}_{0,t}^{(1)} = \frac{4x_{At}}{9} + \frac{17x_{At}^2}{180} + \frac{13253x_{At}^3}{680400} + \frac{4339x_{At}^4}{1058400} + \mathcal{O}\left(x_{At}^5\right).$$

6.8.2. $A \to \gamma\gamma$ in the Limit $m_q \ll M_s \equiv m_{\tilde{q}_1} = m_{\tilde{q}_2} = m_{\tilde{g}}$

Here, the explicit results for the amplitude in the limit $m_q \ll M_S \equiv m_{\tilde{q}_1} = m_{\tilde{q}_2} = m_{\tilde{g}}$, i.e., where we set the SUSY masses equal are displayed. By setting the squark masses to one scale, we do not assume mixing between them. Therefore, this result is independent of the squark mixing angle $\theta_{\tilde{q}}$. In this limit, $M_x = M_s$ (cf. Eqs. (6.22) and (6.23)). In the following, coefficients which are omitted vanish.

For the effects due to sbottoms and gluinos in the photonic decay of the pseudoscalar Higgs boson in NLO we obtain through $\mathcal{O}\left(m_b^4\right)$

$$\mathcal{A}_{0,b\tilde{g},2}^{(1)} = \frac{L_{Ab}}{9}x_{As} + \left(\frac{L_{Ab}}{135} - \frac{L_{As}}{90} + \frac{37}{2700}\right)x_{As}^2 + \left(\frac{L_{Ab}}{1260} - \frac{L_{As}}{1890} - \frac{1147}{793800}\right)x_{As}^3 + \mathcal{O}\left(x_{As}^4\right),$$

$$\mathcal{A}_{0,b\tilde{g},4}^{(1)} = \left(\frac{2L_{Ab}^2}{9} - \frac{2L_{Ab}}{9} - \frac{2}{9}\right)x_{As} + \left(\frac{4L_{Ab}}{135} + \frac{1}{135}\right)x_{As}^2 + \left(\frac{L_{Ab}}{180} - \frac{L_{As}}{126} + \frac{121}{13230}\right)x_{As}^3 + \mathcal{O}\left(x_{As}^4\right),$$

$$\mathcal{A}_{1,b\tilde{g},2}^{(1)} = \frac{L_{Ab}^2}{3} + \left(\frac{L_{Ab}^2}{36} - \frac{L_{bs}}{9} + \frac{2}{27}\right)x_{As} + \left(\frac{L_{Ab}^2}{270} - \frac{L_{bs}}{45} - \frac{1}{2700}\right)x_{As}^2 + \left(\frac{L_{Ab}^2}{1680} - \frac{11L_{bs}}{2520} - \frac{503}{264600}\right)x_{As}^3 + \mathcal{O}\left(x_{As}^4\right),$$

$$\mathcal{A}_{1,b\tilde{g},4}^{(1)} = -\frac{4L_{Ab}}{3} + \left(\frac{L_{Ab}^2}{18} - \frac{L_{Ab}}{9}\right)x_{As} + \left(\frac{L_{Ab}^2}{135} + \frac{7L_{Ab}}{135} - \frac{L_{As}}{15} + \frac{3}{50}\right)x_{As}^2 + \left(\frac{L_{Ab}^2}{840} + \frac{2L_{Ab}}{105} - \frac{3L_{As}}{140} + \frac{403}{44100}\right)x_{As}^3 + \mathcal{O}\left(x_{As}^4\right).$$

The two-loop effects of the mixed top-stop-gluino contributions up to $\mathcal{O}(m_A^4)$ are

$$\mathcal{A}_{0,t\tilde{g},2}^{(1)} = -\frac{1}{27}x_{ts} + \left(-\frac{L_{ts}}{90} - \frac{1}{900}\right)x_{ts}^2 + \left(\frac{29}{6615} - \frac{L_{ts}}{126}\right)x_{ts}^3 + \mathcal{O}\left(x_{ts}^4\right),$$

$$\mathcal{A}_{0,t\tilde{g},4}^{(1)} = -\frac{7x_{ts}}{1620} - \frac{x_{ts}^2}{4050} + \left(-\frac{L_{ts}}{1890} - \frac{629}{793800}\right)x_{ts}^3 + \mathcal{O}\left(x_{ts}^4\right),$$

$$\mathcal{A}_{1,t\tilde{g},0}^{(1)} = -\frac{1}{3} + \left(\frac{1}{54} - \frac{L_{ts}}{9}\right)x_{ts} + \left(\frac{11}{225} - \frac{L_{ts}}{15}\right)x_{ts}^2 + \left(\frac{131}{4900} - \frac{L_{ts}}{35}\right)x_{ts}^3 + \mathcal{O}\left(x_{ts}^4\right),$$

$$\mathcal{A}_{1,t\tilde{g},2}^{(1)} = -\frac{1}{36} - \frac{7x_{ts}}{216} + \left(-\frac{L_{ts}}{45} - \frac{47}{5400}\right)x_{ts}^2 + \left(\frac{409}{58800} - \frac{3L_{ts}}{140}\right)x_{ts}^3 + \mathcal{O}\left(x_{ts}^4\right),$$

$$\mathcal{A}_{1,t\tilde{g},4}^{(1)} = -\frac{1}{270} - \frac{19x_{ts}}{6480} - \frac{x_{ts}^2}{225} + \left(-\frac{11L_{ts}}{2520} - \frac{139}{42336}\right)x_{ts}^3 + \mathcal{O}\left(x_{ts}^4\right).$$

6.8.3. $A \to \gamma\gamma$ in the Limit $m_q \ll m_{\tilde{q}_1} \ll M_{\tilde{g}} \equiv m_{\tilde{q}_2} = m_{\tilde{g}}$

In the limit where $m_q \ll m_{\tilde{q}_1} \ll M_{\tilde{g}} \equiv m_{\tilde{q}_2} = m_{\tilde{g}}$, the newly calculated amplitude for the bottom, sbottom and gluino contributions can be displayed like in the last paragraph but with $M_x = M_{\tilde{g}}$.

For the effects due to sbottoms and gluinos in the photonic decay of the pseudoscalar Higgs boson in NLO we obtain through $\mathcal{O}(m_b^4)$

$$\mathcal{A}^{(1)}_{0,b\tilde{g},0} = \sin^2(2\theta_{\tilde{b}}) \left[\frac{1}{12} + \left(\frac{L_{1\tilde{g}}}{3} + \frac{1}{2}\right) x_{1\tilde{g}} + \frac{17}{324} x_{A\tilde{g}} + \left(\frac{5L_{1\tilde{g}}}{6} + \frac{1}{2}\right) x_{1\tilde{g}}^2 + \left(\frac{4L_{1\tilde{g}}}{9} + \frac{86}{81}\right) x_{A\tilde{g}} x_{1\tilde{g}} + \frac{29 x_{A\tilde{g}}^2}{864}\right] + \mathcal{O}\left(x_{1\tilde{g}}^3, x_{1\tilde{g}}^2 x_{A\tilde{g}}, x_{1\tilde{g}} x_{A\tilde{g}}^2, x_{A\tilde{g}}^3\right),$$

$$\mathcal{A}^{(1)}_{0,b\tilde{g},1} = \sin(2\theta_{\tilde{b}}) \left[\left(-\frac{L_{Ab}^2}{12} - \frac{2L_{Ab}}{9}\right)\sqrt{x_{A\tilde{g}}} + \left(-\frac{L_{Ab}^2}{27} + \frac{L_{Ab}}{20} + \frac{11 L_{b\tilde{g}}}{60} + \frac{19}{5400}\right) x_{A\tilde{g}}^{3/2} + \left[\left(-\frac{L_{1\tilde{g}}}{3} - \frac{7}{12}\right) L_{Ab}^2 + \left(-\frac{2L_{1\tilde{g}}}{3} - 1\right) L_{Ab}\right] x_{1\tilde{g}} \sqrt{x_{A\tilde{g}}}\right] + \mathcal{O}\left(x_{1\tilde{g}}^2 x_{A\tilde{g}}^{1/2}, x_{1\tilde{g}} x_{A\tilde{g}}^{3/2}, x_{A\tilde{g}}^{5/2}\right),$$

$$\mathcal{A}^{(1)}_{0,b\tilde{g},2} = \frac{L_{Ab}^2 \sin^2(2\theta_{\tilde{b}})}{12} + \left(\frac{L_{1\tilde{g}}}{3} + \frac{1}{2}\right) L_{Ab}^2 \sin^2(2\theta_{\tilde{b}}) x_{1\tilde{g}} + \left[\left(\frac{L_{Ab}^2}{27} + \frac{5}{108}\right) \sin^2(2\theta_{\tilde{b}}) + \frac{5L_{Ab}}{18}\right] x_{A\tilde{g}} + \left(\frac{5L_{1\tilde{g}}}{6} + \frac{1}{2}\right) L_{Ab}^2 \sin^2(2\theta_{\tilde{b}}) x_{1\tilde{g}}^2 + \left[\left(\left(\frac{L_{1\tilde{g}}}{3} + \frac{22}{27}\right) L_{Ab}^2 + \frac{L_{1\tilde{g}}}{3} + \frac{20}{27}\right) \sin^2(2\theta_{\tilde{b}}) + \left(\frac{2L_{1\tilde{g}}}{3} + \frac{11}{9}\right) L_{Ab}\right] x_{A\tilde{g}} x_{1\tilde{g}} + \left[\left(\frac{L_{Ab}^2}{48} + \frac{L_{b\tilde{g}}}{36} + \frac{311}{4320}\right) \sin^2(2\theta_{\tilde{b}}) - \frac{4L_{b\tilde{g}}}{45} - \frac{4L_{Ab}}{135} - \frac{1}{10800}\right] x_{A\tilde{g}}^2 + \mathcal{O}\left(x_{1\tilde{g}}^3, x_{1\tilde{g}}^2 x_{A\tilde{g}}, x_{1\tilde{g}} x_{A\tilde{g}}^2, x_{A\tilde{g}}^3\right),$$

$$\mathcal{A}^{(1)}_{0,b\tilde{g},3} = \sin(2\theta_{\tilde{b}}) \left[\left(-\frac{4L_{Ab}^2}{9} + \frac{7L_{Ab}}{9} + \frac{4}{9}\right)\sqrt{x_{A\tilde{g}}} + \left(-\frac{5L_{Ab}^2}{108} - \frac{41 L_{Ab}}{270} - \frac{1}{10}\right) x_{A\tilde{g}}^{3/2} + \left[\left(-\frac{4L_{1\tilde{g}}}{3} - 2\right) L_{Ab}^2 + \left(\frac{8L_{1\tilde{g}}}{3} + \frac{13}{3}\right) L_{Ab} + \frac{4L_{1\tilde{g}}}{3} + 2\right] x_{1\tilde{g}} \sqrt{x_{A\tilde{g}}}\right] + \mathcal{O}\left(x_{1\tilde{g}}^2 x_{A\tilde{g}}^{1/2}, x_{1\tilde{g}} x_{A\tilde{g}}^{3/2}, x_{A\tilde{g}}^{5/2}\right),$$

$$\mathcal{A}^{(1)}_{0,b\tilde{g},4} = -\frac{L_{Ab} \sin^2(2\theta_{\tilde{b}})}{3} + \left(-\frac{4L_{1\tilde{g}}}{3} - 2\right) L_{Ab} \sin^2(2\theta_{\tilde{b}}) x_{1\tilde{g}} + \left[\left(\frac{5\sin^2(2\theta_{\tilde{b}})}{108} + \frac{5}{9}\right) L_{Ab}^2 + \left(-\frac{4\sin^2(2\theta_{\tilde{b}})}{27} - \frac{5}{9}\right) L_{Ab} - \frac{5}{9}\right] x_{A\tilde{g}} + \mathcal{O}\left(x_{1\tilde{g}}^2, x_{1\tilde{g}} x_{A\tilde{g}}, x_{A\tilde{g}}^2\right),$$

$$\mathcal{A}^{(1)}_{1,b\tilde{g},1} = \sin(2\theta_{\tilde{b}})\left[-\frac{\sqrt{x_{A\tilde{g}}}}{6} + \left(-\frac{2L_{1\tilde{g}}}{3} - \frac{7}{6}\right)x_{1\tilde{g}}\sqrt{x_{A\tilde{g}}} - \frac{17x_{A\tilde{g}}^{3/2}}{162}\right.$$
$$\left. - \frac{29x_{A\tilde{g}}^{5/2}}{432} + \left(-\frac{8L_{1\tilde{g}}}{9} - \frac{361}{162}\right)x_{1\tilde{g}}x_{A\tilde{g}}^{3/2} + \left(-\frac{7L_{1\tilde{g}}}{3} - \frac{13}{6}\right)x_{1\tilde{g}}^2\sqrt{x_{A\tilde{g}}}\right]$$
$$+ \mathcal{O}\left(x_{1\tilde{g}}^2 x_{A\tilde{g}}^{1/2}, x_{1\tilde{g}}x_{A\tilde{g}}^{3/2}, x_{A\tilde{g}}^{5/2}\right),$$

$$\mathcal{A}^{(1)}_{1,b\tilde{g},2} = \frac{2L_{Ab}^2}{3} + \left(\frac{2L_{1\tilde{g}}}{3} + \frac{2}{3}\right)L_{Ab}^2 x_{1\tilde{g}} + \left(\frac{L_{Ab}^2}{6} - \frac{4L_{b\tilde{g}}}{9} - \frac{1}{27}\right)x_{A\tilde{g}} + \left(\frac{4L_{1\tilde{g}}}{3} + \frac{2}{3}\right)L_{Ab}^2 x_{1\tilde{g}}^2$$
$$+ x_{1\tilde{g}}x_{A\tilde{g}}\left[\left(\frac{2L_{1\tilde{g}}}{3} + \frac{4}{3}\right)L_{Ab}^2 - \frac{4L_{1\tilde{g}}}{3} + \left(-\frac{4L_{1\tilde{g}}}{3} - \frac{22}{9}\right)L_{b\tilde{g}} - \frac{8\zeta(2)}{3} + \frac{26}{27}\right]$$
$$+ \left(\frac{2L_{Ab}^2}{27} - \frac{4L_{b\tilde{g}}}{15} - \frac{17}{75}\right)x_{A\tilde{g}}^2 + \mathcal{O}\left(x_{1\tilde{g}}^3, x_{1\tilde{g}}^2 x_{A\tilde{g}}, x_{1\tilde{g}}x_{A\tilde{g}}^2, x_{A\tilde{g}}^3\right),$$

$$\mathcal{A}^{(1)}_{1,b\tilde{g},3} = \sin(2\theta_{\tilde{b}})\left[-\frac{1}{6}L_{Ab}^2\sqrt{x_{A\tilde{g}}} + \left(-\frac{2L_{1\tilde{g}}}{3} - \frac{7}{6}\right)L_{Ab}^2 x_{1\tilde{g}}\sqrt{x_{A\tilde{g}}} + \left(-\frac{2L_{Ab}^2}{27} - \frac{5}{54}\right)x_{A\tilde{g}}^{3/2}\right.$$
$$+ \left(-\frac{L_{Ab}^2}{24} - \frac{L_{b\tilde{g}}}{18} - \frac{311}{2160}\right)x_{A\tilde{g}}^{5/2} + \left[\left(-\frac{2L_{1\tilde{g}}}{3} - \frac{46}{27}\right)L_{Ab}^2 - \frac{2L_{1\tilde{g}}}{3} - \frac{85}{54}\right]x_{1\tilde{g}}x_{A\tilde{g}}^{3/2}$$
$$\left. + \left(-\frac{7L_{1\tilde{g}}}{3} - \frac{13}{6}\right)L_{Ab}^2 x_{1\tilde{g}}^2\sqrt{x_{A\tilde{g}}}\right] + \mathcal{O}\left(x_{1\tilde{g}}^3 x_{A\tilde{g}}^{1/2}, x_{1\tilde{g}}^2 x_{A\tilde{g}}^{3/2}, x_{1\tilde{g}}x_{A\tilde{g}}^{5/2}, x_{A\tilde{g}}^{7/2}\right),$$

$$\mathcal{A}^{(1)}_{1,b\tilde{g},4} = -\frac{8L_{Ab}}{3} + \left(-\frac{8L_{1\tilde{g}}}{3} - \frac{8}{3}\right)L_{Ab}x_{1\tilde{g}} + \left(\frac{2L_{Ab}^2}{9} - \frac{2L_{Ab}}{3}\right)x_{A\tilde{g}}$$
$$+ \left(-\frac{16L_{1\tilde{g}}}{3} - \frac{8}{3}\right)L_{Ab}x_{1\tilde{g}}^2 + \left[\left(\frac{2L_{1\tilde{g}}}{3} + \frac{11}{9}\right)L_{Ab}^2 + \left(-\frac{8L_{1\tilde{g}}}{3} - \frac{16}{3}\right)L_{Ab}\right]x_{A\tilde{g}}x_{1\tilde{g}}$$
$$+ \left(\frac{5L_{Ab}^2}{54} - \frac{8L_{Ab}}{27} - \frac{3L_{b\tilde{g}}}{5} + \frac{4}{225}\right)x_{A\tilde{g}}^2 + \mathcal{O}\left(x_{1\tilde{g}}^3, x_{1\tilde{g}}^2 x_{A\tilde{g}}, x_{1\tilde{g}}x_{A\tilde{g}}^2, x_{A\tilde{g}}^3\right),$$

For the contributions due to top quarks and their partners up to $\mathcal{O}(m_A^4)$ we find

$$\mathcal{A}^{(1)}_{0,t\tilde{g},2} = -\frac{\sin^2(2\theta_{\tilde{t}})}{144} + \frac{17\sin(2\theta_{\tilde{t}})\sqrt{x_{t\tilde{g}}}}{108} + \left(-\frac{L_{1\tilde{g}}}{36} - \frac{1}{24}\right)x_{1\tilde{g}}\sin^2(2\theta_{\tilde{t}})$$
$$+ \left(\frac{5\sin^2(2\theta_{\tilde{t}})}{432} - \frac{5}{54}\right)x_{t\tilde{g}} + \left(\frac{11L_{t\tilde{g}}}{60} + \frac{1169}{5400}\right)\sin(2\theta_{\tilde{t}})x_{t\tilde{g}}^{3/2}$$
$$+ \left(\frac{5L_{1\tilde{g}}}{9} + \frac{11}{12}\right)\sin(2\theta_{\tilde{t}})x_{1\tilde{g}}\sqrt{x_{t\tilde{g}}} + \mathcal{O}\left(x_{1\tilde{g}}^2, x_{1\tilde{g}}x_{t\tilde{g}}, x_{t\tilde{g}}^2\right),$$

$$\begin{aligned}\mathcal{A}^{(1)}_{0,t\tilde{g},4} &= -\frac{\sin^2(2\theta_{\tilde{t}})}{1080} + \frac{101\sin(2\theta_{\tilde{t}})}{6480}\sqrt{x_{t\tilde{g}}} + \left(-\frac{L_{1\tilde{g}}}{270} - \frac{1}{180}\right)\sin^2(2\theta_{\tilde{t}})x_{1\tilde{g}} \\ &+ \left(-\frac{7\sin^2(2\theta_{\tilde{t}})}{1944} - \frac{7}{648}\right)x_{t\tilde{g}} + \frac{1307\sin(2\theta_{\tilde{t}})}{32400}x_{t\tilde{g}}^{3/2} \\ &+ \left(\frac{29L_{1\tilde{g}}}{540} + \frac{7}{80}\right)\sin(2\theta_{\tilde{t}})x_{1\tilde{g}}\sqrt{x_{t\tilde{g}}} + \mathcal{O}\left(x_{1\tilde{g}}^2, x_{1\tilde{g}}x_{t\tilde{g}}, x_{t\tilde{g}}^2\right), \\ \mathcal{A}^{(1)}_{1,t\tilde{g},0} &= -\frac{2}{3} + \left(-\frac{2L_{1\tilde{g}}}{3} - \frac{2}{3}\right)x_{1\tilde{g}} + \left(-\frac{4L_{t\tilde{g}}}{9} - \frac{7}{27}\right)x_{t\tilde{g}} + \left(-\frac{4L_{1\tilde{g}}}{3} - \frac{2}{3}\right)x_{1\tilde{g}}^2 \\ &+ \left[-2L_{1\tilde{g}} + \left(-\frac{4L_{1\tilde{g}}}{3} - \frac{22}{9}\right)L_{t\tilde{g}} - \frac{8\zeta(2)}{3} - \frac{7}{27}\right]x_{1\tilde{g}}x_{t\tilde{g}} + \left(-\frac{3L_{t\tilde{g}}}{5} - \frac{37}{450}\right)x_{t\tilde{g}}^2 \\ &+ \mathcal{O}\left(x_{1\tilde{g}}^3, x_{1\tilde{g}}^2x_{t\tilde{g}}, x_{1\tilde{g}}x_{t\tilde{g}}^2, x_{1\tilde{g}}^3\right), \end{aligned}$$

$$\begin{aligned}\mathcal{A}^{(1)}_{1,t\tilde{g},2} &= -\frac{1}{18} + \frac{\sin(2\theta_{\tilde{t}})\sqrt{x_{t\tilde{g}}}}{72} + \left(-\frac{L_{1\tilde{g}}}{18} - \frac{1}{18}\right)x_{1\tilde{g}} - \frac{5x_{t\tilde{g}}}{27} + \left(\frac{L_{1\tilde{g}}}{18} + \frac{7}{72}\right) \\ &\sin(2\theta_{\tilde{t}})x_{1\tilde{g}}\sqrt{x_{t\tilde{g}}} - \frac{5}{216}\sin(2\theta_{\tilde{t}})x_{t\tilde{g}}^{3/2} + \left(-\frac{L_{1\tilde{g}}}{9} - \frac{1}{18}\right)x_{1\tilde{g}}^2 \\ &+ \left(-\frac{13L_{1\tilde{g}}}{18} - \frac{155}{108}\right)x_{t\tilde{g}}x_{1\tilde{g}} + \left(-\frac{4L_{t\tilde{g}}}{15} - \frac{1769}{5400}\right)x_{t\tilde{g}}^2 + \mathcal{O}\left(x_{1\tilde{g}}^2x_{t\tilde{g}}^{1/2}, x_{1\tilde{g}}x_{t\tilde{g}}^{3/2}, x_{1\tilde{g}}^{5/2}\right), \end{aligned}$$

$$\begin{aligned}\mathcal{A}^{(1)}_{1,t\tilde{g},4} &= -\frac{1}{135} + \frac{\sin(2\theta_{\tilde{t}})\sqrt{x_{t\tilde{g}}}}{540} + \left(-\frac{L_{1\tilde{g}}}{135} - \frac{1}{135}\right)x_{1\tilde{g}} - \frac{53x_{t\tilde{g}}}{3240} + \frac{7}{972}\sin(2\theta_{\tilde{t}})x_{t\tilde{g}}^{3/2} \\ &+ \left(\frac{L_{1\tilde{g}}}{135} + \frac{7}{540}\right)\sin(2\theta_{\tilde{t}})x_{1\tilde{g}}\sqrt{x_{t\tilde{g}}} + \left(-\frac{2L_{1\tilde{g}}}{135} - \frac{1}{135}\right)x_{1\tilde{g}}^2 \\ &+ \left(-\frac{17L_{1\tilde{g}}}{270} - \frac{101}{810}\right)x_{t\tilde{g}}x_{1\tilde{g}} - \frac{1343x_{t\tilde{g}}^2}{16200} + \mathcal{O}\left(x_{1\tilde{g}}^2x_{t\tilde{g}}^{1/2}, x_{1\tilde{g}}x_{t\tilde{g}}^{3/2}, x_{1\tilde{g}}^{5/2}\right). \end{aligned}$$

6.8.4. $A \to \gamma\gamma$ in the Limit $m_q \ll m_{\tilde{q}_1} \ll m_{\tilde{q}_2} \ll M_{\tilde{g}}$

The limit where $m_q \ll m_{\tilde{q}_1} \ll m_{\tilde{q}_2} \ll M_{\tilde{g}}$ is the most general one where we set all the appearing mass scales unequal and the gluino is assumed to be larger than the squarks. By convention, $m_{\tilde{q}_2} > m_{\tilde{q}_1}$. For four different scales, the expressions get larger. Therefore, we include less terms. Here, $M_x = M_{\tilde{g}}$.

For the effects due to sbottoms and gluinos in the photonic decay of the pseudoscalar Higgs boson in NLO we obtain through $\mathcal{O}(m_b^4)$

$$\begin{aligned}\mathcal{A}^{(1)}_{0,b\tilde{g},0} &= \sin^2(2\theta_{\tilde{b}})\left[\left(\frac{L_{12}}{3} + \frac{1}{6}\right)x_{1\tilde{g}} + \frac{x_{2\tilde{g}}}{6} + \left(\left(\frac{L_{12}}{3} + \frac{2}{3}\right)x_{12} + \frac{x_{A2}}{36} + \frac{1}{18}\right)x_{A\tilde{g}}\right] \\ &+ \mathcal{O}\left(x_{2\tilde{g}}^2, x_{2\tilde{g}}x_{A\tilde{g}}, x_{1\tilde{g}}x_{A\tilde{g}}, x_{1\tilde{g}}^2, x_{A\tilde{g}}^2\right), \end{aligned}$$

$$\mathcal{A}^{(1)}_{0,b\tilde{g},1} = \sin\left(2\theta_{\tilde{b}}\right)\left[L^2_{Ab}\left(\left(-\frac{L_{12}}{3}-\frac{1}{3}\right)x_{12}-\frac{x_{A2}}{18}-\frac{1}{6}\right)\sqrt{x_{A\tilde{g}}}+L_{1\tilde{g}}\left(\frac{2L^2_{Ab}}{3}-\frac{4L_{Ab}}{3}\right)\right.$$
$$\left. x^{3/2}_{1\tilde{g}}+L_{2\tilde{g}}\left(\frac{4L_{Ab}}{3}-\frac{2L^2_{Ab}}{3}\right)x^{3/2}_{2\tilde{g}}\right]+\mathcal{O}\left(x^{5/2}_{2\tilde{g}},x^{5/2}_{1\tilde{g}},x^2_{2\tilde{g}}x^{1/2}_{A\tilde{g}},x^2_{1\tilde{g}}x^{1/2}_{A\tilde{g}}\right),$$

$$\mathcal{A}^{(1)}_{0,b\tilde{g},2} = \frac{1}{6}L^2_{Ab}\sin^2\left(2\theta_{\tilde{b}}\right)x_{2\tilde{g}}+\left[\left(\frac{L_{12}}{3}+\frac{1}{6}\right)L^2_{Ab}+\left(\frac{L_{12}}{3}+\frac{2}{3}\right)x_{A2}L^2_{Ab}\right]\sin^2\left(2\theta_{\tilde{b}}\right)x_{1\tilde{g}}$$
$$+\left(\left(\frac{x_{A2}}{36}+\frac{1}{18}\right)L^2_{Ab}\sin\left(2\theta_{\tilde{b}}\right)^2+\frac{4L_{Ab}}{9}\right)x_{A\tilde{g}}+\left[-\frac{L^2_{Ab}}{3}+\frac{2L_{Ab}}{3}\right.$$
$$\left.+L_{1\tilde{g}}\left(2L_{Ab}-L^2_{Ab}\right)\right]x^2_{1\tilde{g}}+\left(-\frac{L^2_{Ab}}{3}+\frac{2L_{Ab}}{3}+L_{2\tilde{g}}\left(2L_{Ab}-L^2_{Ab}\right)\right)x^2_{2\tilde{g}}$$
$$+\mathcal{O}\left(x^3_{2\tilde{g}},x^2_{2\tilde{g}}x_{A\tilde{g}},x_{2\tilde{g}}x^2_{A\tilde{g}},x^3_{1\tilde{g}},x^3_{A\tilde{g}}\right),$$

$$\mathcal{A}^{(1)}_{0,b\tilde{g},3} = \sin\left(2\theta_{\tilde{b}}\right)\left[L_{1\tilde{g}}\left(\frac{8}{3}-\frac{16L_{Ab}}{3}\right)\sqrt{x_{1A}}x^{3/2}_{1\tilde{g}}+L_{2\tilde{g}}\left(\frac{16L_{Ab}}{3}-\frac{8}{3}\right)\sqrt{x_{2A}}x^{3/2}_{2\tilde{g}}\right.$$
$$+\left[L^2_{Ab}-2L_{Ab}+L_{1\tilde{g}}\left(\frac{2L^2_{Ab}}{3}-\frac{4L_{Ab}}{3}\right)\right]x_{1\tilde{g}}\sqrt{x_{A\tilde{g}}}$$
$$\left.+\left[-L^2_{Ab}+2L_{Ab}+L_{2\tilde{g}}\left(\frac{4L_{Ab}}{3}-\frac{2L^2_{Ab}}{3}\right)\right]x_{2\tilde{g}}\sqrt{x_{A\tilde{g}}}\right]$$
$$+\mathcal{O}\left(x^{5/2}_{2\tilde{g}},x^{5/2}_{1\tilde{g}},x^2_{2\tilde{g}}x^{1/2}_{A\tilde{g}},x^2_{1\tilde{g}}x^{1/2}_{A\tilde{g}}\right),$$

$$\mathcal{A}^{(1)}_{0,b\tilde{g},4} = \left(-\frac{4L_{12}}{3}-\frac{2}{3}\right)L_{Ab}\sin^2\left(2\theta_{\tilde{b}}\right)x_{1\tilde{g}}-\frac{2}{3}L_{Ab}\sin^2\left(2\theta_{\tilde{b}}\right)x_{2\tilde{g}}$$
$$+\left[\frac{8L^2_{Ab}}{9}-\frac{8L_{Ab}}{9}-\frac{8}{9}+\sin\left(2\theta_{\tilde{b}}\right)^2\left(L_{Ab}\left(\left(-\frac{4L_{12}}{3}-\frac{8}{3}\right)x_{12}-\frac{2}{9}\right)\right.\right.$$
$$\left.\left.-\frac{L_{Ab}x_{A2}}{9}\right)\right]x_{A\tilde{g}}+\mathcal{O}\left(x^2_{2\tilde{g}},x_{2\tilde{g}}x_{A\tilde{g}},x_{1\tilde{g}}x_{A\tilde{g}},x^2_{1\tilde{g}},x^2_{A\tilde{g}}\right),$$

$$\mathcal{A}^{(1)}_{1,b\tilde{g},1} = \left(\left(-\frac{2L_{12}}{3}-\frac{2}{3}\right)x_{12}-\frac{x_{A2}}{9}-\frac{1}{3}\right)\sqrt{x_{A\tilde{g}}}+\mathcal{O}\left(x_{1\tilde{g}}x^{1/2}_{A\tilde{g}},x_{2\tilde{g}}x^{1/2}_{A\tilde{g}},x^{3/2}_{A\tilde{g}}\right),$$

$$\mathcal{A}^{(1)}_{1,b\tilde{g},2} = L^2_{Ab}\left(-\frac{2L_{2\tilde{g}}}{3}+\frac{2L_{12}x_{12}}{3}+\frac{x_{A2}}{3}\right)+\mathcal{O}\left(x_{1\tilde{g}},x_{2\tilde{g}},x_{A\tilde{g}}\right),$$

$$\mathcal{A}^{(1)}_{1,b\tilde{g},3} = \sin\left(2\theta_{\tilde{b}}\right)\left[\left(-\frac{2L_{12}}{3}-\frac{2}{3}\right)x_{12}L^2_{Ab}+\left(-\frac{x_{A2}}{9}-\frac{1}{3}\right)L^2_{Ab}\right]\sqrt{x_{A\tilde{g}}}$$
$$+\mathcal{O}\left(x_{1\tilde{g}}x^{1/2}_{A\tilde{g}},x_{2\tilde{g}}x^{1/2}_{A\tilde{g}},x^{3/2}_{A\tilde{g}}\right),$$

$$\mathcal{A}^{(1)}_{1,b\tilde{g},4} = L_{Ab}\left(\frac{8L_{2\tilde{g}}}{3}-\frac{4x_{A2}}{3}\right)-\frac{8L_{12}L_{Ab}x_{12}}{3}+\mathcal{O}\left(x_{1\tilde{g}},x_{2\tilde{g}},x_{A\tilde{g}}\right),$$

For the contributions due to top quarks and their partners we compute up to $\mathcal{O}(m_A^4)$

$$\begin{aligned}
\mathcal{A}^{(1)}_{0,t\tilde{g},2} &= \left[\left(\frac{L_{12}}{3}+\frac{1}{3}\right)x_{12}+\frac{1}{6}\right]\sin\left(2\theta_{\tilde{t}}\right)\sqrt{x_{t\tilde{g}}}-\frac{4x_{t\tilde{g}}}{27}-\frac{x_{2\tilde{g}}\sin^2\left(2\theta_{\tilde{t}}\right)}{72}\\
&+\left(-\frac{L_{12}}{36}-\frac{1}{72}\right)x_{1\tilde{g}}\sin^2\left(2\theta_{\tilde{t}}\right)+\mathcal{O}\left(x_{1\tilde{g}}^{3/2},x_{2\tilde{g}}^{3/2},x_{2\tilde{g}}x_{t\tilde{g}}^{1/2},x_{2\tilde{g}}x_{t\tilde{g}}^{1/2}\right),\\
\mathcal{A}^{(1)}_{0,t\tilde{g},4} &= \sin\left(2\theta_{\tilde{t}}\right)\left[\left(\left(\frac{L_{12}}{36}+\frac{1}{36}\right)x_{12}+\frac{1}{18}x_{t2}+\frac{1}{72}\right)\sqrt{x_{t\tilde{g}}}\right]\\
&+\sin^2\left(2\theta_{\tilde{t}}\right)\left[\left(-\frac{L_{12}}{270}-\frac{1}{540}\right)x_{12}-\frac{1}{540}\right]x_{2\tilde{g}}+\left[-\frac{7}{405}+\sin^2\left(2\theta_{\tilde{t}}\right)\right.\\
&\left.\left(\left(-\frac{L_{12}}{36}-\frac{1}{18}\right)x_{12}-\frac{1}{216}\right)\right]x_{t\tilde{g}}+\mathcal{O}\left(x_{1\tilde{g}}^{3/2},x_{2\tilde{g}}^{3/2},x_{2\tilde{g}}x_{t\tilde{g}}^{1/2},x_{2\tilde{g}}x_{t\tilde{g}}^{1/2}\right),\\
\mathcal{A}^{(1)}_{1,t\tilde{g},0} &= -\frac{2L_{12}x_{12}}{3}+\frac{2L_{2\tilde{g}}}{3}+\mathcal{O}\left(x_{1\tilde{g}},x_{2\tilde{g}},x_{t\tilde{g}}\right),\\
\mathcal{A}^{(1)}_{1,t\tilde{g},2} &= -\frac{L_{12}x_{12}}{18}+\frac{L_{2\tilde{g}}}{18}-\frac{x_{t2}}{3}+\sin\left(2\theta_{\tilde{t}}\right)\\
&\left[\left(\frac{L_{12}}{18}+\frac{1}{18}\right)x_{12}+\frac{1}{36}\right]\sqrt{x_{t\tilde{g}}}+\mathcal{O}\left(x_{1\tilde{g}},x_{2\tilde{g}},x_{t\tilde{g}}\right),\\
\mathcal{A}^{(1)}_{1,t\tilde{g},4} &= \frac{L_{2\tilde{g}}}{135}-\frac{L_{12}}{135}x_{12}-\frac{x_{t2}}{36}+\left[\left(\frac{L_{12}}{135}+\frac{1}{135}\right)x_{12}\right.\\
&\left.+\frac{x_{t2}}{108}+\frac{1}{270}\right]\sin\left(2\theta_{\tilde{t}}\right)\sqrt{x_{t\tilde{g}}}+\mathcal{O}\left(x_{1\tilde{g}},x_{2\tilde{g}},x_{t\tilde{g}}\right).
\end{aligned}$$

6.8.5. Explicit Expressions for the Amplitude $h \to \gamma\gamma$

In this paragraph we will give explicit expressions for the amplitude in the process of $h \to \gamma\gamma$. The structure of the amplitude for the decay of scalar Higgs bosons into two photons for the bottom sector can be expressed through

$$\begin{aligned}
\mathcal{H}_{b\tilde{b}} &= \frac{\sin\alpha}{\cos\beta}\mathcal{H}_{0,b\tilde{b}}+\frac{\mu_{susy}}{M_x}\frac{\cos\left(\alpha-\beta\right)}{\cos^2\beta}\mathcal{H}_{1,b\tilde{b}}-\frac{M_Z^2}{M_x^2}\sin\left(\alpha+\beta\right)\mathcal{H}_{2,b\tilde{b}}\\
&-\frac{M_Z^2}{M_x^2}\frac{2}{3}\sin^2\theta_W\sin\left(\alpha+\beta\right)\mathcal{H}_{3,b\tilde{b}},
\end{aligned} \tag{6.24}$$

with

$$\mathcal{H}_{i,b\tilde{b}} = \sum_n \left(\frac{m_b}{m_h}\right)^n \mathcal{H}_{i,b\tilde{b},n}. \tag{6.25}$$

For the top sector the structure of the amplitude is given by

$$\boxed{\begin{aligned}\mathcal{H}_{t\tilde{t}} = &\frac{\cos\alpha}{\sin\beta}\mathcal{H}_{0,t\tilde{t}} + \frac{\mu_{susy}}{M_x}\frac{\cos(\alpha-\beta)}{\sin^2\beta}\mathcal{H}_{1,t\tilde{t}} + \frac{M_Z^2}{M_x^2}\sin(\alpha+\beta)\,\mathcal{H}_{2,t\tilde{t}} \\ &+ \frac{M_Z^2}{M_x^2}\frac{4}{3}\sin^2\theta_W\sin(\alpha+\beta)\,\mathcal{H}_{3,t\tilde{t}},\end{aligned}} \tag{6.26}$$

with

$$\mathcal{H}_{i,t\tilde{t}} = \sum_n \left(\frac{m_h}{m_t}\right)^n \mathcal{H}_{i,t\tilde{t},n}. \tag{6.27}$$

Furthermore,

$$\mathcal{H}_{i,q\tilde{q}} = \mathcal{H}^{(0)}_{i,q\tilde{q}} + \frac{\alpha_s}{\pi}\mathcal{H}^{(1)}_{i,q\tilde{q}} + \mathcal{O}\left(\alpha_s^2\right), \qquad q\tilde{q} = t\tilde{t},\, b\tilde{b}$$

and

$$\mathcal{H}^{(j)}_{i,q\tilde{q}} = \mathcal{H}^{(j)}_{i,q} + \mathcal{H}^{(j)}_{i,\tilde{q}\tilde{g}} = \mathcal{H}^{(j)}_{i,q} + \mathcal{H}^{(j)}_{i,\tilde{q}} + \mathcal{H}^{(j)}_{i,q\tilde{g}}.$$

The analogous decomposition applies to the coefficients $\mathcal{H}_{i,q\tilde{q},n}$. It should be noted that $\mathcal{H}^{(j)}_{i,\tilde{q}\tilde{g}}$ denotes corrections to the amplitude that contain at least one supersymmetric scale whereas $\mathcal{H}^{(j)}_{i,q\tilde{g}}$ only refers to contributions from gluinos. Again, M_x denotes the heaviest mass scale in the certain limit under consideration. The mass of the Z (W) bosons, M_Z (M_W), occur at the $h\tilde{q}\tilde{q}$ couplings together with $\sin\theta_W = \sqrt{1 - M_W^2/M_Z^2}$. In the following sections, coefficients which are omitted vanish.

The SM bottom contributions are given by

$$\begin{aligned}\mathcal{H}^{(0)}_{0,b} = &\left(\frac{3L_{hb}^2}{2} - 6\right)x_{bh} + \left(-6L_{hb}^2 + 6L_{hb}\right)x_{bh}^2 + (-15L_{hb}+6)x_{bh}^3 \\ &- (16L_{hb}+6)x_{bh}^4 + \mathcal{O}\left(x_{bh}^5\right),\end{aligned}$$

We take the NLO-QCD result for the amplitude from the literature [76].

$$\begin{aligned}\mathcal{H}^{(1)}_{0,b,2} = &-\frac{L_{hb}^4}{12} - L_{hb}^3 - \frac{2\pi^2 L_{hb}^2}{3} + \left(12 + \frac{2\pi^2}{3} + 16\zeta(3)\right)L_{hb} \\ &+ 4\zeta(3) - \frac{\pi^4}{5} - 20,\end{aligned}$$

$$\begin{aligned}\mathcal{H}^{(1)}_{0,b,4} = &\frac{L_{hb}^4}{3} + 12L_{hb}^3 + \left(10 + \frac{8\pi^2}{3}\right)L_{hb}^2 + (-16 - 64\zeta(3))L_{hb} \\ &+ 16\zeta(3) + \frac{4\pi^4}{5} - \frac{4\pi^2}{3} - 64,\end{aligned}$$

For the top contributions we obtain

$$\mathcal{H}_{0,t}^{(0)} = 1 + \frac{7x_{ht}}{120} + \frac{x_{ht}^2}{168} + \frac{13x_{ht}^3}{16800} + \frac{2x_{ht}^4}{17325} + \mathcal{O}\left(x_{ht}^5\right),$$

$$\mathcal{H}_{0,t}^{(1)} = -1 + \frac{61x_{ht}}{270} + \frac{554x_{ht}^2}{14175} + \frac{104593x_{ht}^3}{15876000} + \frac{87077x_{ht}^4}{74844000} + \mathcal{O}\left(x_{ht}^5\right).$$

6.8.6. $h \to \gamma\gamma$ in the Limit $m_q \ll M_s \equiv m_{\tilde{q}_1} = m_{\tilde{q}_2} = m_{\tilde{g}}$

For the scalar case, we also have to account for sbottoms as well as stops at leading order. For the LO contributions from sbottoms we get the following non-vanishing results for the amplitude

$$\mathcal{H}_{0,\tilde{b},2}^{(0)} = -\frac{x_{hs}}{2} - \frac{x_{hs}^2}{15} - \frac{3x_{hs}^3}{280}, \quad \mathcal{H}_{1,\tilde{b}}^{(0)} = 0,$$

$$\mathcal{H}_{2,\tilde{b},0}^{(0)} = -\frac{1}{8} - \frac{x_{hs}}{60} - \frac{3x_{hs}^2}{1120}, \quad \mathcal{H}_{3,\tilde{b}}^{(0)} = 0.$$

We calculate the results for the LO squark contributions in the limit where the squark masses are considered to be significantly larger than the Higgs mass since the two-loop squark contributions are evaluated in this limit as well.

In next-to-leading order we obtain the following expression for the pure SUSY parts of the amplitude which arise from sbottom and/or gluino insertions in the Feynman diagrams (see Fig. 6.8) through $\mathcal{O}(m_b^4)$

$$\mathcal{H}_{0,\tilde{b}\tilde{g},2}^{(1)} = \left(-\frac{2L_{bs}}{3} + \frac{L_{hb}}{6} - 1\right) x_{hs} + \left(-\frac{13L_{bs}}{180} + \frac{L_{hb}}{20} - \frac{2011}{5400}\right) x_{hs}^2 + \left(-\frac{17L_{bs}}{1260} + \frac{17L_{hb}}{2520} - \frac{125821}{1587600}\right) x_{hs}^3 + \mathcal{O}\left(x_{hs}^4\right),$$

$$\mathcal{H}_{0,\tilde{b}\tilde{g},4}^{(1)} = \left(\frac{L_{hb}^2}{3} - \frac{L_{hb}}{3} - \frac{7}{3}\right) x_{hs} + \left(\frac{L_{hb}^2}{15} - \frac{4L_{hb}}{15} - \frac{2L_{bs}}{15} - \frac{118}{225}\right) x_{hs}^2 + \left(\frac{L_{hb}^2}{105} - \frac{L_{hb}}{40} - \frac{L_{bs}}{420} - \frac{37879}{264600}\right) x_{hs}^3 + \mathcal{O}\left(x_{hs}^4\right),$$

$$\mathcal{H}_{1,\tilde{b}\tilde{g},2}^{(1)} = -\frac{L_{hb}^2}{2} + 2 + \left(-\frac{L_{hb}^2}{24} + \frac{L_{bs}}{6} + \frac{7}{36}\right) x_{hs} + \left(-\frac{L_{hb}^2}{180} + \frac{L_{bs}}{30} + \frac{83}{1080}\right) x_{hs}^2 + \left(-\frac{L_{hb}^2}{1120} + \frac{11L_{bs}}{1680} + \frac{6757}{352800}\right) x_{hs}^3 + \mathcal{O}\left(x_{hs}^4\right),$$

$$\mathcal{H}_{1,\tilde{b}\tilde{g},3}^{(1)} = -\frac{1}{3}\pi x_{hs}^{3/2} - \frac{4}{45}\pi x_{hs}^{5/2} - \frac{3}{140}\pi x_{hs}^{7/2} + \mathcal{O}\left(x_{hs}^{9/2}\right),$$

$$\mathcal{H}^{(1)}_{1,\tilde{b}\tilde{g},4} = 2L_{hb}^2 + 2L_{hb} + \left(\frac{L_{hb}^2}{12} + \frac{L_{hb}}{6} + \frac{1}{3}\right) x_{hs} + \left(\frac{L_{hb}^2}{90} + \frac{L_{hb}}{45} - \frac{4L_{bs}}{15} + \frac{127}{300}\right) x_{hs}^2 + \left(\frac{L_{hb}^2}{560} + \frac{L_{hb}}{280} - \frac{31L_{bs}}{360} + \frac{149}{1400}\right) x_{hs}^3 + \mathcal{O}\left(x_{hs}^4\right),$$

$$\mathcal{H}^{(1)}_{2,\tilde{b}\tilde{g},0} = -\frac{1}{2} - \frac{119x_{hs}}{1080} - \frac{10583x_{hs}^2}{453600} + \mathcal{O}\left(x_{hs}^3\right),$$

$$\mathcal{H}^{(1)}_{2,\tilde{b}\tilde{g},2} = \frac{L_{hb}^2}{6} - \frac{2}{3} + \left(\frac{L_{hb}^2}{60} + \frac{L_{bs}}{30} - \frac{349}{1800}\right) x_{hs} + \left(\frac{L_{hb}^2}{420} + \frac{L_{bs}}{105} - \frac{4399}{132300}\right) x_{hs}^2 + \mathcal{O}\left(x_{hs}^3\right),$$

$$\mathcal{H}^{(1)}_{2,\tilde{b}\tilde{g},3} = \frac{1}{12}\pi x_{hs}^{3/2} + \frac{1}{45}\pi x_{hs}^{5/2} + \mathcal{O}\left(x_{hs}^{7/2}\right),$$

$$\mathcal{H}^{(1)}_{2,\tilde{b}\tilde{g},4} = -\frac{2L_{hb}^2}{3} - \frac{2L_{hb}}{3} + \left(-\frac{L_{hb}^2}{24} - \frac{L_{hb}}{15} - \frac{1}{10}\right) x_{hs} + \left(-\frac{L_{hb}^2}{180} - \frac{L_{hb}}{105} + \frac{29L_{bs}}{280} - \frac{4153}{29400}\right) x_{hs}^2 + \left(\frac{L_{bs}}{90} - \frac{1}{45}\right) x_{hs}^3 + \mathcal{O}\left(x_{hs}^4\right),$$

$$\mathcal{H}^{(1)}_{3,\tilde{b}\tilde{g}} = 0.$$

The LO stop contributions are given by

$$\mathcal{H}^{(0)}_{0,\tilde{t},0} = \frac{x_{ts}}{2}, \quad \mathcal{H}^{(0)}_{0,\tilde{t},2} = \frac{x_{ts}^2}{15}, \quad \mathcal{H}^{(0)}_{0,\tilde{t},4} = \frac{3x_{ts}^3}{280}, \quad \mathcal{H}^{(0)}_{1,\tilde{t}} = 0,$$

$$\mathcal{H}^{(0)}_{2,\tilde{t},0} = -\frac{1}{8}, \quad \mathcal{H}^{(0)}_{2,\tilde{t},2} = -\frac{x_{ts}}{60}, \quad \mathcal{H}^{(0)}_{2,\tilde{t},4} = -\frac{3x_{ts}^2}{1120}, \quad \mathcal{H}^{(0)}_{3,\tilde{t}} = 0.$$

For the two-loop contributions from tops and their superpartners and gluinos we obtain up to $\mathcal{O}(m_h^4)$

$$\mathcal{H}^{(1)}_{0,\tilde{t}\tilde{g},0} = \left(\frac{2L_{ts}}{3} + \frac{5}{6}\right) x_{ts} + \left(\frac{2L_{ts}}{15} + \frac{113}{225}\right) x_{ts}^2 - \frac{1}{3}\pi x_{ts}^{5/2} + \left(\frac{508}{1225} - \frac{19L_{ts}}{70}\right) x_{ts}^3 + \mathcal{O}\left(x_{ts}^{7/2}\right),$$

$$\mathcal{H}^{(1)}_{0,\tilde{t}\tilde{g},2} = \frac{x_{ts}}{30} + \left(\frac{13L_{ts}}{180} + \frac{13}{45}\right) x_{ts}^2 + \left(\frac{L_{ts}}{420} + \frac{10223}{88200}\right) x_{ts}^3 + \mathcal{O}\left(x_{ts}^{7/2}\right),$$

$$\mathcal{H}^{(1)}_{0,\tilde{t}\tilde{g},4} = \frac{11x_{ts}}{3780} + \frac{38x_{ts}^2}{4725} + \left(\frac{17L_{ts}}{1260} + \frac{1027}{14700}\right) x_{ts}^3 + \mathcal{O}\left(x_{ts}^4\right),$$

$$\mathcal{H}^{(1)}_{1,\tilde{t}\tilde{g},0} = -\frac{1}{3} + \left(-\frac{L_{ts}}{6} - \frac{1}{12}\right) x_{ts} + \frac{1}{3}\pi x_{ts}^{3/2} + \left(\frac{4L_{ts}}{15} - \frac{39}{100}\right) x_{ts}^2 - \frac{1}{24}\pi x_{ts}^{5/2} + \left(\frac{11L_{ts}}{210} - \frac{893}{88200}\right) x_{ts}^3 + \mathcal{O}\left(x_{ts}^{7/2}\right),$$

$$\mathcal{H}^{(1)}_{1,\tilde{t}\tilde{g},2} = -\frac{7}{360} - \frac{67x_{ts}}{2160} + \left(-\frac{L_{ts}}{30} - \frac{677}{10800}\right) x_{ts}^2 + \frac{4}{45}\pi x_{ts}^{5/2} + \left(\frac{31L_{ts}}{360} - \frac{5111}{50400}\right) x_{ts}^3 + \mathcal{O}\left(x_{ts}^{7/2}\right),$$

$$\mathcal{H}^{(1)}_{1,\tilde{t}\tilde{g},4} = -\frac{1}{504} - \frac{59x_{ts}}{30240} - \frac{953x_{ts}^2}{226800} + \left(-\frac{11L_{ts}}{1680} - \frac{5111}{302400}\right) x_{ts}^3 + \mathcal{O}\left(x_{ts}^{7/2}\right).$$

$$\mathcal{H}^{(1)}_{2,\tilde{t}\tilde{g},0} = -\frac{11}{18} + \left(\frac{L_{ts}}{30} - \frac{259}{1800}\right) x_{ts} + \frac{1}{12}\pi x_{ts}^{3/2} + \left(\frac{29L_{ts}}{280} - \frac{11339}{88200}\right) x_{ts}^2 - \frac{1}{96}\pi x_{ts}^{5/2} + \frac{x_{ts}^3}{144} + \mathcal{O}\left(x_{ts}^{7/2}\right),$$

$$\mathcal{H}^{(1)}_{2,\tilde{t}\tilde{g},2} = -\frac{7}{1080} - \frac{2641x_{ts}}{21600} + \left(\frac{L_{ts}}{105} - \frac{7027}{264600}\right) x_{ts}^2 + \frac{1}{45}\pi x_{ts}^{5/2} + \left(\frac{L_{ts}}{90} - \frac{1}{45}\right) x_{ts}^3 + \mathcal{O}\left(x_{ts}^{7/2}\right),$$

$$\mathcal{H}^{(1)}_{2,\tilde{t}\tilde{g},4} = -\frac{1}{1512} - \frac{113x_{ts}}{151200} - \frac{26557x_{ts}^2}{1058400} + \mathcal{O}\left(x_{ts}^3\right),$$

$$\mathcal{H}^{(1)}_{3,\tilde{t}\tilde{g}} = 0.$$

6.8.7. $h \to \gamma\gamma$ in the Limit $m_q \ll m_{\tilde{q}_1} \ll m_{\tilde{q}_2} \ll M_{\tilde{g}}$

For the limit $m_q \ll m_{\tilde{q}_1} \ll m_{\tilde{q}_2} \ll M_{\tilde{g}}$ we explicitly write down the results only for the bottom sector. Here, the large scale is $M_{\tilde{g}} = M_x$. Again, the pure SUSY part due to bottoms, sbottom and gluinos can be written in the form of Eq. (6.24). In leading order, the sbottom contributions through $\mathcal{O}(m_b^2)$ are given by

$$\mathcal{H}^{(0)}_{0,\tilde{b},0} = \sin^2 2\theta_{\tilde{b}} \left(\frac{x_{12}}{16} + \frac{x_{21}}{16} - \frac{x_{h1}}{120} - \frac{x_{h2}}{120} - \frac{1}{8}\right), \quad \mathcal{H}^{(0)}_{0,\tilde{b},2} = -\frac{x_{h1}}{4} - \frac{x_{h2}}{4},$$

$$\mathcal{H}^{(0)}_{1,\tilde{b},1} = \sin 2\theta_{\tilde{b}} \left(-\frac{1}{8}\sqrt{x_{h1}}\sqrt{x_{\tilde{g}1}} + \frac{1}{8}\sqrt{x_{h2}}\sqrt{x_{\tilde{g}2}}\right),$$

$$\mathcal{H}^{(0)}_{2,\tilde{b},0} = \left(-\frac{\cos 2\theta_{\tilde{b}}}{16} - \frac{1}{16}\right) x_{\tilde{g}1} + \left(\frac{\cos 2\theta_{\tilde{b}}}{16} - \frac{1}{16}\right) x_{\tilde{g}2},$$

$$\mathcal{H}^{(0)}_{3,\tilde{b},0} = \frac{\cos 2\theta_{\tilde{b}} x_{\tilde{g}1}}{8} - \frac{\cos 2\theta_{\tilde{b}} x_{\tilde{g}2}}{8},$$

The two-loop contributions due to sbottoms through $\mathcal{O}(m_b^2)$ are given by

$$\begin{aligned}
\mathcal{H}^{(1)}_{0,\tilde{b}\tilde{g},0} = {} & \left[\frac{L_{12}}{12} - \frac{L_{\tilde{b}_2}}{6} + \left(\frac{L_{12}}{16} - \frac{L_{\tilde{b}_2}}{6} - \frac{1}{8}\right) x_{21}\right] \sin^4(2\theta_{\tilde{b}}) + \left[-\frac{L_{12}}{12} + \frac{L_{\tilde{b}_2}}{6} + \left(-\frac{L_{12}}{8}\right.\right. \\
& \left.\left. + \frac{L_{\tilde{b}_2}}{6} + \frac{13}{48}\right) x_{21} - \frac{1}{3}\right] \sin^2 2\theta_{\tilde{b}} + \left[\left(-\frac{L_{12}}{36} - \frac{L_{\tilde{b}_2}}{45} - \frac{59}{1440}\right) \sin^4 2\theta_{\tilde{b}} + \left(\frac{11 L_{12}}{360}\right.\right. \\
& \left.\left. + \frac{L_{\tilde{b}_2}}{45} - \frac{7}{1080}\right) \sin^2 2\theta_{\tilde{b}} + \frac{L_{2\tilde{g}}}{90}\right] x_{h2} + x_{h1} \left[\left(\frac{L_{12}}{120} - \frac{L_{\tilde{b}_2}}{45} - \frac{59}{1440}\right) \sin^4 2\theta_{\tilde{b}}\right. \\
& + \left(-\frac{L_{12}}{90} + \frac{L_{\tilde{b}_2}}{45} - \frac{7}{1080}\right) \sin^2 2\theta_{\tilde{b}} + \frac{L_{1\tilde{g}}}{90} + \left(\left(-\frac{23 L_{12}}{2520} + \frac{L_{\tilde{b}_2}}{280} - \frac{25}{3024}\right) \sin^4 2\theta_{\tilde{b}}\right. \\
& \left.\left. + \left(\frac{23 L_{12}}{2520} - \frac{L_{\tilde{b}_2}}{280} + \frac{9}{1120}\right) \sin^2 2\theta_{\tilde{b}}\right) x_{h2}\right] + \left(-\frac{L_{12}}{12} - \frac{1}{48}\right) x_{1\tilde{g}} \sin^2 2\theta_{\tilde{b}} \\
& + \left[\left(-\frac{x_{12}}{72} - \frac{x_{21}}{72} + \frac{11 x_{h1}}{10080} + \frac{11 x_{h2}}{10080} + \frac{1}{30}\right) \sin^2 2\theta_{\tilde{b}} + \frac{L_{12}}{90} + \frac{L_{2\tilde{g}}}{45}\right] x_{h\tilde{g}} \\
& + \left(\frac{L_{12}}{12} + \frac{x_{21}}{72} - \frac{1}{48}\right) x_{2\tilde{g}} \sin^2 2\theta_{\tilde{b}} + \mathcal{O}(x_{1\tilde{g}} x_{h\tilde{g}}^{1/2}, x_{2\tilde{g}} x_{h\tilde{g}}^{1/2}),
\end{aligned}$$

$$\begin{aligned}
\mathcal{H}^{(1)}_{0,\tilde{b}\tilde{g},1} = {} & \sin 2\theta_{\tilde{b}} \left[\left[\left(\frac{2 L_{1\tilde{g}}}{45} - \frac{4 L_{\tilde{g}}}{45} - \frac{4}{45}\right) \sin^2 2\theta_{\tilde{b}} - \frac{2 L_{1\tilde{g}}}{45} + \frac{4 L_{\tilde{g}}}{45} + \frac{4}{45}\right] \sqrt{x_{\tilde{g}2}} x_{h1} \sqrt{x_{h2}} + \left[\left(-\frac{L_{12}}{4}\right.\right. \right. \\
& \left.\left. - \frac{1}{2}\right) L_{hb}^2 + L_{12} + \left(\left(\frac{1}{2} - \frac{L_{12}}{4}\right) L_{hb}^2 + L_{12} - 2\right) x_{12} + 2\right] \sqrt{x_{2\tilde{g}}} \sqrt{x_{2h}} \sin^2 2\theta_{\tilde{b}} + \left[\frac{L_{hb}^2}{4}\right. \\
& + \frac{L_{12}}{6} + \left(\left(\frac{L_{12}}{2} + \frac{1}{2}\right) L_{hb}^2 - \frac{11 L_{12}}{6} + \frac{L_{2\tilde{g}}}{6} - \frac{47}{24}\right) x_{12} + \left(-\frac{L_{2\tilde{g}}}{6} - \frac{1}{24}\right) x_{21} + \left(\frac{1}{9} - \frac{L_{h\tilde{g}}}{12}\right) \\
& x_{h1} + \left(\frac{L_{hb}^2}{12} + \frac{L_{h\tilde{g}}}{12} + \frac{\sqrt{x_{12}}}{45} - \frac{19}{45}\right) x_{h2} + \sin^2 2\theta_{\tilde{b}} \left(-\frac{L_{hb}^2}{4} + \left(\left(-\frac{L_{12}}{2} - \frac{13}{24}\right) L_{hb}^2 + 2 L_{12}\right.\right. \\
& \left.\left. + \frac{13}{6}\right) x_{12} + \left(\frac{L_{hb}^2}{24} - \frac{1}{6}\right) x_{21} + \left(-\frac{L_{hb}^2}{240} - \frac{1}{180}\right) x_{h1} + \left(-\frac{19 L_{hb}^2}{240} - \frac{\sqrt{x_{12}}}{45} + \frac{19}{60}\right) x_{h2}\right. \\
& \left.\left. - \frac{\sqrt{x_{12}}}{12} - \frac{\sqrt{x_{h1}} \sqrt{x_{h2}}}{90} + \frac{1}{12\sqrt{x_{12}}} + 1\right) + \frac{\sqrt{x_{12}}}{12} + \frac{\sqrt{x_{h1}} \sqrt{x_{h2}}}{90} - \frac{1}{12\sqrt{x_{12}}} - 1\right] \sqrt{x_{h\tilde{g}}}\Bigg] \\
& + \mathcal{O}(x_{1\tilde{g}} x_{h\tilde{g}}^{1/2}, x_{2\tilde{g}} x_{h\tilde{g}}^{1/2}),
\end{aligned}$$

$$\mathcal{H}^{(1)}_{0,\tilde{b}\tilde{g},2} = \left[-\frac{L_{12}\sin^2 2\theta_{\tilde{b}}}{12} + \frac{L_{2\tilde{g}}}{6} - \frac{L_{b\tilde{g}}}{2} - \frac{11}{12}\right] x_{h2} + x_{h1}\left[\frac{L_{12}\sin^2 2\theta_{\tilde{b}}}{12} + \frac{x_{h2}\sin^2 2\theta_{\tilde{b}}}{36} + \frac{L_{12}}{6} + \frac{L_{2\tilde{g}}}{6} - \frac{L_{b\tilde{g}}}{2} - \frac{11}{12}\right] + \left[L_{12}\left(\frac{L_{hb}^2}{4} - 1\right)\sin^2 2\theta_{\tilde{b}} + L_{12}\left(1 - \frac{L_{hb}^2}{4}\right) x_{12}\sin^2 2\theta_{\tilde{b}}\right] x_{2\tilde{g}} + \left[\left(\frac{L_{hb}^2}{12} - \frac{1}{3}\right)\sin^2 2\theta_{\tilde{b}} - \frac{L_{12}}{2} - L_{2\tilde{g}} + \frac{4L_{b\tilde{g}}}{3} + \frac{2L_{hb}}{3} + \left(\left(-\frac{L_{hb}^2}{24} - \frac{L_{b\tilde{g}}}{24} + \frac{1}{12}\right)\sin^2 2\theta_{\tilde{b}} - \frac{L_{1\tilde{g}}}{6} - \frac{1}{12}\right) x_{12} + \left(\left(-\frac{L_{hb}^2}{24} - \frac{L_{b\tilde{g}}}{24} + \frac{1}{12}\right)\sin^2 2\theta_{\tilde{b}} - \frac{L_{2\tilde{g}}}{6} - \frac{1}{12}\right) x_{21} + \frac{2}{9}\right] x_{h\tilde{g}} + \mathcal{O}(x_{1\tilde{g}}^2, x_{h\tilde{g}}^2, x_{2\tilde{g}}^2),$$

$$\mathcal{H}^{(1)}_{1,\tilde{b}\tilde{g},0} = \frac{\sin 2\theta_{\tilde{b}}}{360}\left(L_{1\tilde{g}}\sqrt{x_{h1}}\sqrt{x_{\tilde{g}1}} - L_{2\tilde{g}}\sqrt{x_{h2}}\sqrt{x_{\tilde{g}2}}\right) + \frac{\sin^2 2\theta_{\tilde{b}}}{24}\left(L_{1\tilde{g}}\left(1 - x_{12}\right) + L_{2\tilde{g}}\left(1 - x_{21}\right)\right) + \sin 2\theta_{\tilde{b}}\frac{L_{12}}{360}\sqrt{x_{h\tilde{g}}} + \frac{\sin^2 2\theta_{\tilde{b}}}{24}\left(L_{1\tilde{g}}x_{1\tilde{g}} + L_{2\tilde{g}}\left(1 - x_{21}\right)x_{2\tilde{g}}\right) + \mathcal{O}(x_{1\tilde{g}}x_{h\tilde{g}}^{1/2}, x_{2\tilde{g}}x_{h\tilde{g}}^{1/2}),$$

$$\mathcal{H}^{(1)}_{1,\tilde{b}\tilde{g},1} = \left[\left(\frac{L_{12}}{24} + \frac{1}{12}\right)\sin^2 2\theta_{\tilde{b}} + \left(\frac{L_{12}}{12} - \frac{L_{b\tilde{g}}}{8} + \frac{L_{2\tilde{g}}}{6} - \frac{1}{2}\right)\right]\sin 2\theta_{\tilde{b}}x_{h1}\sqrt{x_{\tilde{g}1}} + \left[\left(\frac{L_{12}}{24} - \frac{1}{12}\right)\sin^2 2\theta_{\tilde{b}} + \left(-\frac{L_{12}}{12} + \frac{L_{b\tilde{g}}}{8} - \frac{L_{2\tilde{g}}}{6} + \frac{1}{2}\right)\right]\sin 2\theta_{\tilde{b}}x_{h2}\sqrt{x_{\tilde{g}2}} + \sqrt{x_{1\tilde{g}}}\left(L_{1\tilde{g}}\left(\frac{x_{12}}{48} - \frac{3}{16}\right) + L_{2\tilde{g}}\left(\frac{3}{16} - \frac{x_{21}}{48}\right)\right) + \mathcal{O}(x_{1\tilde{g}}x_{h\tilde{g}}^{1/2}, x_{2\tilde{g}}x_{h\tilde{g}}^{1/2}),$$

$$\mathcal{H}^{(1)}_{1,\tilde{b}\tilde{g},2} = \frac{\sqrt{x_{\tilde{g}2}}x_{h2}}{48} - \frac{\sqrt{x_{\tilde{g}1}}x_{h1}}{48} + \left[L_{hb}^2 + L_{12}\left(\frac{L_{hb}^2}{2} - 2\right) + L_{12}\left(L_{hb}^2 - 4\right)x_{12} - 4\right]\sin^2 2\theta_{\tilde{b}} + L_{2\tilde{g}}\left(L_{hb}^2 - 4\right) + L_{12}\left(4 - L_{hb}^2\right)x_{12} + \left[-\frac{L_{hb}^2}{2} + \left(\frac{5L_{hb}^2}{12} - \frac{41}{24}\right)\sin^2 2\theta_{\tilde{b}} + \frac{49}{24}\right] x_{h2} + x_{h1}\left(\left(\frac{7}{24} - \frac{L_{hb}^2}{12}\right)\sin^2 2\theta_{\tilde{b}} + \frac{1}{24} + \frac{x_{h2}}{45}\left(\sin^2 2\theta_{\tilde{b}} - 1\right)\right) + \left(\frac{1}{12} - \frac{\sin^2 2\theta_{\tilde{b}}}{12}\right)\sqrt{x_{h1}}\sqrt{x_{h2}} + \sin 2\theta_{\tilde{b}}\left[-\frac{L_{12}}{48} + \left(\frac{L_{1\tilde{g}}}{48} + \frac{1}{48}\right)x_{12} + \left(-\frac{L_{2\tilde{g}}}{48} - \frac{1}{48}\right)x_{21} + \frac{x_{h1}}{720} - \frac{x_{h2}}{720}\right]\sqrt{x_{h\tilde{g}}} + \mathcal{O}(x_{1\tilde{g}}, x_{h\tilde{g}}, x_{2\tilde{g}}),$$

$$\begin{aligned}\mathcal{H}^{(1)}_{2,\tilde{b}\tilde{g},0} = &\left[\frac{L_{12}\sin^2 2\theta_{\tilde{b}}}{48} + \frac{L_{1\tilde{g}}}{24} + \cos 2\theta_{\tilde{b}}\left(\left(\frac{L_{12}}{48}+\frac{1}{24}\right)\sin^2 2\theta_{\tilde{b}} + \frac{L_{1\tilde{g}}}{24} - \frac{7}{24}\right) - \frac{7}{24}\right] x_{\tilde{g}1} \\ &+ \left[-\frac{L_{12}\sin^2 2\theta_{\tilde{b}}}{48} + \frac{L_{2\tilde{g}}}{24} + \cos 2\theta_{\tilde{b}}\left(\left(\frac{L_{12}}{48}-\frac{1}{24}\right)\sin^2 2\theta_{\tilde{b}} - \frac{L_{2\tilde{g}}}{24} + \frac{7}{24}\right) - \frac{7}{24}\right] x_{\tilde{g}2} \\ &+ \left(-\frac{\cos 2\theta_{\tilde{b}}}{12} - \frac{1}{12}\right) L_{1\tilde{g}} + \left(\frac{\cos 2\theta_{\tilde{b}}}{12} - \frac{1}{12}\right) L_{2\tilde{g}} + \left(\frac{\cos 2\theta_{\tilde{b}}}{72} + \frac{1}{72}\right) x_{h1} \\ &+ \left(\frac{1}{72} - \frac{\cos 2\theta_{\tilde{b}}}{72}\right) x_{h2} - \frac{1}{8} + \left(\frac{\cos 2\theta_{\tilde{b}}}{144} + \frac{1}{144}\right) x_{1\tilde{g}} + \left(\frac{1}{144} - \frac{\cos 2\theta_{\tilde{b}}}{144}\right) x_{2\tilde{g}} \\ &+ \mathcal{O}(x_{1\tilde{g}} x_{h\tilde{g}}^{1/2}, x_{2\tilde{g}} x_{h\tilde{g}}^{1/2}),\end{aligned}$$

$$\begin{aligned}\mathcal{H}^{(1)}_{2,\tilde{b}\tilde{g},1} = &\left[\sqrt{x_{\tilde{g}h}}\left[L_{12}\left(\frac{L_{hb}^2}{4}-1\right) + \cos 2\theta_{\tilde{b}}\left(\frac{L_{hb}^2}{2} + L_{12}\left(1+2x_{12}\right)\left(\frac{L_{hb}^2}{4}-1\right) - 2\right)\right]\right. \\ &+\sqrt{x_{\tilde{g}1}}\left[\cos 2\theta_{\tilde{b}}\sqrt{x_{h1}}\left(\frac{7}{48} - \frac{L_{hb}^2}{24}\right) + \left(\frac{1}{6} - \frac{L_{hb}^2}{24}\right)\sqrt{x_{h1}}\right] + \sqrt{x_{\tilde{g}2}}\left(\sqrt{x_{h2}}\left(\frac{L_{hb}^2}{24} - \frac{1}{6}\right)\right. \\ &+ \cos 2\theta_{\tilde{b}}\left(\left(\frac{5L_{hb}^2}{24} - \frac{41}{48}\right)\sqrt{x_{h2}} - \frac{\sqrt{x_{h1}}}{24}\right)\Big) + \sqrt{x_{1\tilde{g}}}\left[\sqrt{x_{1h}}\left(\left(\frac{L_{1\tilde{g}}}{2}+\frac{1}{4}\right)L_{hb}^2\right.\right. \\ &\left.\left.-2L_{1\tilde{g}} - 1\right) + \cos 2\theta_{\tilde{b}}\left(\sqrt{x_{1h}}\left(\frac{L_{hb}^2}{4} - 1\right) + L_{12}\left(\frac{L_{hb}^2}{2} - 2\right)\sqrt{x_{1h}}\right)\right] + \sqrt{x_{2\tilde{g}}} \\ &\left[\cos 2\theta_{\tilde{b}}\sqrt{x_{2h}}\left(\frac{L_{hb}^2}{4} - 1\right) + L_{12}\left(\frac{L_{hb}^2}{2} - 2\right)\sqrt{x_{2h}} + \left(\left(-\frac{L_{1\tilde{g}}}{2} - \frac{1}{4}\right)L_{hb}^2 + 2L_{1\tilde{g}} + 1\right)\right. \\ &\left.\sqrt{x_{2h}}\right] + \left[L_{12}\left(-\frac{L_{hb}^2}{8} - \frac{L_{b\tilde{g}}}{2} - \frac{1}{3}\right) + \cos 2\theta_{\tilde{b}}\left(-\frac{5L_{hb}^2}{24} - L_{b\tilde{g}} + L_{12}\left(-\frac{L_{hb}^2}{8} - \frac{L_{b\tilde{g}}}{2} - \frac{1}{3}\right)\right.\right. \\ &\left.\left.\left.-\frac{x_{21}}{576} - \frac{\sqrt{x_{12}}}{144} - \frac{1}{144\sqrt{x_{12}}} - \frac{27}{32} + \left(\frac{L_{hb}^2}{2} + L_{12}\left(-L_{b\tilde{g}} - \frac{5}{3}\right) - \frac{1153}{576}\right)x_{12}\right)\right]\sqrt{x_{h\tilde{g}}}\right] \\ &\sin 2\theta_{\tilde{b}} + \mathcal{O}(x_{2\tilde{g}} x_{h\tilde{g}}^{1/2}, x_{1\tilde{g}} x_{h\tilde{g}}^{1/2}, x_{1\tilde{g}}^{1/2} x_{h\tilde{g}}^{1/2} x_{2\tilde{g}}^{1/2}),\end{aligned}$$

$$\begin{aligned}\mathcal{H}^{(1)}_{2,\tilde{b}\tilde{g},2} = &3 + \left(-\frac{L_{2\tilde{g}}}{2} - \frac{3}{4}\right)L_{hb}^2 + 2L_{2\tilde{g}} + \left(1+\cos 2\theta_{\tilde{b}}\right)L_{12}\left(1 - \frac{L_{hb}^2}{4}\right) + \left[\frac{L_{hb}^2}{24} + \frac{L_{b\tilde{g}}}{24}\right. \\ &\left.+ \cos 2\theta_{\tilde{b}}\left(\frac{L_{hb}^2}{24} + \frac{L_{b\tilde{g}}}{24} - \frac{1}{6}\right) - \frac{1}{6}\right] x_{h1} + \left[\frac{L_{hb}^2}{24} + \frac{L_{b\tilde{g}}}{24} + \cos 2\theta_{\tilde{b}}\left(-\frac{L_{hb}^2}{24}\right.\right. \\ &\left.\left.-\frac{L_{b\tilde{g}}}{24} + \frac{1}{6}\right) - \frac{1}{6}\right] x_{h2} + \left(\frac{L_{b\tilde{g}}}{12} + \frac{1}{8}\right) x_{h\tilde{g}} + \mathcal{O}(x_{1\tilde{g}} x_{h\tilde{g}}^{1/2}, x_{2\tilde{g}} x_{h\tilde{g}}^{1/2}),\end{aligned}$$

$$\mathcal{H}^{(1)}_{3,\tilde{b}\tilde{g},0} = \left[\left(-\frac{L_{12}}{24} - \frac{1}{12}\right)\sin^2 2\theta_{\tilde{b}} - \frac{L_{1\tilde{g}}}{12} + \frac{7}{12}\right] x_{\tilde{g}1} + x_{\tilde{g}2}\left[\left(-\frac{L_{12}}{24} + \left(-\frac{L_2}{45} - \frac{23}{360}\right) x_{h1} + \frac{1}{12}\right)\sin^2 2\theta_{\tilde{b}} + \frac{L_{2\tilde{g}}}{12} - \frac{7}{12}\right] + \frac{L_{12}}{6} - \frac{x_{h1}}{36} + \frac{x_{h2}}{36} + \frac{x_{2\tilde{g}}}{72} - \frac{x_{1\tilde{g}}}{72} + \mathcal{O}(x_{1\tilde{g}} x_{h\tilde{g}}^{1/2}, x_{2\tilde{g}} x_{h\tilde{g}}^{1/2}),$$

$$\mathcal{H}^{(1)}_{3,\tilde{b}\tilde{g},1} = \sqrt{x_{\tilde{g}1}}\sqrt{x_{h1}}\left(\frac{L_{hb}^2}{12} - \frac{7}{24} - \frac{x_{h2}}{45}\right) + \sqrt{x_{\tilde{g}2}}\left[\sqrt{x_{h2}}\left(\frac{41}{24} - \frac{5L_{hb}^2}{12}\right) + \frac{\sqrt{x_{h1}}}{12}\right] + \Big(-L_{hb}^2 + L_{12}\left(2 - \frac{L_{hb}^2}{2}\right) + 4\Big)\sqrt{x_{\tilde{g}h}} + \sqrt{x_{2\tilde{g}}}\sqrt{x_{2h}}\left(2 - \frac{L_{hb}^2}{2}\right) + \sqrt{x_{1\tilde{g}}}\sqrt{x_{1h}}\left(-\frac{1}{2}L_{hb}^2 + L_{12}\left(4 - L_{hb}^2\right) + 2\right) + \left[\frac{5L_{hb}^2}{12} + 2L_{b\tilde{g}} + L_{12}\left(\frac{L_{hb}^2}{4} + L_{b\tilde{g}} + \frac{2}{3}\right) + \Big(-L_{hb}^2 + L_{12}\left(2L_{b\tilde{g}} + \frac{10}{3}\right) + \frac{1153}{288}\Big) x_{12} + \frac{x_{21}}{288} + x_{h1}\left(-\frac{L_{hb}^2}{30} - \frac{L_{b\tilde{g}}}{6} - \frac{x_{h2}}{840} - \frac{13}{90}\right) + \left(\frac{2L_{hb}^2}{15} + \frac{5L_{b\tilde{g}}}{6} + \frac{77}{90}\right) x_{h2} + \frac{\sqrt{x_{12}}}{72} + \frac{1}{72\sqrt{x_{12}}} + \frac{27}{16}\right]\sqrt{x_{h\tilde{g}}} + \mathcal{O}(x_{1\tilde{g}} x_{h\tilde{g}}^{1/2}, x_{2\tilde{g}} x_{h\tilde{g}}^{1/2}, x_{1\tilde{g}}^{1/2} x_{h\tilde{g}}^{1/2} x_{2\tilde{g}}^{1/2}),$$

$$\mathcal{H}^{(1)}_{3,\tilde{b}\tilde{g},2} = L_{12}\left(\frac{L_{hb}^2}{2} - 2\right) + \left(-\frac{L_{hb}^2}{12} - \frac{L_{b\tilde{g}}}{12} + \frac{1}{3}\right) x_{h1} + \left(\frac{L_{hb}^2}{12} + \frac{L_{b\tilde{g}}}{12} - \frac{1}{3}\right) x_{h2} + \mathcal{O}(x_{1\tilde{g}}, x_{h\tilde{g}}, x_{2\tilde{g}}).$$

6.9. Results for the Partial Decay Width $\Gamma(\phi \longrightarrow \gamma\gamma)$

In the following we investigate the results for the partial decay widths of a Higgs decaying into two photons schematically. The effects through bottoms/sbottoms are compared with the top/stop effects. First, the decay of CP-odd Higgs bosons is under investigation. For this case the NLO-SUSY parts are particularly important since there is no contribution from SUSY particles in LO. Afterwards, the decay of the lightest scalar MSSM Higgs boson into two photons is examined. For this process, already at leading order there are contributions originating from stops and sbottoms.

If not mentioned otherwise, the parameters we use in the following are set to

$$m_t = 172.4\ \text{GeV},\ m_b = 4.2\ \text{GeV},\ \overline{m}_b(2\,\text{GeV}) = 4.2\ \text{GeV},$$
$$\alpha_s(M_Z) = 0.1176,\ M_Z = 91.1876\ \text{GeV},\ \mu_R = m_\phi.$$

For the photonic decay of scalar as well as pseudoscalar Higgs bosons, we investigate the limiting cases given by

$$\begin{aligned} &m_q \ll M_s \equiv m_{\tilde{q}_1} = m_{\tilde{q}_2} = m_{\tilde{g}}, \\ &m_q \ll m_{\tilde{q}_1} = m_{\tilde{q}_2} \ll m_{\tilde{g}} \\ &m_q \ll m_{\tilde{q}_1} \ll m_{\tilde{q}_2} = m_{\tilde{g}}, \\ &m_q \ll m_{\tilde{q}_1} \ll m_{\tilde{q}_2} \ll m_{\tilde{g}}, \end{aligned}$$

where $q\tilde{q} = t\tilde{t},\, b\tilde{b}$.

6.9.1. $A \to \gamma\gamma$

For the process $A \to \gamma\gamma$, the decay width in NLO-SQCD is given by (cf. Eq. (6.12))

$$\begin{aligned} \Gamma_{SQCD}\left(A \to \gamma\gamma\right) =& \frac{G_F \alpha^2 m_A^3}{128\sqrt{2}\pi^3} \left| N_c \sum_{q\tilde{q}=t\tilde{t},b\tilde{b}} Q_q^2 \left(\mathcal{A}_{q\tilde{q}}^{(0)} + \frac{\alpha_s}{\pi} \mathcal{A}_{q\tilde{q}}^{(1)} \right) + \mathcal{O}\left(\alpha_s^2\right) \right|^2 \\ =& \frac{G_F \alpha^2 m_A^3}{128\sqrt{2}\pi^3} \left| N_c \left[Q_t^2\, \mathcal{A}_t^{(0)} + Q_b^2\, \mathcal{A}_b^{(0)} + \frac{\alpha_s}{\pi} \left[Q_t^2\, \mathcal{A}_t^{(1)} + Q_b^2\, \mathcal{A}_b^{(1)} \right] \right.\right. \\ &\left.\left. + \frac{\alpha_s}{\pi} \left[Q_t^2\, \mathcal{A}_{t\tilde{g}}^{(1)} + Q_b^2\, \mathcal{A}_{b\tilde{g}}^{(1)} \right] + \mathcal{O}\left(\alpha_s^2\right) \right] \right|^2 . \end{aligned}$$

Being interested in the NLO part of the decay width, at this order, we include the LO squared parts of the amplitude plus the interference terms consisting of the one-loop (label (0)) times the two-loop (label (1)) parts of the amplitude. One has to pay attention that the absolute square values of the pure NLO contributions are already contributing to higher orders, which are not considered here. Therefore, those are not included in the plots shown later on.

We compare the QCD results of top and bottom quarks with the contributions obtained by taking into account their superpartners and the gluino at the two-loop level. Although the pseudoscalar Higgs boson is not a SM particle, "QCD part" refers to only taking into account SM particles like quarks and gluons in the loops. The two-loop QCD results to the amplitude are taken from [76]. For this process we then calculate the NLO-SQCD corrections. The influence of the contribution of bottom squarks on the partial decay width is examined. This is closely connected to examining the dependence of the results on different values for $\tan\beta$.

As expected and shown in Fig. 6.9, the contribution for the LO top part decreases with growing $\tan\beta$ whereas the bottom contribution increases with growing $\tan\beta$. The graphs display the contributions to the partial decay widths for the LO parts in dependence of the mass of the pseudoscalar Higgs boson m_A. The contributions of the tops and bottoms

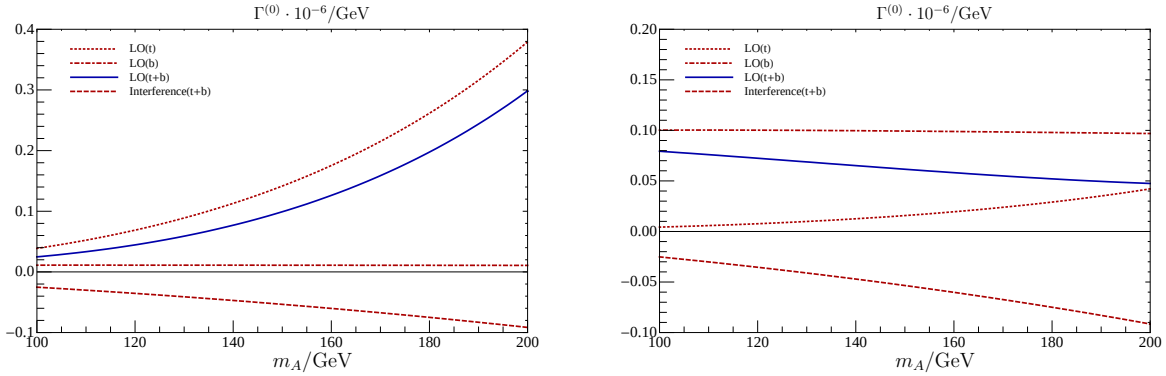

(a) $\tan\beta = 5$ (b) $\tan\beta = 15$

Figure 6.9.: *The LO partial decay width* $\Gamma^{(0)}$ *is displayed in dependence of* m_A*. It is shown for (a)* $\tan\beta = 5$ *and (b)* $\tan\beta = 15$ *(top: dotted red; bottom: dashed-dotted red; sum: solid blue; interference term: dashed red).*

to the LO are plotted separately and combined as well as their interference term which is negative. The diagram Fig. 6.9(a) is done for $\tan\beta = 5$ whereas in 6.9(b) $\tan\beta = 15$.

In order to clarify the dependence of the LO partial decay width on $\tan\beta$, Fig. 6.10(a) is plotted. There, the LO curves for the top parts, bottom parts and their sum are displayed in dependence of $\tan\beta$ for $m_A = 200$ GeV. The color coding is identical to the one in Fig. 6.9. Here, one clearly observes that the contributions from top quarks dominate for values of $\tan\beta$ of up to about 12. Beyond that value, the contributions from bottom quarks form the shape of the LO partial decay widths.

Furthermore, the running of the bottom mass is taken into account. As we investigate the results for the decay widths at the scale of the order of the top mass and larger, it seems appropriate to replace the bottom pole mass with the running bottom mass. First, the effect of only replacing the pole bottom mass at the Higgs-bottom Yukawa coupling with the running bottom mass is examined. Subsequently, all pole masses are replaced with a running bottom mass.

Fig. 6.10(b) illustrates the effects of these different assumptions for the bottom mass on the partial decay width in dependence of $\tan\beta$ with a Higgs mass set to $m_A = 200$ GeV. For the range of $\tan\beta$ where the top quarks account for the dominant contributions to the LO decay width, the influence of a running bottom mass is practically not visible in the diagram. The observation is that the partial decay width decreases for larger $\tan\beta$ if one replaces the pole bottom mass at the Higgs-bottom Yukawa coupling with the running bottom mass. $\Gamma^{(0)}$ decreases even further in case all bottom pole masses are replaced with the running bottom mass.

In the next step the NLO-QCD contributions from quarks of the third family are included. These are taken from [76] and dressed with the appropriate prefactors to include them into

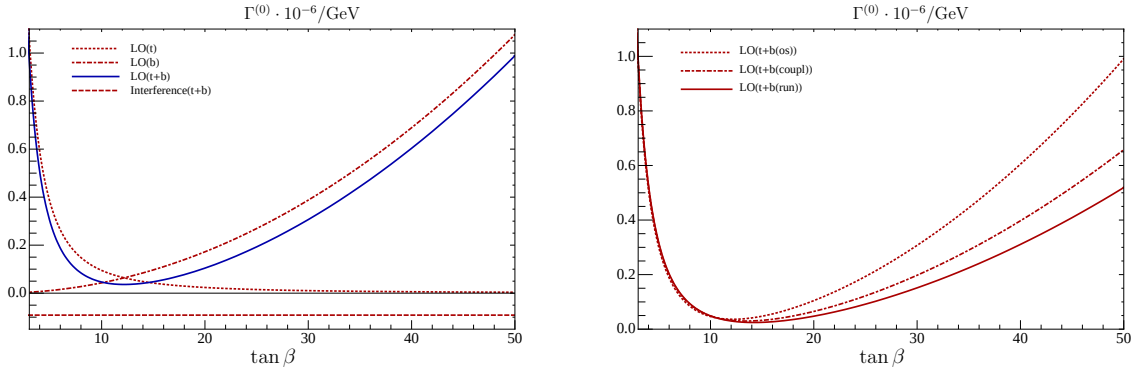

(a) (b)

Figure 6.10.: *The LO partial decay width* $\Gamma^{(0)}$ *is displayed in dependence of* $\tan\beta$ *for* $m_A = 200$ *GeV. (a) It is shown for the top parts (dotted red) the bottom parts (dashed-dotted red) and their sum (solid blue) as well as their interference term which is constant and negative (dashed red). (b)* $\Gamma^{(0)}$ *is shown for an on-shell bottom mass (dotted line) compared to a running bottom mass for the coupling (dashed-dotted) and to all bottom masses being replaced by the running one (solid).*

our calculation.

Fig. 6.11 depicts a comparison between the LO and NLO-QCD partial decay widths with an on-shell bottom mass, only the bottom mass at the Higgs-bottom Yukawa coupling replaced by the running bottom mass and all bottom masses replaced by the running ones. For $\tan\beta = 5$ (see Fig. 6.11 (a)) one almost cannot distinguish between the leading order and NLO-QCD parts and a running or on-shell bottom mass. As the contributions from top quarks dominate the result for smaller values of $\tan\beta$ the effects through taking a running bottom mass instead of the pole bottom mass become more pronounced for larger $\tan\beta$ (see Fig. 6.11 (b),(c)). In contrast, for $\tan\beta = 15$ and $\tan\beta = 25$ one can clearly distinguish the NLO from the LO. The convergence of the NLO compared to the LO order also gets better by taking the bottom mass at the coupling to be running and the distance of the NLO and LO order curves is smallest if one takes all the bottom masses to be the running ones.

Since we observe a better convergence for taking the bottom masses to be running ones, in the following we only display diagrams in which all bottom masses are replaced by the running bottom mass.

The next figures display the results for the partial decay widths in NLO-SQCD. Here, all the effects due to supersymmetric particles in the NLO are due to mixed gluino-quark-squark diagrams for the decay of pseudoscalar Higgs bosons into two photons (cf. Fig. 6.8). This means that all the SUSY effects we investigate originate from gluinos.

In the following diagrams, if not mentioned otherwise, all the SUSY mass scales are set to $M_s = 350$ GeV and $\mu_{susy} = 200$ GeV.

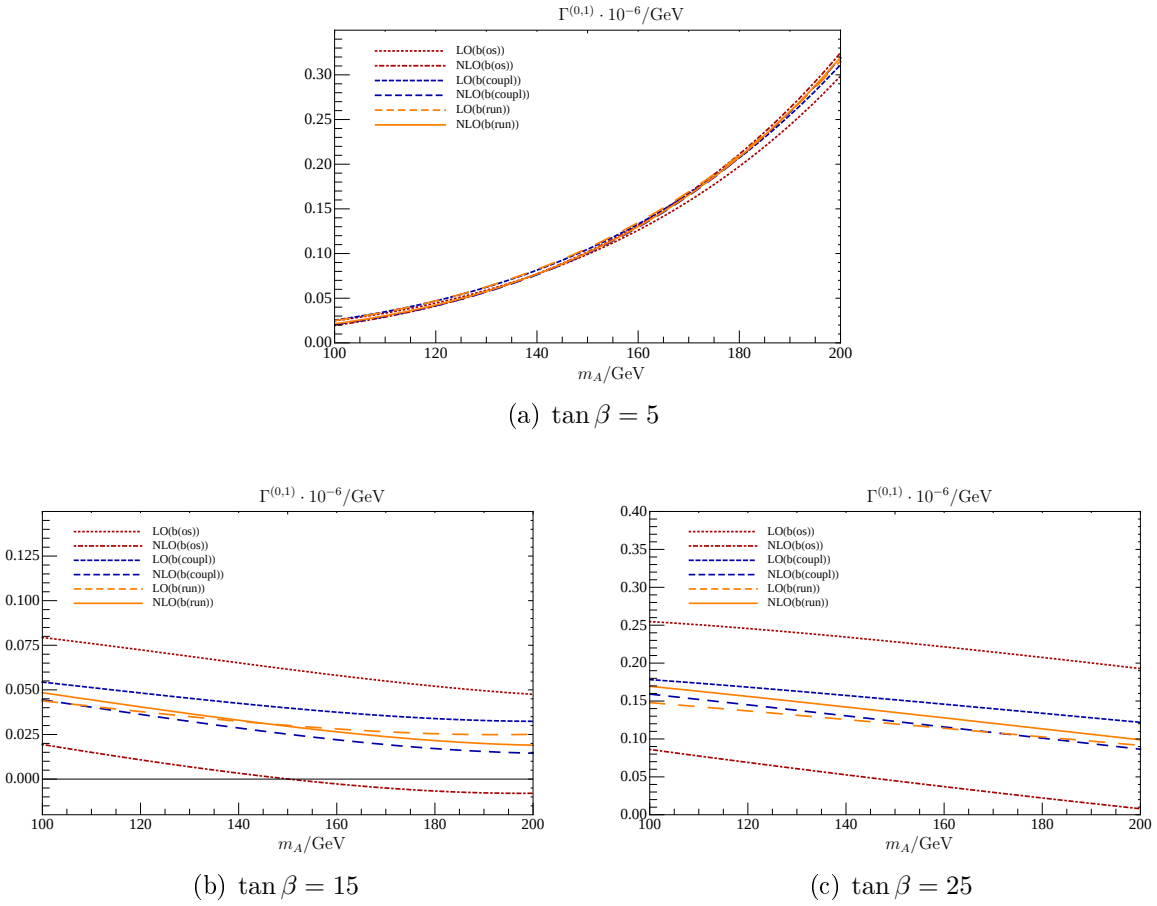

(a) $\tan\beta = 5$

(b) $\tan\beta = 15$

(c) $\tan\beta = 25$

Figure 6.11.: *The LO and NLO-QCD partial decay widths* $\Gamma^{(0,1)}$ *are displayed in dependence of* m_A *for different values of* $\tan\beta$*. We investigate the effect on the LO and NLO-QCD partial decay widths by taking an on-shell bottom mass (red; b(os); LO: dotted, NLO: dashed-dotted) compared to a running bottom mass at the coupling (blue; b(coupl); LO: dashed; NLO: long-dashed) and to taking all bottom masses to be running ones (yellow; b(run); LO: long-dashed; NLO: solid). Different scales were chosen on the vertical axes.*

In Fig. 6.12 we investigate the effect of squarks on the NLO decay rate in dependence of m_A for the case where $M_s \equiv m_{\tilde{q}_1} = m_{\tilde{q}_2} = m_{\tilde{g}},\ \tilde{q} = \tilde{t}, \tilde{b}$, i.e., where we set the SUSY mass scales to one scale. The LO decay width is shown in blue. The red curves display the NLO decay widths of which we show the NLO-QCD and NLO-QCD plus stop curves, i.e., the ones where in addition to the QCD effects only the effects through stops are included, and the entire NLO-SQCD results. We observe that the — previously unknown — sbottom contributions do have a significant effect on the decay width for larger $\tan\beta$. Because the LO-SQCD part for $\Gamma(A \to \gamma\gamma)$ only contains contributions from top and bottom quarks, squarks first arise in the calculation at NLO-SQCD.

We find that the contributions of top squarks are up to 8% compared to the NLO-QCD partial decay width. But taking into account the effects through bottom squarks as well to obtain the entire NLO-SQCD result, we observe a strong suppression of the decay width for large $\tan\beta$. This can be seen in Fig. 6.12(b)-(d), where the solid curves display the NLO-SQCD partial decay width which include the sbottoms. In Fig. 6.12(a) (Fig. 6.12(b)) the sbottoms are responsible for a change up to 2% (22%) compared to the NLO partial decay width that includes the top sector as well as the two-loop bottom effects. For $\tan\beta = 25$ (Fig. 6.12(c)) the size of the two-loop sbottom contributions amounts to 33% and for $\tan\beta = 35$ (Fig. 6.12(d)) their size is up to 47% compared to the NLO-QCD plus stop result. Since $M_s = 350$ GeV was taken to be rather small in these plots, we have to keep in mind that the corrections get smaller, the larger the SUSY masses are chosen.

It was checked that by keeping μ_{susy} fixed and letting the SUSY masses tend to infinity that the SUSY effects disappear and the QCD result is recovered in that limiting case which we denote the "SM-limit" (see Sec. 6.7.2). In this sense the SUSY particles decouple.

Fig. 6.13 again compares the effects on the NLO decay widths due to stops and sbottoms in dependence of m_A. For all four graphs we take $\tan\beta = 25$. The result obtained in the limit $m_t \ll m_{\tilde{t}_1} \ll m_{\tilde{t}_2} = m_{\tilde{g}}$ and $m_b \ll m_{\tilde{b}_1} \ll m_{\tilde{b}_2} = m_{\tilde{g}}$ is analyzed. The plot styles and colors are chosen analogously to Fig. 6.12. From Fig. 6.13 (a)-(c) the SUSY masses are gradually increased and the observation is as expected in that the NLO-SQCD decay widths approaches the NLO-QCD result the larger the SUSY masses get. Furthermore, effects from sbottoms are sizable in the NLO-SQCD result for the partial decay widths. In Fig. 6.13 the sbottom (stop) effects account for up to 35% (8%), in (b) 25% (6%) in (c) 14% (4%) and in (d) 6% (1%) of the NLO partial decay widths.

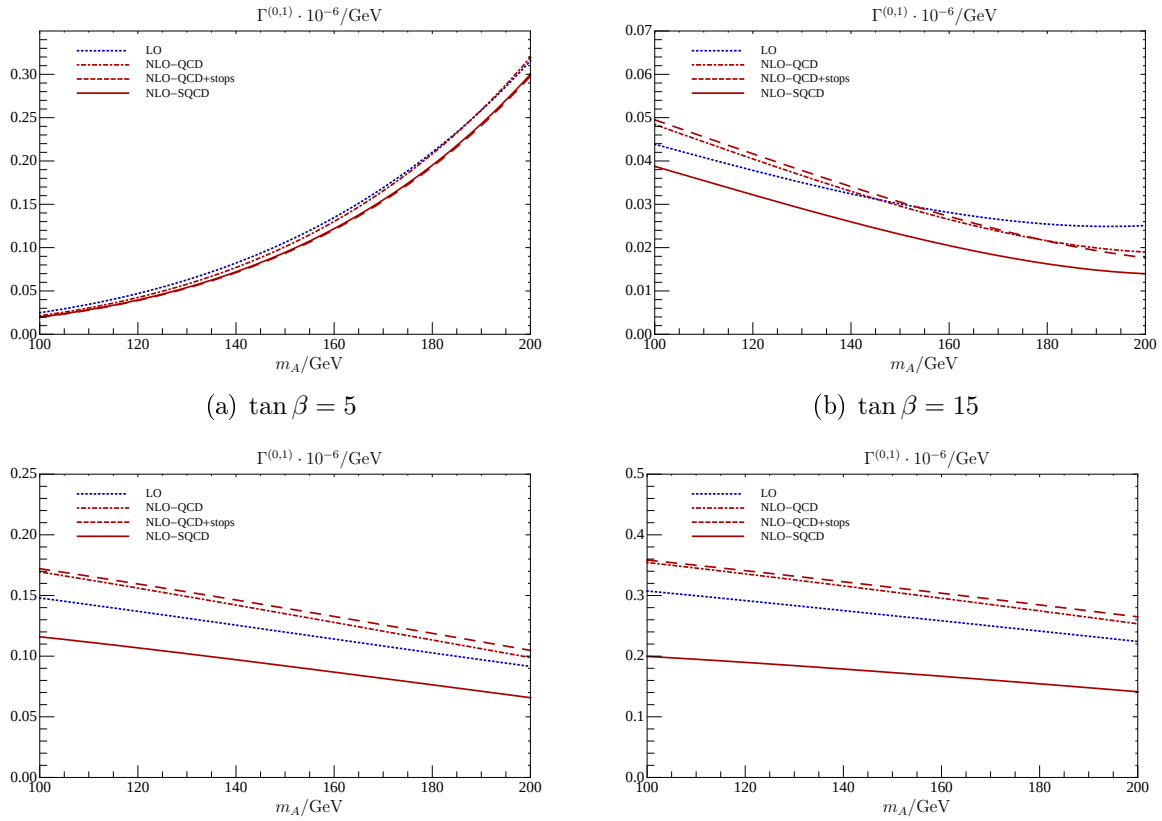

(a) $\tan\beta = 5$ (b) $\tan\beta = 15$

(c) $\tan\beta = 25$ (d) $\tan\beta = 35$

Figure 6.12.: *The LO and NLO partial decay width* $\Gamma^{(0,1)}$ *illustrated in dependence of* m_A *and a fixed value of* $\tan\beta$*. All the bottom masses are taken to be running ones. The LO curve is given in blue (dotted). We exhibit the NLO partial decay widths (red) by successively including first, the effects due to top squarks to the SM result and finally, the sbottom effects as well to obtain the entire NLO-SQCD result. The NLO-QCD (dashed-dotted) parts, the NLO-QCD+*$\tilde{t}$ *(dashed) and the NLO-SQCD (solid) decay widths are compared to each other. Here, all the SUSY mass scales are chosen to be equal, i.e.,* $M_s \equiv m_{\tilde{q}_1} = m_{\tilde{q}_2} = m_{\tilde{g}}$*,* $\tilde{q} = \tilde{t}, \tilde{b}$ *with* $M_s = 350$ *GeV.*

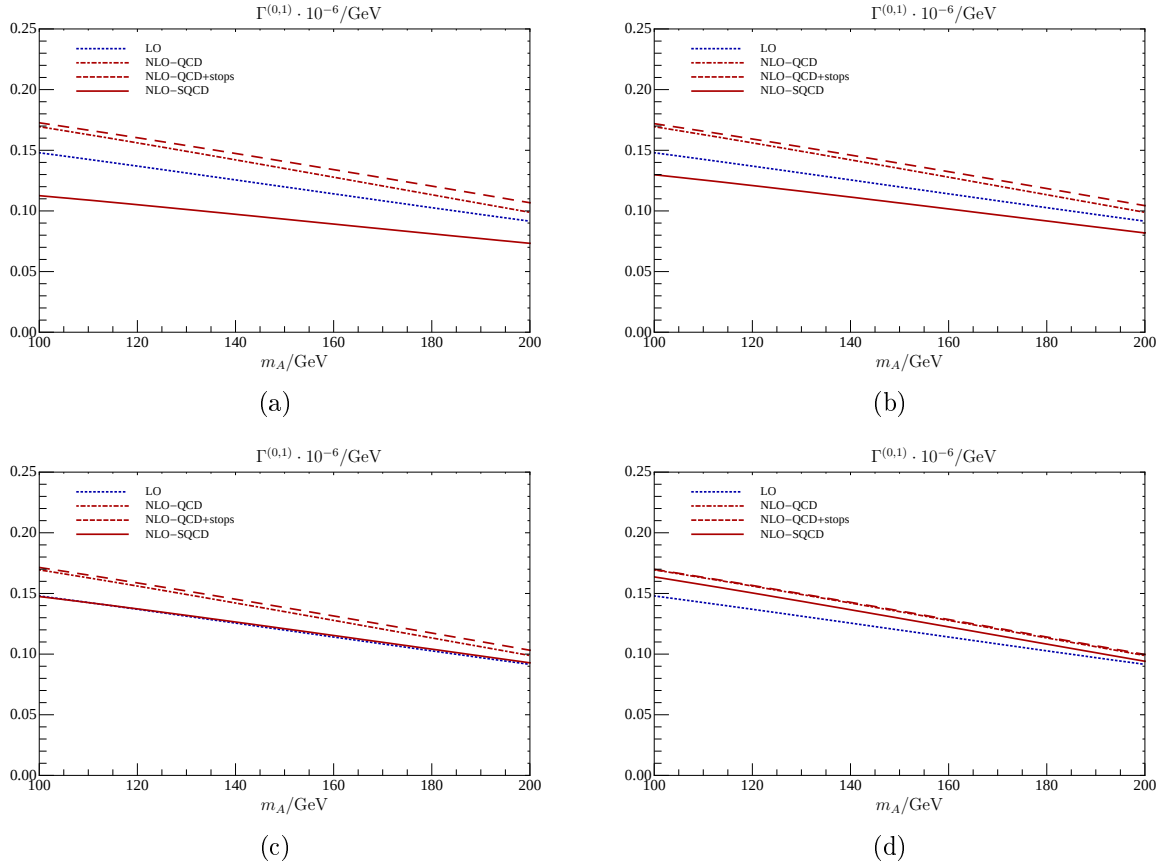

Figure 6.13.: *Here, we examine the behavior of the LO and NLO partial decay widths by successively including first the effects due to top squarks and finally the sbottom effects as well.* Γ *is displayed in dependence of* m_A *with* $\tan\beta = 25$. *The LO is shown in blue (dotted). The NLO parts are coded in red. The solid curves depict the NLO-QCD parts, the dashed-dotted curves the NLO-QCD+*$\tilde{t}$ *results and the long-dashed curves are the ones for the full NLO-SQCD decay width. We consider the limiting case where* $m_q \ll m_{\tilde{q}_1} \ll m_{\tilde{q}_2} = m_{\tilde{g}}$, $q\tilde{q} = t\tilde{t}, b\tilde{b}$. *The masses of the SUSY particles vary as follows (a)* $m_{\tilde{t}_1} = 250\ GeV$, $m_{\tilde{b}_1} = 250\ GeV$, $m_{\tilde{g}} = 450\ GeV$ *(b)* $m_{\tilde{t}_1} = 250\ GeV$, $m_{\tilde{b}_1} = 350\ GeV$, $m_{\tilde{g}} = 600\ GeV$ *(c)* $m_{\tilde{t}_1} = 300\ GeV$, $m_{\tilde{b}_1} = 500\ GeV$, $m_{\tilde{g}} = 800\ GeV$ *(d)* $m_{\tilde{t}_1} = 1000\ GeV$, $m_{\tilde{b}_1} = 2000\ GeV$, $m_{\tilde{g}} = 5000\ GeV$.

6.9.2. Evaluation of the Results in the SPS 1a-Scenario

Next, we examine the results obtained in the limit $m_q \ll m_{\tilde{q}_1} \ll m_{\tilde{q}_2} \ll m_{\tilde{g}}$, $q\tilde{q} = t\tilde{t}, b\tilde{b}$. In this limit we can investigate the NLO-SQCD decay width depending on five different MSSM mass scales, i.e., the four squark masses and the gluino mass, appearing in the loops. The aim is to obtain an estimate of the size of the NLO partial decay widths in a so-called MSSM benchmark-scenario. The effect of the sbottom contributions on the decay width is examined.

The unconstrained version of the MSSM does not assume a distinct mechanism of the breaking of SUSY. It contains more than 100 new parameters in addition to the SM parameters. In order to restrict the parameter space, tangible SUSY-breaking scenarios are assumed. Common scenarios like minimal supergravity (mSUGRA), gauge-mediated SUSY-breaking (GMSB) and anomaly-mediated SUSY-breaking (AMSB) reduce the number of parameters with respect to the unconstrained MSSM. To reduce the number of parameters even further, one assumes so-called benchmark scenarios. This means that one only takes special parameter points or a one-dimensional parameter-space (model line) which displays the features of the MSSM parameter space. In Ref. [85] some representative SUSY scenarios are defined. In general, a benchmark scenario consists of a model line (slope), which corresponds to a continuous set of parameters that runs through the benchmark point.

In this thesis we investigate our results in the SPS 1a scenario which is a mSUGRA scenario. The SPS 1a point is characterized by [85]

$$m_0 = 100 \text{ GeV}, \quad m_{1/2} = 250 \text{ GeV}, \quad A_0 = -100 \text{ GeV}, \quad \tan\beta = 10, \quad \text{sign}(\mu_{susy}) = +1,$$

with the slope defined as

$$m_0 = -A_0 = 0.4\, m_{1/2}, \quad m_{1/2} \text{ varies.}$$

m_0 is the scalar mass parameter, $m_{1/2}$ the gaugino mass parameter and A_0 the trilinear coupling. The sign of the Higgs mixing parameter is chosen to be positive. With the help of the renormalization group equations in the MSSM, m_0 and $m_{1/2}$ at the mSUGRA scale are evaluated down to the MSSM scale and thus the masses of the matter particles are obtained. From the running of m_0 the masses of the scalar particles are calculated and analogously from $m_{1/2}$ the masses of the fermions are obtained. For the calculation of the spectrum, the following parameters are chosen as an input

$$M_Z = 91.1876 \text{ GeV}, \ \overline{m}_b = 4.2 \text{ GeV}, \ m_t = 172.4 \text{ GeV}, \ m_\tau = 1.777 \text{ GeV}, \ \mu_R = m_\phi,$$
$$\alpha^{-1}(M_Z) = 127.934 \text{ GeV}, \ G_F = 1.16637 \times 10^{-5} \text{ GeV}^{-2}, \ \alpha_s(M_Z) = 0.118,$$

where m_τ is the mass of the τ lepton, $\alpha(M_Z)$ is the fine structure constant at M_Z (not to be mixed up with the Higgs mixing angle that is denoted by α as well) and G_F is the Fermi constant.

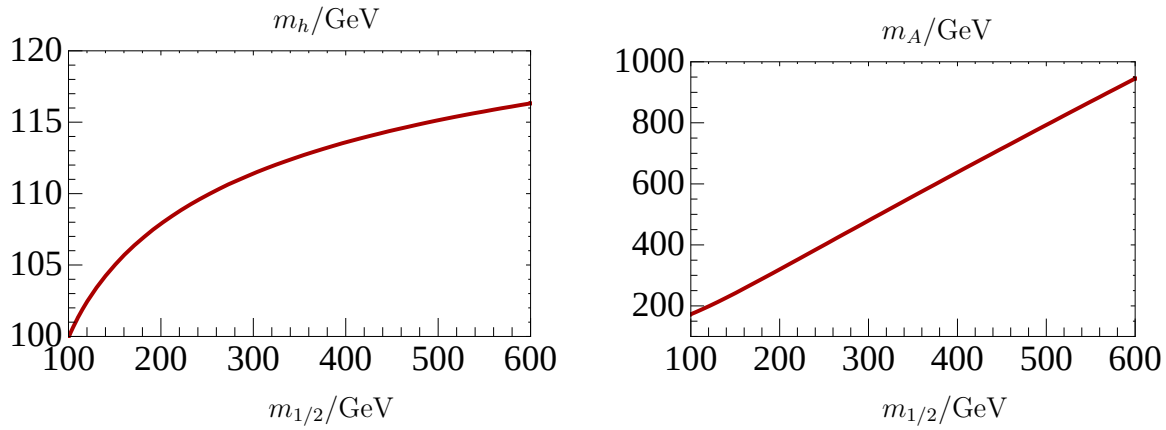

Figure 6.14.: *The scalar and pseudoscalar Higgs masses in dependence of $m_{1/2}$ along the slope of SPS 1a.*

The SUSY spectrum belonging to SPS1a which fixes the masses of the squarks, gluinos and Higgs bosons, the squark mixing angles $\theta_{\tilde{t}}$, $\theta_{\tilde{b}}$, the Higgs mixing angle α and μ_{susy} for varying $m_{1/2}$ is evaluated with the help of the program `suspect` [86]. For $m_{1/2} \in [100\text{ GeV}, 600\text{ GeV}]$ the variation of the parameters relevant for our calculations are

$$\begin{aligned}
99\text{ GeV} \leq m_h &\leq 116\text{ GeV},\\
148\text{ GeV} \leq m_A &\leq 896\text{ GeV},\\
172\text{ GeV} \leq m_{\tilde{t}_1} &\leq 945\text{ GeV},\\
327\text{ GeV} \leq m_{\tilde{t}_2} &\leq 1190\text{ GeV},\\
227\text{ GeV} \leq m_{\tilde{b}_1} &\leq 1153\text{ GeV},\\
327\text{ GeV} \leq m_{\tilde{b}_2} &\leq 1202\text{ GeV},\\
266\text{ GeV} \leq m_{\tilde{g}} &\leq 1360\text{ GeV},\\
144\text{ GeV} \leq \mu_{susy} &\leq 775\text{ GeV},\\
0.6488 \geq \theta_{\tilde{b}} &\geq 0.1991,\\
0.8638 \geq \theta_{\tilde{t}} &\geq 0.1181,\\
-0.2259 \leq \alpha &\leq -0.1057.
\end{aligned}$$

In the chosen mass range of $m_{1/2}$, besides m_h the masses of the sparticles vary linearly with $m_{1/2}$. The dependence of the Higgs masses and squark masses on $m_{1/2}$ is shown in Figs. 6.14 and 6.15. As can be seen in Fig. 6.15 the gluino mass gets larger than all of the squark masses for about $m_{1/2} = 220$ GeV and higher values of $m_{1/2}$. In the limiting case under consideration the gluino mass was chosen to be the largest SUSY scale, that is why for $m_{1/2} \geq 220$ GeV the hierarchy among the SUSY masses is a better approximation to our case. In the following diagrams all the bottom masses are taken to be running in

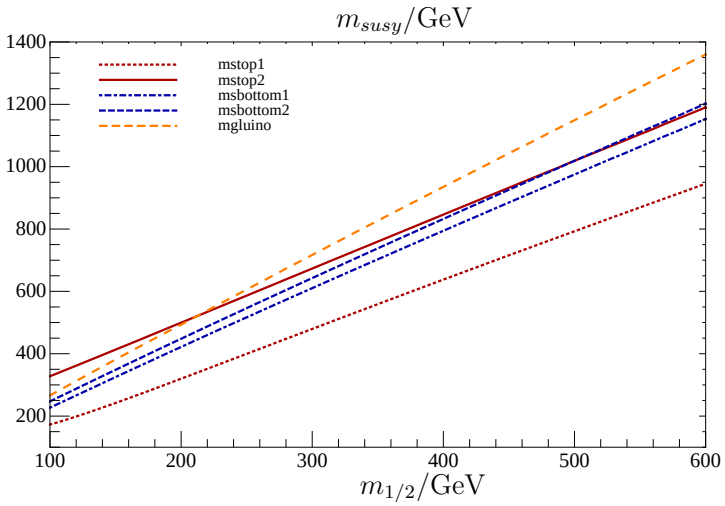

Figure 6.15.: *The masses of the top squarks, bottom squarks and gluino in dependence of $m_{1/2}$ along the slope of SPS 1a.*

dependence of the Higgs mass scale.

Fig. 6.16 displays the results for the partial decay widths in dependence of $m_{1/2}$ in the SPS 1a scenario. The LO-SQCD (dotted red) and NLO-QCD (dashed-dotted red) results are compared to the NLO-QCD plus stop (dashed blue) and NLO-SQCD (solid blue) results for the partial decay widths. In addition, the pure top/stop result without any effects from bottoms/sbottoms is shown in yellow. In case of the decay of the pseudoscalar Higgs boson the graphs in Fig. 6.16(a) show a peak at $m_{1/2} \approx 220$ GeV, which corresponds to $m_A \approx 345\,\text{GeV} \approx 2m_t$. It comes from the threshold which the process possesses. The result does contain an imaginary part in case $4m_t^2 < m_A^2$. The threshold is at $m_A = 2m_t$. In Fig. 6.16(b) we zoom into the region below the threshold. Including (above) the threshold, the stop effects amount to about 22% (5%) compared to the NLO-QCD partial decay widths. The sbottom effects including (above) the threshold are of a size of up to 28% (9%). In the SPS 1a scenario, the sbottom and stop effects on the NLO partial decay width are of comparable size. Below the threshold, the SUSY effects change the partial decay widths thus that they are larger than the QCD contributions and the picture reverses above the threshold. We observe a large increase of the LO partial decay width with growing $m_{1/2}$. This is a result of the large increase of m_A with $m_{1/2}$. For large values of $m_{1/2}$, m_A is up to about 900 GeV.

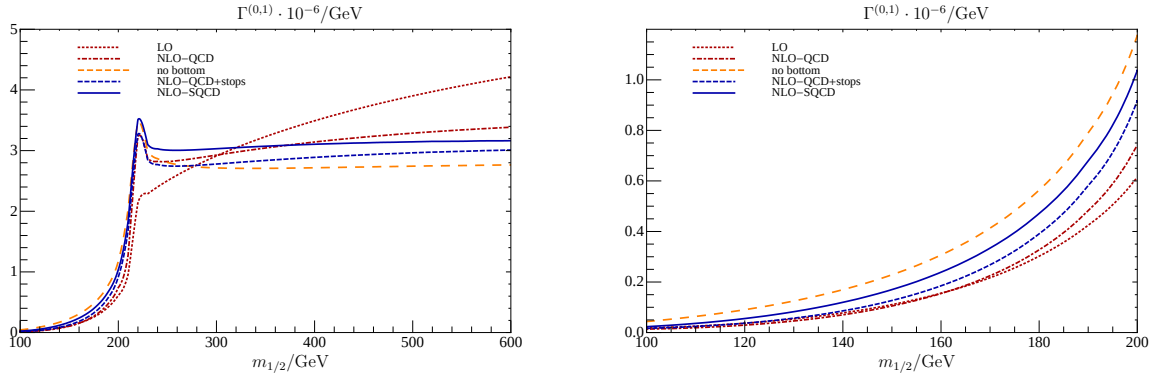

Figure 6.16.: *The partial decay widths for the process $A \to \gamma\gamma$ in dependence of $m_{1/2}$ along the slope of SPS 1a. The dotted (red) curve is the LO-SQCD result, the dashed curve (red) depicts the NLO-QCD result, the dashed-dotted (blue) curve is the NLO-QCD plus stop result and the solid line (blue) is the full NLO-SQCD decay width. In yellow (dashed-dotted) only the top/stop, i.e, no bottom effects are displayed. (a) including the threshold (b) zoom into the region below the threshold.*

6.9.3. $h \to \gamma\gamma$

The decay width for the decay of the lightest scalar MSSM Higgs boson into two photons in NLO-SQCD (cf. Eq. (6.11)) is given by

$$\begin{aligned}\Gamma_{SQCD}(h \to \gamma\gamma) = &\frac{G_F \alpha^2 m_h^3}{128\sqrt{2}\pi^3} \left| N_c \sum_{q\tilde{q}=t\tilde{t},b\tilde{b}} Q_q^2 \left(\mathcal{H}_{q\tilde{q}}^{(0)} + \frac{\alpha_s}{\pi} \mathcal{H}_{q\tilde{q}}^{(1)} \right) + \mathcal{O}\left(\alpha_s^2\right) \right|^2 \\ = &\frac{G_F \alpha^2 m_h^3}{128\sqrt{2}\pi^3} \left| N_c \left[Q_t^2 \mathcal{H}_t^{(0)} + Q_b^2 \mathcal{H}_b^{(0)} + Q_t^2 \mathcal{H}_{\tilde{t}}^{(0)} + Q_b^2 \mathcal{H}_{\tilde{b}}^{(0)} + \frac{\alpha_s}{\pi} \left[Q_t^2 \mathcal{H}_t^{(1)} + Q_b^2 \mathcal{H}_b^{(1)} \right] \right.\right. \\ &\left.\left. + \frac{\alpha_s}{\pi} \left[Q_t^2 \mathcal{H}_{\tilde{t}}^{(1)} + Q_b^2 \mathcal{H}_{\tilde{b}}^{(1)} \right] + \frac{\alpha_s}{\pi} \left[Q_t^2 \mathcal{H}_{t\tilde{g}}^{(1)} + Q_b^2 \mathcal{H}_{b\tilde{g}}^{(1)} \right] + \mathcal{O}\left(\alpha_s^2\right) \right] \right|^2 .\end{aligned}$$

There are two main differences between the decay of scalar and pseudoscalar Higgs bosons into two photons. For the scalar case already at leading order perturbation theory there exists a contribution from the scalar partners of the quarks (see Fig. 6.6). Furthermore, not all of the SUSY contributions in NLO are due to gluinos. Also, contributions from pure squark diagrams exist (see Fig. 6.8). The coupling of squarks to scalar Higgs bosons is different from the one to pseudoscalar Higgs bosons (see App. A).

As in the previous section, the influence of the SUSY particles on the partial decay width Γ in LO and NLO perturbation theory is investigated. In particular, the effects due to sbottom insertions at NLO will be discussed. These were not known before.

As we take the common convention to use the mass of the pseudoscalar Higgs boson m_A and the ratio of the two vacuum expectation values $\tan\beta$ to be the input parameters of the MSSM Higgs sector, the scalar Higgs mass cannot be assumed to be a free parameter. Therefore, we should take a radiatively corrected scalar Higgs mass in the investigation of the partial decay width of $h \to \gamma\gamma$. The SUSY parameter space will be examined with the help of *FeynHiggs* [87]. Its online version is available on the web page *www.feynhiggs.de*. *FeynHiggs* is a Fortran program for the calculation of the masses of the CP-even Higgs bosons in the MSSM. It includes the complete one-loop on-shell results, some leading order two-loop QCD and electroweak results and higher order corrections to the Higgs self-energy are accounted for. We employ the online version of this program where we take our choice for the squark masses, m_A and $\tan\beta$ as input parameters and let the program generate the related loop corrected values for the scalar Higgs mass m_h and the Higgs mixing angle α, as an output.

First, we examine the partial decay width, by assuming all the squark masses to be equal with no-mixing, i.e., $\theta_{\tilde{q}} = 0$, namely $m_q \ll m_{\tilde{q}} \equiv m_{\tilde{q}_1} = m_{\tilde{q}_2} \ll m_{\tilde{g}},\ q\tilde{q} = t\tilde{t},\ b\tilde{b}$. In addition, we set the stop mass equal to the sbottom mass, i.e., $m_{\tilde{q}} = m_{\tilde{t}} = m_{\tilde{b}}$. All bottom masses are set to the running one that varies with the Higgs mass through $\mu = m_h$. Actually, for the examined parameter spaces the curves where the bottom masses are taken to be running ones practically coincide with the curves where the bottom mass is taken to be on-shell. In the following we examine the impact of the SUSY effects on the partial decay widths. The QCD corrections are affected by the variation of m_h and the Higgs mixing angle α.

In Fig. 6.17 the partial decay widths $\Gamma^{(0,1)}$ are examined in dependence of $\tan\beta$. We display the LO and NLO-QCD (red) decay width in comparison with the LO and NLO-SQCD (blue) decay width. In yellow the NLO-QCD plus the full NLO stop dependence, i.e., with no sbottom effects are shown. The observation is that the NLO effect due to sbottoms is very small. A steep increase of the partial decay widths for values of $\tan\beta$ up to 15 is observed. For $\tan\beta > 15$, the curves almost do not exhibit a dependence on this parameter. As indicated in the caption in Fig. 6.17, the change in the scalar Higgs mass is largest for values of up to $\tan\beta = 15$. For larger values of $\tan\beta$, the Higgs mass remains almost constant. For all four graphs, the effects of the sbottoms compared to the partial decay widths that include the top sector as well as the bottom effects are below one percent. Here, the effects through stops clearly dominate since those amount to 11% in Fig. 6.17(a), 6% in Fig. 6.17(a), 2% in Fig. 6.17(c) and 6.17(d) compared to the NLO-QCD partial decay widths. We observe that the decay widths grow with larger squark masses and that the QCD and SQCD results move closer together the larger the squark and pseudoscalar Higgs mass. This is as expected since for very large SUSY masses the SM limit should be recovered.

In Fig. 6.18 the partial decay widths are shown in dependence of $\tan\beta$. The curves are denoted as in Fig. 6.17 and we set $m_A = 200$ GeV, $\mu_{susy} = 200$ GeV. We compare

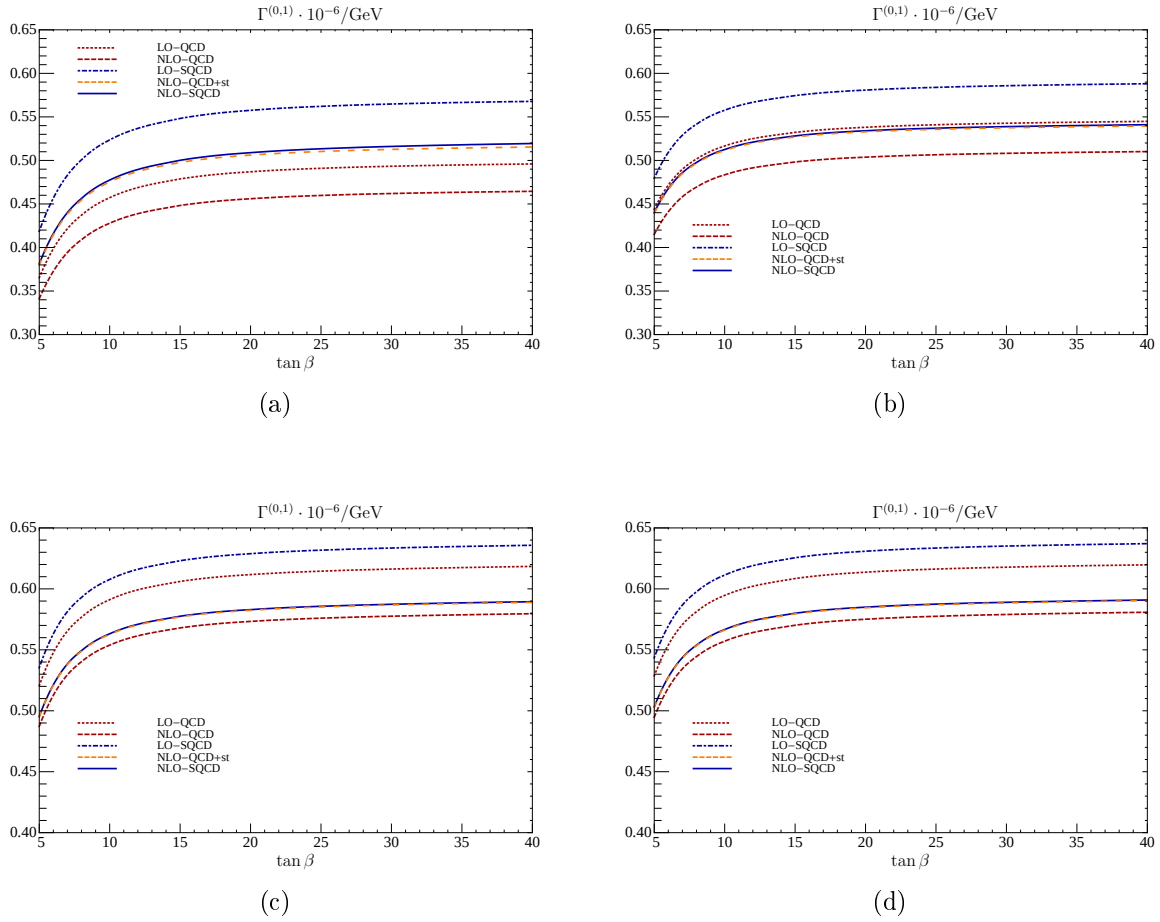

Figure 6.17.: *The partial decay widths* $\Gamma^{(0,1)}$ *are shown in dependence of* $\tan\beta$*. We illustrate the LO-QCD (dotted red) and the NLO-QCD (dashed red) partial decay width for all bottom masses taken to be running ones. The blue curves contain the complete SQCD parts in LO (dashed-dotted) and in NLO-SQCD (solid). In addition, in yellow, nearly on top of the entire NLO-SQCD result, the NLO-QCD+stop (dashed) result is displayed. The results are given in the limiting case* $m_q \ll m_{\tilde{q}} = m_{\tilde{q}_1} = m_{\tilde{q}_2} \ll m_{\tilde{g}}$*,* $q\tilde{q} = t\tilde{t}, b\tilde{b}$*.* $m_{\tilde{q}} = m_{\tilde{t}} = m_{\tilde{b}}$*,* $\mu_{susy} = 200$ *GeV and* $m_{\tilde{g}} = 1600$ *GeV. (a)* $m_A = 200$ *GeV,* $m_{\tilde{q}} = 450$ *GeV,* $\tan\beta \in [5, 15]$ *corresponds to* $m_h \in [98.6\,\mathrm{GeV}, 105.3\,\mathrm{GeV}]$ *and the Higgs mass increases only up to* $m_h = 106.8$ *GeV for* $\tan\beta = 40$*; (b)* $m_A = 350$ *GeV,* $m_{\tilde{q}} = 600$ *GeV* $\tan\beta \in [5, 15]$ *corresponds to* $m_h \in [103.1\,\mathrm{GeV}, 108.5\,\mathrm{GeV}]$ *and for* $\tan\beta = 40$*,* $m_h = 109.5$ *GeV; (c)* $m_A = 500$ *GeV,* $m_{\tilde{q}} = 1000$ *GeV,* $\tan\beta \in [5, 15]$ *corresponds to* $m_h \in [108.1\,\mathrm{GeV}, 112.9\,\mathrm{GeV}]$ *and for* $\tan\beta = 40$*,* $m_h = 114$ *GeV; (d)* $m_A = 1000$ *GeV and* $m_{\tilde{q}} = 1000$ *GeV,* $\tan\beta \in [5, 15]$ *corresponds to* $m_h \in [108.4\,\mathrm{GeV}, 113\,\mathrm{GeV}]$ *and for* $\tan\beta = 40$*,* $m_h = 114$ *GeV.*

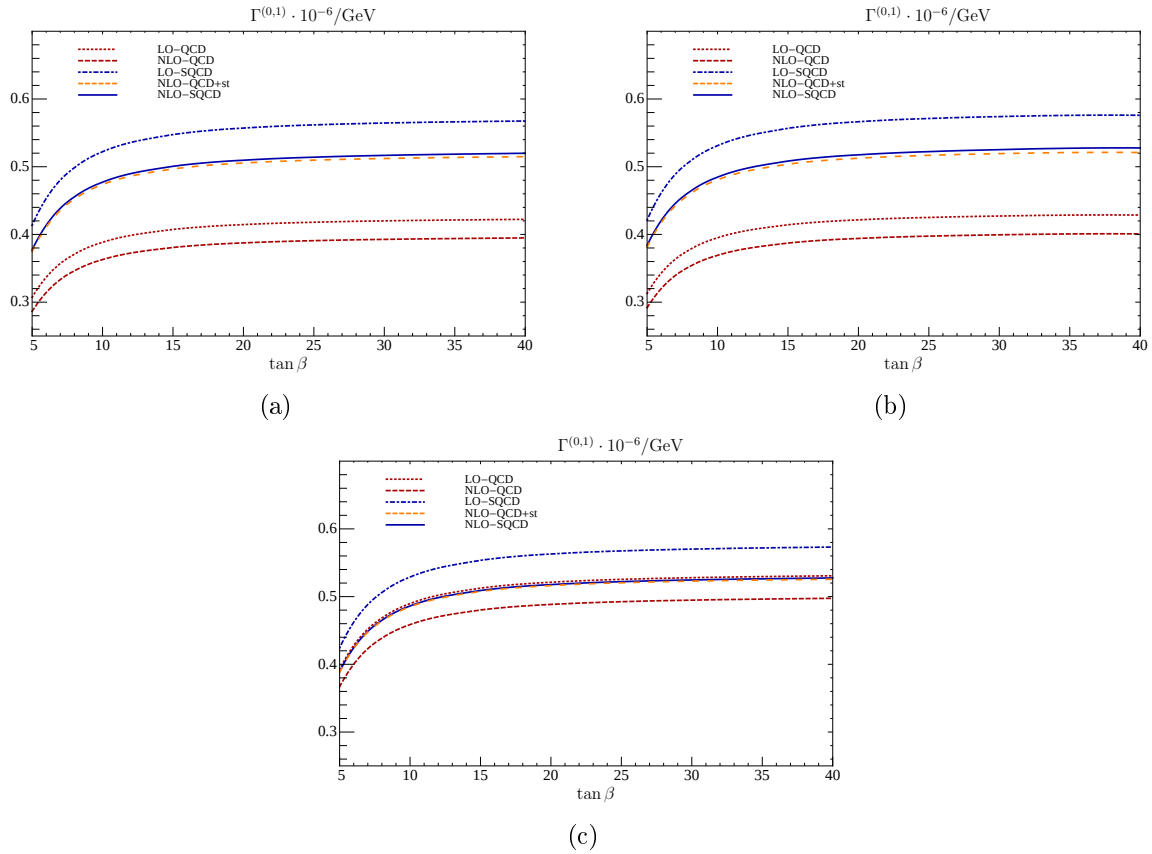

Figure 6.18.: $\Gamma^{(0,1)}$ *is displayed in dependence of* $\tan\beta$ *for the limiting case* $m_q \ll m_{\tilde{q}} \equiv m_{\tilde{q}_1} = m_{\tilde{q}_2} \ll m_{\tilde{g}}$, $q\tilde{q} = t\tilde{t}, b\tilde{b}$. $m_{\tilde{q}} = m_{\tilde{t}} = m_{\tilde{b}}$, $\mu_{susy} = 200\ GeV$ *and* $m_A = 200\ GeV$. *The LO-QCD (dotted red) , NLO-QCD (dashed red), LO-SQCD (dashed-dotted blue), NLO-QCD plus stop effects (dashed yellow) and NLO-SQCD (solid blue) decay widths are displayed. (a)* $m_{\tilde{q}} = 300\ GeV$, $m_{\tilde{g}} = 500\ GeV$, $m_h \in [93\ GeV, 102\ GeV]$ *(b)* $m_{\tilde{q}} = 300\ GeV$, $m_{\tilde{g}} = 1000\ GeV$, $m_h \in [93\ GeV, 102\ GeV]$ *(c)* $m_{\tilde{q}} = 600\ GeV$, $m_{\tilde{g}} = 1000\ GeV$ *and* $m_h \in [101\ GeV, 109\ GeV]$.

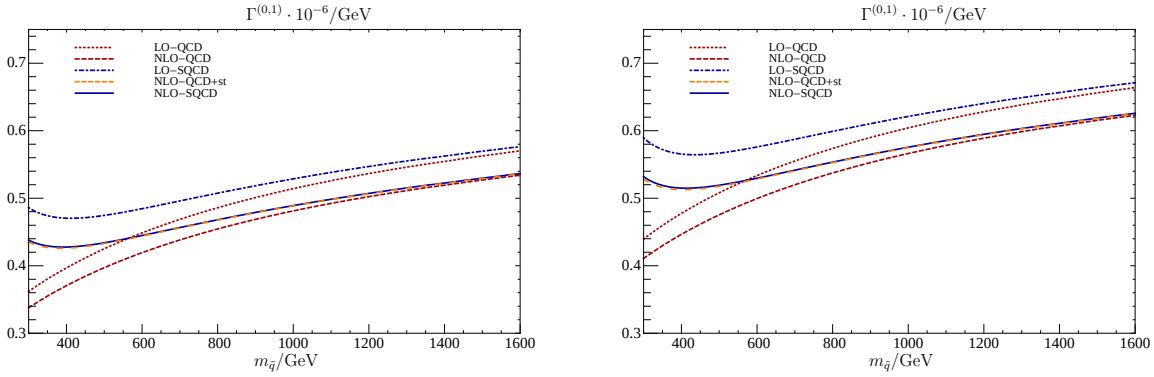

(a) $\tan\beta = 5$ (b) $\tan\beta = 15$

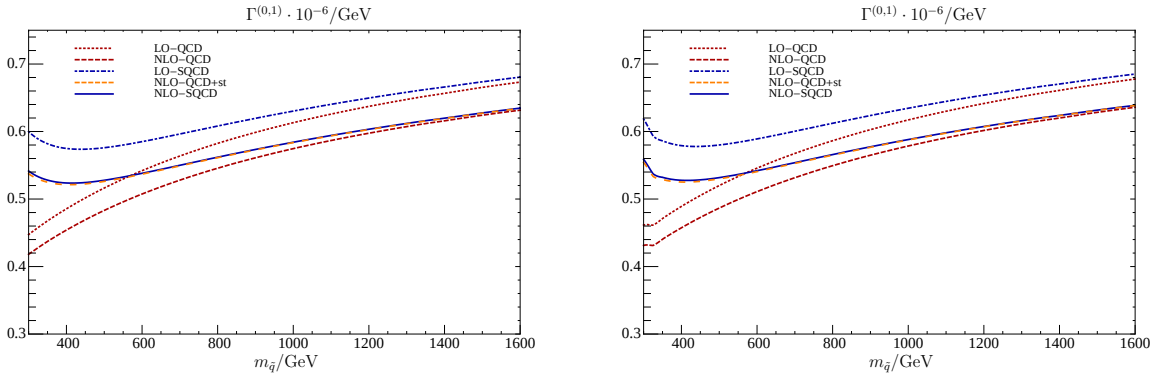

(c) $\tan\beta = 25$ (d) $\tan\beta = 40$

Figure 6.19.: $\Gamma^{(0,1)}$ *is displayed in dependence of one SUSY mass scale* $m_{\tilde{q}}$*, i.e., for the limiting case* $m_q \ll m_{\tilde{q}} \equiv m_{\tilde{q}_1} = m_{\tilde{q}_2} \ll m_{\tilde{g}}$*,* $q\tilde{q} = t\tilde{t}, b\tilde{b}$*.* $m_{\tilde{q}} = m_{\tilde{t}} = m_{\tilde{b}}$*,* $\mu_{susy} = 200\ GeV$*,* $m_{\tilde{g}} = 1600\ GeV$ *and* $m_A = 400\ GeV$*. The LO-QCD (dotted red) , NLO-QCD (dashed red), LO-SQCD (dashed-dotted blue), NLO-QCD plus stop effects (dashed yellow) and NLO-SQCD (solid blue) decay widths are displayed. The four diagrams differ in the value of* $\tan\beta$ *given below the diagrams. (a)* $m_h \in [94.5\ GeV, 111.5\ GeV]$ *(b)-(c)* $m_h \in [100\ GeV, 117.4\ GeV]$*.*

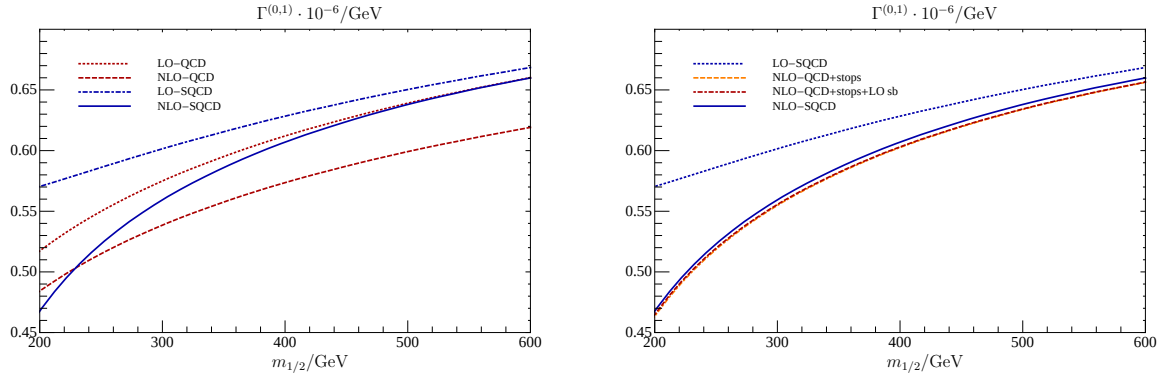

Figure 6.20.: *The partial decay widths for the process $h \to \gamma\gamma$ in dependence of $m_{1/2}$ along the slope of SPS 1a. $m_h \in [107\,GeV, 116\,GeV]$ and $\tan\beta = 10$. (a) We compare the LO-QCD (dotted red) with the NLO-QCD (dashed red), LO-SQCD (dashed-dotted blue) and the full NLO-SQCD (solid blue) results. (b) The LO-SQCD (dotted blue), the NLO-QCD+stop (dashed-dotted red) and NLO-QCD+stop+LO sbottom (dashed yellow) and NLO-SQCD results are compared.*

Fig. 6.18(a) with Fig. 6.18(b) where only $m_{\tilde{g}}$ is changed. The change for doubling the gluino mass is almost not visible in the diagrams. For Fig. 6.18(a),(b) the corrections from sbottoms (stops) are up to 1% (25%) and for Fig. 6.18(c) they are below 1% (6%).

Fig. 6.19 displays the partial decay widths in dependence of $m_{\tilde{q}}$. The curves are denoted as in Fig. 6.17. We observe the expected tendency that from squark mass scales of about 1 TeV onwards, the SQCD curves lie on top of the QCD curves. For lower SUSY masses, we observe a larger effect through the inclusion of squarks in comparison with the QCD result. The SQCD curves exhibit a dip at about $m_{\tilde{q}} = 400$ GeV and grow with larger squark masses. For the given choice of parameters the decay widths grow by about 18% in the change from $\tan\beta = 5$ (Fig. 6.19(a)) to $\tan\beta = 15$ (Fig. 6.19(b)). Changing from $\tan\beta = 15$ to $\tan\beta = 25$ (Fig. 6.19(c)) amounts to an increase of 2% and further augmenting to $\tan\beta = 40$ (Fig. 6.19(d)), the effect on the partial decay widths is a rise of about 3%. For all curves the NLO-SQCD decay width lies on top of the NLO decay width that includes the complete NLO-QCD and in addition, only stop/gluino effects in NLO. This means that, for this choice of parameters, the LO and NLO sbottom contributions only lead to corrections of one percent and smaller and practically do not have an impact on the partial decay width. The stop effects compared to the NLO-QCD result amount to about 25% for smaller $m_{\tilde{q}}$.

As in Sec. 6.9.2 in the pseudoscalar case, for taking the full mass dependency, i.e., the limiting case where we assume $m_q \ll m_{\tilde{q}_1} \ll m_{\tilde{q}_2} \ll m_{\tilde{g}}$, we investigate the results along the slope of the SPS 1a benchmark point. For $m_{1/2} \in [200\,\text{GeV}, 600\,\text{GeV}]$ the variation of

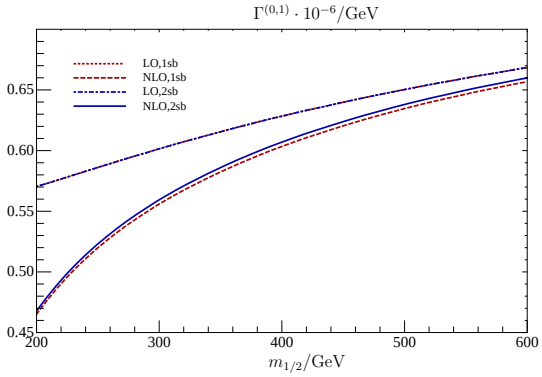

Figure 6.21.: *The partial decay widths for the process $h \to \gamma\gamma$ in dependence of $m_{1/2}$ along the slope of SPS 1a. We compare the results in which we take all the SUSY masses to be different in the LO-SQCD (dashed-dotted blue) and the NLO-SQCD result (solid blue) with the LO-SQCD (dotted,red) and NLO-SQCD (dashed red) result in which we assume equal sbottom masses $m_{\tilde{b}_1} = m_{\tilde{b}_2}$ since their mass splitting is not large along the slope of SPS 1a.*

the scalar Higgs mass is given by $m_h \in [107\,\text{GeV}, 116\,\text{GeV}]$.

Fig. 6.20 displays the partial decay widths along the slope of SPS 1a in dependence of $m_{1/2}$. In Fig. 6.20(a) the LO and NLO-QCD are compared with the LO and NLO-SQCD decay widths. The deviation of the NLO-SQCD with respect to the NLO-QCD partial decay widths is up to 6%. In Fig. 6.20(b) the LO-SQCD and three NLO curves are displayed. In yellow the NLO-QCD plus stop partial decay width, in red the NLO-QCD plus stop plus LO sbottom decay width and in blue the full NLO-SQCD decay width is shown. The effects of stops compared to the QCD effects amount to about 6%. We observe that by including the LO sbottom effects in addition to the QCD and entire stop effects the deviations are not visible in the plot and are numerically below one percent. Further including the NLO sbottom effects amounts to a change of the corrections of less than one percent. In total, including the sbottom contributions to the partial decay width amounts to a deviation of up to one percent compared to the result that only includes the effects of the top sector and bottom quarks. For the SPS 1a scenario, the observed two-loop SUSY effects on the amplitude are almost entirely from the top sector.

In Fig. 6.21 the LO and NLO-SQCD partial decay widths are displayed in dependence of $m_{1/2}$. The result with the full dependence on all SUSY mass scales is compared to the one where the masses of the sbottoms are equal, i.e., $m_{\tilde{b}_1} = m_{\tilde{b}_2}$ and set to the arithmetic mean of the two sbottom masses along the slope of SPS 1a (see Fig. 6.15). We observe that these results coincide in LO-SQCD and they do not differ to a great amount in NLO-SQCD. This demonstrates that the two limits where $m_q \ll m_{\tilde{q}_1} \ll m_{\tilde{q}_2} \ll m_{\tilde{g}}$ and $m_q \ll m_{\tilde{q}_1} = m_{\tilde{q}_2} \ll m_{\tilde{g}}$ are in good agreement if the sbottom masses do not differ much from each other. The deviation of the curves is below one percent.

Chapter 7
Higgs Production

After a short overview about the production mechanisms of scalar and pseudoscalar Higgs bosons at the LHC, we will focus on the production of Higgs bosons via the gluon fusion channel. For this process, we will present results for the NLO-SQCD corrections, including the top and bottom quarks as well as their superpartners and the gluino. We discuss some subtleties about the renormalization of the two-loop amplitudes we calculate. Subsequently, we present explicit results for the expansions of the virtual two-loop SUSY contributions to the amplitudes in the leading terms for various limiting cases. Finally, we investigate the two-loop virtual contributions to the amplitude. For the production of pseudoscalar Higgs bosons an estimate of the size of the sbottom effects on the hadronic cross section is given.

7.1. Higgs Production at the LHC

This section shall provide an overview over the production of scalar and pseudoscalar Higgs bosons at the LHC. If not stated otherwise, $\phi = \{h, A\}$ denotes scalar and pseudoscalar Higgs bosons, respectively. The expression $\mathcal{H} = \{h\}$ only refers to scalar Higgs bosons, where h denotes the SM Higgs boson as well as the lightest MSSM Higgs boson which possesses the closest similarity to the SM Higgs boson. For examining the production of Higgs bosons at the LHC one has to know their production mechanisms. The main parts of protons which are accelerated at the LHC are massless gluons and very light quarks. As the Higgs coupling is proportional to the mass of the particles coupling to the Higgs, the Higgs production has to be mediated by massive intermediate particles which couple to gluons or light quarks (u, d).

The four main production channels for generating Higgs bosons at the LHC are [28]

1. Associated production with electroweak gauge bosons (Higgs strahlung):
   $q\bar{q} \to W\mathcal{H}$, $Z\mathcal{H}$ (Fig. 7.2(a))

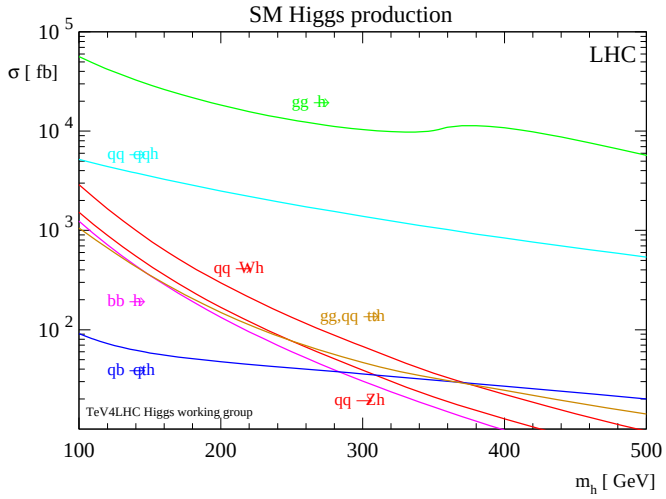

Figure 7.1.: *Inclusive cross sections for SM Higgs production at the LHC. Taken from [88].*

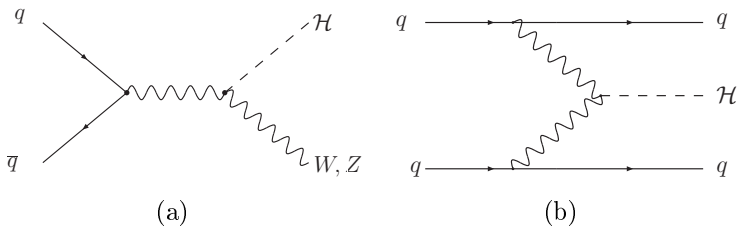

Figure 7.2.: *Leading order Feynman diagrams for (a) the Higgs strahlung and (b) weak boson fusion.*

2. Fusion of weak gauge bosons (vector boson fusion (VBF)):
   $qq \to \mathcal{H}qq$ via W^+W^-, $ZZ \to \mathcal{H}$ (Fig. 7.2(b))

3. Associated production with a top quark respectively a bottom quark pair:
   $gg, q\bar{q} \to t\bar{t}\phi$, $b\bar{b}\phi$ (Fig. 7.3(a)).

4. Gluon fusion: $gg \to \Phi$ (Fig. 7.3(b))

The cross sections for the processes listed above are illustrated in Fig. 7.1 for the production of SM Higgs bosons. For a Higgs mass between 100 GeV and 500 GeV the process of the gluon fusion is the one with the largest cross section at the LHC. For an up to date review about Higgs production the reader is referred to [29, 68].

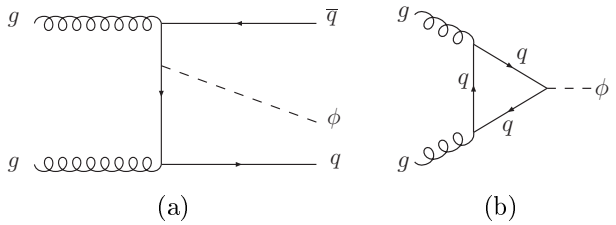

Figure 7.3.: *Leading order to (a) the associated $q\overline{q}\,\phi$ ($q = t, b$) production and (b) the gluon fusion process.*

Higgs Strahlung

The Feynman diagram for the leading order in the process of the Higgs strahlung is displayed in Fig. 7.2(a). The Higgs boson is produced together with a weak gauge boson. Although the cross section is almost an order of magnitude smaller than for the gluon fusion, in this channel one has the advantage that the bottom quarks from the decay can be distinguished from the background. This is possible by measuring the decay products of the W- and Z-bosons, which were generated together with the Higgs boson. This channel is very well under control from the theory side because up to NNLO-QCD as well as NLO-electroweak effects are known (cf. references in [89]). This production channel does not provide a contribution for the pseudoscalar Higgs boson A as a coupling of the form AVV does not exist.

Fusion of Weak Gauge Bosons (VBF)

The production of Higgs bosons via the fusion of weak gauge bosons results in the second largest cross section at the LHC (see Fig. 7.1). The leading order is displayed in Fig. 7.2(b). The Higgs is produced together with two jets which are not color-connected. This results in a small hadronic activity in the rapidity region between these jets. On the other hand, the Higgs decay products are found at central rapidities. Thus, suitable cuts and jet vetoes allow for a significant background reduction [89]. The VBF is important especially in the regions with lower Higgs masses [90]. The fusion of weak gauge bosons is an important production channel for Higgs bosons from which one expects information beyond discovery and mass determination of Higgs bosons. One expects fundamental information about Higgs boson couplings to gauge bosons and fermions from the VBF process. The QCD corrections to VBF are known up to NLO and are moderate such that the theoretical prediction for the cross section is under control [91]. In combination with the gluon fusion and the associated $t\bar{t}H$ production one can determine ratios of the Higgs couplings and with limitations the total Higgs decay width [90, 92]. Nevertheless, this process, as the Higgs strahlung does not exist for pseudoscalar Higgs bosons, as the coupling of the form AVV with vector bosons V does not exist.

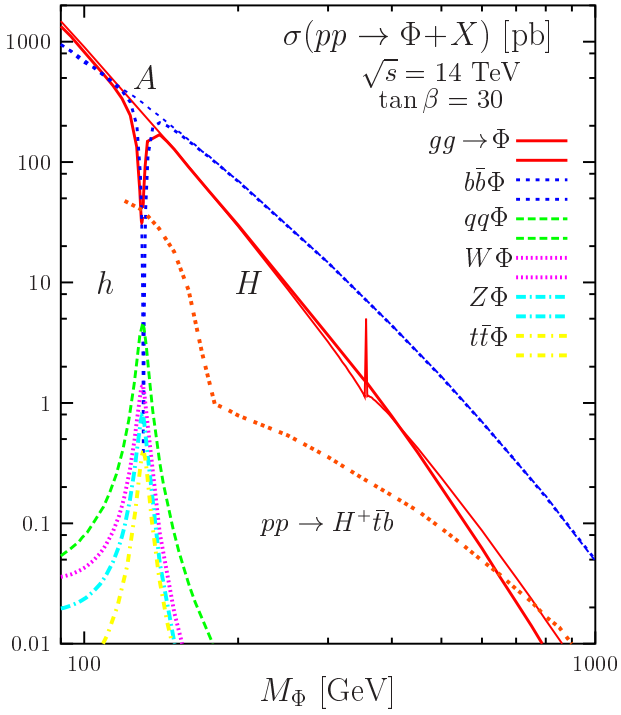

Figure 7.4.: *Production cross sections for neutral Higgs bosons ϕ at the LHC as functions of the Higgs mass for* $\tan\beta = 30$ *[68].*

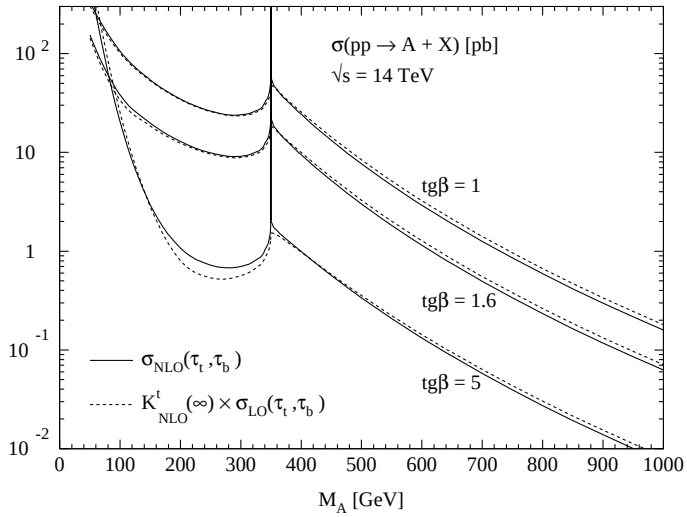

Figure 7.5.: *Comparison between the exact and approximate NLO cross section* $\sigma(pp \to A + X)$ *at the LHC for a cms energy of* $\sqrt{s} = 14$ *TeV. The solid lines display the exactly calculated cross section with the complete top and bottom quark dependency. The dashed lines show the results in the limit of large top masses. Taken from [81].*

$t\bar{t}\phi$ and $b\bar{b}\phi$ Associated Production

Although the cross section is rather small in this case, the $t\bar{t}\phi$ channel has a distinct signature: four bottom quarks in combination with two W bosons. Furthermore, this process is directly sensitive to the top Yukawa coupling for $t\bar{t}\phi$ and the bottom Yukawa coupling for $b\bar{b}\phi$. The largest contribution in leading order at the LHC is depicted in Fig. 7.3(a). For the $t\bar{t}\phi$ associated production the NLO in QCD is known exactly [93, 94] as well as in the limit of large top masses [95]. In Fig. 7.4 [68] it is shown that the cross section for the associated $b\bar{b}H$ and $b\bar{b}A$-production for Higgs masses up to about 130 GeV and $\tan\beta = 30$ GeV is about the same order of magnitude as the cross section for the gluon fusion. For larger Higgs masses it even gets dominant.

7.2. Gluon Fusion

In the SM the coupling of gluons to the Higgs boson is mediated through a top quark loop. The large gluon luminosity as well as the large top Yukawa coupling both compensate that this process is suppressed by loop level. Already at leading order perturbation theory there is a dependence of the cross section on $\alpha_s^2(\mu_R)$, as it is a one-loop process (Fig. 7.3(b)). This corresponds to a large dependence on the renormalization scale μ_R, which one has to reduce by including higher order corrections. However, the exact calculation of higher order corrections is difficult as the leading order is already a one-loop process. The NLO electroweak corrections were obtained in [96]. The process is known in QCD up to NLO [81,97] exactly and NNLO in the limit of large top masses [98–100]. Especially the NNLO-QCD results demonstrate the expected reduction of the dependence of the cross section on μ_R as well as the factorization scale μ_F. This dependence is significantly reduced by the transition from two- to three-loops. Therefore, it can be assumed that the perturbative approach works well in the gluon fusion process.

In the MSSM the cross sections are known in NLO in the limit of large top masses [59, 60, 79, 82]. In this limit, it is assumed that the top quark mass is a lot larger than the Higgs boson mass. Admittedly, this does not seem to be a good approximation for $m_t = 172.4$ GeV and $m_h \geq 114$ GeV. Nevertheless, the expansion in the masses is not given by m_ϕ/m_t, but by $\tau = m_\phi^2/(4m_t^2)$. That is why one can assume that the expansion in τ converges for $m_\phi < 2m_t$. One can perform the calculation (a) in an approximation and (b) exactly. In case (a) the cross section in NLO is calculated in an approximation in which the entire top mass dependence is kept at leading order $\left(\sigma_t^{LO}\right)$ and at NLO the QCD corrections are calculated in the limit of large top masses $\left(\sigma_\infty^{NLO}\right)$. Mathematically, the approach in (a) can be written in the following way

$$\sigma_t^{NLO} \approx K_\infty \sigma_t^{LO},$$

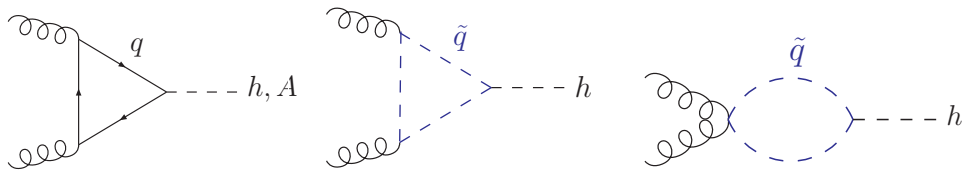

Figure 7.6.: *LO-SQCD contributions to the Higgs production via the gluon fusion.*

with

$$K_\infty = \frac{\sigma_\infty^{NLO}}{\sigma_\infty^{LO}}.$$

By comparing the two results in the case of the production of scalar Higgs bosons one observes that the approximation (a) does agree with the exact result (b) up to 2%. This holds up to a threshold of $m_\phi = 2m_t$. Even at a Higgs mass of about $m_\phi = 1$ TeV there is only a deviation of about 10% [73, 101].

The limit of large top masses is a good approximation even for an MSSM calculation as can be seen in Fig. 7.5. This graph shows a large dependence on $\tan\beta$ for the calculation of the top and bottom quark effects. The bottom quark effects are not negligible even for small $\tan\beta$ for the production of pseudoscalar Higgs bosons [81]. Clearly, this is a motivation for investigating the influence of bottom quarks and their superpartners on the amplitude and the cross section.

Since the main goal in this thesis is to determine the contributions of the bottom and sbottom quarks in NLO-SQCD, the approach of large quark masses it not applicable any longer. The bottom quark cannot in the least be assumed to be larger than the Higgs mass. Therefore, new routines were implemented, to account for the dependence on the external momenta of the gluons in order to calculate the bottom subloops arising in the asymptotic expansions of the Feynman diagrams (see Sec. 5.4). The NLO-SQCD virtual corrections with the inclusion of the bottom and sbottom quarks have been presented in [46]. Later on we will compare our results with these which have not been obtained in any limiting case. Only the squark contributions without the gluino have been given in [102, 103].

7.3. Diagrams in LO and NLO-SQCD in the Gluon Fusion

The LO diagrams for the gluon fusion process are displayed in Fig. 7.6. Analogously to the decay of Higgs bosons into two photons, for the pseudoscalar Higgs bosons the entire LO-SQCD part arises from quark insertions in the loop. As before, for the production of scalar Higgs bosons however, already at LO we obtain contributions from squarks circulating in the loop. Again, we only take into account the effects of top and bottom quarks as well as their superpartners.

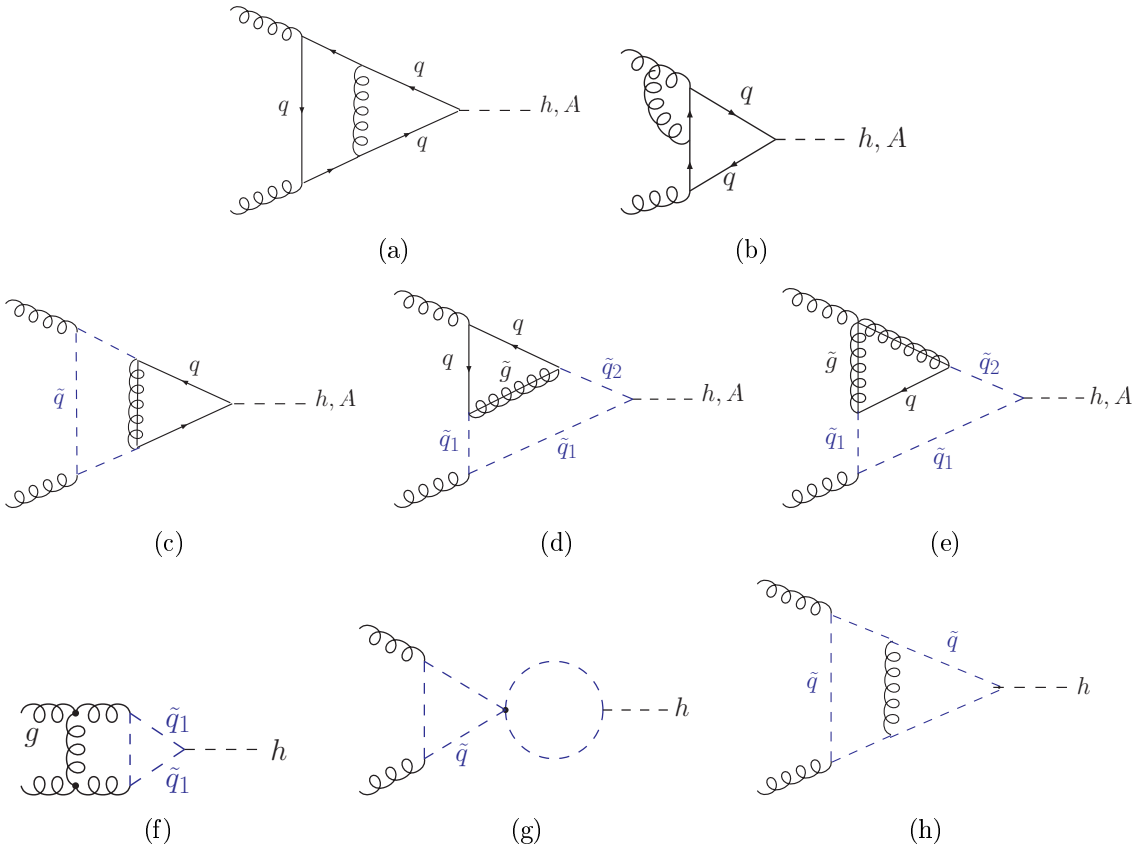

Figure 7.7.: *NLO-SQCD contributions for the Higgs production via gluon fusion: (a),(b): pure quark contributions; (c)-(e): mixed quark/squark/gluino contributions; (f)-(h): pure squark contributions*

The contributions one obtains for the gluon fusion process in NLO-SQCD are very similar to the case of Higgs bosons decaying into two photons in NLO-SQCD. However, for the Higgs production process via the gluon fusion, more diagrams and a more complicated structure are obtained due to the allowed emission of real gluons that was prohibited by color conservation in the case of the Higgs decaying into two photons. Additionally, two-loop diagrams with more than one internal gluon line exist. There are $\mathcal{O}(100)$ diagrams which contribute to the cross section for the production of pseudoscalar Higgs bosons via the gluon fusion in NLO-SQCD for the top sector as well as the bottom sector. For the scalar case there are $\mathcal{O}(300)$ diagrams.

The contributions to the Higgs production (h, A) can be categorized according to

1. pure quark contributions (SM or QCD-contributions) (Fig. 7.7(a), 7.7(b))

2. mixed quark-squark-gluino contributions ($q\tilde{g}$ contributions) (Fig. 7.7(c)-7.7(e))

3. pure squark contributions ($\tilde{q}$ contributions) (Fig. 7.7(f)-7.7(h))

For the production of scalar Higgs bosons there exist more diagrams in NLO-SQCD because of the allowed possible diagonal couplings of $h\tilde{q}_i\tilde{q}_i$, $i = 1, 2$. In order to categorize the contributions to the amplitude the same notation as in Sec. 6.6 is applied.

7.4. Renormalization of the New Contributions

The renormalization procedure for the contributions to the gluon fusion process is more complicated than for the decay of Higgs bosons into two photons. As for the Higgs decay, we only calculate the SUSY parts of the two-loop diagrams.

The QCD contributions to the hadronic cross section are publicly available in the program `HIGLU` [104]. This program allows to evaluate the total Higgs production cross section in the gluon fusion process at hadron colliders including the next-to-leading order QCD corrections of top quarks as well as bottom quarks. The cross sections can be evaluated for the scalar as well as pseudoscalar Higgs boson.

For the production of pseudoscalar Higgs bosons, the QCD contributions to the cross section can be taken from `HIGLU` [104] which accounts for the virtual two-loop quark diagrams as well as the real radiation of gluons in NLO. The mixed quark-squark-gluino diagrams we calculate do not contain contributions from real gluon radiation in NLO-SQCD. Due to the absence of squark contributions at LO, by just the inclusion of the two-loop mixed quark-squark-gluino diagrams, the full NLO-SQCD result is derived. Thus, for the pseudoscalar case no SUSY diagrams with real gluon emission exist at NLO-SQCD.

The production of scalar Higgs bosons is somewhat more complicated, since already at LO there exist contributions from squarks. The program `HIGLU` provides for the real and virtual QCD contributions to the cross section. But it does not provide for expressions of the interference terms for the real QCD parts with the real SUSY parts. The full two-loop virtual QCD contributions are available to us [76].

The structure of the two-loop SUSY parts to the amplitude of the scalar Higgs production is more complex than for the Higgs decay. In addition to the diagrams containing gluinos, pure squark diagrams with insertions of more than one internal gluon line exist.

For the production of scalar and pseudoscalar Higgs bosons through the fusion of gluons, in addition to the renormalization of the mass scales and the squark mixing angle, the strong coupling constant α_s has to be renormalized as well. Furthermore, the gluon wave functions have to be renormalized.

7.4.1. Renormalization in the Effective Theory vs. the Full Theory

As an important check of our calculation of the SUSY parts that include contributions from top and bottom quarks as well as their superpartners, we calculate the top/stop/gluino

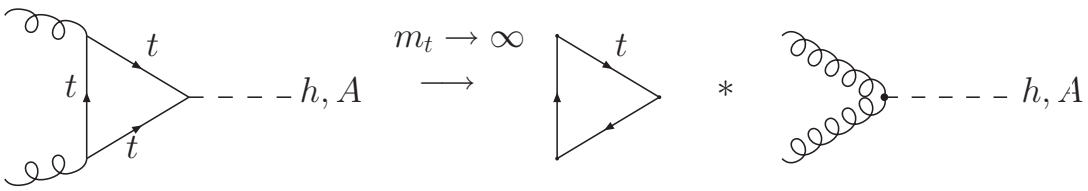

Figure 7.8.: *Diagrammatic illustration of the LO in the effective theory where the top quark is integrated out.*

parts of the amplitude in an effective theory where the top quark is integrated out, i.e., it is assumed to be much heavier than the Higgs boson. In addition, the stops and gluino are integrated out as well.

The calculation in the effective theory is performed along the lines of [60, 82]. We will briefly recollect the renormalization of α_s and the decoupling of the heavy particles in the effective theory.

The effective $gg\phi$ ($\phi = h, A$) coupling in leading order in m_ϕ can be expressed by

$$\mathcal{L}_{eff}^{\phi} = -\frac{\phi}{v} C_{1,\phi}^{B} \mathcal{O}_{1,\phi}^{B} \text{ with } \mathcal{O}_{1,h}^{B} = \frac{1}{4} G_{\mu\nu}^{B,a} G^{B,a\mu\nu} \text{ and } \mathcal{O}_{1,A}^{B} = \frac{1}{4} G_{\mu\nu}^{B,a} \tilde{G}^{B,a\mu\nu}.$$

Since the top quark has been integrated out, $G_{\mu\nu}^{B}$ is the bare gluon field strength tensor in five-flavor QCD. The dual field strength tensor is denoted $\tilde{G}_{\mu\nu}^{B}$. In the effective theory, the goal is to determine the dimensionless so-called Wilson coefficient $C_{1,\phi}^{B}$. This coefficient only depends on the bare quantities of the full theory and is a function of α_s. In particular, it contains the effects of the heavy particles that are integrated out.

Diagramatically (cf. Fig. 7.8) the LO top quark contribution decomposes into a product of two factors if the top is integrated out. The first diagram with vanishing external momenta contains the full top quark dependence and the second part depends on the kinematics of the process but does not contain any massive internal lines. In order to determine $C_{1,\phi}$ in NLO-SQCD, vacuum diagrams that contain massive internal lines of the top quark, top squarks and the gluino have to be evaluated up to the two-loop level.

For both, the production of scalar and pseudoscalar Higgs bosons in the effective theory the renormalization of α_s and the decoupling of the heavy particles are described below. First, the top quark and its supersymmetric partners and the gluino are decoupled from the bare coupling constant

$$\tilde{\alpha}_s^B = \frac{1}{(\zeta_g^B)^2} \alpha_s^B.$$

$\tilde{\alpha}_s^B$ denotes the bare coupling in the full theory (SQCD) including the tops, stops and gluino. α_s^B is the bare coupling in five-flavor QCD. The decoupling factor is given by [82]

$$\frac{1}{(\zeta_g^B)^2} = 1 + \frac{\alpha_s}{\pi} \left[\frac{1}{\epsilon} \left(\frac{1}{6} C_A + \frac{1}{2} T \right) + L(\epsilon) \right] + \mathcal{O}(\alpha_s^2), \tag{7.1}$$

with $C_A = 3$, $T = 1/2$ and

$$\begin{aligned} L(\epsilon) =& \frac{1}{12}\left(2C_A L_{\tilde{g}} + T\left(L_{\tilde{t}_1} + L_{\tilde{t}_2} + 4L_{t_1}\right)\right) \\ &+ \frac{\epsilon}{12}\left(C_A L_{\tilde{g}}^2 + \frac{1}{2}\left(L_{\tilde{t}_1}^2 + L_{\tilde{t}_2}^2\right) + 2TL_t^2 + (C_A + 3T)\,\zeta_2\right), \end{aligned} \tag{7.2}$$

where

$$L_t = \ln\frac{\mu_R^2}{m_t^2}, \quad L_{\tilde{t}_i} = \ln\frac{\mu_R^2}{m_{\tilde{t}_i}^2}, \quad L_{\tilde{g}} = \ln\frac{\mu_R^2}{m_{\tilde{g}}^2}.$$

The renormalization scale is denoted with μ_R. The renormalization of the bare coupling α_s^B is given by [82]

$$\alpha_s^B = \left[1 + \frac{\alpha_s}{\pi}\frac{1}{\epsilon}\left(-\frac{11}{12}C_A + \frac{1}{3}Tn_l\right)\right]\alpha_s^{\overline{DR}}. \tag{7.3}$$

$\alpha_s^{\overline{DR}}$ is the coupling in the $\overline{DR}$-scheme and n_l ($n_l = 5$) denotes the number of light flavors. The gluon field $\tilde{G}_\mu^B$ of the entire theory is reduced to the one in the effective theory G_μ^B by [82]

$$\tilde{G}_\mu^B = \frac{1}{\sqrt{\zeta_3^B}}G_\mu^B, \tag{7.4}$$

with

$$\zeta_3^B = 1 + \frac{\alpha_s}{\pi}\left(\frac{1}{\epsilon}\left(\frac{1}{6}C_A + \frac{1}{2}T\right) + L(\epsilon)\right) + \mathcal{O}(\alpha_s^2). \tag{7.5}$$

In addition, the renormalized Wilson coefficient C_1 is obtained through [80]

$$C_1 = Z_{11}^{-1}C_1^B, \tag{7.6}$$

$$Z_{11}^{-1} = \left[1 - \frac{\alpha_s}{\pi}\frac{1}{\epsilon}\left(-\frac{11}{12}C_A + \frac{1}{3}Tn_l\right)\right]. \tag{7.7}$$

To conclude, the application of Eqs. (7.1), (7.3), (7.4) and (7.6) of which we only need the terms up to $\mathcal{O}(\alpha_s)$ in our two-loop calculation results in a net zero effect.

In the calculation in the full theory, the result will be expressed in terms of $\alpha_s^{\overline{DR}}$ in five-flavor QCD. There, the heavy particles, i.e., the top quark, the squarks and the gluino have to be decoupled as in Eq. (7.1). Furthermore, the bare strong coupling has to be renormalized as given in Eq. (7.3). In addition, the gluon wave function has to be renormalized. In the effective theory, ζ_3^B is obtained by [105]

$$\zeta_3^B = 1 + \Pi_G^B(0).$$

$\Pi_G^B(0)$ is determined by the one-loop corrections to the gluon propagator that are mediated by the heavy particles at zero momentum transfer. Those are the top quark, squarks and gluino as can be seen in Fig. 7.9.

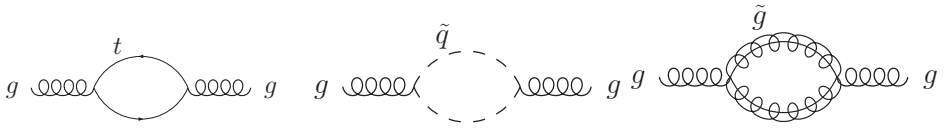

Figure 7.9.: *Contributions to the gluon wave function renormalization.*

It coincides with the on-shell gluon wave function renormalization in the full theory. Thus, in the full theory, the gluon wave function is renormalized with the factor given in Eq. (7.4). The decoupling and the renormalization of the gluon wave functions lead to a net zero effect.

Limitation of the Approach

Our approach to the production of scalar and pseudoscalar Higgs bosons via the gluon fusion is guided by the intention of the inclusion of the bottom quarks. Clearly, the bottom quarks cannot be assumed to be heavier than the Higgs boson and the effective theory is not applicable.

In addition we do not determine the pure QCD bottom contributions to the amplitude. Therefore, we have to split the calculation into QCD parts and SUSY parts. We only determine the latter and have to ensure that these are separately finite by a modified renormalization procedure and can be added to the QCD parts in order to obtain the entire SQCD result.

In the pseudoscalar case, the SUSY contributions are entirely from gluino insertions at the two-loop level. The corresponding Feynman diagrams are determined with the help of the new routines (cf. Sec. 5.4).

In the scalar case we perform an additional splitting of the SUSY contributions into pure squark diagrams and diagrams containing at least one gluino as an internal particle. This is due to the fact that we cannot perform the exact calculation of the pure squark diagrams with several gluon insertions with our setup.

We obtain the pure squark contributions only in an effective theory where we assume the masses of the top and bottom squarks to be much larger than the Higgs mass, i.e., $m_{\tilde{b}_{1,2}}, m_{\tilde{t}_{1,2}} \gg m_h$. The assumption of the squark masses being heavier than the Higgs boson seems to be a fair approximation. The pure sbottom diagrams are calculated with the help of asymptotic expansions and the application of d'Alembert operators.

In contrast to the Higgs decay, diagrams contributing to the pure squark parts at the two-loop level do not only consist of the ones where only squark lines or at most one gluon line appear as internal lines. Additionally, diagrams dressed with more than one gluon propagator exist. An example diagram is given to the left of Fig. 7.10. Since we cannot perform the calculation of this diagram directly, we apply the approach of the effective theory in which the squarks are integrated out as illustrated to the right of Fig. 7.10.

The diagrams to the left of * are vacuum diagrams. The dependence on the external

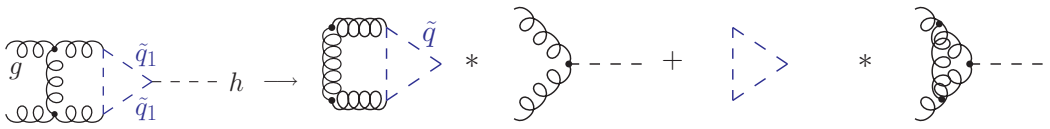

Figure 7.10.: *A squark diagram that is evaluated in the effective theory where the squarks are integrated out.*

momenta is contained in the effective ggh vertex, given by the vertices to the right of *. This effective vertex, with the dependence on the external momenta can be taken from [73]. The Wilson coefficient is determined by applying asymptotic expansions to the pure squark diagrams in certain hierarchies among the two squark masses and the evaluation of one- and two-loop vacuum diagrams. It is the coefficient of $(m_h^2)^0$ and thus independent of the Higgs mass.

It should be noted that in splitting the amplitude into QCD and SUSY contributions and dividing the latter into smaller pieces, one has to carefully think about which part of the renormalization of the leading order counts to which renormalized NLO piece.

7.4.2. Renormalization of the Amplitude for $gg \to h$

In the renormalization of the production of scalar Higgs bosons we obtain additional parts in comparison to the pseudoscalar case due to the appearance of SUSY particles, namely squarks in leading order. Therefore, we have to perform additional renormalizations, which are the ones of the squark masses and of the squark mixing angle. For the scalar cases we do not calculate the QCD effects. These can be extracted from `HIGLU` [104].

As described above, we perform an additional splitting of the amplitude into pure squark diagrams and the ones containing gluinos.

It should be noted that by calculating the pure stop or pure sbottom contributions for $gg \to h$ in the effective theory, in principle, the only adjustment that would have to be performed is a change in $L(\epsilon)$ in Eq. (7.2), where one would have to separate the gluino effects from the squark effects and just apply the squark effects. But this separation is dispensable since those shifts occur in Eq. (7.1) as well as in Eq. (7.4) with opposite signs, i.e., with a net zero effect.

The mixed gluino-quark-squark effects are evaluated with the new routines (cf. Sec. 5.4). In the bottom case, these cannot be computed in the effective theory. If we perform the renormalization of the gluino diagrams separately from the pure squark diagrams, we only have to include the effects from gluinos (label $\tilde{g}$) to the decoupling of the strong coupling from the full theory in Eq. (7.1). In addition, only effects from gluinos are taken into account in the on-shell gluon wave function renormalization. To sum up, the bare amplitude is renormalized with a factor that is given by $\zeta_3^{B,\tilde{g}}(\zeta_g^{B,\tilde{g}})^2 = 1$ up to order α_s to accommodate for the renormalization of the gluon wave functions and the decoupling

of the full theory to five flavors. The renormalization of the strong coupling does not contribute to the gluino parts of the amplitude that are finite after the renormalization of the appearing mass scales and squark mixing angle. Its renormalization only contributes to the QCD and pure squark corrections at NLO-SQCD.

Performing the calculation with the new routines for the top sector without the assumption of an effective theory leads to the same coefficient for $(m_\phi^2)^0$ as in the effective theory. This provides for a welcome check of the new results.

7.4.3. Separation of the Contributions from Gluinos and Squarks

For the production of scalar Higgs bosons in the gluon fusion process an additional partitioning of the SUSY parts, namely into the pure squark ones and the contributions that contain the effects of gluinos, is performed. Therefore, the squark and gluino contributions to the NLO amplitude are renormalized separately. This separation also permits to clearly tell apart terms originating from gluino effects and their renormalization from those coming from the squarks and their renormalization.

Altogether, the entire NLO-SUSY amplitude is given by

$$\mathcal{H}_{susy} = \sum_{q\tilde{q}=t\tilde{t},b\tilde{b}} \left(\mathcal{H}_{q\tilde{g}} + \mathcal{H}_{\tilde{q}}\right).$$

where

$$\begin{aligned} \mathcal{H}_{\tilde{q}} &= \left(\frac{\alpha_s}{\pi}\right)\mathcal{H}_{\tilde{q}}^{(0)} + \left(\frac{\alpha_s}{\pi}\right)^2 \mathcal{H}_{\tilde{q}}^{(1)}. \\ \mathcal{H}_{q\tilde{g}} &= \left(\frac{\alpha_s}{\pi}\right)^2 \left(\mathcal{H}_q^{(0),\mathrm{ren}} + \mathcal{H}_{\tilde{q}}^{(0),\mathrm{ren}}\right) + \left(\frac{\alpha_s}{\pi}\right)^2 \mathcal{H}_{\tilde{g}}^{(1)}. \end{aligned} \tag{7.8}$$

Eq. (7.8) tries to express that the LO contributions are not counted twice. To the pure SUSY parts, in LO only the squark diagrams contribute. These are included in $\mathcal{H}_{\tilde{q}}$. In order to obtain a finite NLO gluino part of the amplitude, we renormalize the LO quark as well as the LO squark parts and take their contributions through gluinos to $\mathcal{O}(\alpha_s^2)$ (label (0),ren) from the renormalization into $\mathcal{H}_{q\tilde{g}}$. $\mathcal{H}_q^{(0)}$ is counted to the QCD parts of the amplitude.

Gluino Contributions to the Amplitude

Clearly, for including the bottom quarks the approach of the effective theory is not valid. First, we discuss the renormalization of the mixed gluino-squark-quark Feynman diagrams. For the gluino parts (label $\tilde{g}$), we take the complete LO amplitude and renormalize the

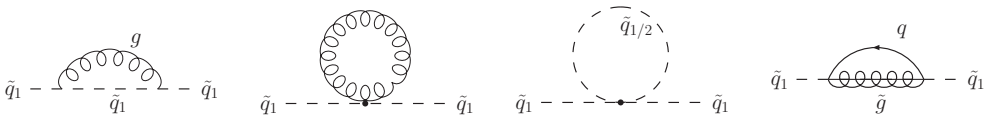

Figure 7.11.: *Contributions to the squark mass counterterm $Z_{m_{\tilde{q}_1}}$. In order to obtain the mass counterterm that is independent of gluino effects the diagram to the right is omitted in the calculation.*

mass scales and the squark mixing angle according to

$$\begin{aligned}
\delta Z^{\tilde{g},\mathrm{DRED}}_{m_q} &= \delta Z^{\mathrm{DRED}}_{m_q} - \delta Z^{\mathrm{DRED}}_{m_q,\mathrm{QCD}},\\
\delta Z^{\tilde{g},\mathrm{DREG}}_{m_q} &= \delta Z^{\mathrm{DREG}}_{m_q} - \delta Z^{\mathrm{DREG}}_{m_q,\mathrm{QCD}},\\
\delta Z^{\tilde{g}}_{m_{\tilde{q}_1}} &= \delta Z_{m_{\tilde{q}_1}} - \delta Z^{\mathrm{no}\,\tilde{g}}_{m_{\tilde{q}_1}},\\
\delta Z^{\tilde{g}}_{m_{\tilde{q}_2}} &= \delta Z_{m_{\tilde{q}_2}} - \delta Z^{\mathrm{no}\,\tilde{g}}_{m_{\tilde{q}_2}},\\
\delta Z^{\tilde{g}}_{\theta_{\tilde{q}}} &= \delta Z_{\theta_{\tilde{q}}} - \delta Z^{\mathrm{no}\,\tilde{g}}_{\theta_{\tilde{q}}}.
\end{aligned}$$

The renormalization constants Z_{x_i} ($x_i = m_q, m_{\tilde{q}_1}, m_{\tilde{q}_2}, \theta_{\tilde{q}}$) with no additional label denote the full MSSM ones that are given in App. B. In order to obtain the counterterms $Z^{\mathrm{no}\,\tilde{g}}_{x_i}$ (labeled "no $\tilde{g}$") without gluino contributions, the counterterms are calculated without the diagrams that contain gluinos. They are explicitly listed in App. B.

We do not have to evaluate Feynman diagrams to obtain $Z^{\mathrm{no}\,\tilde{g}}_{m_q}$. As the only effects from SUSY particles to the quark mass counterterm involve gluinos, this counterterm is just the difference of the complete MSSM quark mass counterterm and the QCD quark mass counterterm. Only for the quark mass counterterm there is a distinction whether the calculation is performed in DRED or DREG.

The complete counterterms $Z_{m_{\tilde{q}_1}}$ and $Z_{m_{\tilde{q}_2}}$ are obtained by the calculation of the one-loop corrected squark propagators for real squarks, i.e., the external momentum $p^2 = m^2_{\tilde{q}_i}$. The loop insertions are internal squark, quark, gluon and gluino lines. The contributions are illustrated in Fig. 7.11. To get the counterterms without gluinos $Z^{\mathrm{no}\,\tilde{g}}_{m_{\tilde{q}_1}}$, $Z^{\mathrm{no}\,\tilde{g}}_{m_{\tilde{q}_2}}$, only the one-loop diagrams that contain no gluinos are evaluated. For the determination of these counterterms, the right diagram in Fig. 7.11 is omitted in the calculation. We implement a new subroutine in order to calculate the contribution in which the squark emits a gluon and re-absorbs it again. The diagrams that contribute to the counterterm of the squark mixing angle are shown in Fig. 7.12.

It should be noted that just modifying the renormalization of the masses and the squark mixing angle for the calculation of the pure gluino parts does not lead to a finite result. That is why, in addition to the new counterterms which do not contain squark parts, we find that we need additional counterterms at the Higgs-squark-squark couplings in order to obtain a finite result for the pure gluino contributions. These are calculated with the help of the known results for the top case, which were obtained in the effective theory [82].

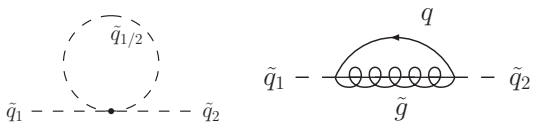

Figure 7.12.: *Contributions to the squark mixing angle counterterm $Z_{\theta_{\tilde{q}}}$. In order to obtain the squark mixing angle counterterm without effects from gluinos the right diagram is omitted in the calculation.*

In this case we could explicitly check if the splitting of the counterterms works. We could reproduce the complete NLO-SQCD result in the limit of large top/stop and gluino masses by renormalizing the SUSY and QCD parts separately and adding them together afterwards to obtain the known result.

The Higgs-squark-squark couplings can be split as follows [82]:

$$g^h_{\tilde{q},ij} = g^{h,ew}_{\tilde{q},ij} + g^{h,\mu}_{\tilde{q},ij} + g^{h,\alpha}_{\tilde{q},ij}.$$

The detailed expressions are given in App. A. For the renormalization of the couplings only the diagonal couplings $g^h_{\tilde{q},ii}, i = 1, 2$ have to be taken into account because only these occur in the leading order. First at two-loop level the non-diagonal couplings exist, where squarks of a different kind couple to Higgs bosons ($g^h_{\tilde{q},ij}, i \neq j$) due to the gluino or four squark insertions.

The single parts of the Higgs coupling to squarks have to be dressed with additional counterterms in order to obtain a finite amplitude. These are given by

$$g^{h,ew,\tilde{g}}_{\tilde{q},ii} = Z^{ew,\tilde{g}}\, g^{h,ew}_{\tilde{q},ii},$$
$$g^{h,\mu,\tilde{g}}_{\tilde{q},ii} = Z^{\mu,\tilde{g}}\, g^{h,\mu}_{\tilde{q},ii}.$$

We find that the new minimal counterterms are given by

$$Z^{ew,\tilde{g}} = 1 + \frac{\alpha_s}{\pi}\frac{1}{\epsilon}\frac{2}{3},$$
$$Z^{\mu,\tilde{g}} = 1 + \frac{\alpha_s}{\pi}\frac{1}{\epsilon}\frac{1}{3}.$$

For the last term in the coupling we find a more complicated structure:

$$g^{h,\alpha,\tilde{g}}_{\tilde{q},11} = c_{\tilde{q}}\left(2Z^{\alpha,\tilde{g}}_A + Z^{\alpha,\tilde{g}}_B\,\frac{1}{2}\frac{\left(m^2_{\tilde{q}_1} - m^2_{\tilde{q}_2}\right)}{m^2_q}\sin^2 2\theta_{\tilde{q}}\right),$$

$$g^{h,\alpha,\tilde{g}}_{\tilde{q},22} = c_{\tilde{q}}\left(2Z^{\alpha,\tilde{g}}_A - Z^{\alpha,\tilde{g}}_B\,\frac{1}{2}\frac{\left(m^2_{\tilde{q}_1} - m^2_{\tilde{q}_2}\right)}{m^2_q}\sin^2 2\theta_{\tilde{q}}\right),$$

where $c_{\tilde{t}} = -\cos\alpha/\sin\beta$ and $c_{\tilde{b}} = \sin\alpha/\cos\beta$ (cf. App. A).
The corresponding counterterms are expressed by

$$Z_A^{\alpha,\tilde{g}} = 1 - \frac{\alpha_s}{\pi}\frac{1}{\epsilon}\frac{4}{3},$$
$$Z_B^{\alpha,\tilde{g}} = 1 + \frac{\alpha_s}{\pi}\frac{1}{\epsilon}0.$$

These counterterms are the same for the bottom sector of the calculation as for the top sector of the calculation.

Squark Contributions to the Amplitude

The pure squark contributions to NLO are computed in the effective theory. The renormalization procedure is modified according to our needs. In the leading order only the pure squark diagrams are taken into account.
The counterterms applied are given by

$$\begin{aligned}
\delta Z_{m_q}^{\tilde{q},\mathrm{DRED}} &= \delta Z_{m_q,\mathrm{QCD}}^{\mathrm{DRED}},\\
\delta Z_{m_q}^{\tilde{q},\mathrm{DREG}} &= \delta Z_{m_q,\mathrm{QCD}}^{\mathrm{DREG}},\\
\delta Z_{m_{\tilde{q}_1}}^{\tilde{q}} &= \delta Z_{m_{\tilde{q}_1}}^{\mathrm{no}\,\tilde{g}},\\
\delta Z_{m_{\tilde{q}_2}}^{\tilde{q}} &= \delta Z_{m_{\tilde{q}_2}}^{\mathrm{no}\,\tilde{g}},\\
\delta Z_{\theta_{\tilde{q}}}^{\tilde{q}} &= \delta Z_{\theta_{\tilde{q}}}^{\mathrm{no}\,\tilde{g}}.
\end{aligned}$$

Their explicit expressions are displayed in App. B. In order to obtain a finite result for the pure squark contributions, again we have to introduce finite counterterms at the $h\tilde{q}\tilde{q}$ couplings. This goes about the same way as for the gluino parts.
We obtain

$$\begin{aligned}
Z^{ew,\mathrm{no}\,\tilde{g}} &= 1 + \frac{\alpha_s}{\pi}\frac{1}{\epsilon}\left(-\frac{2}{3}\right),\\
Z^{\mu,\mathrm{no}\,\tilde{g}} &= 1 + \frac{\alpha_s}{\pi}\frac{1}{\epsilon}\left(-\frac{1}{3}\right),\\
Z_A^{\alpha,\mathrm{no}\,\tilde{g}} &= 1 - \frac{\alpha_s}{\pi}\frac{1}{\epsilon}\left(-\frac{4}{3}\right),\\
Z_B^{\alpha,\mathrm{no}\,\tilde{g}} &= 1 + \frac{\alpha_s}{\pi}\frac{1}{\epsilon}0.
\end{aligned}$$

Here, we can observe that we performed the renormalization correctly as these new counterterms for the squark and gluino parts add up to zero.

7.4.4. Renormalization of the Amplitude $gg \to A$

For the production of pseudoscalar Higgs bosons via the gluon fusion, besides the pure QCD parts only the ones where at least one gluino occurs as an internal particle exist at the two-loop level. Therefore, no splitting into squark and gluino parts as in the scalar case is required.

The mixed gluino-quark-squark effects are evaluated with the help of the new routines (cf. Sec. 5.4). If we perform the renormalization of the gluino diagrams separately from the quark diagrams, we only have to include the effects from gluinos and squarks (label $\tilde{q}\tilde{g}$) in the decoupling of the strong coupling from the full theory in Eq. (7.1). In addition, only effects from gluinos and squarks are taken into account in the on-shell gluon wave function renormalization. To sum up, the bare amplitude is renormalized with a factor that is given by $\zeta_3^{B,\tilde{q}\tilde{g}}(\zeta_g^{B,\tilde{q}\tilde{g}})^2 = 1$ up to order α_s to accommodate for the renormalization of the gluon wave functions and the decoupling of the full theory to five flavors. The renormalization of the strong coupling does not contribute to the gluino parts of the amplitude that are finite after the renormalization of the quark mass.

In addition, only the quark mass has to be renormalized in analogy to the procedure described for the process $A \to \gamma\gamma$ (cf. Sec. 6.7.1).

For the production of pseudoscalar Higgs bosons we evaluated the NLO-SQCD cross section in the effective theory in the large top/stop/gluino limit in [60].

An important check is that the expansion of the newly obtained results for the top sector in an expansion in the parameter $m_A^2/(4m_t^2)$ agree with the result of the effective theory. There, the first term of the expansion, i.e., the coefficient of $(m_A^2)^0$ has to agree.

Again, we have to be careful to obtain the SM limit by keeping the couplings fixed and letting the SUSY masses tend to infinity. For the SUSY parts we obtain that this limit vanishes as required since we take the QCD parts from elsewhere. For the effective theory, i.e., the limit of large SUSY as well as top masses is given explicitly below. As required, the QCD result is obtained in the SM limit.

In this limit, the SUSY parts decouple as demonstrated below

$$\mathcal{A}_{t\tilde{t}} = \frac{\alpha_s}{\pi}\cot\beta\left[1 + \frac{\alpha_s}{\pi}\left(\frac{4}{3}l + \frac{2}{3}\tilde{q} - 2q\right)\right] = \frac{\alpha_s}{\pi}\cot\beta\left(1 + 0\cdot\frac{\alpha_s}{\pi}\right).$$

Here, the terms are labeled such that q ($q = 1$) denotes the part arising from the two-loop QCD effects and $\tilde{q}$ denotes the two-loop contribution from supersymmetric particles (in SUSY: $\tilde{q} = 1$, in QCD: $\tilde{q} = 0$). The label l ($l = 1$) denotes the term originating from the renormalization of the LO part of the amplitude. This has already been observed in [60] and suggests that in MSSM calculations there is a non-trivial interplay of the QCD parts with the SUSY parts.

Validation and Conclusions

Given that we only compute the NLO-SUSY contributions to the amplitude, it should be ensured that we do not obtain contributions from the renormalization of the leading order quark amplitude that are already included in the two-loop QCD result. Therefore, our newly calculated results have to vanish in the SM limit. We explicitly checked that the SUSY effects decouple if we keep the couplings fixed and consider the limit of very large SUSY masses. For all the amplitudes we calculate, the SUSY effects vanish in that limit. Of course, all our SUSY results are separately finite. The pole parts for the top case as well as the bottom case of the amplitudes are analytically zero.

We find agreement if we perform the renormalization in DRED and DREG with the appropriate on-shell quark mass counterterms. In DREG, the $h\tilde{q}\tilde{q}$ coupling has to be renormalized as described in Sec. 4.5.

For the production of the lightest scalar Higgs boson we renormalize the pure squark contributions separately from the gluino contributions to the amplitude. A check of the sum of $\mathcal{H}_{\tilde{t}}+\mathcal{H}_{t\tilde{g}}$ is to renormalize the gluino and stop parts together in one procedure in the effective theory. Thereby, the newly introduced counterterms for the $h\tilde{t}\tilde{t}$ couplings and the splitting of the other counterterms into parts that contain gluinos and "no $\tilde{g}$" parts are not applied. Of course, for calculating the SUSY parts together, we take the entire LO MSSM contribution to the amplitude. By calculating the SUSY parts without the NLO QCD contributions to the amplitude, we perform the renormalization in analogy to the scalar Higgs decay where we did not split the SUSY contributions into ones from gluinos and ones from squarks. There, we changed the entire quark mass counterterm by subtracting the QCD part and the $h\tilde{q}\tilde{q}$ coupling was renormalized with the full MSSM quark mass counterterm. Finally, we find that the result where one renormalizes the stop and gluino parts separately agrees with the one where the two parts are renormalized together in the effective theory. This is an important check of the newly obtained counterterms.

Our result is limited by the pure squark contributions that were obtained in the effective theory. By taking the pure squark parts of the two-loop amplitude from elsewhere, respectively providing the gluino result for others, one could obtain a more general result.

In principle, the calculation can be extended to apply it to the heavier of the two CP-even Higgs bosons H. In doing so, we need to change the Higgs couplings to squarks and quarks. But one has to keep in mind that this is assumed to be much heavier than h and therefore the assumption of the squark masses being larger than the Higgs mass might not be a good assumption any more.

7.5. Explicit Results as an Expansion in Leading Terms

Some limiting cases for the virtual SUSY contributions to the NLO amplitudes in the gluon fusion process will be explicitly listed below. For this process the leading order Feynman

diagrams are already proportional to α_s caused by the two gluons appearing as external particles. The amplitude for the scalar and pseudoscalar Higgs production via the gluon fusion is denoted by

$$\mathcal{H}\left(gg \to h\right) = \sum_{q\tilde{q}=t\tilde{t},b\tilde{b}} \mathcal{H}_{q\tilde{q}} = \sum_{q\tilde{q}=t\tilde{t},b\tilde{b}} \left(\frac{\alpha_s}{\pi} \mathcal{H}^{(0)}_{q\tilde{q}} + \left(\frac{\alpha_s}{\pi}\right)^2 \mathcal{H}^{(1)}_{q\tilde{q}} \right) + \mathcal{O}\left(\alpha_s^2\right),$$

$$\mathcal{A}\left(gg \to A\right) = \sum_{q\tilde{q}=t\tilde{t},b\tilde{b}} \mathcal{A}_{q\tilde{q}} = \sum_{q\tilde{q}=t\tilde{t},b\tilde{b}} \left(\frac{\alpha_s}{\pi} \mathcal{A}^{(0)}_{q\tilde{q}} + \left(\frac{\alpha_s}{\pi}\right)^2 \mathcal{A}^{(1)}_{q\tilde{q}} \right) + \mathcal{O}\left(\alpha_s^2\right).$$

This has to be understood in the sense that $q\tilde{q} = t\tilde{t}, b\tilde{b}$ denotes the top (bottom) case which, in addition to quarks, includes the stops (sbottoms) and gluinos. Since we do not calculate the QCD parts of the amplitude in the gluon fusion process, the results given in this section arise from two-loop virtual contributions to the amplitude from supersymmetric particles, i.e., they contain at least one supersymmetric particle as an internal line. For our newly obtained results we explicitly checked that they all vanish in the SM-limit and that the expansions of the top/stop results agree with the result in the effective theory to $(m_\phi^2)^0$. In addition, we checked that our on-shell results agree in DREG and DRED. Because of the simple structure of the $A\tilde{q}\tilde{q}$ coupling, for the production of pseudoscalar Higgs bosons we tested that the bottom/sbottom results agree with the one for the top/stops with the replacements $m_t \to m_b$, $m_{\tilde{t}_1} \to m_{\tilde{b}_1}$, $m_{\tilde{t}_2} \to m_{\tilde{b}_2}$, $\cot\beta \to \tan\beta$. For the scalar Higgs bosons, the corresponding replacements at the coupling to squarks can be read off in App. A.

The notation applied in the next sections is the one already taken for the amplitudes in the Higgs decay. For the expansion parameters the notation given in Eq. (6.21) is applied.

7.5.1. Explicit Expressions for the Amplitude for $gg \to A$

For the pure SUSY part due to bottoms, sbottom and gluinos we can write down the amplitude in the following form

$$\boxed{\mathcal{A}_{b\tilde{b}} = \tan\beta\, \mathcal{A}_{0,b\tilde{b}} + \frac{\mu_{susy}}{M_x}\left(1+\tan^2\beta\right)\mathcal{A}_{1,b\tilde{b}},} \tag{7.9}$$

with

$$\mathcal{A}_{i,b\tilde{b}} = \sum_n \left(\frac{m_b}{m_A}\right)^n \mathcal{A}_{i,b\tilde{b},n}.$$

The analogous part of the amplitude for the top sector reads

$$\boxed{\mathcal{A}_{t\tilde{t}} = \cot\beta \mathcal{A}_{0,t\tilde{t}} + \frac{\mu_{susy}}{M_x}\left(1+\cot^2\beta\right)\mathcal{A}_{1,t\tilde{t}},} \tag{7.10}$$

with

$$\mathcal{A}_{i,t\tilde{t}} = \sum_n \left(\frac{m_A}{m_t}\right)^n \mathcal{A}_{i,t\tilde{t},n}.$$

Furthermore,

$$\mathcal{A}_{i,q\tilde{q}} = \frac{\alpha_s}{\pi}\mathcal{A}^{(0)}_{i,q\tilde{q}} + \left(\frac{\alpha_s}{\pi}\right)^2 \mathcal{A}^{(1)}_{i,q\tilde{q}} + \mathcal{O}\left(\alpha_s^3\right), \qquad q\tilde{q} = t\tilde{t},\, b\tilde{b}$$

and

$$\mathcal{A}^{(j)}_{i,q\tilde{q}} = \mathcal{A}^{(j)}_{i,q} + \mathcal{A}^{(j)}_{i,q\tilde{g}}.$$

The analogous decomposition applies to the coefficients $\mathcal{A}_{i,q\tilde{q},n}$. The largest SUSY mass scale that we chose in our limiting case is denoted by M_x.

The leading order contribution for the production of pseudoscalar Higgs bosons via the gluon fusion does not contain contributions from squarks. The leading order contributions of bottom quarks read

$$\begin{aligned}\mathcal{A}^{(0)}_{0,b} = &-L^2_{Ab}x_{bA} - 4L_{Ab}x^2_{bA} + (6L_{Ab}-4)x^3_{bA} + \left(\frac{40L_{Ab}}{3} - 12\right)x^4_{bA} \\ &+ \left(35L_{Ab} - \frac{107}{3}\right)x^5_{bA} + \left(\frac{504L_{Ab}}{5} - 110\right)x^6_{bA} + \mathcal{O}\left(x^7_{bA}\right).\end{aligned}$$

The amplitude in LO from top effects is given by

$$\mathcal{A}^{(0)}_{0,t} = 1 + \frac{x_{At}}{12} + \frac{x^2_{At}}{90} + \frac{x^3_{At}}{560} + \frac{x^4_{At}}{3150} + \mathcal{O}\left(x^5_{At}\right).$$

In the following, coefficients that are omitted vanish.

7.5.2. $gg \to A$ in the Limit $m_q \ll M_s \equiv m_{\tilde{q}_1} = m_{\tilde{q}_2} = m_{\tilde{g}}$

First we examine the case, where the masses of the supersymmetric particles are set to one scale, M_s, i.e., $M_x = M_s$.

For the bottom sector we obtain through $\mathcal{O}\left(m_b^4\right)$

$$\begin{aligned}\mathcal{A}^{(1)}_{0,b\tilde{g},2} = &\left(\frac{1}{4} - \frac{5L_{Ab}}{36}\right)x_{As} + \left(-\frac{L_{Ab}}{108} - \frac{71L_{As}}{720} + \frac{1073}{5400}\right)x^2_{As} \\ &+ \left(-\frac{L_{Ab}}{1008} - \frac{67L_{As}}{7560} + \frac{24959}{3175200}\right)x^3_{As} + \mathcal{O}\left(x^4_{As}\right),\end{aligned}$$

$$\mathcal{A}^{(1)}_{0,b\tilde{g},4} = \left(-\frac{L_{Ab}^2}{36} + \frac{5L_{Ab}}{18} + \frac{5}{18}\right) x_{As} + \left(\frac{203L_{Ab}}{1080} + \frac{287}{1080}\right) x_{As}^2 + \left(\frac{277L_{Ab}}{5040} - \frac{191L_{As}}{2520} + \frac{73249}{529200}\right) x_{As}^3 + \mathcal{O}\left(x_{As}^4\right),$$

$$\mathcal{A}^{(1)}_{1,b\tilde{g},2} = \frac{L_{Ab}^2}{3} + \left(\frac{L_{Ab}^2}{36} + \frac{5L_{bs}}{36} - \frac{16}{27}\right) x_{As} + \left(\frac{L_{Ab}^2}{270} + \frac{L_{bs}}{36} - \frac{113}{864}\right) x_{As}^2 + \left(\frac{L_{Ab}^2}{1680} + \frac{11L_{bs}}{2016} - \frac{15091}{529200}\right) x_{As}^3 + \mathcal{O}\left(x_{As}^4\right),$$

$$\mathcal{A}^{(1)}_{1,b\tilde{g},4} = -\frac{4L_{Ab}}{3} + \left(\frac{L_{Ab}^2}{18} - \frac{L_{Ab}}{9}\right) x_{As} + \left(\frac{L_{Ab}^2}{135} - \frac{2L_{Ab}}{135} - \frac{7L_{bs}}{60} - \frac{7}{600}\right) x_{As}^2 + \left(\frac{L_{Ab}^2}{840} - \frac{L_{Ab}}{420} - \frac{31L_{bs}}{560} - \frac{9463}{352800}\right) x_{As}^3 + \mathcal{O}\left(x_{As}^4\right).$$

The pure SUSY contributions arising from top, stop and gluino contributions to the amplitude up to $\mathcal{O}\left(m_A^6\right)$ are given by

$$\mathcal{A}^{(1)}_{0,t\tilde{g},2} = \frac{11}{432} x_{ts} + \left(-\frac{71L_{ts}}{720} - \frac{43}{3600}\right) x_{ts}^2 + \left(\frac{40973}{1058400} - \frac{191L_{ts}}{2520}\right) x_{ts}^3 + \mathcal{O}\left(x_{ts}^4\right),$$

$$\mathcal{A}^{(1)}_{0,t\tilde{g},4} = \frac{17}{6480} x_{ts} + \frac{1199}{64800} x_{ts}^2 + \left(-\frac{67L_{ts}}{7560} - \frac{15809}{3175200}\right) x_{ts}^3 + \mathcal{O}\left(x_{ts}^4\right),$$

$$\mathcal{A}^{(1)}_{0,t\tilde{g},6} = \frac{23}{60480} x_{ts} + \frac{17}{9072} x_{ts}^2 + \frac{9883 x_{ts}^3}{4233600} + \mathcal{O}\left(x_{ts}^4\right),$$

$$\mathcal{A}^{(1)}_{1,t\tilde{g},0} = -\frac{1}{3} + \left(\frac{5L_{ts}}{36} - \frac{35}{54}\right) x_{ts} + \left(-\frac{7L_{ts}}{60} - \frac{41}{1800}\right) x_{ts}^2 + \left(\frac{1069}{19600} - \frac{23L_{ts}}{280}\right) x_{ts}^3 + \mathcal{O}\left(x_{ts}^4\right),$$

$$\mathcal{A}^{(1)}_{1,t\tilde{g},2} = -\frac{1}{36} - \frac{7}{216} x_{ts} + \left(\frac{L_{ts}}{36} - \frac{601}{4320}\right) x_{ts}^2 + \left(-\frac{31L_{ts}}{560} - \frac{1137}{39200}\right) x_{ts}^3 + \mathcal{O}\left(x_{ts}^4\right),$$

$$\mathcal{A}^{(1)}_{1,t\tilde{g},4} = -\frac{1}{270} - \frac{19}{6480} x_{ts} - \frac{x_{ts}^2}{225} + \left(\frac{11L_{ts}}{2016} - \frac{6329}{211680}\right) x_{ts}^3 + \mathcal{O}\left(x_{ts}^4\right),$$

$$\mathcal{A}^{(1)}_{1,t\tilde{g},6} = -\frac{1}{1680} - \frac{37}{90720} x_{ts} - \frac{559 x_{ts}^2}{1360800} - \frac{4577 x_{ts}^3}{6350400} + \mathcal{O}\left(x_{ts}^4\right).$$

7.5.3. $gg \to A$ in the Limit $m_q \ll m_{\tilde{q}_1} \ll M_{\tilde{g}} \equiv m_{\tilde{q}_2} = m_{\tilde{g}}$

Again, the pure SUSY part due to bottoms, sbottoms and gluinos can be written in the form of Eq. (7.9), but with $M_x = M_{\tilde{g}}$.

The individual parts for the bottom sector through $\mathcal{O}(m_b^4)$ are given by

$$\mathcal{A}^{(1)}_{0,b\tilde{g},0} = \sin^2 2\theta_{\tilde{b}} \left[\frac{1}{12} + \left(\frac{L_{1\tilde{g}}}{3} + \frac{1}{2}\right) x_{1\tilde{g}} + \frac{137}{5184} x_{A\tilde{g}}\right] + \mathcal{O}\left(x_{A\tilde{g}}^2, x_{1\tilde{g}} x_{A\tilde{g}}, x_{1\tilde{g}}^2\right),$$

$$\mathcal{A}^{(1)}_{0,b\tilde{g},1} = \sin 2\theta_{\tilde{b}}\sqrt{x_{A\tilde{g}}}\left(-\frac{L^2_{Ab}}{12}+\frac{11L_{Ab}}{72}-\frac{3}{8}\right)+\mathcal{O}\left(x^{3/2}_{A\tilde{g}},x_{1\tilde{g}}x^{1/2}_{A\tilde{g}}\right),$$

$$\begin{aligned}\mathcal{A}^{(1)}_{0,b\tilde{g},2} = {}& \sin^2 2\theta_{\tilde{b}}\left[\frac{L^2_{Ab}}{12}+\left(\frac{L_{1\tilde{g}}}{3}+\frac{1}{2}\right)L^2_{Ab}x_{1\tilde{g}}\right]\\ &+x_{A\tilde{g}}\left[\left(\frac{L^2_{Ab}}{27}+\frac{5}{108}\right)\sin^2 2\theta_{\tilde{b}}-\frac{2L_{Ab}}{9}+\frac{1}{2}\right]+\mathcal{O}\left(x^2_{A\tilde{g}},x_{1\tilde{g}}x_{A\tilde{g}},x^2_{1\tilde{g}}\right),\end{aligned}$$

$$\mathcal{A}^{(1)}_{0,b\tilde{g},3} = \sin 2\theta_{\tilde{b}}\sqrt{x_{A\tilde{g}}}\left(-\frac{5L^2_{Ab}}{72}+\frac{L_{Ab}}{36}-\frac{11}{36}\right)+\mathcal{O}\left(x^{3/2}_{A\tilde{g}},x_{1\tilde{g}}x^{1/2}_{A\tilde{g}}\right),$$

$$\begin{aligned}\mathcal{A}^{(1)}_{0,b\tilde{g},4} = {}& \sin^2 2\theta_{\tilde{b}}\left[-\frac{L_{Ab}}{3}+\left(-\frac{4L_{1\tilde{g}}}{3}-2\right)L_{Ab}x_{1\tilde{g}}\right]\\ &+x_{A\tilde{g}}\left[\frac{L^2_{Ab}}{18}+\frac{4L_{Ab}}{9}+\left(\frac{5L^2_{Ab}}{108}-\frac{4L_{Ab}}{27}\right)\sin^2 2\theta_{\tilde{b}}+\frac{4}{9}\right]+\mathcal{O}\left(x^2_{A\tilde{g}},x_{1\tilde{g}}x_{A\tilde{g}},x^2_{1\tilde{g}}\right),\end{aligned}$$

$$\mathcal{A}^{(1)}_{1,b\tilde{g},1} = \sin 2\theta_{\tilde{b}}\left[-\frac{1}{6}\sqrt{x_{A\tilde{g}}}-\frac{137x^{3/2}_{A\tilde{g}}}{2592}+\left(-\frac{2L_{1\tilde{g}}}{3}-\frac{7}{6}\right)x_{1\tilde{g}}\sqrt{x_{A\tilde{g}}}\right]+\mathcal{O}\left(x^{5/2}_{A\tilde{g}},x^2_{1\tilde{g}}x^{1/2}_{A\tilde{g}}\right),$$

$$\mathcal{A}^{(1)}_{1,b\tilde{g},2} = \frac{2L^2_{Ab}}{3}+\left(\frac{2L_{1\tilde{g}}}{3}+\frac{2}{3}\right)L^2_{Ab}x_{1\tilde{g}}+\left(\frac{L^2_{Ab}}{6}+\frac{11L_{b\tilde{g}}}{36}-\frac{85}{108}\right)x_{A\tilde{g}}+\mathcal{O}\left(x^2_{A\tilde{g}},x_{1\tilde{g}}x_{A\tilde{g}},x^2_{1\tilde{g}}\right),$$

$$\begin{aligned}\mathcal{A}^{(1)}_{1,b\tilde{g},3} = {}& \sin 2\theta_{\tilde{b}}\left[-\frac{L^2_{Ab}}{6}\sqrt{x_{A\tilde{g}}}+\left(-\frac{2L_{1\tilde{g}}}{3}-\frac{7}{6}\right)L^2_{Ab}x_{1\tilde{g}}\sqrt{x_{A\tilde{g}}}\right.\\ &\left.+\left(-\frac{2L^2_{Ab}}{27}-\frac{5}{54}\right)x^{3/2}_{A\tilde{g}}\right]+\mathcal{O}\left(x^{5/2}_{A\tilde{g}},x^2_{1\tilde{g}}x^{1/2}_{A\tilde{g}}\right),\end{aligned}$$

$$\mathcal{A}^{(1)}_{1,b\tilde{g},4} = -\frac{8L_{Ab}}{3}+\left(-\frac{8L_{1\tilde{g}}}{3}-\frac{8}{3}\right)x_{1\tilde{g}}L_{Ab}+\left(\frac{2L^2_{Ab}}{9}-\frac{2L_{Ab}}{3}\right)x_{A\tilde{g}}+\mathcal{O}\left(x^2_{A\tilde{g}},x_{1\tilde{g}}x_{A\tilde{g}},x^2_{1\tilde{g}}\right).$$

For the pure SUSY part arising due to the top, stop and gluino contributions to the amplitude we obtain up to $\mathcal{O}\left(m_A^4\right)$

$$\begin{aligned}\mathcal{A}^{(1)}_{0,t\tilde{g},2} = {}& -\frac{\sin^2 2\theta_{\tilde{t}}}{144}+\frac{55\sin 2\theta_{\tilde{t}}}{864}\sqrt{x_{t\tilde{g}}}+\left(-\frac{L_{1\tilde{g}}}{36}-\frac{1}{24}\right)\sin^2 2\theta_{\tilde{t}}x_{1\tilde{g}}+\left(\frac{7}{216}-\frac{25\sin^2 2\theta_{\tilde{t}}}{1728}\right)x_{t\tilde{g}}\\ &+\left(\frac{71L_{t\tilde{g}}}{960}+\frac{30179}{86400}\right)\sin 2\theta_{\tilde{t}}x^{3/2}_{t\tilde{g}}+\left(\frac{53L_{1\tilde{g}}}{144}+\frac{35}{48}\right)\sin 2\theta_{\tilde{t}}x_{1\tilde{g}}\sqrt{x_{t\tilde{g}}}+\left(-\frac{5L_{1\tilde{g}}}{72}-\frac{1}{24}\right)\\ &\sin^2 2\theta_{\tilde{t}}x^2_{1\tilde{g}}+\left[\left(-\frac{L_{1\tilde{g}}}{24}-\frac{29}{864}\right)\sin^2 2\theta_{\tilde{t}}-\frac{5L_{1\tilde{g}}}{144}-\frac{109}{864}\right]x_{t\tilde{g}}x_{1\tilde{g}}+\left[\left(\frac{29}{21600}-\frac{7L_{t\tilde{g}}}{720}\right)\right.\\ &\left.\sin^2 2\theta_{\tilde{t}}-\frac{281L_{t\tilde{g}}}{1440}-\frac{49}{225}\right]x^2_{t\tilde{g}}+\mathcal{O}\left(x^{5/2}_{t\tilde{g}},x^{1/2}_{t\tilde{g}}x^2_{1\tilde{g}}\right),\end{aligned}$$

$$\mathcal{A}^{(1)}_{0,t\tilde{g},4} = -\frac{\sin^2 2\theta_{\tilde{t}}}{1080} + \frac{67\sin 2\theta_{\tilde{t}}}{12960}\sqrt{x_{t\tilde{g}}} + \left(-\frac{L_{1\tilde{g}}}{270} - \frac{1}{180}\right)\sin^2 2\theta_{\tilde{t}} x_{1\tilde{g}}$$
$$+ \left(-\frac{7\sin^2 2\theta_{\tilde{t}}}{1944} + \frac{1}{324}\right) x_{t\tilde{g}} + \frac{1039\sin 2\theta_{\tilde{t}}}{64800} x_{t\tilde{g}}^{3/2} + \left(\frac{71L_{1\tilde{g}}}{2160} + \frac{1}{15}\right)\sin 2\theta_{\tilde{t}} x_{1\tilde{g}}\sqrt{x_{t\tilde{g}}}$$
$$+ \left(-\frac{L_{1\tilde{g}}}{108} - \frac{1}{180}\right)\sin^2 2\theta_{\tilde{t}} x_{1\tilde{g}}^2 + \left[\left(-\frac{17L_{1\tilde{g}}}{540} - \frac{37}{486}\right)\sin^2 2\theta_{\tilde{t}} - \frac{11L_{1\tilde{g}}}{2160}\right.$$
$$\left. - \frac{211}{12960}\right] x_{t\tilde{g}} x_{1\tilde{g}} + \left(\frac{5009}{129600} - \frac{151\sin^2 2\theta_{\tilde{t}}}{12960}\right) x_{t\tilde{g}}^2 + \mathcal{O}\left(x_{t\tilde{g}}^{5/2}, x_{t\tilde{g}}^{1/2} x_{1\tilde{g}}^2\right),$$

$$\mathcal{A}^{(1)}_{1,t\tilde{g},0} = -\frac{2}{3} + \left(-\frac{2L_{1\tilde{g}}}{3} - \frac{2}{3}\right) x_{1\tilde{g}} + \left(\frac{11L_{t\tilde{g}}}{36} - \frac{109}{108}\right) x_{t\tilde{g}} + \left(-\frac{4L_{1\tilde{g}}}{3} - \frac{2}{3}\right) x_{1\tilde{g}}^2$$
$$+ \left(\frac{L_{t\tilde{g}}L_{1\tilde{g}}}{6} - \frac{L_{1\tilde{g}}}{2} - \frac{7L_{t\tilde{g}}}{36} + \frac{\zeta(2)}{3} - \frac{109}{108}\right) x_{t\tilde{g}} x_{1\tilde{g}} + \left(-\frac{7L_{t\tilde{g}}}{20} - \frac{673}{1800}\right) x_{t\tilde{g}}^2$$
$$+ \mathcal{O}\left(x_{t\tilde{g}}^{5/2}, x_{t\tilde{g}}^{1/2} x_{1\tilde{g}}^2\right),$$

$$\mathcal{A}^{(1)}_{1,t\tilde{g},2} = -\frac{1}{18} + \frac{\sin 2\theta_{\tilde{t}}}{72}\sqrt{x_{t\tilde{g}}} + \left(-\frac{L_{1\tilde{g}}}{18} - \frac{1}{18}\right) x_{1\tilde{g}} - \frac{5x_{t\tilde{g}}}{27} + \frac{25}{864}\sin 2\theta_{\tilde{t}}\, x_{t\tilde{g}}^{3/2}$$
$$+ \left(\frac{L_{1\tilde{g}}}{18} + \frac{7}{72}\right)\sin 2\theta_{\tilde{t}} x_{1\tilde{g}}\sqrt{x_{t\tilde{g}}} + \left(-\frac{L_{1\tilde{g}}}{9} - \frac{1}{18}\right) x_{1\tilde{g}}^2 + \left(-\frac{13L_{1\tilde{g}}}{18} - \frac{155}{108}\right) x_{t\tilde{g}} x_{1\tilde{g}}$$
$$+ \left(\frac{67L_{t\tilde{g}}}{480} - \frac{14377}{43200}\right) x_{t\tilde{g}}^2 + \mathcal{O}\left(x_{t\tilde{g}}^{5/2}, x_{t\tilde{g}}^{1/2} x_{1\tilde{g}}^2\right),$$

$$\mathcal{A}^{(1)}_{1,t\tilde{g},4} = -\frac{1}{135} + \frac{\sin 2\theta_{\tilde{t}}}{540}\sqrt{x_{t\tilde{g}}} + \left(-\frac{L_{1\tilde{g}}}{135} - \frac{1}{135}\right) x_{1\tilde{g}} - \frac{53x_{t\tilde{g}}}{3240} + \frac{7}{972}\sin 2\theta_{\tilde{t}}\, x_{t\tilde{g}}^{3/2}$$
$$+ \left(\frac{L_{1\tilde{g}}}{135} + \frac{7}{540}\right)\sin 2\theta_{\tilde{t}} x_{1\tilde{g}}\sqrt{x_{t\tilde{g}}} + \left(-\frac{2L_{1\tilde{g}}}{135} - \frac{1}{135}\right) x_{1\tilde{g}}^2$$
$$+ \left(-\frac{17L_{1\tilde{g}}}{270} - \frac{101}{810}\right) x_{t\tilde{g}} x_{1\tilde{g}} - \frac{1343x_{t\tilde{g}}^2}{16200} + \mathcal{O}\left(x_{t\tilde{g}}^{5/2}, x_{t\tilde{g}}^{1/2} x_{1\tilde{g}}^2\right).$$

7.5.4. $gg \to A$ in the Limit $m_q \ll m_{\tilde{q}_1} \ll m_{\tilde{q}_2} \ll M_{\tilde{g}}$

For this limiting case we take $M_x = M_{\tilde{g}}$. For the SUSY parts of the amplitude in the bottom sector we obtain through $\mathcal{O}(m_b^2)$

$$\mathcal{A}^{(1)}_{0,b\tilde{g},0} = \sin^2 2\theta_{\tilde{b}}\left[\left(\frac{L_{12}}{3} + \frac{1}{6}\right) x_{1\tilde{g}} + \frac{x_{A\tilde{g}}}{18} + \frac{x_{2\tilde{g}}}{6} + x_{A2}\left(\left(\frac{L_{12}}{3} + \frac{2}{3}\right) x_{1\tilde{g}} + \frac{x_{A\tilde{g}}}{36}\right)\right]$$
$$+ \mathcal{O}\left(x_{A\tilde{g}}^2, x_{1\tilde{g}}x_{2\tilde{g}}, x_{A\tilde{g}}x_{1\tilde{g}}, x_{A\tilde{g}}x_{2\tilde{g}}, x_{2\tilde{g}}^2\right),$$

$$\mathcal{A}^{(1)}_{0,b\tilde{g},1} = \sqrt{x_{A\tilde{g}}} L_{Ab}^2 \sin 2\theta_{\tilde{b}}\left[-\frac{1}{6} + \left(-\frac{L_{12}}{3} - \frac{1}{3}\right) x_{12} - \frac{x_{A2}}{18}\right] + \mathcal{O}\left(x_{A\tilde{g}}^{3/2}, x_{A\tilde{g}}^{1/2} x_{1\tilde{g}}, x_{A\tilde{g}}^{1/2} x_{2\tilde{g}}\right),$$

$$\mathcal{A}^{(1)}_{0,b\tilde{g},2} = \sin^2 2\theta_{\tilde{b}} L^2_{Ab} \left[x_{2\tilde{g}} \frac{1}{6} + x_{1\tilde{g}} \left(\left(\frac{L_{12}}{3} + \frac{1}{6} \right) + \left(\frac{L_{12}}{3} + \frac{2}{3} \right) x_{A2} \right) \right] + \left[-\frac{11 L_{Ab}}{36} + \frac{3}{4} + \left(\frac{1}{18} + \frac{x_{A2}}{36} \right) L^2_{Ab} \sin^2 2\theta_{\tilde{b}} \right] x_{A\tilde{g}} + \mathcal{O}\left(x^2_{A\tilde{g}}, x_{1\tilde{g}} x_{2\tilde{g}}, x_{A\tilde{g}} x_{1\tilde{g}}, x_{A\tilde{g}} x_{2\tilde{g}}, x^2_{2\tilde{g}}, x^2_{1\tilde{g}} \right),$$

$$\mathcal{A}^{(1)}_{1,b\tilde{g},1} = \sin 2\theta_{\tilde{b}} \sqrt{x_{A\tilde{g}}} \left(-\frac{1}{3} + x_{12} \left(-\frac{2L_{12}}{3} - \frac{2}{3} \right) - \frac{x_{A2}}{9} \right) + \mathcal{O}\left(x^{3/2}_{A\tilde{g}}, x^{1/2}_{A\tilde{g}} x_{1\tilde{g}}, x^{1/2}_{A\tilde{g}} x_{2\tilde{g}} \right),$$

$$\mathcal{A}^{(1)}_{1,b\tilde{g},2} = L^2_{Ab} \left(-\frac{2L_{2\tilde{g}}}{3} + \frac{2L_{12}}{3} x_{12} + \frac{x_{A2}}{3} \right) + \mathcal{O}\left(x_{A\tilde{g}}, x_{1\tilde{g}}, x_{2\tilde{g}} \right).$$

For the SUSY parts of the amplitude in the top sector up to $\mathcal{O}(m_A^4)$ we obtain

$$\mathcal{A}^{(1)}_{0,t\tilde{g},2} = \sqrt{x_{t\tilde{g}}} \sin 2\theta_{\tilde{t}} \left[\frac{1}{6} + \left(\frac{L_{12}}{3} + \frac{1}{3} \right) x_{12} \right] + \left[\left(-\frac{L_{12}}{36} - \frac{1}{72} \right) x_{1\tilde{g}} - \frac{x_{2\tilde{g}}}{72} \right] \sin^2 2\theta_{\tilde{t}} + \frac{17}{432} x_{t\tilde{g}} + \mathcal{O}\left(x^{3/2}_{t\tilde{g}}, x^{1/2}_{t\tilde{g}} x_{1\tilde{g}}, x^{1/2}_{t\tilde{g}} x_{2\tilde{g}} \right),$$

$$\mathcal{A}^{(1)}_{0,t\tilde{g},4} = \sqrt{x_{t\tilde{g}}} \sin 2\theta_{\tilde{t}} \left[\frac{1}{72} + \left(\frac{L_{12}}{36} + \frac{1}{36} \right) x_{12} + \frac{x_{t2}}{18} \right] + \left[-\frac{1}{540} + \left(-\frac{1}{540} - \frac{L_{12}}{270} \right) x_{12} \right] \sin^2 2\theta_{\tilde{t}} \; x_{2\tilde{g}} + \left[-\frac{1}{216} + \left(-\frac{L_{12}}{36} - \frac{1}{18} \right) x_{12} \right] \sin^2 2\theta_{\tilde{t}} x_{t\tilde{g}} + \frac{23 x_{t\tilde{g}}}{6480} + \mathcal{O}\left(x^{3/2}_{t\tilde{g}}, x^{1/2}_{t\tilde{g}} x_{1\tilde{g}}, x^{1/2}_{t\tilde{g}} x_{2\tilde{g}} \right),$$

$$\mathcal{A}^{(1)}_{1,t\tilde{g},0} = -\frac{2L_{12} x_{12}}{3} + \frac{2L_{2\tilde{g}}}{3} + \mathcal{O}\left(x_{t\tilde{g}}, x_{1\tilde{g}}, x_{2\tilde{g}} \right),$$

$$\mathcal{A}^{(1)}_{1,t\tilde{g},2} = \frac{L_{2\tilde{g}}}{18} - \frac{x_{t2}}{3} - \frac{L_{12}}{18} x_{12} + \left[\frac{1}{36} + \left(\frac{L_{12}}{18} + \frac{1}{18} \right) x_{12} \right] \sin 2\theta_{\tilde{t}} \sqrt{x_{t\tilde{g}}} + \mathcal{O}\left(x_{t\tilde{g}}, x_{1\tilde{g}}, x_{2\tilde{g}} \right),$$

$$\mathcal{A}^{(1)}_{1,t\tilde{g},4} = \frac{L_{2\tilde{g}}}{135} - \frac{x_{t2}}{36} - \frac{L_{12}}{135} x_{12} + \left[\frac{x_{t2}}{108} + \frac{1}{270} + \left(\frac{L_{12}}{135} + \frac{1}{135} \right) x_{12} \right] \sin 2\theta_{\tilde{t}} \sqrt{x_{t\tilde{g}}} + \mathcal{O}\left(x^{3/2}_{t\tilde{g}}, x^{1/2}_{t\tilde{g}} x_{1\tilde{g}}, x^{1/2}_{t\tilde{g}} x_{2\tilde{g}} \right).$$

7.5.5. Explicit Expressions for the Amplitude $gg \to h$

The structure of the amplitude for the production of scalar Higgs bosons in the gluon fusion process for the bottom as well as top sector can be expressed through

$$\boxed{\begin{aligned} \mathcal{H}_{b\tilde{b}} = {} & \frac{\sin\alpha}{\cos\beta} \mathcal{H}_{0,b\tilde{b}} + \frac{\mu_{susy}}{M_x} \frac{\cos(\alpha-\beta)}{\cos^2\beta} \mathcal{H}_{1,b\tilde{b}} - \frac{M_Z^2}{M_x^2} \sin(\alpha+\beta) \mathcal{H}_{2,b\tilde{b}} \\ & - \frac{M_Z^2}{M_x^2} \frac{2}{3} \sin^2\theta_W \sin(\alpha+\beta) \mathcal{H}_{3,b\tilde{b}}, \end{aligned}} \tag{7.11}$$

with

$$\mathcal{H}_{i,b\tilde{b}} = \sum_n \left(\frac{m_b}{m_A}\right)^n \mathcal{H}_{i,b\tilde{b},n}. \tag{7.12}$$

$$\begin{aligned}\mathcal{H}_{t\tilde{t}} = {} & \frac{\cos\alpha}{\sin\beta}\mathcal{H}_{0,t\tilde{t}} + \frac{\mu_{susy}}{M_x}\frac{\cos(\alpha-\beta)}{\sin^2\beta}\mathcal{H}_{1,t\tilde{t}} + \frac{M_Z^2}{M_x^2}\sin(\alpha+\beta)\,\mathcal{H}_{2,t\tilde{t}} \\ & + \frac{M_Z^2}{M_x^2}\frac{4}{3}\sin^2\theta_W \sin(\alpha+\beta)\,\mathcal{H}_{3,t\tilde{t}},\end{aligned} \tag{7.13}$$

with

$$\mathcal{H}_{i,t\tilde{t}} = \sum_n \left(\frac{m_h}{m_t}\right)^n \mathcal{H}_{i,t\tilde{t},n}. \tag{7.14}$$

Furthermore,

$$\mathcal{H}_{i,q\tilde{q}} = \frac{\alpha_s}{\pi}\mathcal{H}^{(0)}_{i,q\tilde{q}} + \left(\frac{\alpha_s}{\pi}\right)^2 \mathcal{H}^{(1)}_{i,q\tilde{q}} + \mathcal{O}\left(\alpha_s^3\right), \qquad q\tilde{q} = t\tilde{t},\, b\tilde{b}$$

and

$$\mathcal{H}^{(j)}_{i,q\tilde{q}} = \mathcal{H}^{(j)}_{i,q} + \mathcal{H}^{(j)}_{i,\tilde{q}\tilde{g}} = \mathcal{H}^{(j)}_{i,q} + \mathcal{H}^{(j)}_{i,\tilde{q}} + \mathcal{H}^{(j)}_{i,q\tilde{g}}.$$

The analogous decomposition applies to the coefficients $\mathcal{H}_{i,q\tilde{q},n}$. It should be noted that $\mathcal{H}^{(j)}_{i,\tilde{q}\tilde{g}}$ denotes corrections to the amplitude that contain at least one supersymmetric scale whereas $\mathcal{H}^{(j)}_{i,q\tilde{g}}$ only refers to contributions from gluinos. Again, M_x denotes the heaviest mass scale in the certain limit under consideration.

We only display the QCD results in LO since we do not calculate the NLO-QCD parts. The bottom contributions are given by

$$\mathcal{H}^{(0)}_{0,b} = \left(\frac{L_{hb}^2}{2} - 2\right) x_{bh} + \left(-2L_{hb}^2 - 2L_{hb}\right) x_{bh}^2 + (5L_{hb}+2)x_{bh}^3 + \left(\frac{16}{3}L_{hb} - 2\right) x_{bh}^4 + \mathcal{O}\left(x_{bh}^5\right),$$

For the top contributions we obtain

$$\mathcal{H}^{(0)}_{0,t} = \frac{1}{3} + \frac{7x_{ht}}{360} + \frac{x_{ht}^2}{504} + \frac{13x_{ht}^3}{50400} + \frac{2x_{ht}^4}{51975} + \mathcal{O}\left(x_{ht}^5\right),$$

In the following, coefficients that are omitted vanish.

7.5.6. $gg \to h$ in the Limit $m_q \ll M_s \equiv m_{\tilde{q}_1} = m_{\tilde{q}_2} = m_{\tilde{g}}$

We split the NLO-SUSY contributions to the amplitude into the ones due to gluinos (label $\tilde{g} = 1$) and the pure sbottom (label $\tilde{b} = 1$) ones. The parts which are not marked result from the renormalization of the two-loop gluino effects.

For the LO sbottom contributions we get through $\mathcal{O}(m_b^4)$

$$\mathcal{H}^{(0)}_{0,\tilde{b},2} = -\frac{1}{6}x_{hs},\ \mathcal{H}^{(0)}_{1,\tilde{b}} = 0,\ \mathcal{H}^{(0)}_{2,\tilde{b},0} = -\frac{1}{24},\ \mathcal{H}^{(0)}_{3,\tilde{b}} = 0.$$

In NLO we obtain for the bottom sector up to $\mathcal{O}(m_b^4)$

$$\begin{aligned}\mathcal{H}^{(1)}_{0,\tilde{b}\tilde{g},2} &= \left(\frac{L_{hb}^2}{3} - \frac{2L_{hb}}{3} - \frac{4}{3}\right)L_{\tilde{b}} + \left(-\frac{2L_{\tilde{b}}}{9} - \frac{2}{9}\right)x_{hs} + \tilde{b}\left(-\frac{L_{bs}}{3} + \frac{2L_{\tilde{b}}}{9} - \frac{7}{12}\right)x_{hs} \\ &\quad + \tilde{g}\left[\left(-\frac{L_{hb}^2}{3} + \frac{2L_{hb}}{3} + \frac{4}{3}\right)L_{\tilde{b}} + \left(\frac{5L_{hb}}{72} - \frac{5L_{hs}}{36} + \frac{43}{72}\right)x_{hs}\right] + \mathcal{O}\left(x_{hs}^2\right) \\ &= \left(\frac{29L_{hb}}{72} - \frac{17L_{hs}}{36} - \frac{5}{24}\right)x_{hs} + \mathcal{O}\left(x_{hs}^2\right),\end{aligned}$$

$$\begin{aligned}\mathcal{H}^{(1)}_{0,\tilde{b}\tilde{g},4} &= -\frac{x_{hs}^2}{54} + \left(\frac{L_{hb}^2}{18} - \frac{L_{hb}}{9} - \frac{2}{9}\right)x_{hs} + \left(\frac{4}{3} - \frac{8L_{hb}^2}{3}\right)L_{\tilde{b}} \\ &\quad + \tilde{g}\left[\left(\frac{8L_{hb}^2}{3} - \frac{4}{3}\right)L_{\tilde{b}} + \left(\frac{13L_{hb}^2}{72} + \frac{L_{hb}}{4} - \frac{11}{36}\right)x_{hs}\right] + \mathcal{O}\left(x_{hs}^3\right) \\ &= \left(\frac{17L_{hb}^2}{72} + \frac{5L_{hb}}{36} - \frac{19}{36}\right)x_{hs} - \frac{x_{hs}^2}{54} + \mathcal{O}\left(x_{hs}^3\right),\end{aligned}$$

$$\mathcal{H}^{(1)}_{1,\tilde{b}\tilde{g},2} = \tilde{g}\left(\frac{2}{3} - \frac{L_{hb}^2}{6}\right) + \mathcal{O}\left(x_{hs}\right) \quad \text{and} \quad \mathcal{H}^{(1)}_{1,\tilde{b}\tilde{g},4} = \tilde{g}\left(\frac{2L_{hb}^2}{3} + \frac{2L_{hb}}{3}\right) + \mathcal{O}\left(x_{hs}\right).$$

$$\begin{aligned}\mathcal{H}^{(1)}_{2,\tilde{b}\tilde{g},0} &= \frac{L_{\tilde{b}}}{36} + \left(-\frac{L_{\tilde{b}}}{36} - \frac{41}{144}\right)\tilde{b} + \frac{25}{288} + \mathcal{O}\left(x_{hs}\right) = -\frac{19}{96} + \mathcal{O}\left(x_{hs}\right), \\ \mathcal{H}^{(1)}_{2,\tilde{b}\tilde{g},2} &= \tilde{g}\left(\frac{L_{hb}^2}{18} - \frac{2}{9}\right) + \mathcal{O}\left(x_{hs}\right), \quad \mathcal{H}^{(1)}_{2,\tilde{b}\tilde{g},4} = \tilde{g}\left(-\frac{2L_{hb}^2}{9} - \frac{2L_{hb}}{9}\right) + \mathcal{O}\left(x_{hs}\right),\end{aligned}$$

$$\mathcal{H}^{(1)}_{3,\tilde{b}\tilde{g}} = 0.$$

For the top case the SUSY parts of the amplitude are up to $\mathcal{O}(m_h^4)$

$$\mathcal{H}^{(0)}_{0,\tilde{t},2} = \frac{1}{6}x_{ts},\ \mathcal{H}^{(0)}_{1,\tilde{t}} = 0,\ \mathcal{H}^{(0)}_{2,\tilde{t},0} = -\frac{1}{24},\ \mathcal{H}^{(0)}_{3,\tilde{t}} = 0.$$

Analogously, the SUSY effects in the top sector are split into the ones due to gluinos (label $\tilde{g}=1$) and the pure stop (label $\tilde{t}=1$) ones. The parts that are not marked result from the renormalization of the two-loop gluino effects. The stop effects up to $\mathcal{O}(m_h^4)$ read

$$\begin{aligned}\mathcal{H}^{(1)}_{0,\tilde{t}\tilde{g},0} &= \left(\frac{2L_t}{9}+\tilde{g}\left(\frac{5L_{ts}}{36}-\frac{5}{18}\right)+\frac{2L_{ts}}{9}+\left(-\frac{2L_t}{9}+\frac{L_{ts}}{9}+\frac{7}{12}\right)\tilde{t}+\frac{2}{9}\right)x_{ts}+\frac{x_{ts}^2}{54}\\ &\quad+\mathcal{O}\left(x_{ts}^3\right)=\left(\frac{17L_{ts}}{36}+\frac{19}{36}\right)x_{ts}+\frac{x_{ts}^2}{54}+\mathcal{O}\left(x_{ts}^3\right),\end{aligned}$$

$$\begin{aligned}\mathcal{H}^{(1)}_{0,\tilde{t}\tilde{g},2} &= -\frac{7L_t}{540}-\frac{7L_{ts}}{540}-\frac{7x_{ts}}{3240}-\frac{7x_{ts}^2}{32400}+\tilde{g}\left(\frac{7L_t}{540}+\frac{7L_{ts}}{540}+\frac{37x_{ts}}{12960}\right)+\mathcal{O}\left(x_{ts}^3\right)\\ &= \frac{x_{ts}}{1440}-\frac{7x_{ts}^2}{32400}+\mathcal{O}\left(x_{ts}^3\right),\\ \mathcal{H}^{(1)}_{0,\tilde{t}\tilde{g},4} &= -\frac{L_t}{378}-\frac{L_{ts}}{378}-\frac{x_{ts}}{2268}-\frac{x_{ts}^2}{22680}+\tilde{g}\left(\frac{L_t}{378}+\frac{L_{ts}}{378}+\frac{13x_{ts}}{18144}\right)+\mathcal{O}\left(x_{ts}^3\right)\\ &= \frac{5x_{ts}}{18144}-\frac{x_{ts}^2}{22680}+\mathcal{O}\left(x_{ts}^3\right),\end{aligned}$$

$$\mathcal{H}^{(1)}_{1,\tilde{t}\tilde{g},0}=-\frac{\tilde{g}}{9}+\mathcal{O}\left(x_{ts}\right),\quad \mathcal{H}^{(1)}_{1,\tilde{t}\tilde{g},2}=-\frac{7\tilde{g}}{1080}+\mathcal{O}\left(x_{ts}\right),\quad \mathcal{H}^{(1)}_{2,4}=-\frac{\tilde{g}}{1512}+\mathcal{O}\left(x_{ts}\right).$$

$$\begin{aligned}\mathcal{H}^{(1)}_{2,\tilde{t}\tilde{g},0} &= -\frac{L_t}{12}+\tilde{g}\left(\frac{L_t}{9}+\frac{L_{ts}}{9}+\frac{91}{864}\right)-\frac{L_{ts}}{12}+\left(-\frac{L_{ts}}{36}-\frac{L_{ts}}{36}-\frac{41}{144}\right)\tilde{t}-\frac{1}{18}+\mathcal{O}\left(x_{ts}\right)\\ &= -\frac{203}{864}+\mathcal{O}\left(x_{ts}\right),\end{aligned}$$

$$\mathcal{H}^{(1)}_{2,\tilde{t}\tilde{g},2}=-\frac{7\tilde{g}}{3240}+\mathcal{O}\left(x_{ts}\right),\qquad\text{and}\qquad \mathcal{H}^{(1)}_{2,\tilde{t}\tilde{g},4}=-\frac{\tilde{g}}{4536}+\mathcal{O}\left(x_{ts}\right)$$

$$\mathcal{H}^{(1)}_{3,\tilde{t}\tilde{g}}=0.$$

7.5.7. $gg\to h$ in the Limit $m_q \ll m_{\tilde{q}_1} \ll m_{\tilde{q}_2} \ll M_{\tilde{g}}$

For the limit $m_q \ll m_{\tilde{q}_1} \ll m_{\tilde{q}_2} \ll M_{\tilde{g}}$ we explicitly write down the results only for the bottom sector. In this paragraph, the large scale is $M_x = M_{\tilde{g}}$. Again, the pure SUSY part due to bottoms, sbottom and gluinos can be written in the form of Eq. (7.11).

The sbottom contributions to the leading order up to $\mathcal{O}\left(m_b^2\right)$ read

$$\mathcal{H}^{(0)}_{0,\tilde{b}\tilde{g},0}=\sin^2 2\theta_{\tilde{b}}\left(\frac{x_{12}}{48}+\frac{x_{21}}{48}-\frac{x_{h1}}{360}-\frac{x_{h2}}{360}-\frac{1}{24}\right),\ \mathcal{H}^{(0)}_{0,\tilde{b}\tilde{g},2}=\sin^2 2\theta_{\tilde{b}}\left(-\frac{x_{h1}}{12}-\frac{x_{h2}}{12}\right),$$

$$\mathcal{H}^{(0)}_{1,\tilde{b}\tilde{g},1} = \sin 2\theta_{\tilde{b}} \left(-\frac{1}{24}\sqrt{x_{h1}}\sqrt{x_{\tilde{g}1}} + \frac{1}{24}\sqrt{x_{h2}}\sqrt{x_{\tilde{g}2}} \right),$$

$$\mathcal{H}^{(0)}_{2,\tilde{b}\tilde{g},0} = \left(-\frac{\cos 2\theta_{\tilde{b}}}{48} - \frac{1}{48} \right) x_{\tilde{g}1} + \left(\frac{\cos 2\theta_{\tilde{b}}}{48} - \frac{1}{48} \right) x_{\tilde{g}2},$$

$$\mathcal{H}^{(0)}_{3,\tilde{b}\tilde{g},0} = \frac{\cos 2\theta_{\tilde{b}} x_{\tilde{g}1}}{24} - \frac{\cos 2\theta_{\tilde{b}} x_{\tilde{g}2}}{24}.$$

The individual parts for two-loop effects of the bottom sector through $\mathcal{O}(m_b^2)$ are given by

$$\begin{aligned}
\mathcal{H}^{(1)}_{0,\tilde{b}\tilde{g},0} = {} & \left[\left(-\frac{L_{12}}{144} - \frac{1}{72} \right) x_{21} + \left(\frac{L_{12}}{144} - \frac{1}{72} \right) x_{12} + \frac{1}{36} \right] \sin^4 2\theta_{\tilde{b}} + \left[\left(-\frac{L_{12}}{72} + \frac{3}{32} \right) x_{21} \right. \\
& \left. + \left(\frac{L_{12}}{72} + \frac{3}{32} \right) x_{12} - \frac{29}{144} \right] \sin^2 2\theta_{\tilde{b}} + \left(\frac{\sin^2 2\theta_{\tilde{b}}}{1080} + \frac{L_{1\tilde{g}}}{270} \right) x_{h1} + \left(\frac{\sin^2 2\theta_{\tilde{b}}}{1080} + \frac{L_{2\tilde{g}}}{270} \right) x_{h2} \\
& + \left(-\frac{17 L_{12}}{288} - \frac{1}{144} \right) \sin^2 2\theta_{\tilde{b}} x_{1\tilde{g}} + \left(\frac{17 L_{12}}{288} + \frac{x_{21}}{216} - \frac{1}{144} \right) \sin^2 2\theta_{\tilde{b}} x_{2\tilde{g}} + \left[\left(-\frac{17}{1728} \right. \right. \\
& \left. \left. (x_{12} + x_{21}) + \frac{107(x_{h1} + x_{h2})}{120960} + \frac{31}{1440} \right) \sin^2 2\theta_{\tilde{b}} + \frac{L_{1\tilde{g}}}{270} + \frac{L_{2\tilde{g}}}{270} \right] x_{h\tilde{g}} + \mathcal{O}\left(x_{2\tilde{g}}^2, x_{1\tilde{g}}^2, x_{h\tilde{g}}^2 \right),
\end{aligned}$$

$$\begin{aligned}
\mathcal{H}^{(1)}_{0,\tilde{b}\tilde{g},1} = {} & \left(\frac{2L_{\tilde{g}}}{135} + \frac{2L_{\tilde{b}_1}}{135} + \frac{4}{135} \right) x_{h1}\sqrt{x_{h2}} \cos^2 2\theta_{\tilde{b}} \sin 2\theta_{\tilde{b}} \sqrt{x_{\tilde{g}2}} + \left[\left(-\frac{L_{12}}{12} - \frac{1}{6} \right) L_{hb}^2 + \frac{L_{12}}{3} + \frac{2}{3} \right. \\
& \left. + \left[\left(\frac{1}{6} - \frac{L_{12}}{12} \right) L_{hb}^2 + \frac{L_{12}}{3} - \frac{2}{3} \right] x_{12} \right] \sin^3 2\theta_{\tilde{b}} \sqrt{x_{2h}}\sqrt{x_{2\tilde{g}}} + \left[\frac{L_{hb}^2}{12} + \frac{L_{12}}{18} + \left(-\frac{L_{2\tilde{g}}}{18} - \frac{1}{72} \right) \right. \\
& x_{21} + \left[\left(\frac{L_{12}}{6} + \frac{1}{6} \right) L_{hb}^2 - \frac{11 L_{12}}{18} + \frac{L_{2\tilde{g}}}{18} - \frac{47}{72} \right] x_{12} + \left(\frac{1}{27} - \frac{L_{h\tilde{g}}}{36} \right) x_{h1} + \left(\frac{L_{hb}^2}{36} + \frac{L_{h\tilde{g}}}{36} \right. \\
& \left. + \frac{\sqrt{x_{12}}}{135} - \frac{19}{135} \right) x_{h2} + \frac{\sqrt{x_{h1}}\sqrt{x_{h2}}}{270} + \sin^2 2\theta_{\tilde{b}} \left[-\frac{L_{hb}^2}{12} + \left(\frac{L_{hb}^2}{72} - \frac{1}{18} \right) x_{21} - \frac{\sqrt{x_{12}}}{36} + \frac{\sqrt{x_{21}}}{36} \right. \\
& + \frac{1}{3} + \left(\left(-\frac{L_{12}}{6} - \frac{13}{72} \right) L_{hb}^2 + \frac{2L_{12}}{3} + \frac{13}{18} \right) x_{12} + \left(-\frac{L_{hb}^2}{720} - \frac{1}{540} \right) x_{h1} + \left(-\frac{19 L_{hb}^2}{720} - \frac{\sqrt{x_{12}}}{135} \right. \\
& \left. \left. \left. + \frac{19}{180} \right) x_{h2} - \frac{\sqrt{x_{h1}}\sqrt{x_{h2}}}{270} \right] + \frac{\sqrt{x_{12}}}{36} - \frac{\sqrt{x_{21}}}{36} - \frac{1}{3} \right] \sin 2\theta_{\tilde{b}} \sqrt{x_{h\tilde{g}}} + \mathcal{O}\left(x_{2\tilde{g}} x_{h\tilde{g}}^{1/2}, x_{1\tilde{g}} x_{h\tilde{g}}^{1/2} \right),
\end{aligned}$$

$$\mathcal{H}^{(1)}_{0,\tilde{b}\tilde{g},2} = \left(\frac{L_{12}\sin^2 2\theta_{\tilde{b}}}{36} + \frac{L_{1\tilde{g}}}{18} - \frac{L_{b\tilde{g}}}{6} - \frac{31}{72}\right) x_{h1} + \left(-\frac{L_{12}\sin^2 2\theta_{\tilde{b}}}{36} + \frac{L_{2\tilde{g}}}{18} - \frac{L_{b\tilde{g}}}{6} - \frac{31}{72}\right) x_{h2} + \left(\frac{L_{hb}^2}{12} - \frac{1}{3}\right)(1 - x_{12}) L_{12}\sin^2 2\theta_{\tilde{b}} x_{2\tilde{g}} + \left[\left(\frac{L_{hb}^2}{36} - \frac{1}{9}\right)\sin^2 2\theta_{\tilde{b}} - \frac{7L_{12}}{24} - \frac{7L_{2\tilde{g}}}{12} - \frac{11L_{b\tilde{g}}}{36} - \frac{11L_{hb}}{72} + \left[\left(-\frac{L_{hb}^2}{72} - \frac{L_{b\tilde{g}}}{72} + \frac{1}{36}\right)\sin^2 2\theta_{\tilde{b}} - \frac{L_{2\tilde{g}}}{18} - \frac{1}{36}\right] x_{21} - \frac{65}{216} + \left[\left(-\frac{L_{hb}^2}{72} - \frac{L_{b\tilde{g}}}{72} + \frac{1}{36}\right)\sin^2 2\theta_{\tilde{b}} - \frac{L_{1\tilde{g}}}{18} - \frac{1}{36}\right] x_{12}\right] x_{h\tilde{g}} + \mathcal{O}\left(x_{2\tilde{g}}^2, x_{1\tilde{g}}^2, x_{h\tilde{g}}^2, x_{2\tilde{g}}x_{h\tilde{g}}, x_{1\tilde{g}}x_{h\tilde{g}}\right),$$

$$\mathcal{H}^{(1)}_{1,\tilde{b}\tilde{g},0} = \sin 2\theta_{\tilde{b}}\left[\frac{L_{1\tilde{g}}\sqrt{x_{h1}}}{1080}\sqrt{x_{\tilde{g}1}} - \frac{L_{2\tilde{g}}\sqrt{x_{h2}}}{1080}\sqrt{x_{\tilde{g}2}}\right] + \left[L_{1\tilde{g}}\left(\frac{1}{72} - \frac{x_{12}}{72}\right) + L_{2\tilde{g}}\left(\frac{1}{72} - \frac{x_{21}}{72}\right)\right] \sin^2 2\theta_{\tilde{b}} + \frac{L_{12}\sqrt{x_{h\tilde{g}}}}{1080}\sin 2\theta_{\tilde{b}} + \sin^2 2\theta_{\tilde{b}}\left[\frac{L_{1\tilde{g}}}{72}x_{1\tilde{g}} + L_{2\tilde{g}}\left(\frac{1}{72} - \frac{x_{21}}{72}\right)x_{2\tilde{g}}\right] + \mathcal{O}\left(x_{2\tilde{g}}x_{h\tilde{g}}^{1/2}, x_{1\tilde{g}}x_{h\tilde{g}}^{1/2}\right),$$

$$\mathcal{H}^{(1)}_{1,\tilde{b}\tilde{g},1} = \left[\left(\frac{L_{12}}{72} + \frac{1}{36}\right)\sin^3 2\theta_{\tilde{b}} + \left(\frac{L_{12}}{36} + \frac{L_{2\tilde{g}}}{18} - \frac{L_{b\tilde{g}}}{24} - \frac{11}{48}\right)\sin 2\theta_{\tilde{b}}\right] x_{h1}\sqrt{x_{\tilde{g}1}} + \left[\left(\frac{L_{12}}{72} - \frac{1}{36}\right)\sin^3 2\theta_{\tilde{b}} + \left(-\frac{L_{12}}{36} - \frac{L_{2\tilde{g}}}{18} + \frac{L_{b\tilde{g}}}{24} + \frac{11}{48}\right)\sin 2\theta_{\tilde{b}}\right] x_{h2}\sqrt{x_{\tilde{g}2}} + \sqrt{x_{1\tilde{g}}}\sin 2\theta_{\tilde{b}}\left[L_{1\tilde{g}}\left(\frac{x_{12}}{144} - \frac{1}{8}\right) + L_{2\tilde{g}}\left(\frac{1}{8} - \frac{x_{21}}{144}\right)\right] + \frac{17}{864}(x_{h1} - x_{h2})\sqrt{x_{hgl}} + \left[\left(\frac{1}{216} - \frac{L_{1\tilde{g}}}{144}\right)\sqrt{x_{h\tilde{g}}}x_{1\tilde{g}} + \left[L_{2\tilde{g}}\left(\frac{1}{144} - \frac{x_{21}}{144}\right) - \frac{1}{216}\right]\sqrt{x_{h\tilde{g}}}x_{2\tilde{g}}\right]\sin 2\theta_{\tilde{b}} + \mathcal{O}\left(x_{2\tilde{g}}^2 x_{h\tilde{g}}^{1/2}, x_{1\tilde{g}}^2 x_{h\tilde{g}}^{1/2}\right),$$

$$\mathcal{H}^{(1)}_{1,\tilde{b}\tilde{g},2} = \sin 2\theta_{\tilde{b}}\left[\frac{\sqrt{x_{\tilde{g}2}}x_{h2}}{144} - \frac{\sqrt{x_{\tilde{g}1}}x_{h1}}{144}\right] + \left[\frac{L_{hb}^2}{3} + L_{12}\left(\frac{L_{hb}^2}{6} - \frac{2}{3}\right) + L_{12}\left(\frac{L_{hb}^2}{3} - \frac{4}{3}\right)x_{12} - \frac{4}{3}\right]\sin^2 2\theta_{\tilde{b}} + L_{2\tilde{g}}\left(\frac{L_{hb}^2}{3} - \frac{4}{3}\right) + L_{12}\left(\frac{4}{3} - \frac{L_{hb}^2}{3}\right)x_{12} + \left[-\frac{L_{hb}^2}{6} + \left(\frac{5L_{hb}^2}{36} - \frac{41}{72}\right)\sin^2 2\theta_{\tilde{b}} + \frac{49}{72}\right] x_{h2} + x_{h1}\left[\left(\frac{7}{72} - \frac{L_{hb}^2}{36}\right)\sin^2 2\theta_{\tilde{b}} + \left(\frac{\sin^2 2\theta_{\tilde{b}}}{135} - \frac{1}{135}\right)x_{h2} + \frac{1}{72}\right] + \left(\frac{1}{36} - \frac{\sin^2 2\theta_{\tilde{b}}}{36}\right)\sqrt{x_{h1}}\sqrt{x_{h2}} + \sin 2\theta_{\tilde{b}}\left[-\frac{L_{12}}{144} + \left(\frac{L_{1\tilde{g}}}{144} + \frac{1}{144}\right)x_{12} + \left(-\frac{L_{2\tilde{g}}}{144} - \frac{1}{144}\right)x_{21} + \frac{x_{h1}}{2160} - \frac{x_{h2}}{2160}\right]\sqrt{x_{h\tilde{g}}} + \mathcal{O}\left(x_{2\tilde{g}}, x_{1\tilde{g}}, x_{h\tilde{g}}\right),$$

$$\mathcal{H}^{(1)}_{2,\tilde{b}\tilde{g},0} = \left[\frac{L_{12}\sin^2 2\theta_{\tilde{b}}}{144} + \frac{L_{1\tilde{g}}}{72} + \cos 2\theta_{\tilde{b}}\left[\left(\frac{L_{12}}{144}+\frac{1}{72}\right)\sin^2 2\theta_{\tilde{b}} + \frac{L_{1\tilde{g}}}{72} - \frac{37}{288}\right] - \frac{37}{288}\right] x_{\tilde{g}1}$$
$$+ \left[-\frac{L_{12}\sin^2 2\theta_{\tilde{b}}}{144} + \frac{L_{2\tilde{g}}}{72} + \cos 2\theta_{\tilde{b}}\left[\left(\frac{L_{12}}{144}-\frac{1}{72}\right)\sin^2 2\theta_{\tilde{b}} - \frac{L_{2\tilde{g}}}{72} + \frac{37}{288}\right] - \frac{37}{288}\right] x_{\tilde{g}2}$$
$$+ \left(-\frac{17\cos 2\theta_{\tilde{b}}}{288} - \frac{17}{288}\right) L_{1\tilde{g}} + \left(\frac{17\cos 2\theta_{\tilde{b}}}{288} - \frac{17}{288}\right) L_{2\tilde{g}} + \left(\frac{17\cos 2\theta_{\tilde{b}}}{1728} + \frac{17}{1728}\right) x_{h1}$$
$$+ \left(\frac{17}{1728} - \frac{17\cos 2\theta_{\tilde{b}}}{1728}\right) x_{h2} - \frac{5}{48} + \left(\frac{\cos 2\theta_{\tilde{b}}}{432} + \frac{1}{432}\right) x_{1\tilde{g}} + \left(\frac{1}{432} - \frac{\cos 2\theta_{\tilde{b}}}{432}\right) x_{2\tilde{g}}$$
$$+ \mathcal{O}\left(x^2_{1\tilde{g}}, x^2_{2\tilde{g}}\right),$$

$$\mathcal{H}^{(1)}_{2,\tilde{b}\tilde{g},1} = \sin 2\theta_{\tilde{b}}\left[\sqrt{x_{\tilde{g}h}}\left[L_{12}\left(\frac{L^2_{hb}}{12}-\frac{1}{3}\right) + \cos 2\theta_{\tilde{b}}\left(\left(\frac{L^2_{hb}}{6}-\frac{2}{3}\right)(1+L_{12}x_{12}) + L_{12}\left(\frac{L^2_{hb}}{12}\right.\right.\right.\right.$$
$$\left.\left.\left.\left.-\frac{1}{3}\right)\right)\right] + \sqrt{x_{\tilde{g}1}}\left[\cos 2\theta_{\tilde{b}}\sqrt{x_{h1}}\left(\frac{7}{144} - \frac{L^2_{hb}}{72}\right) + \left(\frac{1}{18} - \frac{L^2_{hb}}{72}\right)\sqrt{x_{h1}}\right] + \sqrt{x_{\tilde{g}2}}\left[\sqrt{x_{h2}}\right.\right.$$
$$\left.\left.\left(\frac{L^2_{hb}}{72} - \frac{1}{18}\right) + \cos 2\theta_{\tilde{b}}\left(\left(\frac{5L^2_{hb}}{72} + \frac{x_{h1}}{270} - \frac{41}{144}\right)\sqrt{x_{h2}} - \frac{\sqrt{x_{h1}}}{72}\right)\right] + \sqrt{x_{1\tilde{g}}}\left[\sqrt{x_{1h}}\right.\right.$$
$$\left.\left.\left(\left(\frac{L_{1\tilde{g}}}{6}+\frac{1}{12}\right)L^2_{hb} - \frac{2L_{1\tilde{g}}}{3} - \frac{1}{3}\right) + \cos 2\theta_{\tilde{b}}\left(\sqrt{x_{1h}}\left(\frac{L^2_{hb}}{12}-\frac{1}{3}\right) + L_{12}\left(\frac{L^2_{hb}}{6}-\frac{2}{3}\right)\right.\right.\right.$$
$$\left.\left.\left.\sqrt{x_{1h}})\right] + \sqrt{x_{2\tilde{g}}}\left[\cos 2\theta_{\tilde{b}}\sqrt{x_{2h}}\left(\frac{L^2_{hb}}{12}-\frac{1}{3}\right) + L_{12}\left(\frac{L^2_{hb}}{6}-\frac{2}{3}\right)\sqrt{x_{2h}} + \left(\left(-\frac{L_{1\tilde{g}}}{6}-\frac{1}{12}\right)\right.\right.\right.$$
$$\left.\left.\left.L^2_{hb} + \frac{2L_{1\tilde{g}}}{3} + \frac{1}{3}\right)\sqrt{x_{2h}}\right] + \left[L_{12}\left(-\frac{L^2_{hb}}{24} + \frac{L_{b\tilde{g}}}{48} + \frac{29}{144}\right) + \left(\frac{L^2_{hb}}{180} - \frac{L_{b\tilde{g}}}{288} - \frac{121}{4320}\right)\right.$$
$$(x_{h1}-x_{h2}) + \cos 2\theta_{\tilde{b}}\left(-\frac{5L^2_{hb}}{72} + \frac{L_{b\tilde{g}}}{24} + L_{12}\left(-\frac{L^2_{hb}}{24} + \frac{L_{b\tilde{g}}}{48} + \frac{29}{144}\right) - \frac{x_{21}}{1728} - \frac{\sqrt{x_{12}}}{432}\right.$$
$$-\frac{\sqrt{x_{21}}}{432} + \frac{11}{32} + \left(\frac{L^2_{hb}}{6} + L_{12}\left(\frac{L_{b\tilde{g}}}{24}+\frac{5}{72}\right)\right)x_{12} + x_{h1}\left(\frac{L^2_{hb}}{180} - \frac{L_{b\tilde{g}}}{288} + \frac{x_{h2}}{5040} - \frac{121}{4320}\right)$$
$$\left.\left.+\left(-\frac{L^2_{hb}}{45} + \frac{5L_{b\tilde{g}}}{288} + \frac{509}{4320}\right)x_{h2}\right)\right]\sqrt{x_{h\tilde{g}}}\right] + \mathcal{O}\left(x_{2\tilde{g}}x^{1/2}_{h\tilde{g}}, x_{1\tilde{g}}x^{1/2}_{h\tilde{g}}, x^{1/2}_{2\tilde{g}}x^{1/2}_{1\tilde{g}}x^{1/2}_{h\tilde{g}}\right),$$

$$\mathcal{H}^{(1)}_{2,\tilde{b}\tilde{g},2} = 1 - \frac{L_{2\tilde{g}}L^2_{hb}}{6} - \frac{L^2_{hb}}{4} + \frac{2L_{2\tilde{g}}}{3} + (1+\cos 2\theta_{\tilde{b}})L_{12}\left(\frac{1}{3} - \frac{L^2_{hb}}{12}\right)$$
$$+ \left[\frac{L_{b\tilde{g}}}{36} + \frac{1}{24}\right]x_{h\tilde{g}} + \mathcal{O}\left(x^2_{h\tilde{g}}, x^2_{2\tilde{g}}, x^2_{1\tilde{g}}\right),$$

$$\mathcal{H}^{(1)}_{3,\tilde{b}\tilde{g},0} = \cos 2\theta_{\tilde{b}} \left[\left(\left(-\frac{L_{12}}{72} - \frac{1}{36} \right) \sin^2 2\theta_{\tilde{b}} - \frac{L_{1\tilde{g}}}{36} + \frac{37}{144} \right) x_{\tilde{g}1} + \left(\left(\frac{1}{36} - \frac{L_{12}}{72} \right) \sin^2 2\theta_{\tilde{b}} + \frac{L_{2\tilde{g}}}{36} - \frac{37}{144} \right) x_{\tilde{g}2} + \frac{17L_{12}}{144} - \frac{17x_{h1}}{864} + \frac{17x_{h2}}{864} + \frac{x_{2\tilde{g}}}{216} - \frac{x_{1\tilde{g}}}{216} \right] + \mathcal{O}\left(x^2_{2\tilde{g}}, x^2_{1\tilde{g}}\right),$$

$$\begin{aligned}\mathcal{H}^{(1)}_{3,\tilde{b}\tilde{g},1} = \sin 2\theta_{\tilde{b}} \cos 2\theta_{\tilde{b}} \Bigg[& \sqrt{x_{\tilde{g}1}}\sqrt{x_{h1}} \left(\frac{L^2_{hb}}{36} - \frac{7}{72} - \frac{x_{h2}}{135} \right) + \sqrt{x_{\tilde{g}2}} \left(\sqrt{x_{h2}} \left(\frac{41}{72} - \frac{5L^2_{hb}}{36} \right) + \frac{\sqrt{x_{h1}}}{36} \right) + \left(-\frac{L^2_{hb}}{3} + L_{12} \left(\frac{2}{3} - \frac{L^2_{hb}}{6} \right) + \frac{4}{3} \right) \sqrt{x_{\tilde{g}h}} + \sqrt{x_{h\tilde{g}}} \left[\frac{5L^2_{hb}}{36} - \frac{L_{b\tilde{g}}}{12} + L_{12} \left(\frac{L^2_{hb}}{12} - \frac{L_{b\tilde{g}}}{24} - \frac{29}{72} \right) + \frac{x_{21}}{864} + \frac{\sqrt{x_{12}}}{216} + \frac{\sqrt{x_{21}}}{216} - \frac{11}{16} + \left(-\frac{L^2_{hb}}{3} + L_{12} \left(-\frac{L_{b\tilde{g}}}{12} - \frac{5}{36} \right) + \frac{1153}{864} \right) x_{12} + \left(-\frac{L^2_{hb}}{90} + \frac{L_{b\tilde{g}}}{144} + \frac{121}{2160} \right) x_{h1} + \left(\frac{2L^2_{hb}}{45} - \frac{5L_{b\tilde{g}}}{144} - \frac{x_{h1}}{2520} - \frac{509}{2160} \right) x_{h2} \right] + \left[\frac{2}{3} - \frac{L^2_{hb}}{6} + \left(-\frac{L^2_{hb}}{6} + L_{12} \left(\frac{4}{3} - \frac{L^2_{hb}}{3} \right) + \frac{2}{3} \right) x_{12} \right] \sqrt{x_{2h}}\sqrt{x_{2\tilde{g}}} \Bigg] \\ & + \mathcal{O}\left(x_{2\tilde{g}} x^{1/2}_{h\tilde{g}}, x_{1\tilde{g}} x^{1/2}_{h\tilde{g}}, x^{1/2}_{h\tilde{g}} x^{1/2}_{1\tilde{g}} x^{1/2}_{2\tilde{g}} \right),\end{aligned}$$

$$\mathcal{H}^{(1)}_{3,\tilde{b}\tilde{g},2} = \cos 2\theta_{\tilde{b}} \left[L_{12} \left(\frac{L^2_{hb}}{6} - \frac{2}{3} \right) + \left(-\frac{L^2_{hb}}{36} - \frac{L_{b\tilde{g}}}{36} + \frac{1}{9} \right) x_{h1} + \left(\frac{L^2_{hb}}{36} + \frac{L_{b\tilde{g}}}{36} - \frac{1}{9} \right) x_{h2} \right] + \mathcal{O}\left(x_{2\tilde{g}}, x_{2\tilde{g}}\right).$$

7.6. Results for the Virtual Two-Loop Contributions to the Amplitude

In this section, we compare our results with Ref. [46], where the virtual parts of the NLO-SQCD amplitude for the process $gg \to h$ were examined. There, the result for the two-loop virtual contributions to the amplitude that only contains effects from tops/stops/gluinos (no bottom) is compared to the entire SQCD effects that include bottoms/sbottoms/gluinos in addition to the top sector. The result presented in [46] is a complete one in the sense that novel numerical methods were applied and a general result with no approximations was obtained. The variation of the virtual parts of the two-loop amplitude that contains the QCD parts as well as the SUSY parts with respect to the leading order is examined in Ref. [46]. This is done by means of the K-factor that is the ratio of the squared amplitude through $\mathcal{O}(\alpha_s^3)$ divided by the result to $\mathcal{O}(\alpha_s^2)$.

In order to perform the comparison with the publication, we take the parameters chosen there. They are given by

$$\begin{aligned} &m_h = 115 \text{ GeV},\ m_b = 5 \text{ GeV},\ m_t = 172.4 \text{ GeV}, m_{\tilde{t}_1} = 150 \text{ GeV}, m_{\tilde{b}_1} = 350 \text{ GeV}, \\ &m_{\tilde{t}_2} = 370 \text{ GeV}, m_{\tilde{g}} = 500 \text{ GeV},\ q_0 = 200 \text{ GeV}, \alpha = 3°,\ \theta_{\tilde{t}} = 40°,\ \theta_{\tilde{b}} = 40°, \\ &\tan\beta = 20,\ \mu_{susy} = 300 \text{ GeV},\ \mu_R = m_h,\ \alpha_s^{\overline{MS}}(M_Z) = 0.1176. \end{aligned} \tag{7.15}$$

In all the plots the results are taken in terms of $\alpha_s^{\overline{MS}}$. The conversion between $\alpha_s^{\overline{DR}}$ and $\alpha_s^{\overline{MS}}$ was given in Eq. (6.20). We take the two-loop virtual QCD contributions from [76]. With the help of the `mathematica` package `HPL` [106] the harmonic poly logarithms that occur in the QCD result are evaluated numerically.

As our result is limited by the assumption of the hierarchies among the various SUSY mass scales we compare various limits with different mass hierarchies.

We include the bottom result in the limiting cases given by

(B2m) $m_b \ll M_s \equiv m_{\tilde{b}_1} = m_{\tilde{b}_2} = m_{\tilde{g}}$ with $M_s = 500$ GeV.

(B3m) $m_b \ll m_{\tilde{b}_1} \ll m_{\tilde{b}_2} = m_{\tilde{g}}$ with $m_{\tilde{b}_1} = 360$ GeV and $m_{\tilde{g}} = 500$ GeV.

(B3m') $m_b \ll m_{\tilde{b}_1} = m_{\tilde{b}_2} \ll m_{\tilde{g}}$ with $m_{\tilde{b}_1} = 360$ GeV and $m_{\tilde{g}} = 500$ GeV.

(B4m) $m_b \ll m_{\tilde{b}_1} \ll m_{\tilde{b}_2} \ll m_{\tilde{g}}$ with the masses as in Eq. (7.15).

The parameters not mentioned are chosen as in Eq. (7.15). In spite that in [46] the lighter stop mass is taken to be lighter than the top mass we take the four mass case, where (T4m) $m_t \ll m_{\tilde{t}_1} \ll m_{\tilde{t}_2} \ll m_{\tilde{g}}$ into the calculation for the K-factors. We display our results for two light squark masses, i.e., for $m_{\tilde{t}_1} = 150$ GeV and $m_{\tilde{t}_1} = 190$ GeV. Once $m_{\tilde{t}_2}$ becomes larger than the gluino mass, the radius of convergence is left for (T4m).

In Fig. 7.13 we compare our results displayed in Fig. 7.13(b) for the virtual contributions to the K-factor in dependence of $m_{\tilde{t}_2}$ to Fig. 7.13(a) from Ref. [46]. In both diagrams the constant QCD K-factors are shown in green. The top-sector contributions to the K-factor are given by the brown/yellow curves. They are of similar size. Fig. 7.13(a) displays the visible effects of the bottom sector on the K-factors of the virtual parts of the amplitude compared to the top sector. Only for the case (B3m') the K-factor including the bottom sector is larger than the result for the top sector. For $gg \to h$ we find for the $\mathcal{O}(\alpha_s^3)$ contributions of the squared SQCD amplitudes that they decrease with growing $m_{\tilde{t}_2}$. This is due to cancellations between diagrams where a top or light stop couple to the Higgs boson [46]. The $\mathcal{O}(\alpha_s^3)$ contribution ranges from 15% to -40% in [46] and for our squared amplitudes from 10% to 18% to about (-33)% to (-15)% depending on the curve we consider. They become negative for large $m_{\tilde{t}_2}$.

Whereas in [46] the effects of the bottom sector is below 3% the effects we obtain contributions up to 14% depending on which limiting case we include for the bottom sector. To

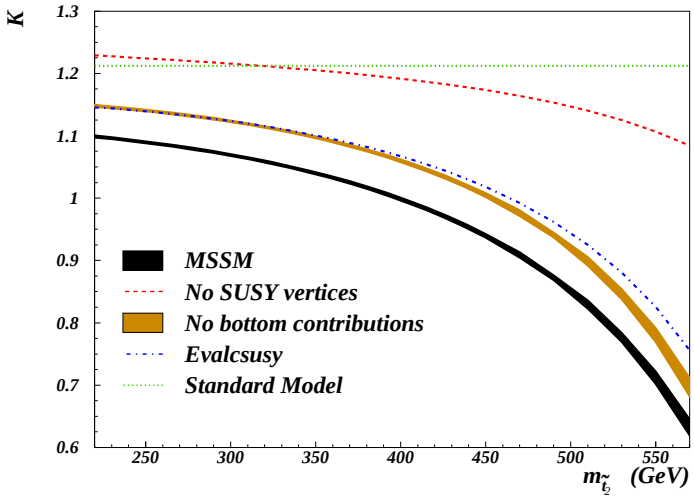

(a) Taken from [46].

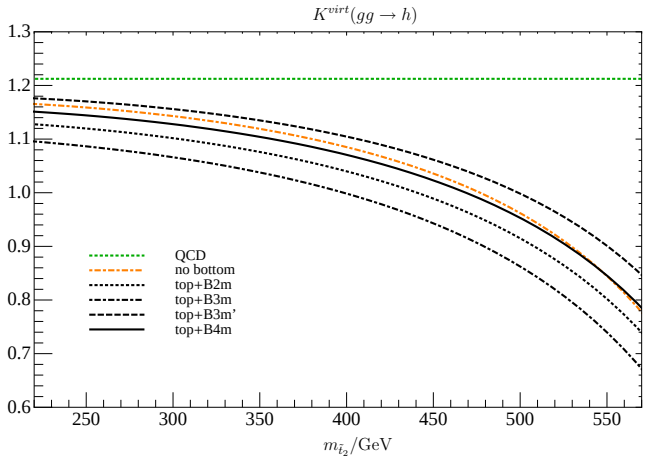

(b) Our result.

Figure 7.13.: *K-factors of the virtual parts of the amplitude in NLO-(S)QCD for the process $gg \to h$ in dependence of $m_{\tilde{t}_2}$. (a) The green (dotted) QCD result is compared to the K-factors that only contains the top sector (no bottoms, solid brown) with the entire SQCD contributions (black). Taken from [46]. (b) Comparison with our result where we give the QCD result (dotted green), only the top sector contributions (dashed-dotted yellow) and in black the whole SQCD K-factor in various limits. For the entire SQCD results we distinguish four cases (B2m, dotted), (B3m, dashed-dotted), (B3m', dashed), (B4m, solid). The corresponding choice of mass parameters is given in the text.*

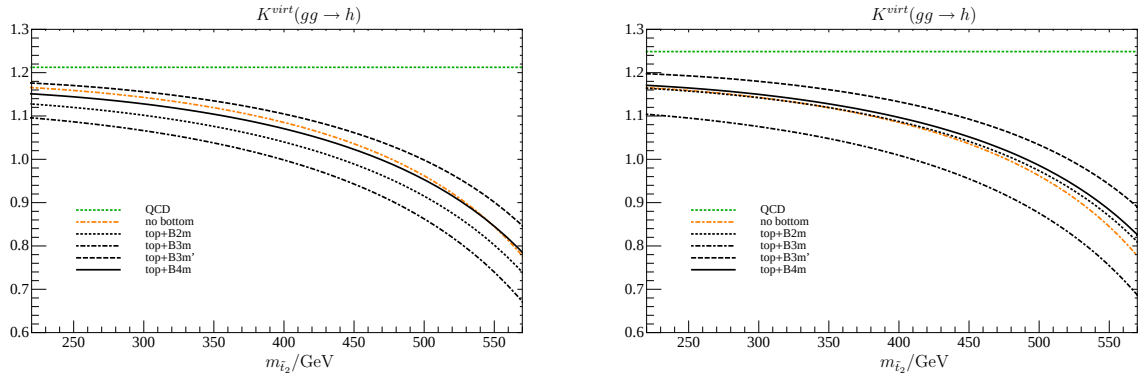

Figure 7.14.: *K-factors of the virtual parts of the squared amplitude in NLO-(S)QCD for the process $gg \to h$ in dependence of $m_{\tilde{t}_2}$. $m_{\tilde{t}_1} = 150$ GeV. In green we give the SM result (dotted), in yellow only the top contributions (dashed-dotted) are included and in black the whole MSSM result is given. For the MSSM results we distinguish four cases (B2m, dotted), (B3m, dashed-dotted), (B3m', dashed), (B4m, solid). (a) $m_b = 5$ GeV (b) running bottom mass.*

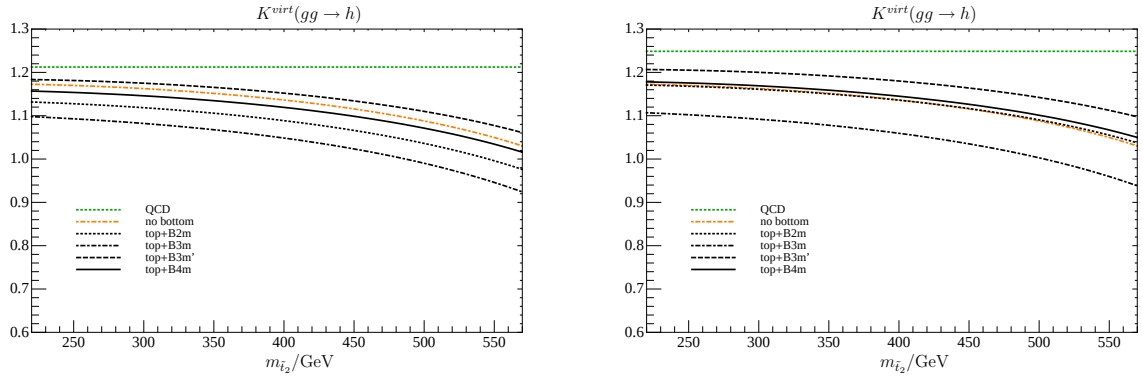

Figure 7.15.: *Same as Fig. 7.14 but with $m_{\tilde{t}_1} = 190$ GeV.*

specify this further, the effects of the bottom sector compared with the top sector are up to 5% for (B2m), 14% for (B3m), 8% for (B3m') and 1% for (B4m). It seems that for this choice of parameters, the cases (B2m) and (B4m) agree best with the publication.

In Fig. 7.14(a) we again display Fig. 7.13(b) where the bottom mass was taken to be 5 GeV and compare it to Fig. 7.14(b) where all the bottom masses are taken to be running ones. We observe that the K factors slightly increase for running bottom masses compared to the assumption of a fixed bottom mass. The effects of the bottom sector compared with the top sector change for running bottom masses and are up to 4% for (B2m), 12% for (B3m), 13% for (B3m') and 6% for (B4m). For (B3m') and (B4m) an enhancement of the bottom/sbottom effects is observed by taking a running bottom mass.

As argued above, the very light stop mass does not suit our limiting case very well. Therefore, we show Fig. 7.15 where the same is illustrated as in Fig. 7.14 but with $m_{\tilde{t}_1} = 190$ GeV. We find that towards lower $m_{\tilde{t}_2}$ the spectrum is practically identical to the one for $m_{\tilde{t}_1} = 150$ GeV but for larger $m_{\tilde{t}_2}$ the curves for the K-factor are a lot flatter than before the $\mathcal{O}(\alpha_s^3)$ contribution only ranges from 18% to -8%. Compared to the top sector the effects of the bottom sector for an on-shell (running) bottom mass amount to about 5% (1%) for (B2m), 10% (9%) for (B3m), 3% (6%) for (B3m') and 2% (2%) for (B4m).

Additionally, the results for the K-factors are examined in the SPS 1a benchmark scenario with the choice of parameters as in Sec. 6.9.2. The squared virtual parts of the amplitude are only a part of the entire NLO-SQCD result. Therefore, this study is performed to obtain an impression of the size of the corrections. In the SPS 1a scenario $\tan\beta = 10$.

In Fig. 7.16 we investigate the $\mathcal{O}(\alpha_s^3)$ effects of the squared (S)QCD amplitude in dependence of $m_{1/2}$. We display the QCD, the top sector (w/o bottoms), the QCD plus contributions (w/o sbottoms), the QCD plus stop and LO sbottom contributions (w LO sbottom) and the entire SQCD K-factors. It can be read off from Fig. 7.16(a) that the effects to the $\mathcal{O}(\alpha_s^3)$ squared amplitude amount to about 1% if in addition to the top sector only the pure bottom parts are included. Including the LO sbottom effects in addition does not lead to a visible effect in the diagram. Further taking into account the two-loop sbottom effects to obtain the entire SQCD virtual contributions to the two-loop amplitude makes up for corrections below one percent. In total, the effect of the bottom sector is below 2% for the virtual contributions.

We compare Fig. 7.16(a) where we take an on-shell bottom mass to Fig. 7.16(b) where all bottom masses are taken to be running ones. Since the SPS 1a scenario along the slope of $m_{1/2}$ suits our limiting cases (B4m) and (T4m) we observe the expected better convergence for taking a running bottom mass because the K-factors decrease in that case compared to taking an on-shell bottom mass. In case we take the bottom masses to be running (on-shell) the effects to the $\mathcal{O}(\alpha_s^3)$ squared amplitude if one includes in addition to the top sector only the pure bottom contributions amount to about 2% (1%). Further, including the LO sbottom effects in addition amounts to contributions below one percent. Therefore, the effect from sbottoms is entirely due to the NLO sbottom contributions which deviate

up to 1% (1%) from the bottom result. Taking all the bottom/sbottom effects into account as well in the end only amounts to corrections of up to 1% (2%) in addition to the top sector.

In Fig. 7.17 we compare the K-factors where we take the limit (B4m) with (B3m'). Setting the sbottom masses to their arithmetic mean in the SPS 1a scenario seems to be a valid assumption since the mass difference between the sbottoms is at most 40 GeV for the mass range of $m_{1/2}$ we chose. Their difference amounts to about 1% towards higher $m_{1/2}$ where the splitting between the sbottoms gets larger.

Next, the K-factors of the virtual squared amplitudes for the process $gg \to A$ are examined. In Fig. 7.18 we take the same parameters as given in Eq. (7.15) and in addition set the pseudoscalar Higgs mass to $m_A = 200$ GeV. For the production of pseudoscalar Higgs bosons in the gluon fusion process, the effects of sbottoms are pure NLO effects. That is why, for the pseudoscalar case, the K-factors of the virtual contributions to the two-loop amplitude without sbottom effects are compared to the ones including the sbottom effects. We observe in Fig. 7.18 that the pure sbottom effects of the K-factor for our choice of $\tan\beta = 20$ and $m_A = 200$ GeV are large. Compared to the K-factor that includes the top sector as well as the bottom effects, the sbottom effects amount to 30% for (B2m), 11% for (B3m), 17% for (B3m') and 32% for (B4m). Taking $m_{\tilde{t}_1} = 190$ GeV instead of $m_{\tilde{t}_1} = 150$ GeV does not change the size of the relative effects. For this choice of parameters the effects from stops only account for up to 4% compared to the QCD K-factor for the virtual effects.

In the SPS 1a scenario examined in Fig. 7.19 the effects to the $\mathcal{O}(\alpha_s^3)$ squared amplitude are shown in dependence of $m_{1/2}$. The diagrams display the threshold ($m_A = 2m_t$) for $m_{1/2} \approx 220$ GeV. We display the K-factors for the QCD effects, the top sector (w/o bottom), the contributions without any sbottom effects (w/o sbottoms) and the entire SQCD virtual effects. The K-factors displayed are for an on-shell bottom mass since the effects of a running bottom mass are small in that case. We find that the two-loop sbottom effects for an on-shell bottom mass amount to about 30% compared to the K-factor without sbottom effects for the given mass range. Here, the stop effects amount to about 15% compared to the K-factor that only contains the QCD effects.

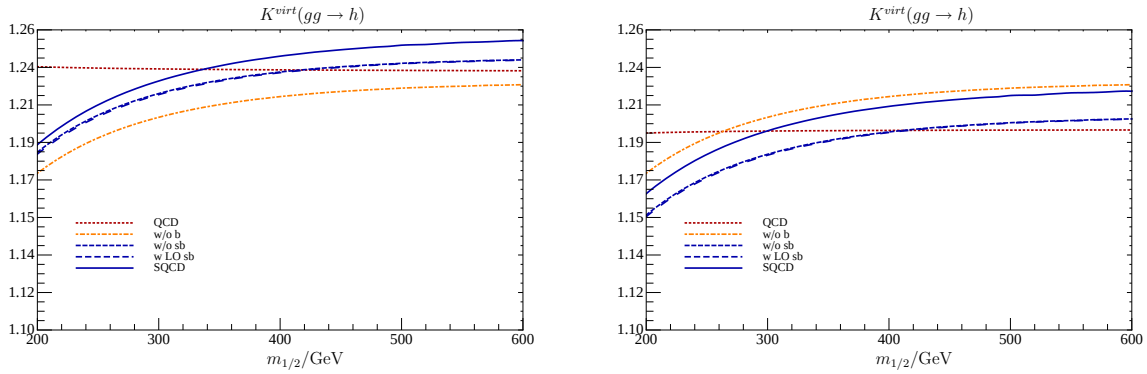

(a) (b)

Figure 7.16.: *K-factors of the virtual parts of the squared amplitude in NLO-(S)QCD for the process $gg \to h$ in dependence of $m_{1/2}$ along the slope of SPS 1a. As a reference, the dotted (red) line displays the SM K-factor. The dashed-dotted curve (yellow) depicts the K-factor for only the top and stop contributions, the dashed (blue) curve includes the bottoms as well, the long-dashed (blue) curve in addition includes the LO sbottom effects and finally the solid (blue) curve is the complete MSSM result. (a) $m_b = 5$ GeV (b) running bottom masses.*

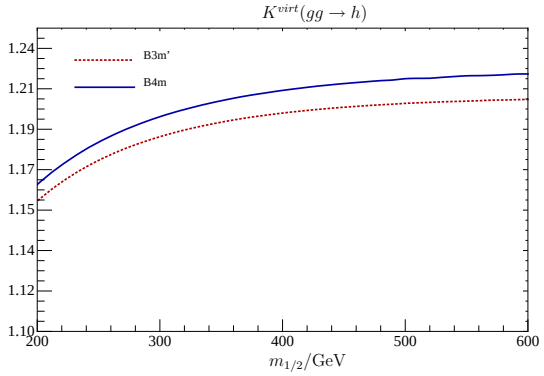

(a)

Figure 7.17.: *K-factors of the virtual parts of the squared amplitude in NLO-(S)QCD for the process $gg \to h$ in dependence of $m_{1/2}$ along the slope of SPS 1a. The MSSM K-factors are shown for setting the two sbottom masses equal (dotted red) vs. the case where the sbottom masses are taken unequal (solid-blue). In these plots, the bottom masses are taken to be running ones.*

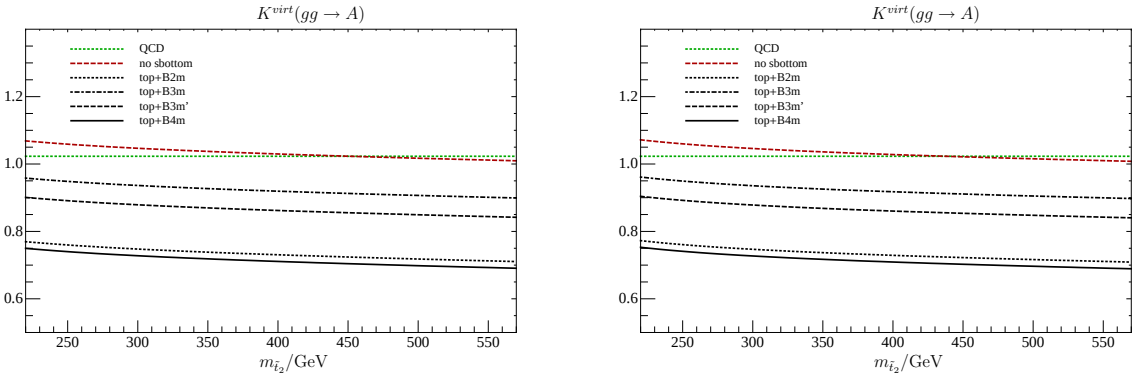

(a) (b)

Figure 7.18.: *K-factors of the virtual parts of the amplitude in NLO-(S)QCD for the process $gg \to A$ in dependence of $m_{\tilde{t}_2}$. The green (dotted) QCD result is compared to the K-factors that contain the top sector and bottom effects (no sbottom, dotted red) with the entire SQCD contributions (black). For the entire SQCD results we distinguish four cases (B2m, dotted), (B3m, dashed-dotted), (B3m', dashed), (B4m, solid). The corresponding choice of mass parameters given in the text. We chose $m_A = 200$ GeV and $\tan\beta = 20$. (a) $m_{\tilde{t}_1} = 150$ GeV (b) $m_{\tilde{t}_1} = 190$ GeV.*

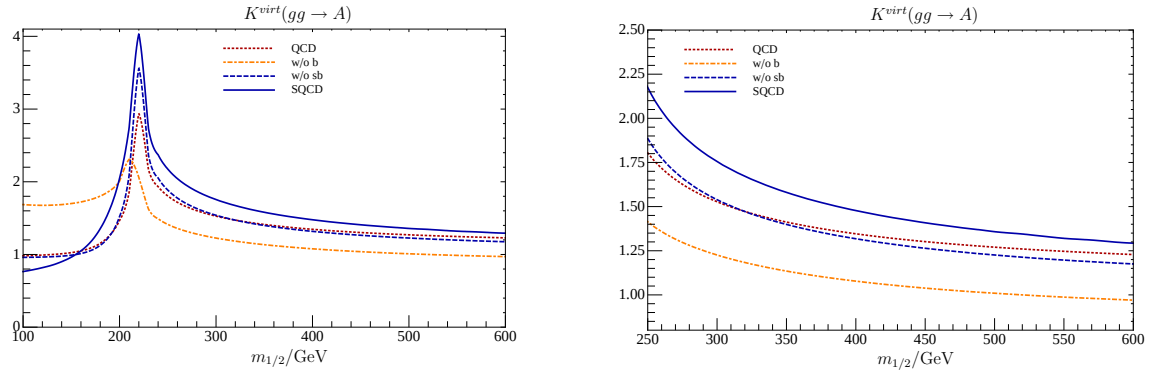

(a) (b)

Figure 7.19.: *K-factors of the virtual parts of the amplitude in NLO for the process $gg \to A$ in dependence of $m_{1/2}$ along the slope of SPS 1a for $m_b = 5$ GeV. The dotted (red) line is the QCD result, the dashed-dotted curve (yellow) depicts the K-factor for only the top and stop contributions, the dashed (blue) curve includes the bottoms as well and finally the solid (blue) curve is the complete MSSM result. (a) Including the threshold (b) zoom above the threshold.*

7.7. The Cross Section in NLO-SQCD for $gg \to \phi$

The partonic cross sections to lowest order in the production of scalar and pseudoscalar Higgs bosons via the gluon fusion read [81]

$$\begin{aligned}
\hat{\sigma}^{\phi}_{LO}\left(gg \to \phi\right) &= \sigma^{\phi}_{o}\delta\left(1-z\right), \\
\sigma^{\phi}_{o} &= \frac{\pi^2}{8m^3_{\phi}}\Gamma_{LO}\left(\phi \to gg\right) \\
\sigma^{h}_{o} &= \frac{G_F\alpha^2_s(\mu_R)}{288\sqrt{2}\pi}\left|\sum_{Q=t,b} g^h_Q H_Q\left(\tau_Q\right) + \sum_{\tilde{Q}=\tilde{t}_1,\tilde{t}_2,\tilde{b}_1,\tilde{b}_2} g^h_{\tilde{Q}} H_{\tilde{Q}}\left(\tau_{\tilde{Q}}\right)\right|^2 \\
\sigma^{A}_{o} &= \frac{G_F\alpha^2_s(\mu_R)}{128\sqrt{2}\pi}\left|\sum_{Q=t,b} g^A_Q A_Q\left(\tau_Q\right)\right|^2,
\end{aligned}$$

where $z = m^2_{\phi}/\hat{s}$ with the partonic center of mass energy squared $\hat{s}$ and $\tau_i = 4m^2_i/m^2_{\phi}$.
The form factors are given by

$$\begin{aligned}
H_Q\left(\tau\right) &= \frac{3}{2}\tau\left[1+\left(1-\tau\right)f(\tau)\right], \\
H_{\tilde{Q}}\left(\tau\right) &= -\frac{3}{4}\tau\left[1-\tau f(\tau)\right], \\
A_Q\left(\tau\right) &= \tau f(\tau).
\end{aligned}$$

The function f has the shape

$$f(\tau) = \begin{cases} \arcsin^2\frac{1}{\sqrt{\tau}} & , \ \tau \geq 1 \\ -\frac{1}{4}\left(\ln\frac{1+\sqrt{1-\tau}}{1-\sqrt{1-\tau}} - i\pi\right)^2 & , \ \tau < 1. \end{cases}$$

The next-to-leading order corrections to the $gg \to \phi$ process consist of virtual and real corrections.
The inclusive NLO hadronic cross section can be written as [29, 81]

$$\sigma(pp \to \phi + X) = \sigma^{\phi}_0\left[1 + C^{\phi}\frac{\alpha_s}{\pi}\right]\tau_{\phi}\frac{d\mathcal{L}^{gg}}{d\tau_{\phi}} + \Delta\sigma^{\phi}_{gg} + \Delta\sigma^{\phi}_{gq} + \Delta\sigma^{\phi}_{q\bar{q}},$$

where $\tau_{\phi} = m^2_{\phi}/s$ with the total center of mass energy squared s. The gluon luminosity is defined by

$$\frac{d\mathcal{L}^{gg}}{d\tau} = \int_{\tau}^{1}\frac{dx}{x}g(x,\mu_F)g(\tau/x,\mu_F)$$

with the gluon density $g(x,\mu_F)$. The renormalization scale μ_R of the strong coupling $\alpha_s(\mu_R)$ and the factorization scale μ_F of the parton densities are given by the Higgs mass

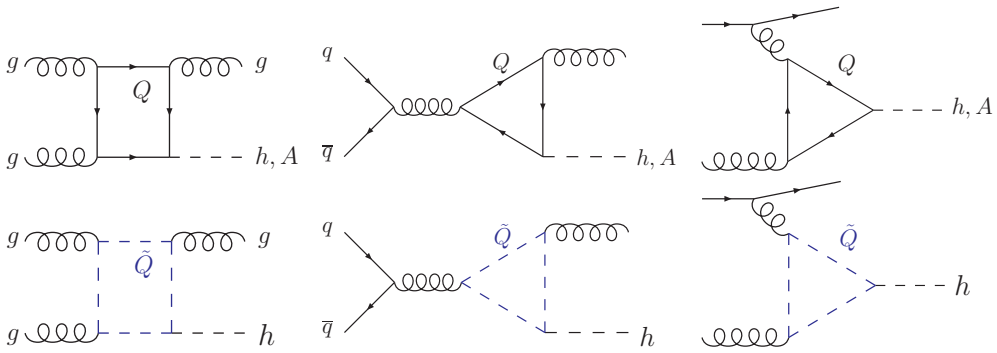

Figure 7.20.: *Typical diagrams for the real corrections to $gg \to \phi$.*

m_ϕ. $\Delta\sigma_{ij}^{\phi}$ are contributions from radiation of quarks and gluons with massless initial state partons $(i, j = g, q, \overline{q})$ corresponding to the subprocesses $gg \to \phi g$, $gq \to \phi q$ and $q\overline{q} \to \phi g$ (cf. Fig. 7.20).

In NLO-SQCD, the coefficients C^ϕ denote contributions from virtual two-loop corrections that depend on

$$C^\phi = C^\phi(m_\phi, m_b, m_t, m_{\tilde{t}_1}, m_{\tilde{t}_2}, m_{\tilde{b}_1}, m_{\tilde{b}_2}, m_{\tilde{g}}).$$

For the production of pseudoscalar Higgs bosons, the virtual corrections consist of the two-loop contributions to the amplitude that contain pure quark effects and mixed quark-squark-gluino effects.

The production of scalar Higgs bosons in addition contains pure squark effects. For the scalar Higgs production in the gluon fusion process, we calculated the virtual two-loop contributions from supersymmetric particles. The program `HIGLU` [104] provides for the final cross sections for the NLO-QCD contributions. In order to obtain the entire cross section we lack the interference term of the real corrections from quarks with the real corrections from squarks that are displayed in Fig. 7.20. These do not exist in the pseudoscalar Higgs production via the gluon fusion process.

In the following we examine the sbottom effects on the cross section for the production of pseudoscalar Higgs bosons. The integration over the parton distribution functions is performed with the help of `ggh@nnlo` [107]. For the purpose of obtaining an estimate of the sbottom effects on the cross section, the top sector is included in the effective theory (cf. [60]). In addition, our newly obtained two-loop bottom-sbottom-gluino effects are included as well. The latter are the only effects from sbottoms that occur in NLO-SQCD.

The numerical results for the cross section are evaluated graphically in the SPS 1a benchmark-scenario that has been introduced in Sec. 6.9.2, where $\tan\beta = 10$. The two-loop sbottom effects are included in the limit where $m_b \ll m_{\tilde{b}_1} \ll m_{\tilde{b}_2} \ll m_{\tilde{g}}$. The size of the newly obtained sbottom effects on the hadronic cross section is investigated. We only investigate the effects of the sbottoms qualitatively since we do not include the NLO

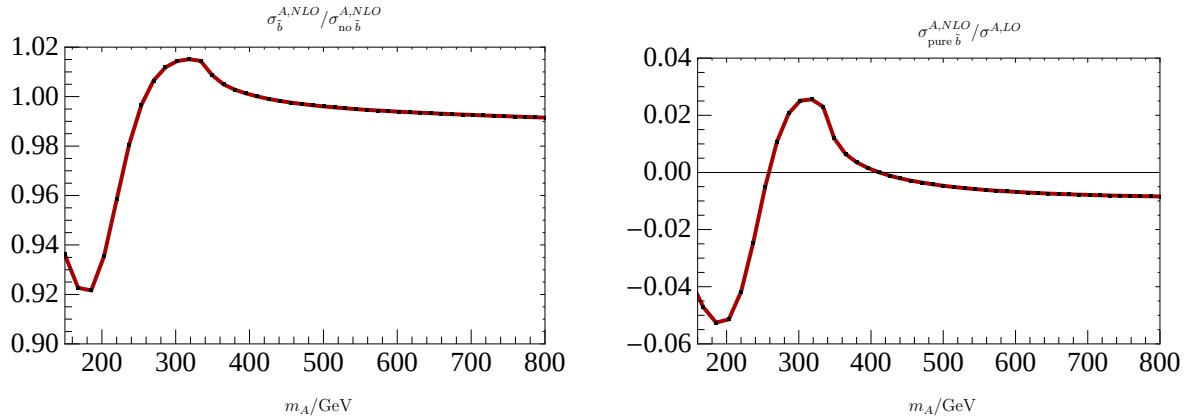

(a) (b)

Figure 7.21.: *(a) This figure displays the ratio of the NLO cross section including the sbottom effects over the cross section without the sbottom effects in dependence of m_A. The effect is thus the share of the sbottom parts to the cross section that includes the NLO top and stop effects. (b) The percentaged fraction of the pure NLO sbottom effects with respect to the LO is shown.*

bottom effects into the calculation.

In order to obtain an estimate of the size of the corrections on the cross section due to sbottoms we display the ratio of the cross section including the sbottom effects over the cross section without sbottom contributions in dependence of m_A in Fig. 7.21(a). The black dots mark the actual data points that we extrapolate in between under the assumption that the curves are smooth. Below the threshold the absolute value of the effects due to sbottoms amount to about 8%. For Higgs masses larger than about 350 GeV the effects from sbottoms on the cross section only amount to about one percent in comparison with the effects without sbottoms. Since the presented NLO hadronic cross sections were obtained for a running bottom mass, we can only qualitatively estimate the effect of the NLO bottom contributions the program `HIGLU` [104] contains. There, the bottom mass is set to its on-shell value. By qualitatively including the NLO bottom effects to the cross section from `HIGLU`, we find that then the pure sbottom effects only contribute approximately one percent to the NLO cross section over the entire mass range of the pseudoscalar Higgs boson displayed in Fig. 7.21(a). In Fig. 7.21(b) the pure NLO sbottom effects are compared to the full LO cross section and the result is that their size amounts up to 5% of the LO.

For comparing the effects of the sbottoms with the stop contributions, Fig. 7.22 is displayed. In order to obtain an estimate of the absolute value of the corrections on the cross section due to stops we show the ratio of the cross section including the stop effects over the cross section without stop contributions in dependence of m_A in Fig. 7.22(a). Below the threshold, the absolute value of the effects due to sbottoms amount up to 17%. Above

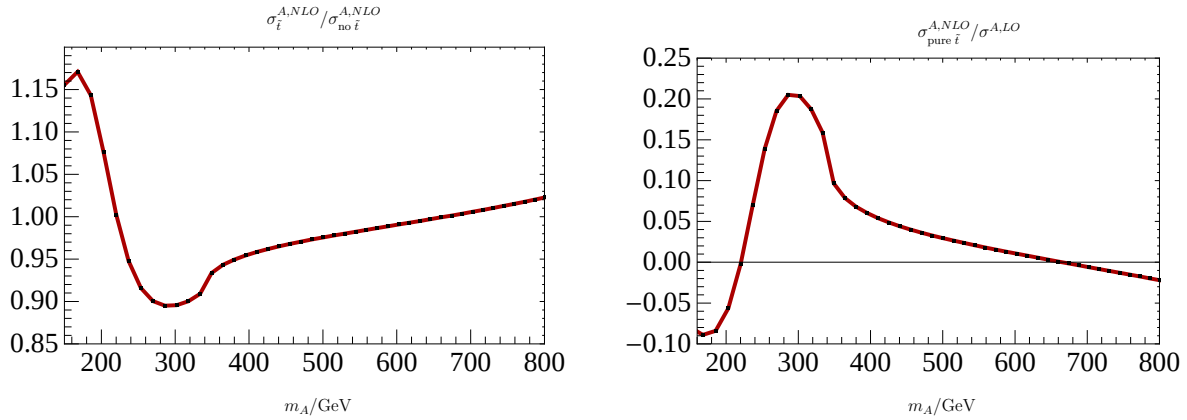

(a) (b)

Figure 7.22.: *(a) This figure displays the ratio of the NLO cross section including the stop effects over the cross section without the stop effects in dependence of m_A. The effect is thus the share of the stop contributions to the cross section that includes the NLO stop effects. (b) The percentaged fraction of the pure NLO stop effects with respect to the LO is displayed.*

the threshold they are up to 5%. By qualitatively including the NLO bottom effects, the pure stop effects only amount to about 7% on the NLO cross section that includes two-loop top as well as bottom effects. In Fig. 7.22(b) the pure NLO stop effects are compared to the entire LO. Their size amounts to about 20% of the LO.

In this estimate of the production cross section of pseudoscalar Higgs bosons in the gluon fusion process, the stop effects are dominant over the sbottom effects. In comparison with the leading order cross section, the stop effects are about a factor of four larger than the sbottom effects. Of course what remains to be done is the inclusion of the NLO bottom effects to obtain the complete NLO-SQCD cross sections.

Chapter 8
8 Conclusions and Outlook

In the present thesis, the influence of the bottom sector on the production of scalar and pseudoscalar Higgs bosons via the gluon fusion process in the framework of the MSSM has been investigated. In addition, we examined the decay of scalar and pseudoscalar Higgs bosons into two photons. For both, the production and the decay of these Higgs bosons, the virtual NLO-SQCD corrections were obtained in the framework of the MSSM. Already at leading order, the processes are at the one-loop level as massive Higgs bosons do not couple to massless gluons or photons directly. Therefore, the next-to-leading order calculation corresponds to the evaluation of up to two-loop Feynman diagrams.

In QCD the top quark provides the dominant contribution to these processes. Within the framework of the MSSM however, the couplings of quarks to Higgs bosons are modified by factors of $\tan\beta$ which can lead to an enhancement of the contributions from bottom quarks together with a suppression of the top contributions. Therefore, the bottom quark has to be considered in an MSSM calculation.

The transition from QCD to SQCD is performed by including the superpartners of the quarks, namely the squarks into the calculation. Each quark obtains two massive superpartners. At the two-loop level the massive superpartner of the gluon, the gluino also has to be taken into account. The contributions from top quarks and top squarks and the gluino were known in the limit of large top and SUSY masses where these were assumed to be much larger than the mass of the Higgs boson. For the calculation in the MSSM, in addition, contributions from the superpartners of the bottoms, the sbottoms, have to be accounted for.

In order to determine the two-loop contributions, the method of asymptotic expansions in various hierarchies among the up to four contributing mass scales (the quark mass, the two squark masses and the gluino mass) for the bottom as well as the top sector was applied. The assumption of the quark being heavier than the Higgs bosons is not valid for the bottom quark. To account for the effects of bottom quarks, one-loop routines were implemented which were applied to subdiagrams during the expansion of the two-loop diagrams.

For the decay of pseudoscalar Higgs bosons into two photons we find that the contributions from sbottoms have an impact on the partial decay widths for large $\tan\beta$. The finding is that the sbottoms may have an effect of up to 47% on the partial decay widths, depending on the limiting case and the value of $\tan\beta$. In evaluating the effects along the slope of the SPS 1a benchmark point, where $\tan\beta = 10$, the size of the sbottom effects amounts to 28%, which is comparable to the size of the stop effects.

Since commonly m_A and $\tan\beta$ are chosen to be the free parameters in the MSSM Higgs sector, the lightest scalar Higgs mass is not a free parameter and depends on the choice of m_A and $\tan\beta$. The partial decay widths for the photonic decay of scalar Higgs bosons were examined with the help of *FeynHiggs* [87] that provides for a loop corrected scalar Higgs mass. There, we found that the sbottom effects have a share of less than one percent on the NLO-SQCD decay width. Along the slope of the SPS 1a benchmark point we find that the sbottoms account for contributions of up to one percent on the NLO partial decay width. For this case, the newly obtained sbottom contributions are small and the effects of supersymmetric particles in that case are mainly due to stops.

Regarding the Higgs production via the gluon fusion mechanism the two-loop virtual effects of the bottom/sbottom contributions to the amplitude were investigated. For scalar Higgs bosons in the SPS 1a scenario these contributions are of the size of up to 2%. In case of the pseudoscalar Higgs bosons the virtual effects of sbottoms amount to approximately 30% and are dominant over the stop contributions. However, one has to keep in mind that the virtual effects of the two-loop amplitudes only provide for a first estimate of the size of the effects. These could be smaller once the real corrections to the process are included into the results.

Finally, the effects of the sbottoms on the hadronic cross section for the production of pseudoscalar Higgs bosons were estimated in the SPS 1a scenario. Without the inclusion of the NLO bottom effects, these extend to 8%. By including an estimate for the NLO bottom effects with the help of the publicly available program `HIGLU` [104], they drop to one percent. The stop effects that were included in the large top limit amount to about 17% and with the estimate of the NLO bottom effects to about 7%. In addition, we observed that the NLO sbottom effects on the hadronic cross section compared to the LO cross section are of up to 5% and the stop effects amount to 20%. In this case, the stop effects are dominant over the sbottom effects.

In case of the decay of scalar and pseudoscalar Higgs bosons into two photons we provided for the entire NLO-SQCD corrections to the partial decay widths. Additionally, we evaluated the two-loop SUSY contributions for the production of scalar and pseudoscalar Higgs bosons via the gluon fusion. For the pseudoscalar case, we estimated the sbottom contributions to the hadronic cross section. The results were obtained in various limiting cases that assumed different hierarchies among the contributing SUSY mass scales. In case the MSSM is the underlying model, one of these should always provide for a good approximation to reality.

As an outlook, it would be interesting to determine the NLO hadronic cross sections including the NLO bottom quarks and our newly obtained effects for both the scalar as well as pseudoscalar Higgs production. Since we provided for the two-loop effects from sbottoms in the Higgs production and decay, these can be included into existing programs for evaluating cross sections and decay rates.

It is important to dispose of predictions for cross sections and decay rates for the Higgs boson production and decay. If the Higgs is found at the LHC, these become precision observables with which one can investigate the SM and in case it exists, the MSSM more closely.

Finally, judging from the differences between leading-order predictions and our NLO results, we do not expect dramatic changes from NNLO corrections. Thus, we think that our results are entirely sufficient to support the ongoing search for supersymmetric particles. However, should experiments — at the LHC or elsewhere — find concrete evidence for the existence of SUSY particles, it would definitely make sense to extend our calculations to the next higher order.

A Appendix A

Couplings $h\tilde{q}\tilde{q}$ and $A\tilde{q}\tilde{q}$

The coupling of two squarks to the pseudoscalar Higgs boson , $\tilde{q}_i\tilde{q}_j A$, is proportional to [31]

$$i\frac{m_q}{v}g^A_{\tilde{q},ij} = i\frac{m_q}{v}\begin{pmatrix} 0 & -A_q\begin{Bmatrix}\cot\beta\\ \tan\beta\end{Bmatrix} - \mu_{susy} \\ A_q\begin{Bmatrix}\cot\beta\\ \tan\beta\end{Bmatrix} + \mu_{susy} & 0 \end{pmatrix}_{ij}. \tag{A.1}$$

It is the same for the mass and flavor eigenstates of the squarks as $(g^A_{\tilde{q}})_{ij}$ is an off-diagonal matrix and $\mathcal{R}$ in Eq. (A.4) is a unitary matrix. The upper entry in {} in Eq. (A.1) holds for the stop and the lower one for the sbottom. Furthermore, we have

$$A_q = \frac{m^2_{\tilde{q}_1} - m^2_{\tilde{q}_2}}{2m_q}\sin 2\theta_{\tilde{q}} + \mu_{susy}\begin{Bmatrix}\cot\beta\\ \tan\beta\end{Bmatrix}. \tag{A.2}$$

A_q is the trilinear coupling of the soft SUSY breaking terms.

The couplings of the CP-even, lightest Higgs boson h to two squarks can be obtained from [31] by expressing the terms in the chiral basis through the mass eigenstates. The $\tilde{q}_i\tilde{q}_j h$ coupling is proportional to [31]

$$i\frac{m_q^2}{v}g^h_{\tilde{q},ij} \equiv i\left[\mathcal{R}^{\tilde{q}}\hat{G}^{\tilde{q}}\left(\mathcal{R}^{\tilde{q}}\right)^T\right]_{ij}, \tag{A.3}$$

$$\mathcal{R}^{\tilde{q}} = \begin{pmatrix}\cos\theta_{\tilde{q}} & \sin\theta_{\tilde{q}} \\ -\sin\theta_{\tilde{q}} & \cos\theta_{\tilde{q}}\end{pmatrix}, \tag{A.4}$$

$$\hat{G}^{\tilde{q}} = \begin{pmatrix} \frac{2M_Z^2}{v}C_{qL}s_{\alpha+\beta} - 2m_q\tilde{h}_q\begin{Bmatrix}c_\alpha\\ -s_\alpha\end{Bmatrix} & -\tilde{h}_q\left(A_q\begin{Bmatrix}c_\alpha\\ -s_\alpha\end{Bmatrix} + \mu_{susy}\begin{Bmatrix}s_\alpha\\ -c_\alpha\end{Bmatrix}\right) \\ -\tilde{h}_q\left(A_q\begin{Bmatrix}c_\alpha\\ -s_\alpha\end{Bmatrix} + \mu_{susy}\begin{Bmatrix}s_\alpha\\ -c_\alpha\end{Bmatrix}\right) & \frac{2M_Z^2}{v}C_{qR}s_{\alpha+\beta} - 2m_q\tilde{h}_q\begin{Bmatrix}c_\alpha\\ -s_\alpha\end{Bmatrix}\end{pmatrix} \tag{A.5}$$

for $\left\{\begin{matrix}\text{up}\\\text{down}\end{matrix}\right\}$-type of the squarks. The following abbreviations are used $s_\alpha = \sin\alpha$, $c_\alpha = \cos\alpha$, $s_{\alpha+\beta} = \sin\alpha + \beta$, $C_{qL} = I_{3L}^q - Q_q \sin^2\theta_W$, $C_{qL} = Q_q \sin^2\theta_W$. The Yukawa-couplings are given by

$$\tilde{h}_t = \frac{m_t}{v\sin\beta}, \quad \tilde{h}_b = \frac{m_b}{v\cos\beta}. \tag{A.6}$$

Altogether in the notation of [82] the couplings of squarks to scalar Higgs bosons can be expressed by

$$\boxed{g_{\tilde{q},ij}^h = g_{\tilde{q},ij}^{h,\mu} + g_{\tilde{q},ij}^{h,ew} + g_{\tilde{q},ij}^{h,\alpha}.} \tag{A.7}$$

For the coupling of top squarks to scalar Higgs bosons find with the help of Eq. (A.3)

$$g_{\tilde{t},11}^{h,ew} = c_1^{ew}\cos^2\theta_{\tilde{t}} + c_2^{ew}\sin^2\theta_{\tilde{t}}, \tag{A.8}$$

with

$$c_1^{ew} = \left(\frac{M_Z}{m_t}\right)^2 \left(1 - \frac{4}{3}\sin^2\theta_W\right)\sin(\alpha+\beta) \tag{A.9}$$

and

$$c_2^{ew} = \left(\frac{M_Z}{m_t}\right)^2 \frac{4}{3}\sin^2\theta_W \sin(\alpha+\beta), \tag{A.10}$$

$$g_{\tilde{t},11}^{h,\mu} = -g_{\tilde{t},22}^{h,\mu} = -\frac{\mu_{susy}}{m_t}\sin(2\theta_{\tilde{t}})\frac{\cos(\alpha-\beta)}{\sin^2\beta}, \tag{A.11}$$

$$g_{\tilde{t},11}^{h,\alpha} = -\frac{\cos\alpha}{\sin\beta}\left(2 + \frac{1}{2}\frac{\left(m_{\tilde{t}_1}^2 - m_{\tilde{t}_2}^2\right)}{m_t^2}\sin^2(2\theta_{\tilde{t}})\right), \tag{A.12}$$

$$g_{\tilde{t},22}^{h,ew} = c_1^{ew}\sin^2\theta_{\tilde{t}} + c_2^{ew}\cos^2\theta_{\tilde{t}}, \tag{A.13}$$

$$g_{\tilde{t},22}^{h,\alpha} = -\frac{\cos\alpha}{\sin\beta}\left(2 - \frac{1}{2}\frac{\left(m_{\tilde{t}_1}^2 - m_{\tilde{t}_2}^2\right)}{m_t^2}\sin^2(2\theta_{\tilde{t}})\right), \tag{A.14}$$

$$g_{\tilde{t},12}^h = g_{\tilde{t},21}^h, \tag{A.15}$$

$$g_{\tilde{t},12}^{h,ew} = \frac{1}{2}(c_2^{ew} - c_1^{ew})\sin(2\theta_{\tilde{t}}), \tag{A.16}$$

$$g_{\tilde{t},12}^{h,\mu} = -\frac{\mu_{susy}}{m_t}\cos(2\theta_{\tilde{t}})\frac{\cos(\alpha-\beta)}{\sin^2\beta}, \tag{A.17}$$

$$g^{h,\alpha}_{\tilde{t},12} = -\frac{\cos\alpha}{\sin\beta}\frac{\left(m^2_{\tilde{t}_1} - m^2_{\tilde{t}_2}\right)}{2m^2_t}\sin\left(2\theta_{\tilde{t}}\right)\cos\left(2\theta_{\tilde{t}}\right). \tag{A.18}$$

For the coupling of sbottoms to h we obtain

$$g^{h,ew}_{\tilde{b},11} = c^{ew}_1\cos^2\theta_{\tilde{b}} + c^{ew}_2\sin^2\theta_{\tilde{b}}, \tag{A.19}$$

with

$$c^{ew}_1 = \left(\frac{M_Z}{m_b}\right)^2\left(-1 + \frac{2}{3}\sin^2\theta_W\right)\sin\left(\alpha+\beta\right) \tag{A.20}$$

and

$$c^{ew}_2 = -\left(\frac{M_Z}{m_b}\right)^2\frac{2}{3}\sin^2\theta_W\sin\left(\alpha+\beta\right), \tag{A.21}$$

$$g^{h,\mu}_{\tilde{b},11} = -g^{h,\mu}_{\tilde{t},22} = \frac{\mu_{susy}}{m_b}\sin\left(2\theta_{\tilde{b}}\right)\frac{\cos\left(\alpha-\beta\right)}{\cos^2\beta}, \tag{A.22}$$

$$g^{h,\alpha}_{\tilde{b},11} = \frac{\sin\alpha}{\cos\beta}\left(2 + \frac{1}{2}\frac{\left(m^2_{\tilde{b}_1} - m^2_{\tilde{b}_2}\right)}{m^2_b}\sin^2\left(2\theta_{\tilde{b}}\right)\right), \tag{A.23}$$

$$g^{h,ew}_{\tilde{b},22} = c^{ew}_1\sin^2\theta_{\tilde{b}} + c^{ew}_2\cos^2\theta_{\tilde{b}}, \tag{A.24}$$

$$g^{h,\alpha}_{\tilde{b},22} = \frac{\sin\alpha}{\cos\beta}\left(2 - \frac{1}{2}\frac{\left(m^2_{\tilde{b}_1} - m^2_{\tilde{b}_2}\right)}{m^2_b}\sin^2\left(2\theta_{\tilde{b}}\right)\right), \tag{A.25}$$

$$g^{h}_{\tilde{b},12} = g^{h}_{\tilde{b},21}, \tag{A.26}$$

$$g^{h,ew}_{\tilde{b},12} = \frac{1}{2}\left(c^{ew}_2 - c^{ew}_1\right)\sin\left(2\theta_{\tilde{b}}\right), \tag{A.27}$$

$$g^{h,\mu}_{\tilde{b},12} = \frac{\mu_{susy}}{m_b}\cos\left(2\theta_{\tilde{b}}\right)\frac{\cos\left(\alpha-\beta\right)}{\cos^2\beta}, \tag{A.28}$$

$$g^{h,\alpha}_{\tilde{b},12} = -\frac{\sin\alpha}{\cos\beta}\frac{\left(m^2_{\tilde{b}_1} - m^2_{\tilde{b}_2}\right)}{2m^2_b}\sin\left(2\theta_{\tilde{b}}\right)\cos\left(2\theta_{\tilde{b}}\right). \tag{A.29}$$

B Appendix B
Counterterms

The quark mass counterterm in QCD is given by

$$\frac{m_q^B}{m_q} = 1 - C_F \frac{\alpha_s}{\pi} \left(\frac{1}{\epsilon} \frac{3}{4} - 1 - \frac{3}{4} L_q \right). \tag{B.1}$$

with $C_F = 4/3$ and $L_q = \ln\left(\mu_R^2/m_q^2\right)$. The quark mass counterterm in QCD is given in DREG. Switching to DRED, the constant "1" becomes "5/4".

Complete SQCD Counterterms

The relations between the bare and renormalized pole masses are given in what follows. For the quark $(q = t, b)$ one has [82]

$$\begin{aligned} \frac{m_q^B}{m_q} = 1 + C_F \frac{\alpha_s}{\pi} \Bigg\{ & -\frac{1}{2\epsilon} - \frac{5}{4} - \frac{3}{4} L_q - \frac{m_{\tilde{g}^2}}{4m_q^2} \left(1 + L_{\tilde{g}}\right) + \sum_{i=1}^{2} \frac{m_{\tilde{q}_i}^2}{8m_q^2} \left(1 + L_{\tilde{q}_i}^2\right) \\ & + \sum_{i=1}^{2} \left[\frac{1}{8} \left(1 + \frac{m_{\tilde{g}}^2}{m_q^2} - \frac{m_{\tilde{q}_i}^2}{m_q^2} + 2(-1)^i \frac{m_{\tilde{g}}}{m_q} \sin 2\theta_{\tilde{q}} \right) B_0^{fin}\left(m_q^2, m_{\tilde{g}}, m_{\tilde{q}_i}\right) \right] \Bigg\}, \end{aligned} \tag{B.2}$$

with

$$L_q = \ln \frac{\mu_R^2}{m_q^2}, \qquad L_{\tilde{q}_i} = \ln \frac{\mu_R^2}{m_{\tilde{q}_i}^2}, \qquad L_{\tilde{g}} = \ln \frac{\mu_R^2}{m_{\tilde{g}}^2}. \tag{B.3}$$

It should be noted that the above given counterterm (B.2) is obtained by using DRED. The corresponding counterterm in DREG is obtained by changing the constant "5/4" to "1" in Eq. (B.2).

The relation between the bare and renormalized squark ($\tilde{q} = \tilde{t}, \tilde{b}$) mass reads [82]

$$\begin{aligned}\frac{m^B_{\tilde{q}_1}}{m_{\tilde{q}_1}} = 1 + C_F \frac{\alpha_s}{\pi} \Bigg\{ & \frac{1}{8m^2_{\tilde{q}_1}\epsilon} \left[4m_{\tilde{g}} m_q \sin 2\theta_{\tilde{q}} - 4m^2_{\tilde{g}} - 4m^2_q + \left(m^2_{\tilde{q}_2} - m^2_{\tilde{q}_1}\right) \sin^2 2\theta_{\tilde{q}}\right] \\ & - \frac{3}{4} - \frac{\sin^2 2\theta_{\tilde{q}}}{8} - \left(\frac{1}{4} + \frac{\sin^2 2\theta_{\tilde{q}}}{8}\right) L_{\tilde{q}_1} - \frac{m^2_{\tilde{g}}}{4m^2_{\tilde{q}_1}} (1 + L_{\tilde{g}}) - \frac{m^2_q}{4m^2_{\tilde{q}_1}} (1 + L_q) \\ & + \frac{m^2_{\tilde{q}_2} \sin^2 2\theta_{\tilde{q}}}{8m^2_{\tilde{q}_1}} (1 + L_{\tilde{q}_2}) + \left[\frac{1}{4} + \frac{2m_{\tilde{g}} m_q \sin 2\theta_{\tilde{q}} - m^2_{\tilde{g}} - m^2_q}{4m^2_{\tilde{q}_1}}\right] B_0^{fin}\left(m^2_{\tilde{q}_1}, m_q, m_{\tilde{g}}\right) \Bigg\}. \end{aligned} \tag{B.4}$$

The result for $m_{\tilde{q}_2}$ is obtained if one exchanges the indices 1 and 2 and switches the sign of $\sin 2\theta_{\tilde{q}}$.

For the renormalization of the mixing angle the following holds [82]

$$\theta^B_{\tilde{q}} = \theta_{\tilde{q}} + \delta\theta_{\tilde{q}}, \tag{B.5}$$

where

$$\begin{aligned}\delta\theta_{\tilde{q}} = C_F \frac{\alpha_s}{\pi} \frac{\cos 2\theta_{\tilde{q}}}{m^2_{\tilde{t}_2} - m^2_{\tilde{q}_1}} \Bigg\{ & \frac{4m_{\tilde{g}} m_q + \left(m^2_{\tilde{q}_1} - m^2_{\tilde{q}_2}\right) \sin 2\theta_{\tilde{q}}}{4\epsilon} \\ & + \frac{\sin 2\theta_{\tilde{q}}}{4} \left[m^2_{\tilde{q}_2} (1 + L_{\tilde{q}_2}) - m^2_{\tilde{q}_1} (1 + L_{\tilde{q}_1})\right] + m_{\tilde{g}} m_q B_0^{fin}\left(q^2_o, m_q, m_{\tilde{g}}\right) \Bigg\}. \end{aligned} \tag{B.6}$$

Counterterms without gluino effects (no $\tilde{g}$)

For the on-shell counterterms without gluinos we find

$$\begin{aligned}\delta Z^{\text{no}\,\tilde{g}}_{m_{\tilde{q}_1}} = C_F \frac{\alpha_s}{\pi} \Bigg[& \frac{1}{2\epsilon} \frac{1}{m^2_{\tilde{q}_1}} \left(-\frac{1}{2} m^2_{\tilde{q}_1} - \left(m^2_{\tilde{q}_2} - m^2_{\tilde{q}_1}\right) \sin^2\theta_{\tilde{q}} + \sin^4\theta_{\tilde{q}} \left(m^2_{\tilde{q}_2} - m^2_{\tilde{q}_1}\right)\right) \\ & - \frac{1}{2} m^2_{\tilde{q}_1} (3 + L_{\tilde{q}_1}) - \frac{1}{4} \sin^2 2\theta_{\tilde{q}}\, m^2_{\tilde{q}_1} (1 + L_{\tilde{q}_1}) + \frac{1}{4} \sin^2 2\theta_{\tilde{q}}\, m^2_{\tilde{q}_2} (1 + L_{\tilde{q}_2})\Bigg], \end{aligned} \tag{B.7}$$

$$\begin{aligned}\delta Z^{\text{no}\,\tilde{g}}_{m_{\tilde{q}_2}} = C_F \frac{\alpha_s}{\pi} \Bigg[& \frac{1}{2\epsilon} \frac{1}{m^2_{\tilde{q}_2}} \left(-\frac{1}{2} m^2_{\tilde{q}_1} - \left(m^2_{\tilde{q}_2} - m^2_{\tilde{q}_1}\right) \sin^2\theta_{\tilde{q}} + \sin^4\theta_{\tilde{q}} \left(m^2_{\tilde{q}_2} - m^2_{\tilde{q}_1}\right)\right) \\ & - \frac{1}{2} m^2_{\tilde{q}_2} (3 + L_{\tilde{q}_2}) + \frac{1}{4} \sin^2 2\theta_{\tilde{q}}\, m^2_{\tilde{q}_1} (1 + L_{\tilde{q}_1}) - \frac{1}{4} \sin^2 2\theta_{\tilde{q}}\, m^2_{\tilde{q}_2} (1 + L_{\tilde{q}_2})\Bigg], \end{aligned} \tag{B.8}$$

$$\begin{aligned}\delta\theta_{\tilde{q}}{}^{\text{no}\,\tilde{g}} = C_F \frac{\alpha_s}{\pi} \Bigg[& \frac{1}{\epsilon} \frac{1}{m^2_{\tilde{q}_1} - m^2_{\tilde{q}_2}} \left(\frac{1}{4} \left(m^2_{\tilde{q}_2} - m^2_{\tilde{q}_1}\right) \sin 2\theta_{\tilde{q}} - \frac{1}{2} \sin 2\theta_{\tilde{q}} \sin^2\theta_{\tilde{q}} \left(m^2_{\tilde{q}_2} - m^2_{\tilde{q}_1}\right)\right) \\ & + \frac{1}{8} \frac{1}{m^2_{\tilde{q}_1} - m^2_{\tilde{q}_2}} \sin 4\theta_{\tilde{q}} \left(m^2_{\tilde{q}_2} (1 + L_{\tilde{q}_2}) - m^2_{\tilde{q}_1} (1 + L_{\tilde{q}_1})\right)\Bigg]. \end{aligned} \tag{B.9}$$

In the calculation of the counterterms integrals of the form

$$I\left(q,m_1,m_2\right)=\frac{\left(2\pi\mu\right)^{4-d}}{i\pi^2}\int d^dl\frac{1}{\left((q+l)^2-m_1^2\right)\left(l^2-m_2^2\right)} \tag{B.10}$$

are obtained. Their finite parts are denoted by $B_0^{fin}\left(q^2,m_1,m_2\right)$. For $q^2\leq\left(m_1-m_2\right)^2$ it is given by [82]

$$B_0^{fin}\left(q^2,m_1,m_2\right)=2-\ln\frac{m_1m_2}{\mu_R^2}+\frac{m_1^2-m_2^2}{q^2}\ln\frac{m_2}{m_1}+\frac{M_+M_-}{q^2}\ln\frac{M_++M_-}{M_+-M_-}, \tag{B.11}$$

with $M_\pm=\sqrt{\left(m_1\pm m_2\right)^2-q^2}$.

For a certain given hierarchy among the masses we calculate

$$\begin{aligned}
B_0^{fin}\left(M^2,M,M\right)&=2-\frac{\pi}{\sqrt{3}}+L_M,\\
B_0^{fin}\left(m^2,M,M\right)&=2+L_M+\sqrt{t-1}\arctan\left(\frac{2\sqrt{t-1}}{t-2}\right),\\
B_0^{fin}\left(M^2,m,M\right)&=2+L_M+\frac{2}{t}\ln\frac{M^2}{m^2}-\frac{4}{t}\sqrt{t-1}\arctan\left(\sqrt{t-1}\right),
\end{aligned} \tag{B.12}$$

with

$$t=\frac{4M^2}{m^2},\qquad L_M=\ln\frac{\mu_R^2}{M^2}. \tag{B.13}$$

Appendix C
Feynman Rules

The Feynman rules relevant for the calculations are taken from [31,82,108].

First, we introduce the notation applied for the Feynman rules. p, p_1, p_2, p_3 and k are four-momenta. We name color triplet indices (r,s,t,u), color octet indices (a,b,c), Lorentz indices (μ,ν,ρ), squark mass eigenstate indices (i,j,k,l) and flavor indices (α,β).

The expressions used below are defined as

$$
\begin{aligned}
&\left[T^a,T^b\right] = if^{abc}T^c, \qquad \left\{T^a,T^b\right\} = \frac{1}{n_c}\delta^{ab} + d^{abc}T^c,\\
&P_L = \frac{1-\gamma_5}{2}, \qquad P_R = \frac{1+\gamma_5}{2},\\
&\mathcal{R}^{\tilde{q}} = \begin{pmatrix} \mathcal{R}^{\tilde{q}}_{11} & \mathcal{R}^{\tilde{q}}_{12} \\ \mathcal{R}^{\tilde{q}}_{21} & \mathcal{R}^{\tilde{q}}_{22} \end{pmatrix} = \begin{pmatrix} \cos\theta_{\tilde{q}} & \sin\theta_{\tilde{q}} \\ -\sin\theta_{\tilde{q}} & \cos\theta_{\tilde{q}} \end{pmatrix},\\
&\mathcal{S}^{\tilde{q}}_{ij} \equiv \mathcal{R}^{\tilde{q}}_{i1}\mathcal{R}^{\tilde{q}}_{j1} - \mathcal{R}^{\tilde{q}}_{i2}\mathcal{R}^{\tilde{q}}_{j2} = \begin{pmatrix} \cos\theta_{\tilde{q}} & \sin\theta_{\tilde{q}} \\ -\sin\theta_{\tilde{q}} & \cos\theta_{\tilde{q}} \end{pmatrix}_{ij}.
\end{aligned}
\tag{C.1}
$$

$i\frac{m_q}{v}g_q^{\phi}$ (see Tab. 3.2)

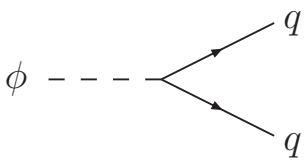

$i\frac{m_q}{v}g^A_{\tilde{q},ij}$, $i\frac{m_q^2}{v}g^h_{\tilde{q},ij}$ (see Eqs. (A.1), (A.3))

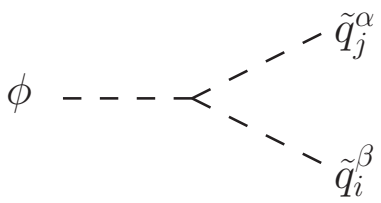

$$ig_s T^a_{rs}\gamma^\mu$$

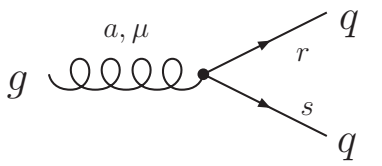

$$ie\, e_q \gamma^\mu$$

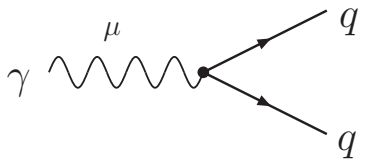

$$g_s f^{abc}\left[(p_1-p_2)^\rho\, g^{\mu\nu} + (p_2-p_3)^\mu\, g^{\nu\rho} + (p_3-p_1)^\nu\, g^{\mu\rho}\right]$$

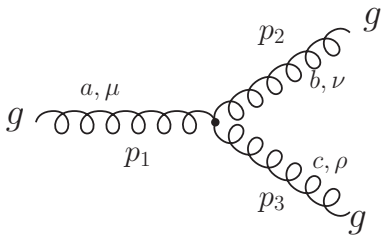

$$g_s f^{abc}\gamma^\mu$$

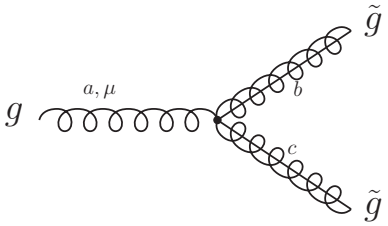

$$ig_s T^a_{rs}\,(p+k)^\mu\,\delta_{ij}$$

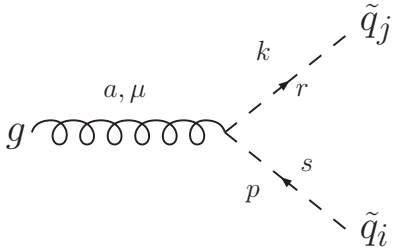

$$ie\, e_q\,(p+k)^\mu\,\delta_{ij}$$

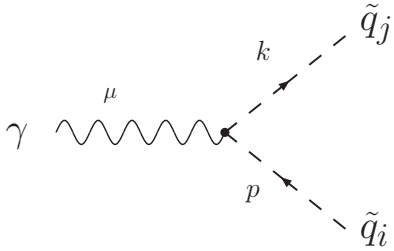

$$\sqrt{2}g_s T^a_{rs}\left(\mathcal{R}^{\tilde{q}}_{i1}P_L - \mathcal{R}^{\tilde{q}}_{i2}P_R\right)$$

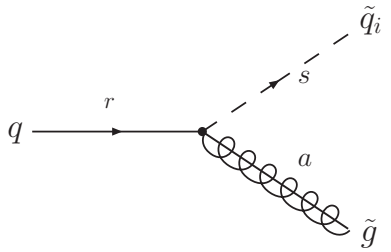

$$\sqrt{2}g_s T^a_{rs}\left(\mathcal{R}^{\tilde{q}}_{i1}P_R - \mathcal{R}^{\tilde{q}}_{i2}P_L\right)$$

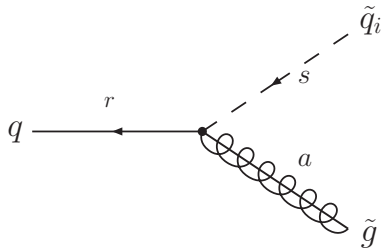

$$-ig_s^2\left(\tfrac{1}{3}\delta_{ab}\delta_{rs} + d_{abc}T^c_{rs}\right)g_{\mu\nu}\delta_{ij}$$

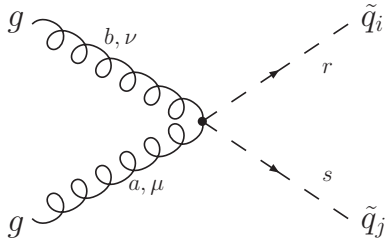

$$-2ie\,e_q g_s T^a_{rs} g_{\mu\nu}\delta_{ij}$$

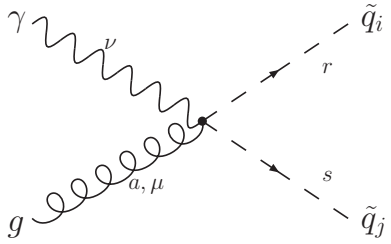

$$2ie^2\,e_q^2 g_{\mu\nu}\delta_{ij}$$

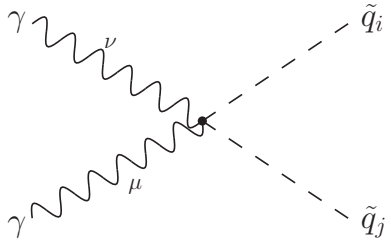

$$ig_s^2\left(T^a_{rs}T^a_{tu}\mathcal{S}^{\alpha}_{ij}\mathcal{S}^{\beta}_{kl} + T^a_{ru}T^a_{ts}\mathcal{S}^{\alpha}_{il}\mathcal{S}^{\alpha}_{kj}\delta_{\alpha\beta}\right)$$

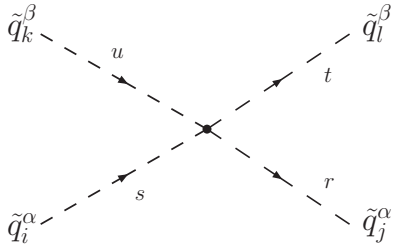

Bibliography

[1] S. L. Glashow, "Partial Symmetries of Weak Interactions," *Nucl. Phys.* **22** (1961) 579–588.

[2] S. Weinberg, "A Model of Leptons," *Phys. Rev. Lett.* **19** (1967) 1264–1266.

[3] A. Salam, *Elementary Particle Theory*, p. 367. Stockholm, 1969.

[4] M. Gell-Mann, "A Schematic Model of Baryons and Mesons," *Phys. Lett.* **8** (1964) 214–215.

[5] G. Zweig, "An SU(3) Model for Strong Interaction Symmetry and its Breaking,". CERN-TH-401.

[6] H. Fritzsch, M. Gell-Mann, and H. Leutwyler, "Advantages of the Color Octet Gluon Picture," *Phys. Lett. B* **47** (1973) 365–368.

[7] D. J. Gross and F. Wilczek, "Ultraviolet Behavior of Non-Abelian Gauge Theories," *Phys. Rev. Lett.* **30** (1973) 1343–1346.

[8] H. D. Politzer, "Reliable Perturbative Results for Strong Interactions?," *Phys. Rev. Lett.* **30** (1973) 1346–1349.

[9] P. W. Higgs, "Broken Symmetries, Massless Particles and Gauge Fields," *Phys. Lett.* **12** (1964) 132–133.

[10] F. Englert and R. Brout, "Broken Symmetry and the Mass of Gauge Vector Mesons," *Phys. Rev. Lett.* **13** (1964) 321–322.

[11] F. Zwicky, "Spectral Displacement of Extra Galactic Nebulae," *Helv. Phys. Acta* **6** (1933) 110–127.

[12] H. Georgi and S. L. Glashow, "Unity of All Elementary Particle Forces," *Phys. Rev. Lett.* **32** (1974) 438–441.

[13] J. C. Pati and A. Salam, "Lepton Number as the Fourth Color," *Phys. Rev. D* **10** (1974) 275–289.

[14] P. Fayet, "About the Origins of the Supersymmetric Standard Model," *Nucl. Phys. Proc. Suppl.* **101** (2001) 81–98, hep-ph/0107228.

[15] S. P. Martin, "A Supersymmetry Primer," hep-ph/9709356.

[16] S. R. Coleman and J. Mandula, "All Possible Symmetries of the S-Matrix," *Phys. Rev.* **159** (1967) 1251–1256.

[17] R. Haag, J. T. Lopuszanski, and M. Sohnius, "All Possible Generators of Supersymmetries of the S-Matrix," *Nucl. Phys. B* **88** (1975) 257.

[18] H. Baer and X. Tata, *Weak scale supersymmetry.* Cambridge, 2006.

[19] J. Wess and B. Zumino, "Supergauge Transformations in Four-Dimensions," *Nucl. Phys. B* **70** (1974) 39–50.

[20] G.L. Kane and M.A. Shifman, editors, *The Supersymmetric World.* World Scientific, 2001.

[21] Y. A. Golfand and E. P. Likhtman, "Extension of the Algebra of Poincaré Group Generators and Violation of P-Invariance," *JETP Lett.* **13** (1971) 323–326.

[22] D. V. Volkov and V. P. Akulov, "Possible Universal Neutrino Interaction," *JETP Lett.* **16** (1972) 438–440.

[23] D. V. Volkov and V. P. Akulov, "Is the Neutrino a Goldstone Particle?," *Phys. Lett. B* **46** (1973) 109–110.

[24] D. V. Volkov and V. A. Soroka, "Higgs Effect for Goldstone Particles with Spin 1/2," *JETP Lett.* **18** (1973) 312–314.

[25] http://pdg.lbl.gov.

[26] M. Shifman, "From Heisenberg to Supersymmetry," *Fortsch. Phys.* **50** (2002) 552–561.

[27] U. Amaldi, W. de Boer, and H. Fürstenau, "Comparison of Grand Unified Theories with Electroweak and Strong Coupling Constants Measured at LEP," *Phys. Lett. B* **260** (1991) 447–455.

[28] J. Gunion, H. Haber, G. Kane, and S. Dawson, *The Higgs Hunter's Guide.* Addison Wesley Publishing Company, 1990.

[29] A. Djouadi, "The Anatomy of Electro-Weak Symmetry Breaking. Tome II: The Higgs Bosons in the Minimal Supersymmetric Model," *Phys. Rept.* **459** (2008) 1–241, hep-ph/0503173.

[30] F. Hofmann, *Erzeugung pseudoskalarer Higgs Bosonen am LHC*. Diplomarbeit, 2005.

[31] S. Kraml, "Stop and Sbottom Phenomenology in the MSSM," hep-ph/9903257.

[32] J. Collins, *Renormalization*. Cambridge University Press, 1984.

[33] H. J. M. Böhm, A. Denner, *Gauge Theories of the Strong and Electroweak Interaction*. B. G. Teubner, 3. Auflage, 2001.

[34] M. Steinhauser, *Übungen zu Strahlungskorrekturen in Eichtheorien*. Herbstschule, Maria Laach, 2003.

[35] G. 't Hooft and M. J. G. Veltman, "Regularization and Renormalization of Gauge Fields," *Nucl. Phys. B* **44** (1972) 189–213.

[36] S. A. Larin, "The Renormalization of the Axial Anomaly in Dimensional Regularization," *Phys. Lett. B* **303** (1993) 113–118, hep-ph/9302240.

[37] W. Beenakker, R. Höpker, and P. M. Zerwas, "SUSY-QCD Decays of Squarks and Gluinos," *Phys. Lett. B* **378** (1996) 159–166, hep-ph/9602378.

[38] W. Hollik, E. Kraus, and D. Stöckinger, "Renormalization and Symmetry Conditions in Supersymmetric QED," *Eur. Phys. J. C* **11** (1999) 365–381, hep-ph/9907393.

[39] W. Hollik and D. Stöckinger, "Regularization and Supersymmetry-Restoring Counterterms in Supersymmetric QCD," *Eur. Phys. J. C* **20** (2001) 105–119, hep-ph/0103009.

[40] P. L. White, "An Analysis of the Cohomology Structure of Super-Yang-Mills Coupled to Matter," *Class. Quant. Grav.* **9** (1992) 1663–1682.

[41] W. Hollik, E. Kraus, and D. Stöckinger, "Renormalization of Supersymmetric Yang-Mills Theories with Soft Supersymmetry Breaking," *Eur. Phys. J. C* **23** (2002) 735–747, hep-ph/0007134.

[42] W. Hollik *et al.*, "Renormalization of the Supersymmetric Minimal Standard Model," *Nucl. Phys. B* **639** (2002) 3–65, hep-ph/0204350.

[43] W. Siegel, "Supersymmetric Dimensional Regularization via Dimensional Reduction," *Phys. Lett. B* **84** (1979) 193.

[44] I. Jack and D. R. T. Jones, "Regularisation of Supersymmetric Theories," hep-ph/9707278.

[45] D. Stöckinger, "Regularization by Dimensional Reduction: Consistency, Quantum Action Principle, and Supersymmetry," *JHEP* **03** (2005) 076, hep-ph/0503129.

[46] C. Anastasiou, S. Beerli, and A. Daleo, "The Two-Loop QCD Amplitude gg -> h,H in the Minimal Supersymmetric Standard Model," *Phys. Rev. Lett.* **100** (2008) 241806, 0803.3065.

[47] K. G. Chetyrkin, J. H. Kühn, and A. Kwiatkowski, "QCD Corrections to the e^+e^- Cross-Section and the Z Boson Decay Rate," hep-ph/9503396.

[48] V. Ahrens, T. Becher, M. Neubert, and L. L. Yang, "Renormalization-Group Improved Prediction for Higgs Production at Hadron Colliders," *Eur. Phys. J. C* **62** (2009) 333–353, 0809.4283.

[49] V. Smirnov, "Asymptotic Expansions in Momenta and Masses and Calculation of Feynman Diagrams," *Mod. Phys. Lett. A* **10** (1995) 1485–1500, hep-th/9412063.

[50] V. A. Smirnov, "Applied Asymptotic Expansions in Momenta and Masses," *Springer Tracts Mod. Phys.* **177** (2002) 1–262.

[51] R. Harlander, "Asymptotic Expansions: Methods and Applications," *Acta Phys. Polon. B* **30** (1999) 3443–3462, hep-ph/9910496.

[52] T. Seidensticker, "Automatic Application of Successive Asymptotic Expansions of Feynman Diagrams," hep-ph/9905298.

[53] R. V. Harlander, T. Seidensticker, and M. Steinhauser, "Complete Corrections of O(alpha alpha(s)) to the Decay of the Z Boson into Bottom Quarks," *Phys. Lett. B* **426** (1998) 125–132, hep-ph/9712228.

[54] P. Nogueira, "Automatic Feynman Graph Generation," *J. Comput. Phys.* **105** (1993) 279–289.

[55] T. Seidensticker. (unpublished).

[56] J. A. M. Vermaseren, "New Features of FORM," math-ph/0010025.

[57] M. Steinhauser, "MATAD: A Program Package for the Computation of Massive Tadpoles," *Comput. Phys. Comm.* **134** (2001) 335–364, hep-ph/0009029.

[58] S. A. Larin, F. V. Tkachov, and J. A. M. Vermaseren, "The FORM Version of MINCER,". NIKHEF-H-91-18.

[59] R. V. Harlander and M. Steinhauser, "Hadronic Higgs Production and Decay in Supersymmetry at next-to-leading Order," *Phys. Lett. B* **574** (2003) 258–268, hep-ph/0307346.

[60] R. V. Harlander and F. Hofmann, "Pseudo-Scalar Higgs Production at next-to-leading Order SUSY-QCD," *JHEP* **03** (2006) 050, hep-ph/0507041.

[61] M. E. Peskin and D. V. Schroeder, *An Introduction to Quantum Field Theory.* Westview Press, 1995.

[62] W. Research, *Mathematica Edition: Version 6.0.* Wolfram Research, Inc. Place of publication: Champaign, Illinois, 2007.

[63] A. I. Davydychev and M. Y. Kalmykov, "Massive Feynman Diagrams and Inverse Binomial Sums," *Nucl. Phys. B* **699** (2004) 3–64, hep-th/0303162.

[64] J. G. Körner, Z. Merebashvili, and M. Rogal, "Laurent Series Expansion of Massive Scalar One-Loop Integrals to $O(epsilson^2)$," *Phys. Rev. D* **71** (2005) 054028, hep-ph/0412088.

[65] http://lepewwg.web.cern.ch/LEPEWWG.

[66] *CDF and DZero* Collaboration, "Combined CDF and DZero Upper Limits on Standard Model Higgs-Boson Production with up to 4.2 fb-1 of Data," 0903.4001.

[67] T. Hambye and K. Riesselmann, "Matching Conditions and Higgs Mass Upper Bounds Revisited," *Phys. Rev. D* **55** (1997) 7255–7262, hep-ph/9610272.

[68] A. Djouadi, "The Anatomy of Electro-Weak Symmetry Breaking. Tome I: The Higgs Boson in the Standard Model," *Phys. Rept.* **457** (2008) 1–216, hep-ph/0503172.

[69] *The ATLAS* Collaboration, G. Aad *et al.*, "Expected Performance of the ATLAS Experiment - Detector, Trigger and Physics," 0901.0512.

[70] J. R. Ellis, M. K. Gaillard, and D. V. Nanopoulos, "A Phenomenological Profile of the Higgs Boson," *Nucl. Phys. B* **106** (1976) 292.

[71] M. A. Shifman, A. I. Vainshtein, M. B. Voloshin, and V. I. Zakharov, "Low-Energy Theorems for Higgs Boson Couplings to Photons," *Sov. J. Nucl. Phys.* **30** (1979) 711–716.

[72] M. B. Gavela, G. Girardi, C. Malleville, and P. Sorba, "A Nonlinear R(xi) Gauge Condition for the Electroweak SU(2) x U(1) Model," *Nucl. Phys. B* **193** (1981) 257.

[73] M. Spira, A. Djouadi, D. Graudenz, and P. M. Zerwas, "Higgs Boson Production at the LHC," *Nucl. Phys. B* **453** (1995) 17–82, hep-ph/9504378.

[74] G. Passarino, C. Sturm, and S. Uccirati, "Complete Two-Loop Corrections to H -> gamma gamma," *Phys. Lett. B* **655** (2007) 298–306, 0707.1401.

[75] J. Fleischer, O. V. Tarasov, and V. O. Tarasov, "Analytical Result for the Two-Loop QCD Correction to the Decay H –> 2gamma," *Phys. Lett. B* **584** (2004) 294–297, hep-ph/0401090.

[76] R. Harlander and P. Kant, "Higgs Production and Decay: Analytic Results at next-to-leading Order QCD," *JHEP* **12** (2005) 015, hep-ph/0509189.

[77] M. Steinhauser, "Corrections of O(alpha(s)**2) to the Decay of an Intermediate-Mass Higgs Boson into two Photons," hep-ph/9612395.

[78] J. Brod, F. Fugel, and B. A. Kniehl, "Two-Loop Electroweak Corrections to the A0 gamma gamma and A0 g g Couplings of the CP-Odd Higgs Boson," *Nucl. Phys. B* **807** (2009) 188–209, 0807.1008.

[79] G. Degrassi and P. Slavich, "On the NLO QCD Corrections to Higgs Production and Decay in the MSSM," *Nucl. Phys. B* **805** (2008) 267–286, 0806.1495.

[80] K. G. Chetyrkin, B. A. Kniehl, M. Steinhauser, and W. A. Bardeen, "Effective QCD Interactions of CP-Odd Higgs Bosons at Three Loops," *Nucl. Phys. B* **535** (1998) 3–18, hep-ph/9807241.

[81] M. Spira, "QCD Effects in Higgs Physics," *Fortsch. Phys.* **46** (1998) 203–284, hep-ph/9705337.

[82] R. V. Harlander and M. Steinhauser, "Supersymmetric Higgs Production in Gluon Fusion at next- to-leading Order," *JHEP* **09** (2004) 066, hep-ph/0409010.

[83] R. Harlander, P. Kant, L. Mihaila, and M. Steinhauser, "Dimensional Reduction Applied to QCD at Three Loops," *JHEP* **09** (2006) 053, hep-ph/0607240.

[84] T. Appelquist and J. Carazzone, "Infrared Singularities and Massive Fields," *Phys. Rev. D* **11** (1975) 2856.

[85] B. C. Allanach *et al.*, "The Snowmass Points and Slopes: Benchmarks for SUSY Searches," *Eur. Phys. J. C* **25** (2002) 113–123, hep-ph/0202233.

[86] A. Djouadi, J.-L. Kneur, and G. Moultaka, "SuSpect: A Fortran Code for the Supersymmetric and Higgs Particle Spectrum in the MSSM," *Comput. Phys. Commun.* **176** (2007) 426–455, hep-ph/0211331.

[87] S. Heinemeyer, W. Hollik, and G. Weiglein, "FeynHiggs: A Program for the Calculation of the Masses of the Neutral CP-even Higgs Bosons in the MSSM," *Comput. Phys. Commun.* **124** (2000) 76–89, hep-ph/9812320.

[88] T. Hahn, S. Heinemeyer, F. Maltoni, G. Weiglein, and S. Willenbrock, "SM and MSSM Higgs Boson Production Cross Sections at the Tevatron and the LHC," hep-ph/0607308.

[89] R. Harlander, "Higgs Production at the Large Hadron Collider: Theoretical Status," *J. Phys. G* **35** (2008) 033001.

[90] D. L. Rainwater and D. Zeppenfeld, "Searching for H –> gamma gamma in Weak Boson Fusion at the LHC," *JHEP* **12** (1997) 005, hep-ph/9712271.

[91] T. Figy, C. Oleari, and D. Zeppenfeld, "Next-to-leading Order Jet Distributions for Higgs Boson Production via Weak-Boson Fusion," *Phys. Rev. D* **68** (2003) 073005, hep-ph/0306109.

[92] M. Dührssen *et al.*, "Determination of Higgs-boson Couplings at the LHC," hep-ph/0407190.

[93] W. Beenakker, S. Dittmaier, M. Kramer, B. Plumper, M. Spira, and P. M. Zerwas, "Higgs Radiation off Top Quarks at the Tevatron and the LHC," *Phys. Rev. Lett.* **87** (2001) 201805, hep-ph/0107081.

[94] L. Reina and S. Dawson, "Next-to-leading Order Results for t anti-t h Production at the Tevatron," *Phys. Rev. Lett.* **87** (2001) 201804, hep-ph/0107101.

[95] S. Dawson and L. Reina, "QCD Corrections to Associated Higgs Boson Production," *Phys. Rev. D* **57** (1998) 5851–5859, hep-ph/9712400.

[96] S. Actis, G. Passarino, C. Sturm, and S. Uccirati, "NLO Electroweak Corrections to Higgs Boson Production at Hadron Colliders," *Phys. Lett. B* **670** (2008) 12–17, 0809.1301.

[97] M. Spira, A. Djouadi, D. Graudenz, and P. M. Zerwas, "SUSY Higgs Production at Proton Colliders," *Phys. Lett. B* (1993) 347–353.

[98] R. V. Harlander and W. B. Kilgore, "Next-to-next-to-leading Order Higgs Production at Hadron Colliders," *Phys. Rev. Lett.* **88** (2002) 201801, hep-ph/0201206.

[99] C. Anastasiou and K. Melnikov, "Higgs Boson Production at Hadron Colliders in NNLO QCD," *Nucl. Phys. B* **646** (2002) 220–256, hep-ph/0207004.

[100] V. Ravindran, J. Smith, and W. L. van Neerven, "NNLO Corrections to the Total Cross Section for Higgs Boson Production in Hadron-Hadron Collisions," *Nucl. Phys. B* **665** (2003) 325–366, hep-ph/0302135.

[101] S. Dawson, "Radiative Corrections to Higgs Boson Production," *Nucl. Phys. B* **359** (1991) 283–300.

[102] M. Mühlleitner and M. Spira, "Higgs Boson Production via Gluon Fusion: Squark Loops at NLO QCD," *Nucl. Phys. B* **790** (2008) 1–27, hep-ph/0612254.

[103] M. Mühlleitner, H. Rzehak, and M. Spira, "MSSM Higgs Boson Production via Gluon Fusion: The Large Gluino Mass Limit," *JHEP* **04** (2009) 023, 0812.3815.

[104] M. Spira, "HIGLU: A Program for the Calculation of the Total Higgs Production Cross Section at Hadron Colliders via Gluon Fusion including QCD Corrections," hep-ph/9510347.

[105] M. Steinhauser, "Results and Techniques of Multi-Loop Calculations," *Phys. Rept.* **364** (2002) 247–357, hep-ph/0201075.

[106] D. Maitre, "HPL, a Mathematica Implementation of the Harmonic Polylogarithms," *Comput. Phys. Commun.* **174** (2006) 222–240, hep-ph/0507152.

[107] R. V. Harlander, "ggh@nnlo,". (unpublished).

[108] J. Rosiek, "Complete Set of Feynman Rules for the MSSM — ERRATUM," hep-ph/9511250.

Danksagung

Mein besonderer Dank gilt Prof. Robert Harlander, der mir eine Dissertation in Bereich der theoretischen Teilchenphysik ermöglicht hat. Ich möchte mich für seinen physikalischen Rat und die vielen Diskussionen bedanken, in denen ich viel von seiner Erfahrung auf dem Gebiet der Teilchenphysik profitiert habe. Ohne seine finanzielle Unterstützung wäre diese Arbeit nicht möglich gewesen. Dafür, dass Prof. Harlander mir die Teilnahme an inspirierenden Sommerschulen in Maria Laach, Schweden und Dubna und bei diversen Konferenzen und Workshops ermöglicht hat, möchte ich ihm ebenfalls ausdrücklich danken.

Prof. Matthias Steinhauser danke ich, dass er sich dazu bereit erklärt hat, das Koreferat dieser Arbeit zu übernehmen.

Meinen BürokollegInnen Christa und Thorsten möchte ich für die angenehme Arbeitsatmosphäre und die vielen Gespräche über physikalische und nicht-physikalische Themen danken, die meinen Arbeitsalltag positiv bereichert haben.

Meinen Korrekturlesern Christa, Kemal, Peter und Jens bin ich ebenfalls zu Dank verpflichtet.